Republic of Iraq
Ministry of Higher Education and Scientific Research
University of Baghdad
College of Engineering
Chemical Engineering Department

Control of Scale Formation in Ceramic Titanium Dioxide Nanofiltration Membrane

A THESIS SUBMITTED TO

THE COLLEGE OF ENGINEERING – UNIVERSITY OF BAGHDAD

IN PARTIAL FULFILLMENT OF THE REQUIREMENTS FOR

THE DEGREE OF DOCTOR OF PHILOSOPHY

IN CHEMICAL ENGINEERING

BY

Mudhaffar Yacoub Hussein AL-Saedi

(B.Sc. Chem. Eng.1988)
(M.Sc. Chem. Eng.2002)

August 2018

(بِسْمِ اَللّٰهِ الرَّحْمنِ الرَّحِيمِ)

"يَرْفَعِ اللَّهُ الَّذِينَ آمَنُوا مِنْكُمْ

وَالَّذِينَ أُوتُوا الْعِلْمَ دَرَجَاتٍ

وَاللَّهُ بِمَا تَعْمَلُونَ خَبِيرٌ"

(صَدقَ اللّٰهُ العَظيم)

سورةالمجادلة-11

Certification of Supervisors

I certify that this thesis entitled

"Control of Scale Formation in Ceramic Titanium Dioxide Nanofiltration Membrane"

Presented by **Mudhaffar Yacoub Hussein** was prepared under my Supervision in Chemical Engineering Department, of the College of Engineering, University of Baghdad, of the Requirements for the Degree of Doctor of Philosophy in Chemical Engineering.

Signature:
Prof. Dr. Ahmed Faiq Al – Alawy
Supervisor
Date: / /2018

Signature:
Dr. Amer Naji Ahmed Al-Naemi
Supervisor
Date: / /2018

In view of the available recommendation I forward this thesis for debate by the committee.

Signature:
Prof Dr. Hussein Qasim Hussein
Head of Chemical Engineering Department
Date: / /2018

Examination Committee Certificate

We certify that we have read this thesis entitled **"Control of Scale Formation in Ceramic Titanium Dioxide Nanofiltration Membrane"** and as an Examining Committee examined the student in its content and that in our opinion it meets the standard of a thesis for the degree of **Doctor of Philosophy in Chemical Engineering** at the University of Baghdad, Department of Chemical Engineering.

Signature:
Prof. Dr. Qusay F. Abd Alhameed
Date: / / 2018
(Chairman)

Signature:
Prof. Dr. Sawsan A. M. Mohammed
Date: / / 2018
(Member)

Signature:
Assist. Prof. Dr. Ibtehal K. Shakir
Date: / / 2018
(Member)

Signature:
Assist. Prof. Dr. Nagam O. Kariem
Date: / / 2018
(Member)

Signature:
Assist. Prof. Dr. Ali H. Abbar
Date: / / 2018
(Member)

Signature:
Prof. Dr. Ahmed Faiq Al – Alawy
Date: / / 2018
(Supervisor)

Signature:
Dr. Amer Naji Ahmed Al-Naemi
Date: / / 2018
(Supervisor)

Approved by the University of Baghdad:

Signature:
Prof. Dr. Saba Jabbar Neamah
Acting Dean of College of Engineering
Date: / / 2018

Dedication

To the Memory of My Father

To My Mother.

To My Wife

And My Lovely boys Ahmed, Ali and My Daughter Ghada

May God To Bless Them.

Mudhaffar 2018

Acknowledgment

First of all I thank Allah who gives me patience and strength and the most important thing is faith to continue.

I wish to express my sincere gratitude and grateful admiration to my supervisors ***Prof.Dr. Ahmed Faiq Al – Alway*** *and* ***Dr. Amer N. Al-Naemi*** *for their overseeing guidance, interests and suggestions which were very helpful for the preparation and completion of this work and I cannot express how much I have learned from them.*

My respectful regards and sincere appreciation to ***Prof Dr. Hussein Qasim Hussein*** *(the head of Chemical Engineering department) for providing the facilities for this work. My deep thank to the staff of Chemical Engineering Department at University of Baghdad as well as to the high studies students and Water Treatment Technology Center, Environment / Water Research Directorate for their assistance and support.*

I would like to express my very deep respect and sincere appreciation to my family in particular my mother and wife whose patience and encouragement gave me hope and support that I feel short of thanks.

Above all, my great thanks to Allah all Mighty for his mercy and blesses.

Mudhaffar 2018

Abstract

The research aims to study the prevention of scaling and calculate the rejection percentage of calcium carbonate ($CaCO_3$) and other salts (NaCl, KCl, $NaHCO_3$, $MgCl_2$, $CaCl_2$, Na_2CO_3, Na_2SO_4 and $MgSO_4$) for a 0.9 nm tubular ceramic titanium dioxide (TiO_2) nanofiltration (NF) membrane. The main parameters that affect the scaling and rejection of NF membrane is charge of membrane surface which were measured by using microelectrophoresis and streaming methods to determine the isoelectric point (IEP) of the membrane. Therefore, two electrodes made locally from composite material consist of pure silver and 4% gold conducting in-situ to measure zeta potential for salts by streaming potential method. Also, flux – pressure profile (step by step) procedure has been applied to estimate the values of critical flux (CF) as function to avoid deposits on the membrane surface and thus increasing the life of the NF membrane.

The measurements of zeta potential for sodium chloride solution as reference salt were conducted at pH ranged from 3 to 9 with different concentration and applied transmembrane pressure (TMP) ranged from 0.25 to 2 bars. The experimental results for the two methods were consistent and the IEP was at pH of (3.3 – 3.5) for NaCl. The IEP of other salts using streaming potential method was at pH of (3.4-3.8). The zeta potential increases with increasing pH value and decreases with increasing concentration.

The parameters studied in the rejection and critical flux experiments concentration which from 5×10^{-5} to 50×10^{-5} M to $CaCO_3$ while the another salts of 0.001 to 0.1 M, pH values from 3 to 9, cross flow velocity 1 m/s and TMP from 1 to 15 bar.

The rejection of $CaCO_3$ increases with increasing pressure and reaches the highest value 61% at TMP equal to 6 bar with concentration equal to 5×10^{-5} M, and then begins to decline with pressure. The rejection percentage increased with increasing of pH and flow velocity, so the increasing of flow velocity from (1 m/s to 2 m/s) caused to increase the rejection within 6% at pH = 6 and concentration 10×10^{-5}. Maximum rejection was found equal to 70% at TMP of 6 bar, concentration 5×10^{-5} M, pH of 9 and velocity 2m/s. In the case of supersaturation, 50×10^{-5} M the rejection from the beginning decreases with increasing of pressure.

Measurements of rejection for other salts showed that the sequence of rejections were Na_2SO_4 > $MgSO_4$ > $MgCl_2$ > $CaCl_2$ > $NaHCO_3$ > NaCl. The highest rejection was (82.2%) for Na_2SO_4. The rejection increases with increasing of (zeta potential, cross flow velocity, transmembrane pressure TMP) and decreases with increasing of concentration.

The obtained results of critical flux showed that the critical flux was reached and exceeded only for saline solutions of $MgSO_4$ at 0.005 M and 0.01M with 79 and 59 $l/m^2.h$ respectively. While for $CaCl_2$ at 0.005,0.01 and 0.015 M with 78.6, 57.5 and 43.3 $l/m^2.h$ respectively. A critical flux is not had in the other salts (NaCl, $NaHCO_3$, and Na_2SO_4). Generally, when the concentration increases, the critical flux occurs at a lower applied transmembrane pressure. While increasing both the pH value and a cross flow velocity leads to a critical flux occurs at higher applied transmembrane pressure.

The treatment of produced water from the Bazargan oilfield in Misan was investigated in this study in order to improve its quality before reinjection and reuse or disposal. The process of treatment consists of a pretreatment step utilizing microfiltration (0.3 μm) and ultrafiltration (0.004 μm), and posttreatment utilizing NF TiO_2 (0.9 nm) and reverse

osmosis (RO) respectively. Total organic carbon (TOC) removal was up (95.8%, 100%), total oil removal reached to (99.4%, 100%) and total removal of total dissolved solid (TDS) was up to (30%, 99.44%) after NF and RO membranes respectively.

Donnan model (DSPM) was used to estimate the rejection for NaCl salt theoretically. The theoretical results were agreement with the experimental results. The highest rejection is equal to 30.3% and 33,6% experimentally and theoretically respectively at TMP 15.0 bar.

Nomenclature

Symbols	Definition	Units
C_b	The solute concentration at external bulk solution	(mol/l)
$C_{i,new}^{permeate}$	New estimated permeate concentration of ion i	(mol/l)
$C_{i,old}^{permeate}$	Old assumed permeate concentration of ion i	(mol/l)
C_i^{feed}	Concentration of ion i in the Feed	(mol/l)
C_i^m	Concentration of ion i in membrane	(mol/l)
$C_p^{permeate}$	Permeate concentration	(mol/l)
A	Membrane one (effective area)	m^2
A_k	Membrane porosity	(dimensionless)
C	Uncharged solute concentration within pore	(mol/l)
C_b	Concentration of ion at external bulk solution	(mol/l)
C_i	Concentration of ion in salt solution	(mol/l)
$C_{i(x=o)}$	Concentration of ion i at feed-membrane interface	(mol/l)
$C_{i(x=\Delta x)}$	Concentration of ion i at feed-permeate interface	(mol/l)
$C_{i,1}$	Concentrations of interned solute	(mol/l)
$C_{i,N}$	Concentration of internal solute	(mol/l)
$C_{iavg.}$	Average concentration of ion i	(mol/l)
C_m	The solute concentration at the surface of membrane	(mol/l)
C_p	The solute concentration at the permeate side	(mol/l)
C_s	The coupling coefficient	V/bar
$D_{i,\infty}$	Molecular diffusion coefficient of ion i at infinite dilution	$(m^2.s^{-1})$
$D_{i,p}$	Hindered diffusivity of ion i	$(m^2.s^{-1})$
e	Elementary charge	$(1.6022 \times 10^{-19}$ C)
E_{str}	Streaming potential	(V)
F	Faraday constant	(96487 C/mol)

F_w	Water flux through membrane	$l/m^2.h$
h	Step size	m
J_{ci}	Critical flux of irreversibility form	$l/m^2.h$
J_{cs}	Strong critical flux	$l/m^2.h$
J_{cw}	Weak critical flux	$l/m^2.h$
Ji	Molar flux of species	(mol/m^2s)
J_{limit}	Limiting critical flux	$l/m^2.h$
J_v	Volume flux	$l/m^2.h$
J_w	Permeate water flux	$l/m^2.h$
k	Bulk conductivity of circulating electrolyte	$(S.m^{-1})$
K^{-1}	Bebye length (thickness of the diffuse double layer)	nm
K_B	Boltzmann constant	$(1.3806 \times 10^{-23}$ J/K)
$K_{i,c}$	Hindered coefficient for convection	(dimensionless)
$K_{i,d}$	Hindered coefficient for diffusion	(dimensionless)
K_w	Water mass transfer coefficient	$l/bar.m^2.h$
M	Solute molar concentration	mol/l
N_A	Avogadro number	$(6.022 \times 10^{23}$ /mol)
N_{steps}	Number of steps	
Pe^*	Modified Peclet number (uncharged solute hydrodynamic model)	
P_{in}	Module inlet pressure.	bar
P_{out}	Module outlet pressure	bar
Q_p	Permeate flow	(l/h)
R%	Salt rejection	
R_{ads}	Resistance of adsorption	1/m
$ratio_i$	Ratio between new and old permeates concentration of ion i.	
relax	Under relaxation factor.	
R_g	The constant of ideal gas	J/mol K
R_i	Rejection of ion (i)	

r_i	Stockes` radius of ion i	m
R_{irrev}	Resistance of inversible	1/m
R_m	Resistance of membrane	1/m
r_p	Effective pore radius	m
R_{rev}	Resistance of reversible	1/m
T	The absolute temperature	k
V	Solute velocity	$(m.s^{-1})$
x	Distance normal to membrane	(m)
X^m	Effective charge density of membrane	C/m^3
Z_i	Valance of ion i	(dimensionless)

Greek symbols	**Definition**	
π	Osmotic pressure	bar
$\gamma_{i,pore}$	Activity coefficient of ion i in the pore side of the interface.	
$\gamma_{i,sol}$	Activity coefficient of ion in the solution side of the interface.	
ϕ	Van't Hoff factor (Osmotic coefficient)	–
δ	Boundary layer thickness	m
μ	Viscosity of fluid	Pa.s
ε	Porosity	–
ψ	Membrane potential	V
$\Delta\pi$	Salt osmotic pressure difference	bar
$\Delta\psi_{Don}$	Donnan potential	V
$(\Delta P-\Delta\pi)$	Net applied pressure, (NAP)	bar
$\psi_{(x)}$	Electrical potential at (x) direction	V
$\Delta E_{stre.}$	Streaming potential (measured electrical)	V

λ_i	Ratio of stocks radius of ion i to the effective pore radius	–
ϕ_i	Steric partioning coefficient of ion i	(dimensionless)
ψ^m	Electrical potential of the membrane	V
ε_o	Permittivity of free space	$8.854\times10^{-12.}$ $C.m^{-1}.v^{-1}$
ψ_o	Initial electrical potential	V
ΔP	Applied pressure difference	bar
ε_r	Relative permittivity of water	78.54 at 25°C
σ^s	Electrical charge on membrane surface	C/m^2
ΔX	Effective thickness of membrane active layer	m
ΔX_e	Equivalent thickness of the membrane layer	m
ζ	Zeta potential	V

Abbreviations

Symbols	Definition	
AFM	Atomic force microscopy	
CF	Critical flux	$l/m^2.h$
CFF	Cross flow filtration	(m/s)
CP	Concentration polarization	
DEF	Dead-end filtration	
DOTM	Direct observation through the membrane	
DSPM	Donnan Steric Pore Model	
DSPM-DE	Donnan steric pore and dielectric exclusion model	
EDL	Electrical double layer	
EDXS	Energy dispersive x-ray spectroscopy	
ENPE	Extended Nernest Plank Equation	
H-S	Helmoholte-Smoluchowski equation	
I.E.P	Iso-electric point	

IC	Ion chromatography	
ICP-AES	Inductively coupled plasma-atomic emission spectroscopy	
KSM	Kedem-Spiegler model	
MF	Microfiltration	
MWCO	Molecular weight cut-off	
NF	Nanofilteration	
ODE	Ordinary differential equation	
ppm	Part per million	
RO	Reverse Osmosis	
SEM	Scanning electron microscopy	
SHP	Steric hindered pore model	
TDS	Total dissolved solid	(mg/l)
TMP	Transmembrane pressure	(bar)
TMS	Theorell, Meyer, and Sievers model	
TOC	Total organic carbon	(mg/l)
UF	Ultrafiltration	

Contents

List of Tables

List of Figure

Chapter one
Introduction

1.1 Introduction

The high performance development and innovative process are important for a sustainable growth of industry. Technology and membrane science is expected to play an increasingly important role in the future for many sectors of industry due to its numerous advantages compared to conventional treatment technology; especially, separation with membranes which have increasingly significant **(Boussu, 2007; Chandan and Sujoy, 2017)**.

Advances in membrane separation technologies have been largely driven by the increasing environmental regulations legislated and the increasing demand of desalinated water**.** The ion exchange resins, membrane separation systems and conventional filters, distillation systems supply high quality products with adequate energy consumption. An additional factor is the economic advantage of using membranes, as they decrease waste disposal expenditure and allow for increasing opportunities for recycling and material recovery. Because these reasons, using membrane in difference market places, such as water and wastewater treatment, as well as beverage and food processing is expanding significantly **(Andrea and Tony, 2018; Vitaly and Gadi, 2016)**. The nature of each membrane process is formed by the membrane itself, that can be considered as a thin film interposed between two fluid phases, the selective permeation across that is governed by molecular size or particle, the mobility of the permeating species within the membrane and chemical affinity to the membrane material **(Stefan, 2014)**. According to the separation processes of membrane; the membrane can be divided into four basic types of membrane system generally used in the industry **(Andrea and Tony, 2018)**:

● Microfiltration (MF) is widely applied in particulate removal process and maintains degreasing.

● Ultrafiltration (UF) is commonly used for water, oil and emulsion separations; the separation of oils, fats or greases in the food industry and paint recovery.

● Nanofiltration (NF) and reverse osmosis (RO) are used widely for water purification, desalination and disinfection.

The NF–RO process makes it possible to bring into being high purity permeate from a single-step RO process without the need for a second desalination step. This process significantly enhances the value of permeate without needing for a second stage with brackish water using RO membranes **(Hassan, 2012; Kurth, et al., 2011)**.

Ceramic membranes have been comprehensively applied in fields such as pharmaceutical and biotechnology, beverage and food industry, industrial and chemical applications, recycling and recovery. The capability of ceramic membranes exclusively heading the distinct requirements of frequent cleaning, high resistance to hard operating conditions and continuous flow in these fields are the major reasons why ceramic membranes favored choice over other kinds of membranes **(Chandan and Sujoy, 2017; Stefan, 2014)**.

In addition the ceramic membranes application has also been expanded to non-aqueous solution separation mostly in petrochemical processing where organic membranes cannot be utilized, titania, alumina, zirconia and silica ultrafiltration, ceramic membranes have been applied to the asphaltene separation from crude oil. Using ceramic membranes for separation and concentration of organic solvent such as hexane and ethanol is considered another interesting applications. Titania, zirconia

and silica membranes, produced by process of a sol-gel, have been succeed effectively employed in separating mixtures of non- aqueous solvent. additionally, ceramic membranes can be applied in separation of super critical fluids particularly, super critical alcohol and super critical CO_2 (**Andrea and Tony, 2018**; **LEO, 2008; Stefan, 2014).**

In NF membrane the basis of all models of the double layer is the theory of the shear (slipping) plane surface. This plane surface detaches the moving part of the electrical double layer from the fixed part. The electric potential at the shear plane called the electrokinetic (or zeta) potential. This potential is considerable and significance to surface and colloids science because the surface potential itself cannot be specified experimentally. Determining the zeta potential is very important for membrane fouling research. This property is normally ignored in efforts to get optimal operating conditions for many types of membranes separation processes. Zeta potential can be specified from one of the following electrokinetic measurements. Streaming potential, electrophoresis, electroosmosis and sedimentation potential. The main parameters that affect the scaling and rejection of NF membrane is charge of membrane surface which were measured by using microelectrophoresis potential and streaming potential methods to determine the isoelectric point (IEP) of the membrane **(Elimelech, et al., 1995)**. The streaming potential and electrophoresis are the base for the most common methods and the other methods may seldom be used **(Herbig, et al., 2003)**.

The streaming potential is the best experimental techniques for electrokinetic characterization of flat and tubular membrane surfaces **(Elimelech, et al., 1995)**. These experimental techniques include measurement of electrical potential through the NF membrane beneath

flow conditions. If the solution of electrolyte is forced across the pores by the pressure gradient, the charges in the moving portion of the double electrical layer are moved towards the ends of pores, producing in accumulation, it makes an electric field and a potential variance per gradient of pressure that is usually called streaming potential **(Szymczyk, et al., 1999)**.

The more widespread components of scale in applications of membrane are calcium carbonate ($CaCO_3$), calcium sulphate ($CaSO_4.2H_2O$), and silica, **(Faller, 1999; Hassan, et al., 2007)**. Together the nucleation and the development of crystal steps of the fouling or operation of scale formation based mostly on the ratio of supersaturation in the concentrate (saline solution feed) of a mineral salt. In operation, providers of membrane counseled not to exceed the product of solubility of each probable combination of scale formation compounds or to put some type of water pretreatment.

(Field, et al., 1995), defined the CF for microfiltration membranes in the form of a theory: "The critical flux hypothesis for membrane is that on start-up there exists a flux below which a decline of flux with time does not occur; above it fouling is observed". The CF can be notable in two forms (strong & weak). The strong form of permeate CF when the flux able to a point is equal to the related flux of pure water at the identical transmembrane pressure (TMP), when the flux diverges from the flux of pure water, but increases linearly with pressure, is aberration point from linearity is known as the weak form of the CF **(Mänttäri and Nyström, 2000)**.

Determine of the critical flux considered a basis parameter for estimating fouling. The concept of critical flux was inserted in this study based on cross flow filtration tests in order to characterize the fouling

(scaling) behavior of hardness alts (magnesium sulphate $MgSO_4$, calcium chloride $CaCl_2$) main scale forming substances and anther salts in tubular ceramic nanofilteration titanium dioxide. The Prediction of critical flux theoretically according to its physio-chemical only is yet hopeless. Based on this, the estimate of critical flux seems to be major since this factor can lead to select the fixed operation conditions that attains a best control of fouling.

Reduction of flux less that of the corresponding flux of pure water (or more commonly flux of pure solvent) can be classified into two separate parts. The first one concentration polarization (CP) is a natural consequence of the selectivity of a membrane. This leads to a solutes or particles accumulation or solutes in a mass transfer boundary layer near to the surface of membrane that influences the flux by minimizing in effective transmembrane pressure driving force (TMP) owing to the osmotic pressure variance between feed solution and filtrate next to the surface of membrane. This phenomenon is inescapable, but is reversible with a minimization in TMP and hence fluxes. Secondly there is fouling which leads to significant further resistance of hydraulic. This is sometimes denoted to as resistance of a cake. Estimate the development of subcritical membrane process has led to decreasing in consumption of energy. So reducing of running costs is partially off-set increased cost of investment **(LEO, 2008; Mänttäri and Nyström, 2000; Patrice, et al., 2006)**.

The concentration of polarization at the membrane surface cannot be avoided but a right excellent in operating circumstances permits one to select those settings where the accumulation of mass merely has a slight influence on the effectiveness of process. Working lower CF can license process over long times without occurring of any important precipitation.

Fouling can also change membrane selectivity. Therefore, understanding the sustainable positions and critical flux will effect process optimization according to both selectivity and productivity **(Chiu and James, 2005; Patrice, et al., 2006)**.

1.2 Objectives and Scope of the Study:

The major objectives of the present study are summarized as the following.

● Two electrodes were manufactured of composite silver and (4% gold) and used to measure the zeta potential of the TiO_2 NF membrane.

● Inspect the charge of TiO_2 NF membrane by measuring the zeta potential at sodium chloride as reference solution.

● Inspection of the rejection behaviour and relationship between zeta potential and the rejection for salts ($CaCO_3$, NaCl, Na_2SO_4, $MgSO_4$, $MgCl_2$, $CaCl_2$, and $NaHCO_3$) for TiO_2 NF membrane at different concentration, pH, transmembrane pressure (TMP) and across flow velocity.

● One of the most important objectives of this work is studying for the first time the rejection behaviour of calcium carbonate salt ($CaCO_3$) for TiO_2 NF ceramic membrane in relation to its zeta potential at different electrolyte concentration (below saturation, saturation and above saturation), transmembrane pressure (TMP) (1-15 bar) and two different across flow velocity.

● Determine the critical flux values of salts ($MgSO_4$, $MgCl_2$, $NaHCO_3$, Na_2SO_4, NaCl) and oilfield produced water by using step by step method at fifteen stepped heights overcoming an applied transmembrane pressure (TMP) range from (1 to 15 bar) in order to describe the forms of critical flux CF and fouling behaviour for all used salts.

● Estimate the development of subcritical membrane process has led to decreasing in consumption of energy. So reducing of running costs is partially off-set increased cost of investment.

● Estimate the effective pore radius of the membrane by using Donnan Steric pore model (DSPM) to determine the rejection of sodium chloride (NaCl) theoretically in order to compare the theoretical results with the experimental rejection (R%).

Chapter Two
Literature Survey

2.1 Introduction

The utilization of membrane in the separation technologies can be dated back to the late (1960 s) when they were gradually being considered as replacements of more classical process like evaporation, distillation and extraction in industrial settings **(Timmer, 2001)**. It is not surprising that the coming of membrane-based filtration processes agreement with the significant developments synthetic in the field of polymer or ceramic chemistry. Processes of membrane are categorized and classified based on the required mechanisms of the driving force and separation. Driving force application such as TMP pressure, temperature, electrical potential, or chemical is the most pivotal step to obtaining separation.

Membrane of pressure driven involve MF, UF, NF and RO. The nanofiltration history, or (loose RO) membranes as they are so frequently termed for offering properties between RO and UF membranes, dates back to the late (1970 s) when the need for a less cost and less energy consumption (compared to reverse osmosis RO process) was evident in the industry. High flux, low operation pressure and selective rejection of multivalent ions are some of several advantages displayed by nanofiltrations. The first industrial application of nanofilreation membranes was in 1978, for the desalination of brighteners and dyes **(Yacubowicz and Yacubowicz, 2005)**. Nanofiltration is now familiar in wastewater, seawater, dry production, dairy, textile, pulp and paper and pharmaceutical industries **(Chandan and Sujoy, 2017)**.

The arrangement of the membranes for MF, UF, NF and RO is demonstrated in **Fig. 2.1**. The figure usually demonstrations the relative size of common retained materials, the pore size of membrane and the

approximated the membranes molecular weight cut-off (MWCO) of the membranes **(Leo, 2008)**.

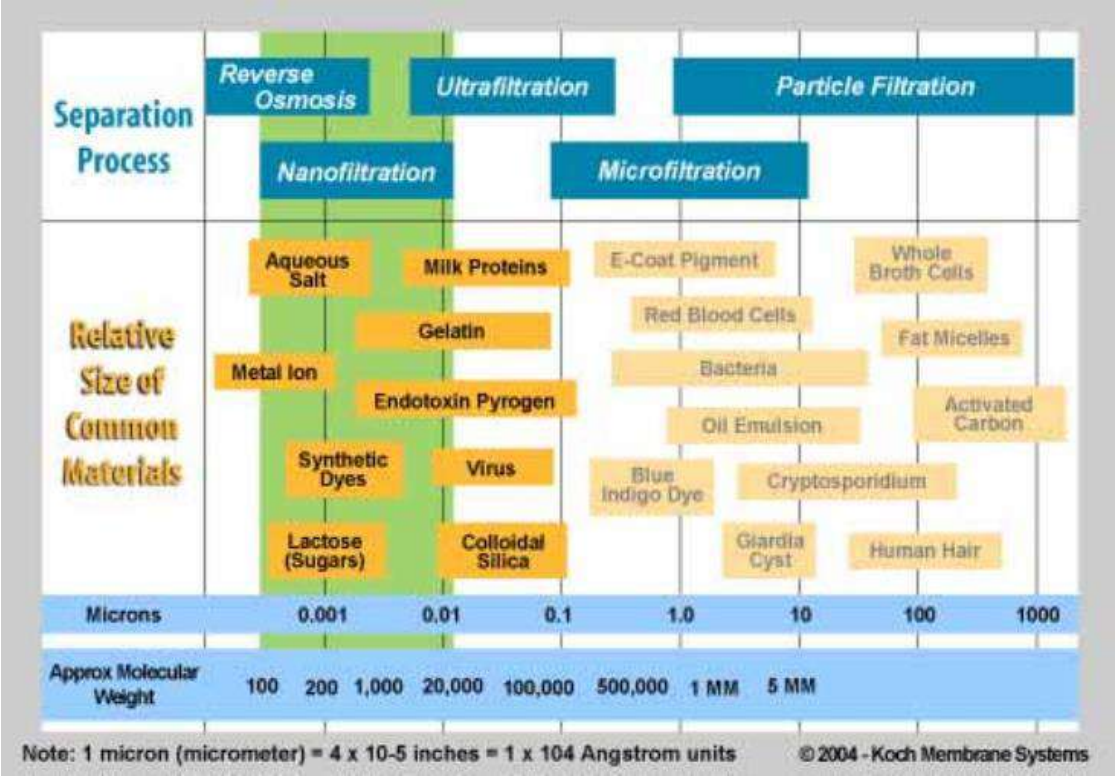

Figure 2.1 The Filtration Spectrum (Leo, 2008).

Using membrane separation correctly can provide financial savings and conserve resources. Maximum benefits are obtained when the output streams from the membrane system are recycled or re-used, thereby reducing process materials requirement and minimizing waste disposal costs.

Membranes of nanofiltration can attain classically a rejection of divalent ions (e.g. SO_4^{-2}) in a extent of (75 – 99%) and for monovalent ions (e.g. Na^+, Cl^-) up to (30 – 50 %), depending on conditions of operational and chemistry of inlet feed water **(AWWA, 1999; Eriksson, et al., 2010)**.

The basic advantages for desalinating seawater plants by utilizing NF as a pretreatment these combinations gives the following:

1. Minimizing of the TDS of inlet sea water by up to 40 %.

2. Minimizing of (SO_4^{-2}, Mg^{+2}, Ca^{+2}) major scale forming substances – by approximately (70 – 98%) depending on the kind of NF membrane and the conditions of operating.

3. Minimizing of turbidity and microorganisms nearly up to (95%)

Nanofiltration is used when liquid-phase separations of low molecular weight organic solutes such as glucose and sucrose or monovalent ions from multivalent salts are desired. Nanofiltration is practically always operated in the cross flow or tangential mode is opposed to the dead-end mode, to minimize the solid filter cake on membrane surface. Nanofiltration membranes are described by (0.5 - 3 nm) pore sizes coinciding to a nominal MWCO of about (200 - 1000 Dalton) **(Hubbard, 2002 ; Yacubowicz and Yacubowicz, 2005)**.

If all water of earth – containing its rivers, lakes, groundwater, seawater and glacial icecaps – were included in a bubble, that bubble diameter would measure (1,385 km). All volume of the water is equal to $(\frac{4}{3}\pi\ (\frac{1385}{2})^3$ = 1,391 million km^3). **Fig. 2.2(a)**, explains the compared of relative size of that water-filled sphere to the earth size. Around (97%) of the existing water is signified by salty water frequently with level of a salinity larger than (35,000) ppm (3.5 wt. %) as presented in **Fig. 2.2(b)**. Consequently, the biggest potential source of alternative water supply needs and will continue to need desalination of saline water **(Nada, 2014)**. maximizing population and rise in their standards of living and requirements, together with the growth activities of agricultural and industrial, there is at all times an increase in request for upright quality water in the world.

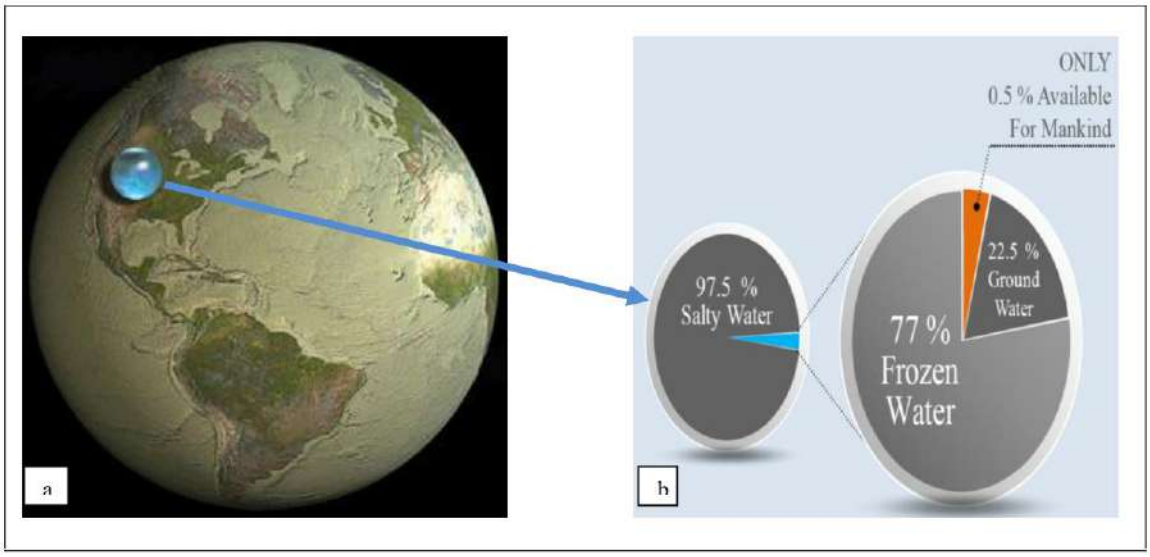

Figure 2.2 (a) Shows all Earth Water Available to the Comparison to Size of the Planet, (b) Abundance of Water on Earth (Nada, 2014).

Additionally, across the world, scarcity of water is being known as impendence to human activity at a present and future. To happen this increase in request, treatment of water, in all its forms, is furthermore on the increase. **(IDA, 2014)**.

2.2 Nanofiltration Principal

Acceptable understand the behavior of nanofiltration (NF) membranes, it is suitable to denote to the concept of RO that is classically appropriate to nanofiltration with the only variance on the magnitude of the TMP needed to drive the water as a result of the pore size. The phenomena of usual osmotic happens across membrane of a semi permeable as the fewer concentrated water will flow to the extra concentrated till accomplishment an equal state between together solutions. The force of driving for the water flow is the variance in chemical potential between the two solutions. The water flow through the membrane efforts a TMP called the pressure of osmotic. Backing the normal path by effecting an exterior TMP on the solution of salty which is divided from the fresh aqueous solution by membrane of a semi permeable allows the flow to go forward the fresh side **Fig. 2.3**. The TMP

to be applied must be more than the solution (equilibrium) osmotic pressure to achieve a reverse flow **(AWWA, 1999; Farah, 2013)**.

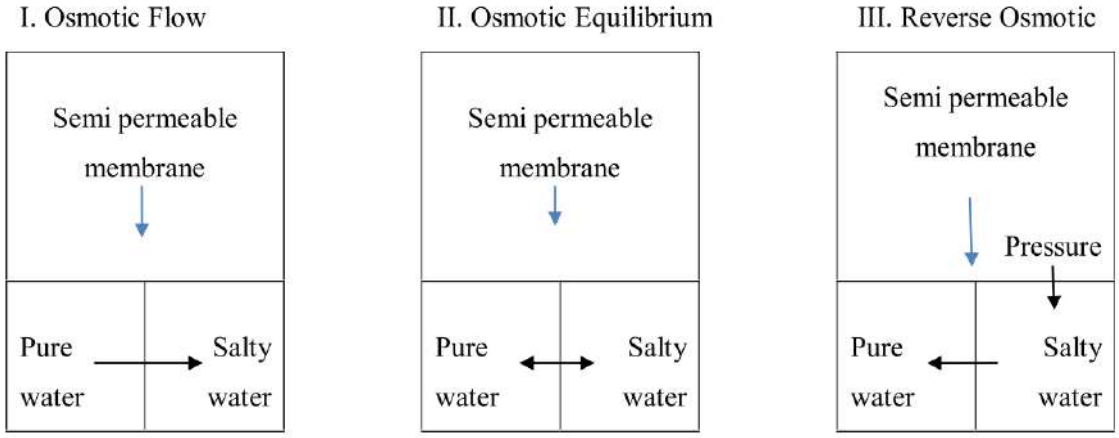

Figure 2.3 Explanation Schematic of Osmotic Phenomena (AWWA, 1999)

The membrane term of semi-permeable denotes to a membrane which selectively allows fixed species to pass across it while retaining others. Actuality, several species will pass across the membrane, however at significantly changed rates. In nanofiltration, the water (solvent) permits across the membrane at a greatly quicker rate than the dissolved solids (salts). The net result is that separation of a solute-solvent happens, with water being the product and with a tough total rejection for salts with weaker rejection of the monovalent ions than the bivalent ions. The connections between salts, water, and the membrane are the greatest significant factors in the mechanism of separation **(ASTM, 2008; Deon, et al., 2011; Meer, et al., 1995; Schaep, et al., 1998)**.

The following schematic diagram **Fig. 2.4** and equations are the greatest generally used for process of nanofiltration membrane to estimate the characteristics of system.

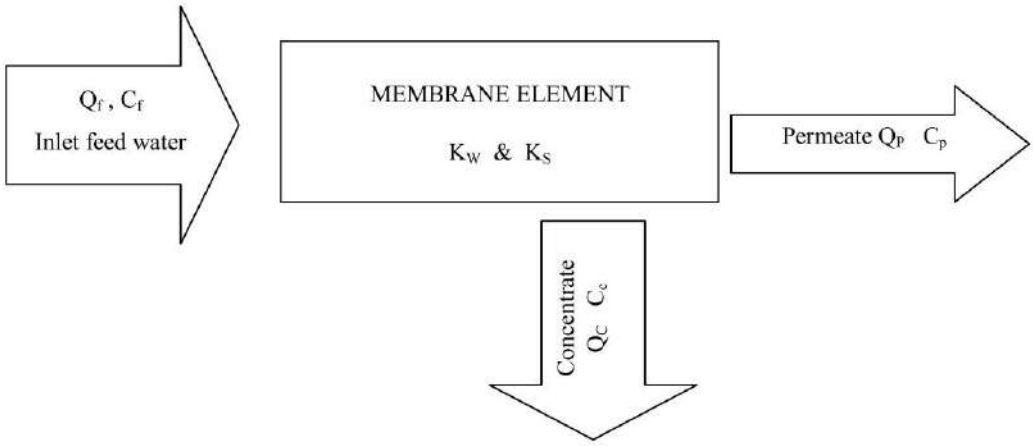

Figure 2.4 Nanofiltration Membrane Flow Streams (ASTM, 2008)

Water flux equation of NF and RO membrane:

$$F_w = K_w (\Delta P - \Delta\pi) = Q_p / A \quad \textbf{(2.1)}$$

Where:

F_w is flux of water across membrane, ($l/m^2.h$).

Q_p is permeate flow (l/h).

K_w is mass transfer coefficient of water, ($l/m^2.h.bar$).

ΔP is difference of applied (TMP), (bar).

$\Delta\pi$ is difference of salt osmotic pressure (bar).

A is effective area of membrane (m^2).

($\Delta P - \Delta\pi$) is net applied TMP, (NAP), (bar).

The pressure of osmotic for a given solution that can be determined from van't Hoff equation is directly linked to the dissolved solute concentration **(Howard, 2003; Khudair, 2011**):

$$\pi = \mathrm{i}\,\Phi R_g T\, C \quad \textbf{(2.2)}$$

Where:

π is the pressure of osmotic (bar).

i is the dissociation factor (Van't Hoff factor).

Φ is the osmotic coefficient.

R_g is the constant of ideal gas (J/mol K).

T is the absolute temperature (K).

C is the concentration (molarity).

In common, Φ depends on the solute concentration and type. When the concentration of the solute goes to zero (dilute) its value of Φ goes to 1 in ideal solution **(Balabel and Kotbb, 2013; Cheremisinoff, 2002)**.

Nanofiltration membranes are suitable for removal of dyes and colouring agents in wastewater treatment of the textile has been studied by many workers. **(Benfer, et al., 2001)** and **(Weber, et al., 2003)** found that the dyes rejection (such as SAC 620, SAC 525, SAC 436 and Direct Red) was as large as (99%). Practically all ceramic membranes are multilayered, forming of a toplayer, interlayer (s) and a membrane support by the sol. gel method **(Van, et al., 2002; Benfer, et al., 2004; Van, et al., 2002)**. Commonly the interlayers are mesoporous (diameter of pore > 2 nm) and made by colloidal sol. gel procedure, that is deposited on support of a macroporous membrane. The latter stage includes the synthesis and deposition of a thin, generally microporous (diameter of pore 2 nm) top layer. This is usually done by using the polymeric sol gel method.

one of separation process is a filtration of membrane which includes o fluid mixture containing two or more species and a membrane. The mixture might contain particles (solids) or dissolved substances like ions. A membrane may be considered as electric barrier between two phases that permits some substances in the fluid to surpass the barrier put

hinders others. Process of the filtration is either in dead- end geometry or tangential flow (also as cross flow filtration).

A schematic illustration of cross flow filtration shown in **Fig. 2.5**. The feed is referred as the flow into the membrane and the major part of the feed pass through tangentially with nanofiltration membrane. The feed cross the membrane and this stream is called the permeate. In addition; another part of the feed that do not cross the membrane is called the retenate. Thus, the required product can be either the retenate or permeate. Either the permeate and retenate are called concentrate in applications whereas some species is concentrated in the retenate or permeate **(Judd and Jefferson, 2003).**

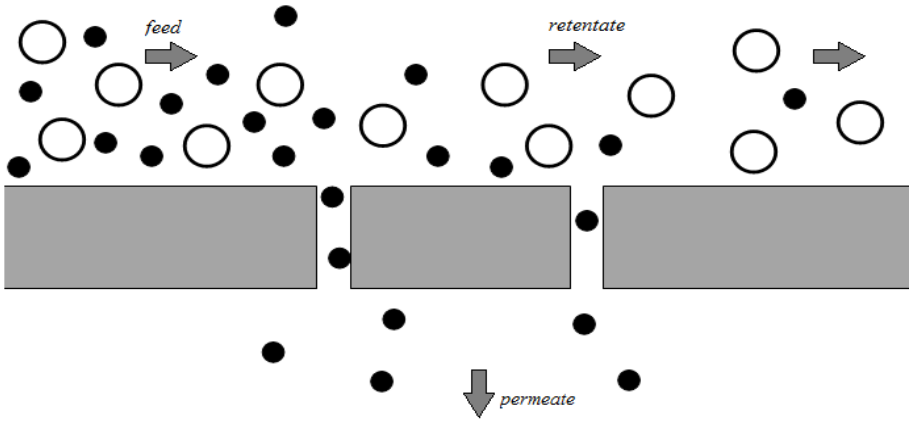

Figure 2.5 Cross Flow Filtration. Here, The Flow of Feed Enters from Left and is Splitted into Retenate and Permeate (Anna, 2015)

In normal once through filtration (also identified as dead – end filtration) the whole feed is pushed across the membrane in normal direction, as shown in **Fig. 2.6**. The species that are discarded by membrane will put down on the surface of membrane and a filter cake is generated. In cross flow filtration no filter cake is generated because the substances that cannot penetrate the membrane is transferred away by the flow of retentate. The filter cake will reduce the ability of penetration for the substances in the mixture **(Judd and Jefferson, 2003).**

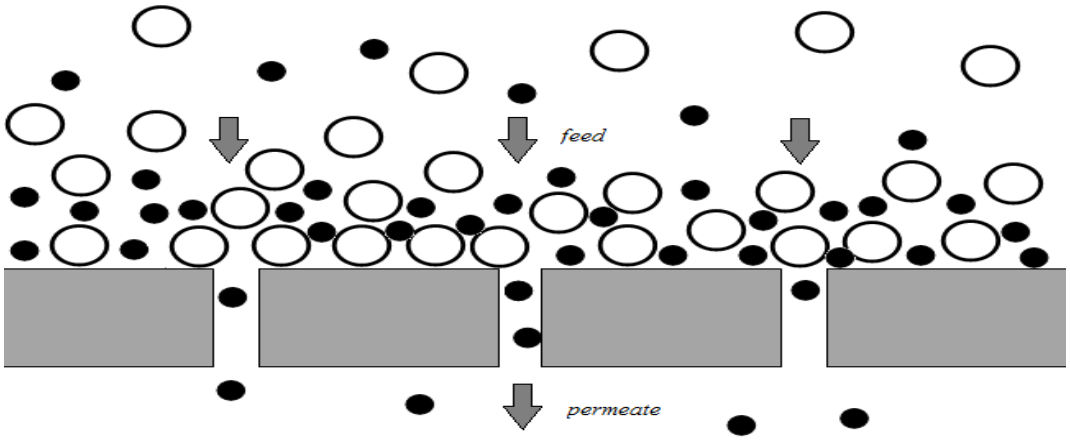

Figure 2.6 Dead End Filtration (Anna, 2015)

There are no similarities among the processes of membrane filtration application. This makes the process hard to alters of fluid properties and each membrane separation device must be accustomed to the fixed application. In comparison with another processes of separations, distillation, evaporation, ion exchangers… etc., membrane filtration usually has the following :

- Chemical additives like flocculants and coagulants are seldom needed.
- Membrane filtration process can be conducted continuously under steady state condition.
- Less energy consumption since the separation does not require any change of phase.

Table 2.1 shows some examples of membrane filter types and under which driving force they are operated by. Driving force, Structure and separation mechanism are explained in the following sub-sections (see Table 2.1).

Table 2.1 Examples of Various Membrane Types (IAEA, 2004)

Membrane type	Driving force	Separation mechanism	Structure
Reversed osmosis	Pressure	Variance in rate of diffusion between solutes and solvent.	Dense
Nanofiltration		Arrangement of variance in rate of diffusion and sieving over micropores (<2nm)	Dense
Ultrafiltration		Sieving over mesopores (2-50 nm)	Porous
Microfiltration		Sieving trough macropores (>50 nm)	Porous
Dialysis	Concentration	Diffusion	Porous
Electrodialysis	Electrical potential	Variance in strength and ionic size	Charged, Porous
Membrane distillation	Temperature	Variance in partial pressure of vapour	Porous

2.3 Ceramic Membranes

Membranes of ceramic are prepared of inorganic materials such as oxides (titania, alumina, zirconia) or some materials of glassy. Though membranes of ceramic are considered to be expensive because the complex fabrication process, the expensive starting materials and less surface of membrane area per volume of a module of membrane; membranes of ceramic stay have a many another advantages on membranes polymeric. Compare to membranes of polymeric, membranes of ceramic have benefits of resistance to solvent, resistance to chemical and thermal stability, as recorded in Table 2.2 Another ceramic membranes advantages are long term durability and high mechanical strength **(Chandan and Sujoy, 2017)**.

Table 2.2 Advantages of Ceramic Membranes (LEO, 2008; Stefan, 2014).

Advantages	Applications and comments
Organic solvents resistance	Non-aqueous separation of systems, oil separation.
Thermal stability	Steam sterilization, separation at high temperature.
Peroxide resistance to	Chemical cleaning, application of textile processing
Chemicals acidic resistance and basic pH	Recovery of acid/base ,chemical cleaning.
Uniform pore size	Dependent upon preparation methods
Mechanical strength Long life-span	Backwashing

In common, membranes ceramic contain thin layers of ceramic supported on porous ceramic as presented in **Fig. 2.7**. Membrane of macroporous supports that afford the major mechanical strength for pressure driven separation processes, are generally synthetic using oxide powders by extrusion or tape casting. The size of pore for supports is commonly higher than a micrometer and the support thickness is generally in order of few millimeters. A middle layer is covered on the support layer in order to reduce the pore size of coating surface for further coating of top layer. Meanwhile, the top layer that has the ability of separation needs to have controlled size of pore that is appropriate for the specific separation **(Chandan and Sujoy, 2017; Stefan, 2014)**.

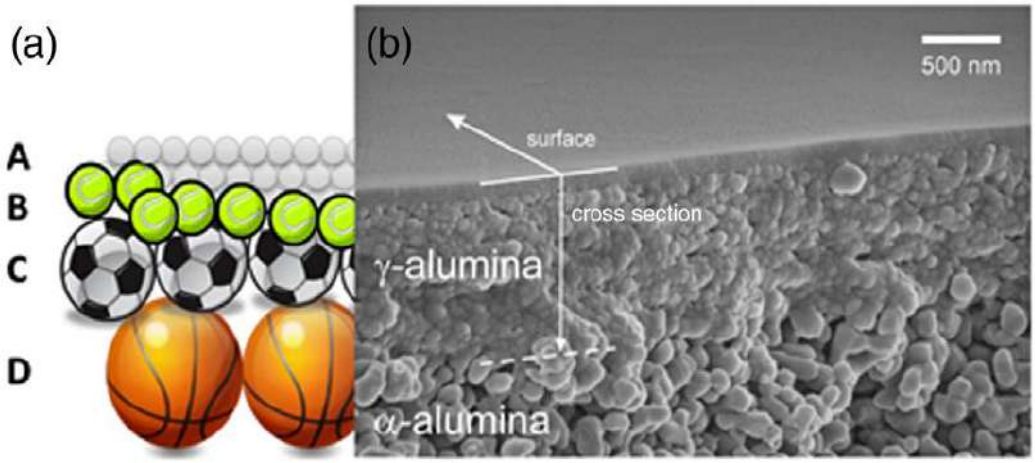

Figure 2.7 (a) Pictorial Representation of Anasymmetric Composite Ceramic Membrane that Consists of a Nanofiltration Modified Separation Layer of 50 nm Depth with Pores Less than 2 nm Wide (A), an Ultrafiltration Layer of 100–500 nm Depth with 10 nm Pores (B), a 1–10 μm Microfiltration Intermediate Layer with Pores 100–200 nm Wide (C) and a Porous Support of 1–1.5 mm Width (D). (b) Scanning Electron Micrograph of a Cross Section of a Ceramic Composite Membrane : γ-Alumina on top of an *α*-Alumina Support (Vitaly and Gadi, 2016).

Structures of membrane are divided depend on the type of their pores. Membranes with sponge-like pores are called *anisotropic* (having asymmetrical pores). Membranes with finger-like pores are called *isotropic* (having symmetrical pores going from one to another membrane side with the same width)., see **Fig. 2.8**. **(Chandan and Sujoy, 2017; LEO, 2008; Vitaly and Gadi, 2016)**.

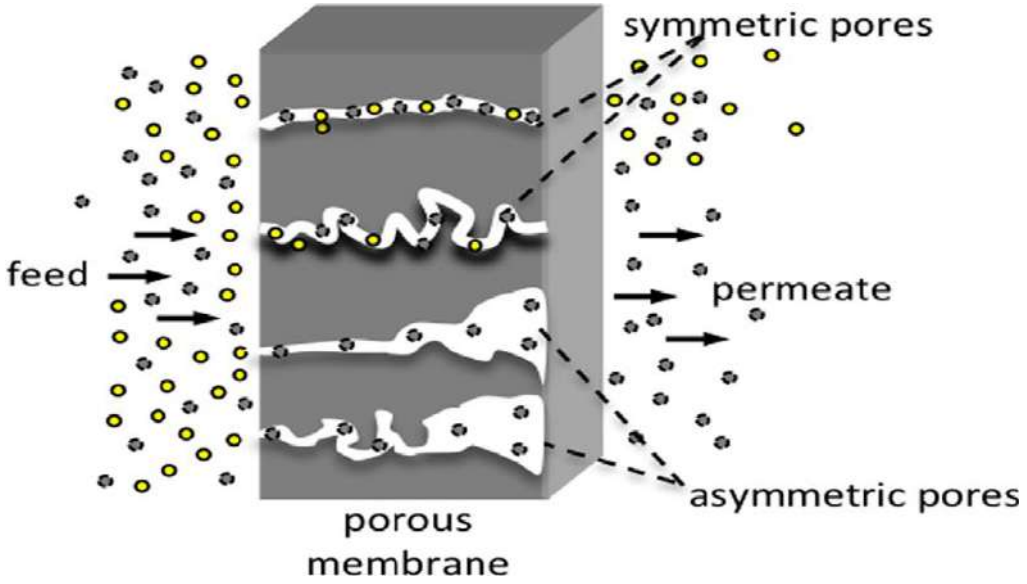

Figure 2.8 Symmetric and asymmetric membrane pores (LEO, 2008).

In structural design, the pore size of an asymmetric ceramic membrane displays a gradient structure from the separation layer to the porous supports, in order to minimize the resistance to permeation through the membrane. There are few methods to produce intermediate layers and separating layers as shown in Table (2.3). The selection separating layer (Silica) Intermediate layer (γ -Alumina) Support (α -Alumina) of a preparation method based on the desired membrane structure and the application of the membrane. Like, sol-gel route is prominent in preparing nanoporous ceramic membranes whilst chemical-vapor deposition is distinguished in producing dense ceramic membranes **(Agoudjil, et al., 2005; LEO, 2008; Vitaly and Gadi, 2016)**.

Table 2.3 Preparation Methods of Ceramic Membranes (LEO, 2008; Van Gestal, et al., 2006).

Process	Materials
Sol-gel	TiO_2, γ-Al_2O_3 , ZrO_2 , SiO_2
Phase separation/ leaching	SiO_2
Chemical vapor deposition	SiO_2
Dynamic membranes	ZrO_2 (Amorphous)
Anodic oxidation	Al_2O_3 (Amorphous)
Hydrothermal treatment	Silicalite
Pyrolysis	SiC, Si_3N_4

2.4 Application of Ceramic Membrane

Widely Ceramic membranes of microfiltration (MF) and ultrafiltration (UF) have been used as a set of filtration process like separation of proteins, microorganism and colloidal solutes. On the other hand, nanofiltration (NF) has largest applications in water treatment, involving waste water counting synthetic dyes and heavy metals. Separation of ion is mainly due to the interaction of electrostatic between

surface charge and ions. The ions with the same charge as the membrane surface (co-ions) , generate repulsion force from the surface charge of membrane that is named as Donnan exclusion. Thus, separation of ion can be successfully conducted using membranes of nanofiltration even though the ions are considerably smaller than pores of membrane **(Andrea and Tony, 2018; Chandan and Sujoy, 2017).**

The main application of ceramic membranes are summarized in Table 2.4.

Table 2.4 Ceramic Membranes Applications in Liquid Phase Separations.

Process	Area	Application examples
NF and UF	Recovery and recycling	Drinking water and wastewater treatment. **(Rautenbach and Linn, 1996; Rautenbach, et al., 2000; Geraldes and de Pinho, 1995)**
NF, MF and UF	Chemical and industrial applications	Separation of oil-water, purification of used oil, removal of precipitated heavy metals and solids. **(Tellez, et al., 1995; Qdaisa and Moussa, 2004)**
NF, MF and UF	Pharmaceutical and Biotechnology industry	Microorganism separation and plasma separation, cell debris filtration. **(Kimura, et al., 2003; Košutić, et al., 2007)**
NF, MF and UF	Food and beverage industry	Milk and protein concentrations, clarification of fruit juice, clearing up of wine, bacteria elimination, microorganism separation from fermented. **(Kim, et al., 2007)**

2.4.1 Treatment of Sea Water

The nanofilteration membrane utilizing as pretreatment for seawater reverse osmosis and multistage flash desalination process. The nanofiltration membrane unit removed residual bacteria, very fine turbidity, reduced total dissolved solid TDS by about (58%) and decreased total hardness by (93%). The completely integrated nanofilteration seawater reverse osmosis and nanofilteration- multistage

flash desalination systems decreased consumption of energy by 25-30% **(Hassan, et al., 1998; Hassan, et al., 2000; A1-Amoudi and Farooque, 2005)**.

2.4.2 Treatment of Oilfield Produced Water

The offshore and onshore transport of natural gas and crude oil is accompanying with the coproduction of important amounts of wastewater, referred to as (produced water). Oilfield produced water is considered the biggest volume waste stream in the investigation and production procedure of gas and oil **(Gilbert, et al., 1995)**. Oilfield produced water has typical characteristics because inorganic and organic matter. Basically, it contains oil hydrocarbons and salts, that may be toxic to the environment. But, its volume and characteristics differ significantly from well to well and depend on the reservoir lifetime **(Nicolaisen, 2002)**. Over time, the percentage of product decline and the percentage of water increases. Therefore, oilfield produced water is problematic to treat. Reuse, reinjection and disposal are the available handling options of produced water **(Evans and Robinson, 1999; Gulde, 2003)**. Produced water reinjection (PWRI) needs skillful arrangement and treatment to meet the quality wanted for reinjection water to avoid formation damage and disposal of produced water needs imperious environmental regulations. In common treatment of produced water is advanced through de-mineralizing and de-oiling before its utilization or disposal. Many methods and technologies exist for produced water treatment. Effective treatment commonly needs a sequence of pretreatment and posttreatment processes to eliminate different contaminants. Old technologies such as clarifiers, dissolved air flotation, hydrocyclones and disposable filters and absorbers respectively **(Shams, et al., 2007)** do not reach the separation efficiency needed **(Kharaka, et**

al., 1998). Membrane technology is used in industrial wastewater treatment, industrial processes, and is utilized currently for treatment of produced water **(Nicolaisen, 2002; Hua FL, et al., 2007; Ebrahimi, et al., 2008)**. Inorganic (or ceramic) membranes have attracted interest because their superior thermal, chemical and mechanical stability.

2.5 Tubular Membrane Model

The membrane configuration includes how the area of the membrane is oriented relative to the flow i.e. the membrane surface geometry. To support and stabilize the membrane, the membrane is placed inside a house, i.e. a module **(Judd and Jefferson, 2003)**.

Configurations of membrane are either based on a cylindrical or planner shape. Choosing the more optimum configuration includes the following considerations:

- Surface area of membrane in relation to the total module volume.
- Production cost.
- Design that allows cleaning.
- Turbulent flow so as to great as possible the mass transport.

A schematic image of cylindrical configuration membrane is shown in **Fig. 2.9**. Tubular modules have alike aspect as shell and tube heat exchangers. The membrane jackets the contained by of one or several tubes. Tubular configuration membranes have advantage of large turbulence step. On drawback is the surface area in relation to volume of module **(Seader, and Henley, 2006; Kullab, 2011)**.

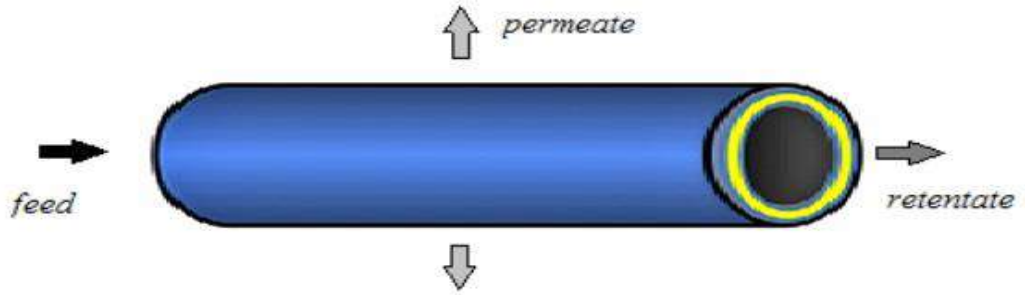

Figure 2.9 The Principle of Tubular Membranes

This kind of configuration has elevated resistance to fouling and simple to clean but it has low packing density and wants high flow rate to operate. Therefore, this model is used for high fouling feed **(Li et al., 2006).**

Ceramic membranes of tubular type are made of an extruded carrier (so-called Support) which has one or more channels on that the layers of membrane are fixed on the surface of cannel by some intermediate layers. Usually, the support is also made of a ceramic material, but there are also some technical alternatives accessible. **Fig. 2.10** shows some typical single- and multi-channel geometries of ceramic membranes. Today a huge number of material and membrane combinations are offered on the market, like for example TiO_2, ZrO_2, Al_2O_3 and SiC **(Chandan and Sujoy, 2017; Stefan, 2014; Van, et al., 2006)**.

Fig. 2.11 shows the design of a typical multi-channel membrane, including the front-side sealing. During operation, the membrane is installed in a housing and the feed flow / raw medium flows through the channels of the ceramic carrier. The surface of the channels are coated with a ceramic membrane layer. The filtration process is done by leading liquid through the membrane layer and separating the components out of the feed medium which are not able to pass the membrane layer. Liquids

and components which can pass through the membrane layer are called "permeate", while the remaining particles, which cannot pass through the membrane layer, are called "concentrate". For a maximum efficiency, it has to be avoided, that feed liquid gets on the permeate side without passing through the membrane layer; otherwise, this would mean a contamination of the permeate flow **(Stefan, 2014; Agoudjil, et al., 2005)**.

Figure 2.10 Shows Some Typical Single and Multi-Channel Membrane (Stefan, 2014)

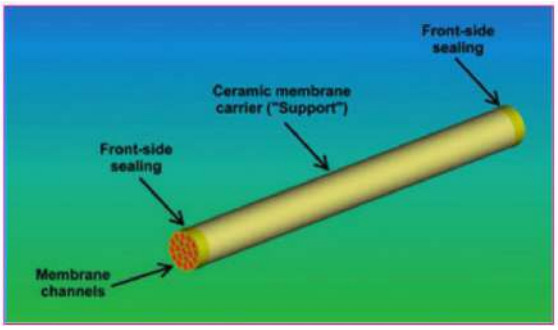

Figure 2.11 Shows Multi-Channel Membrane Including the Front-Side Sealing (Stefan, 2014)

2.6 Fouling and Concentration Polarization

In technology of membrane, fouling is seen as process consequential in reduced performance of membrane because of undesired deposits onto external surface of membrane, within the pore or in the pore openings. The deposit can be hang solids, particles or dissolved substances. Membrane fouling leads to decline of flow through the membrane that in turn will result in a higher energy command to save the performance of the membrane high. Therefore, the total cost for separation will rise and the life-time of membrane will reduce. Techniques of decrease the problem of fouling are depend on cleaning and pretreatment of the membrane. Design of a module that enables cleaning must also be prefer for applications where the feed supposed to include fouling components (i.e. foulants) **(Kullab, 2011)**.

Feed pretreatment can include both chemical modification and prefiltration. Membrane cleaning techniques are based on physically or chemically cracking the bonds forces between the membrane and foulants. The chemical reactions involve solubilization, chelation and hydrolysis. Sometimes membranes are cleaned when the normal flux is decreased by (10-15%) **(IAEA, 2004; Kullab, 2011).**

Commonly, two process control the particle deposition in the filtrations of cross flow. The first is the fouling process that is caused by particles deposition on the surface of membrane. The second is the returning back of the particles from the surface to the bulk stream **(Kim et al., 2008)**. These processes reach an equilibrium in particle transport, at steady state **(Haghighi, 2011)**. These mechanisms might take place instantaneously through filtration process, the degree of fouling based on three basic factors:

- Feed characteristics.
- Membrane characteristics.
- Operating parameters.

The operating parameters are significant to dominate the fouling of membrane. For instance, the increment in transmembrane pressure will rise the permeate flux but it will boost the generation of (Cake/gel) layer of higher density that might lead to complete blocking of pore **(Kumar and Roy, 2008)**.

There are four various fouling mechanisms as shown in **Fig. 2.12**.

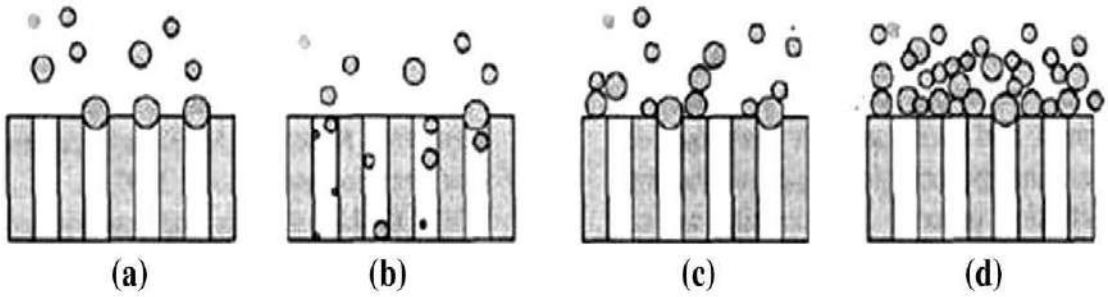

Figure 2.12 Blocking Mechanisms Schematic Representation, a : Complete Pore Blocking, b : Standard Blocking, c : Intermediate Blocking and d : Cake Layer Formation (Salahi, et al., 2010).

Complete blocking mechanism happens if the size of particle/oil is largerer than pores of membrane. As result, these particles will not come in the pores of membrane and do not permeate across the membrane **(Susanto et al., 2009).** Standard blocking mechanism occurs when the particle size is smaller than pores of membrane. The particles will adsorb to pore walls and interior pore blocking happens **(Vela et al., 2008)**. If pore and particle have similar size intermediate blocking will occur. Like these cases, the pores of membrane get clogged near the entrances at the feed part **(Kim et al., 1997).** Mechanism of cake formation happens when the volume of particles are much larger than pore volume. Most fouling of membrane associate flux with time in terms of quadratic or exponential relation by supposing mechanism of fouling for specific operational period **(Salahi, et al., 2010)**.

The principle of membrane filtration products to accumulation of retained solute on surface of membrane and results in concentration gradient at the side of feed. This phenomenon is called as concentration polarization and results of rise in osmotic pressure at the wall of membrane that reduces permeate flux and rises the passage of solute due to rise in concentration gradient. While the convection stream of solute to the surface of membrane is much higher than the diffusion of the solute return to the bulk stream, the concentration polarization happens **(Fig.**

2.13) as a consequence concentration will rise on the surface of membrane **(Song and Elimelech, 1995).**

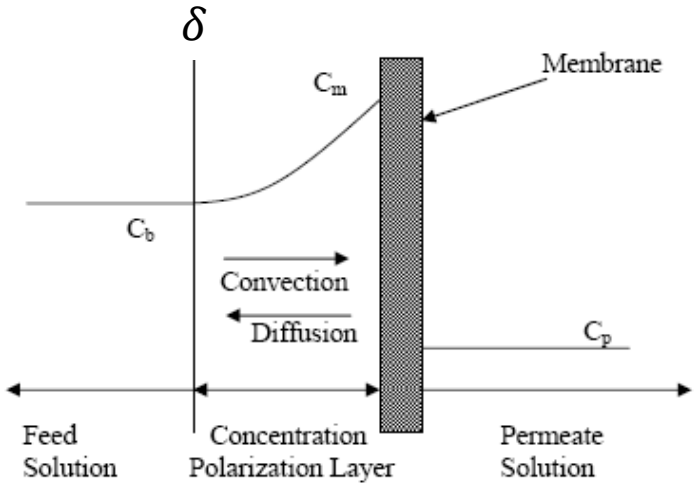

Figure 2.13 Concentration Polarization Concentration Profile (GUPTA, 2003)

Where:

C_b : The solute concentration at external bulk solution (mol/l).

C_m : The solute concentration at the surface of membrane (mol/l).

C_p : The solute concentration at the permeate side (mol/l).

Rising the turbulence close to the surface of membrane increases the transmission rate from the surface to the bulk stream. This is concerning to the design of the membrane element or by redesigning the process of membrane like vibrating or rotating membrane modules **(Jaffrin et al., 2004; Williams and Wakeman, 2000)**.

2.7 Scaling of Calcium Carbonate

The capability to predict scaling is a significant factor in controlling its appearance. The applied technique in membrane plants of water treatment is based on determination of degree of supersaturation that is explained as the activity product of ion of the salt divided by its product of solubility. In specific cases, but, with different moderately

soluble salts ($CaCO_3$, CaF_2, $BaSO_4$) supersaturation with regarding to a mineral salt does not substantially indicate which scaling would take place. In fact, when the ratio of supersaturation, much more than one that lead to formation of scale happens **(Andritsos, et al., 1996; Boerlage, et al., 2000)**.

The growth of a scale is a multistep process, of that adhesion of the scaling or fouling agents to the surface is a main stage. Water quality, flow velocity and temperature are some of factors influencing scaling.

In areas of geographical where ground water and rain water come into touch with bearing rock of carbonate, particularly, chalk and limestone, chemical weathering can happen. Weathering may share up to (50%) of the bicarbonate and carbonate salts existent in natural water. In other areas of non-carbonate rocks the bicarbonate and carbonate originate completely from the soil carbon dioxide and atmosphere carbon dioxide. Concentrations of calcium carbonate in natural waters are normally lower than (15×10^{-5} M), however for waters related with loaded rocks of carbonate, concentrations may attain (30×10^{-5} M to 100×10^{-5} M) **(Chapman, 1992)**.

The possibility for calcium carbonate scaling occurs in most types of feed water, inclusive surface, brackish or well waters. $CaCO_3$ creates a dense, highly adherent precipitation and its deposit in a nanofiltration (NF) or reverse osmoses (RO) factory must be obviated. It is the almost popular kinds of scaling in many systems, containing oil or gas production systems or cooling installation of water. In systems of nanofilration (NF) and reverse osmoses (RO) it shows that the maximum danger of calcium carbonate scaling (as with another salt) occurs in the stream of concentrate at the ends of pores of the of the membrane system.

Fouling is a main problem in processes of nanofiltration (NF) and reverse osmosis (RO), putting critical limitations of performance for membrane`s installation. An investigation of types, mechanisms and major species concerned of scaling in nanofiltration membrane can be sited in Ref. **(Schafer, et al., 2004)**.

Fouling (or scaling of precipitation) products from the raised concentration of fouling species higher than their limits of solubility and leads to deposition on to the membrane. A raised concentration of the fouling creating species in the bulk because withdrawal of permeate, that is further increased in the zone next to the surface of membrane by the influence of the superimpose of concentration polarization, in fact, as water permeates across the NF and RO membranes, the concentration of retained ions in the boundary layer (BL) close to the surface of membrane becomes extremely more than which prevailing in the bulk of electrolyte solution. This impact is higher announced at great fluxes of permeate and less flow velocity. As in other kinds of scaling, fouling tends to decrease flow of permeate and raise pressure drop through the element and affects the efficiency of the performance of the (NF) and (R.O) membranes and reduces rejection. Furthermore, scaling may usually result in physical harm of the membrane because the irreversible pore plugging and to hardness of scale elimination. For that reasons, reduction of fouling or scaling is a significant consideration in the process of generality nanofiltration (NF) and reverse osmoses (RO) operation **(Drak, et al., 2000; Hassan, et al., 1998)**.

2.8 Ceramic Membrane Cleaning

2.8.1 Chemical Cleaning Technique

Membrane cleaning method by chemical cleaning is the most widely, especially in ceramic membranes. In this process of cleaning,

agent of a cleaning (often a mixture of compounds) plays the main role, so the choice of cleaning agent is critical. Commonly, selection of the suitable cleaning agent is done on the basis of type of fouling and membrane material (metal oxides, organic, colloidal, carbonate scales, sulfate scales, silica, etc.). These agents of cleaning dissolve most of the deposited materials on the surface and remove them without damaging the surface of membrane. Generally, acidic cleaning agents, such as nitric, hydrochloric, sulfuric, phosphoric, and citric acids, are used to remove precipitated salts from the membrane surface, while agents of alkaline cleaning are appropriate for the removal of organic foulants. A distinctive cleaning cycle generally entails of the following stages: removal of product, rinsing with water, repetitive cleaning steps and rinsing with water again **(Liikanen, et al., 2002; Chen, et al. 2003)**.

2.8.2 Physical Cleaning Techniques

Procedures physical cleaning by using mechanical forces to remove and dislodge foulants from surface of the membrane. Physical procedures involve cleaning by sponge ball, reverse and forward flushing, backwashing with deionized water, air sparging or air bubbling, and back permeation by gas (preferably CO_2) **(Fouladitajar, et al., 2014; Ghadimkhani, et al., 2016)**. In addition, ultrasonic **(Alventosa, et al., 2014; Popovic, et al., 2010)**, spark discharge **(Kim, et al., 2015)**, electrical field **(Chen and Deng, 2013)**, and magnetic field **(Gryta, 2011)** are other present developed physical cleaning techniques that are generally used for membrane cleaning purposes.

2.8.3 Physicochemical Cleaning Method

Several situations arise where interactions of physicochemical happen between the membrane material and solution species. Properties of physicochemical, involving hydrophobicity and charge effects, cause a

concentration profile and deposition of feed solution over the surface of membrane. The charges on a membrane are strongly dependent upon the material of membrane, the ionic strength, and the pH of the feed solution. In order to minimize the concentration profile, two another cleaning methods are gaining attention; one is the electrochemical technique and the another is the physicochemical method. The physicochemical cleaning ways use physical cleaning methods with the totaling of chemical agents to improve efficiency of cleaning. The applications generally include forward flushing with permeate between cleanings when more than one chemical cleaning is used, but not simultaneous use of physical and chemical cleaning actions **(Ebrahim, 1994)**.

2.8.4 Cleaning of Sponge Ball

For this procedure, sponge balls are incorporated into the modules of membrane for a few seconds to scrub the scalent from the surface of membrane. They are usually used for cleaning big tubular membranes for industrial and wastewater process water **(Psoch and Schiewer, 2006)**.

2.8.5 Flushing

In the method of forward flushing, permeate water is pumped at large cross-flow velocity across the side of feed in order to remove foulants from the surface of membrane **(Ebrahim, 1994)**.

Because high cross-flow velocity and the subsequent turbulence, the absorbed particles inside the wall and pores of membrane are released and discharged (e.g., removal of colloidal matter). The reverse flushing method illustrates permeate flush and for a few seconds in alternative direction the forward direction and a few seconds in the reverse direction.

2.8.6 Backwashing

In this process of filtration, permeate is flushed in a reverse procedure across the membrane to the concentrate side. At the state of porous ceramic membranes, the pores are flushed inside out because higher membrane pressure on the permeate side than the pressure within the membranes when backward flush is applied.

Fig. 2.14 schematically depicts the TMP development over time in reversible and irreversible fouling. Backwashing is generally used in membranes of reverse osmosis either by increasing the permeate pressure or by minimizing operating pressure lower the (π) of the feed solution **(Sagiv and Semiat, 2010)**.

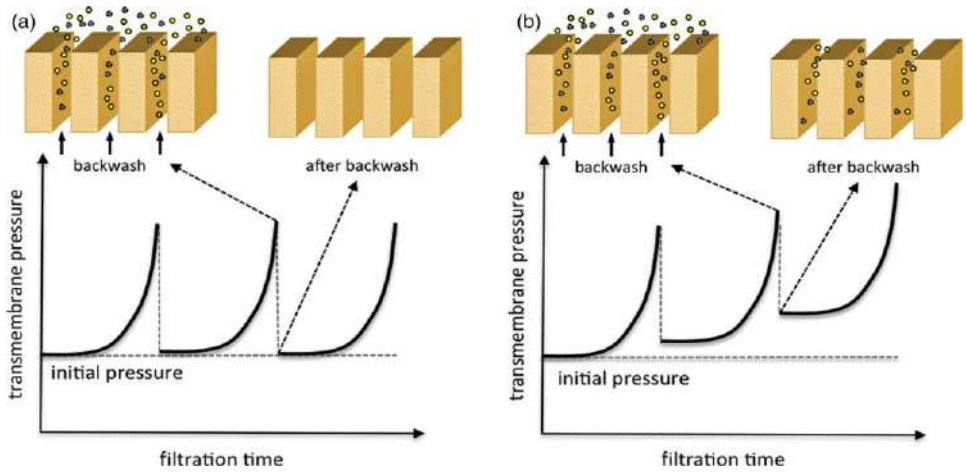

Figure 2.14 Direction Flow for Membrane Cleaning by Backwashing (Reversible Fouling Development (a) and Irreversible Fouling (b)) (Vitaly and Gadi, 2016)

2.8.7 Air Sparging

This technique produces a two-phase flow to eliminate external fouling and thus diminishes the cake layer precipitated on the surface of membrane. Air sparging may be used either during the periodically to remove already formed deposits or course of filtration to minimized deposition of fouling. The types of gases used for the sparging of gas are

water/N2 mixture and water/CO_2 mixture. Air sparging is normally applied in NF, UF and MF membranes with tubular, flat sheet, and, to some extent, spiral wound modules and hollow fiber **(Cabassud, et al., 2001; Cui and Taha, 2003)**.

The purpose of applying air is to obtain an enhanced flux with high separation efficiency in systems of MF and UF. This is possible because the existence of air bubbles, that intensify turbulence in the membrane feed side, thus raising permeate flux as well as efficiency of solute separation **(Ducom and Cabassud, 2003).**

2.8.8 Other Techniques

Several novel and nonconventional procedures, such as electric field **(Jagannadh and Muralidhara, 2006; Saxena, et al., 2009)**, magnetic field and application of ultrasound **(DeLara, et al., 2014; Li, et al., 2002; Lu, et al., 2009; Popovic, et al., 2010)** to the surface of membrane, have been developed to overcome fouling without decreasing the membrane efficiency and lifetime.

2.9 Critical Flux

2.9.1 Critical Flux Theory

A significant characteristic of membrane operation is the limiting flux (J_{limit}) that matches to the highest stable state permeate flux realizable with given suspension or solution. For this limit, furthermore rises in transmembrane pressure TMP do not rise flux. Widely speaking the critical flux was defined in two paths. Either as the permeate flux at that the TMP begins to diverge from the pure water line (the strong form of the CF) or as the permeate flux for that appears on the membrane surface irreversible fouling. Generally, the CF can be defined as the first permeate flux for that fouling become predominant, being then will

distinguished from limiting flux (the last permeate flux accessible). **(Mänttäri and Nyström, 2000; Patrice, et al, 2006)**.

One way of characterizing nanofiltration NF membrane is by estimating its critical flux. The flux where below it no reduce in the flux with time happens is the critical flux, and above it fouling can be monitored. There are two forms of the CF the weak critical flux and strong critical flux. The weak critical flux where all of the magnitudes are less than that of the ultra-pure water flux where the resistance of membrane for the solution is different from that of ultra-pure water, and the resistance of membrane changes with the rising flux after the critical flux is reached (see **Fig. 2.15)**.

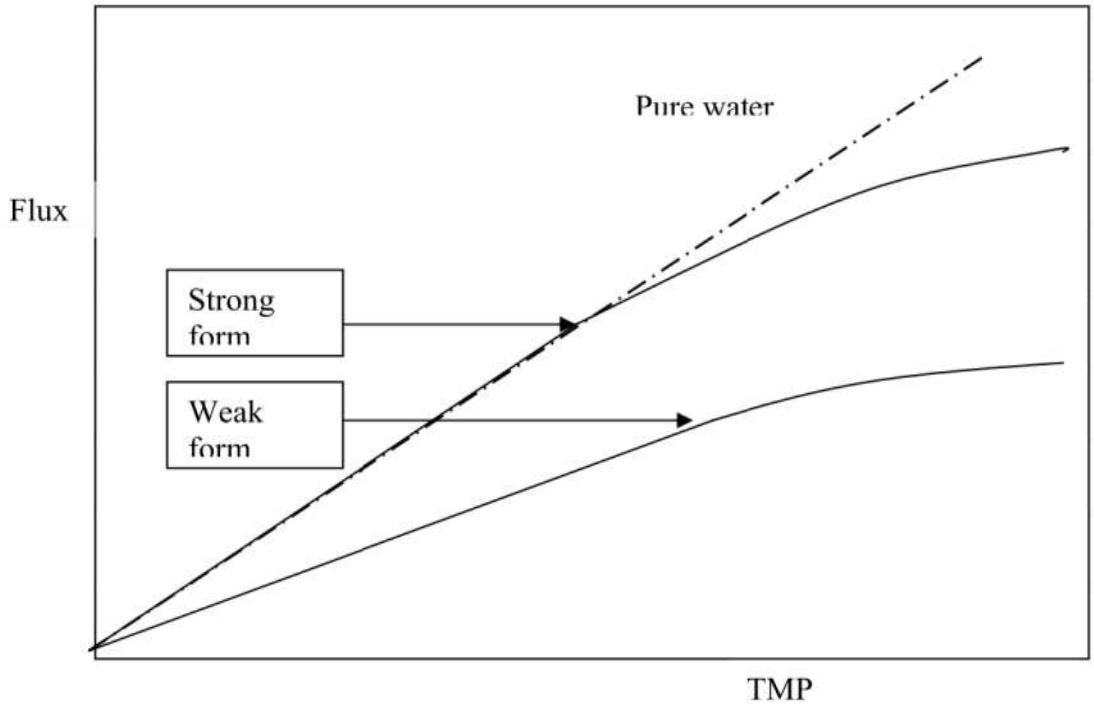

Figure 2.15 Forms of Critical Flux (Patrice, et al., 2006)

The strong is where the TMP begins to diverge from the ultra-pure water, and the resistance of membrane for the solution and ultra-pure water is the same. When ultra-pure water permeate across the membrane, the permeate flux is linearly proportional to the transmembrane pressure.

On the other hand, when a solution permeates across the membrane, the relationship between the transmembrane pressure TMP and the permeate flux is not linearly proportional. Based on that, the critical flux is the flux where the TMP deviates from the ultra-pure flux or it is the flux at that irreversible fouling happens. The critical flux dominates the particle`s repulsion and cusses the coagulate of particles on the surface of membrane **(Rautenbach and Gröschl, 1990; Meng, et al., 2006; Gilron, et al., 2006; Santafé-Moros, et al., 2008)**. Critical flux must be differentiated from the limiting flux. The maximum flux that can be reached by rising the transmembrane pressure TMP is known as the limiting flux. Accordingly, the flux magnitude would not rises by increasing the transmembrane pressure more than the limiting flux value. Add to that, the maximum flux where no fouling occurs is also known as the critical flux. The critical flux rises with increase in cross flow velocity and particle size, and reduces with rise in concentration. The critical flux is determined in different ways, that are as follows.

Foundation theory for the irreversibility or the CF in the study of based on the interaction of colloidal surface. Such approximation can also be observed in the practical testes of who distinct the CF below that the transmembrane pressure TMP continues constant and fouling is reversible **(Chiu and James, 2005; Defrance and Jaffrin, 1999)**. Those researchers view that prior this flux fouling is because adsorption and closing of pore but when it was exceeded TMP raised and did not stabilize because formation of cake at the surface. In spite of the critical flux concept was mainly assumed as a procedure of an obviating fouling it is now shown by several as a concept connected to the fouling minimization. Therefore, the sustainable flux helpful concept has newly advanced particularly in the membrane engineering state.

2.9.2 Critical Flux Definition

It is important before going further to clarify definitions of critical flux which will be related to techniques of experimental features, measurements and theory. It was showed that the term critical flux was used in basically two procedures, either as the first permeate flux for that irreversible fouling appears or as the flux at that the TMP- flux line begins to diverge from linearity. The definitions were given at several levels. A some are from an experimental (naturalistic) point a view while others are from a physical (deterministic) point an opinion (normally defined as the flux that leads to coagulation adjacent to and then deposition on the membrane). The first were normally distinct as the flux leading to a first deviance from a linear variation with transmembrane pressure. Commonly, increase in pressure (or decrease in flux) for fixed flux (pressure) process is related to a filtration law that can be shown as an integral form of the Darcy law in that many mechanisms of fouling operate.

$$J = \frac{\Delta P - \Delta \pi}{\mu(R_m + R_{ads} + R_{rev} + R_{irrev})} \qquad (2.19)$$

An osmotic pressure term ($\Delta\pi$) decreases the performance of the TMP. In addition, resistance of hydraulic are added to the resistance of membrane because of:

● a resistance of fouling driven by the volume of filtered being reversible (cake deposit or possibly blinding of pore), R_{rev}, irreversible (gel formation possibly or cake deposit), R_{irrev}.

● pore or surface adsorption, R_{ads} which independent of solvent transfer.

This classification allows to distinguish other resistances such as adsorption which are independent of the permeate flux and TMP from fouling phenomena driven by the transfer of solvent across the

membrane. Fouling of the latter type can be reversible (R_{rev}) or irreversible (R_{irrev}) when the TMP is reduced.

When considering these mechanisms of fouling, the **strong form of critical flux** (J_{cs}) was developed to identify no fouling conditions (where R_m is the only resistance in Eq. 2.19) from fouling conditions where another resistances also apply. It has been defined as the flux at that the flux - TMP curve begins to diverge from linearity (see **Fig. 2.15)**. Thus with the hypothesis that impacts of osmotic pressure (π) effects are negligible.

$$for\ J < J_{cs}: J = \frac{\Delta P}{\mu R_m} \tag{2.20}$$

$$for\ J > J_{cs}: J = \frac{\Delta P}{\mu(R_m + (R_{rev} + R_{irrev}))} \tag{2.21}$$

Here at least one of (R_{irrev} or R_{rev}) is non-zero and when (R_{ads})is accounted as insignificant.

The critical flux of the weak form (J_{cw}) was used to recognize operation down and higher the point at that the performance is effected by phenomena of fouling which are driven by the transfer of solvent across membrane. Initially the supplemental term was applied only to adsorption happening at the outset of filtration **(Field, et al., 1995).** Latest a dissimilarity was made by **(Wu, et al., 1999)** between more significant ones and very low fouling conditions, with this medium zone being between, J_{cs} and J_{cw}. But in this survey the previous definition is retained.

$$for\ J < J_{cw}: J = \frac{\Delta P}{\mu(R_m + R_{ads})} \tag{2.22}$$

$$for\ J > J_{cw}: J = \frac{\Delta P}{\mu(R_m + R_{ads} + R_{rev} + R_{irrev})} \tag{2.23}$$

Here at least one of (R_{irrev} or R_{rev}) is non-zero.

Define a new term for irreversibility of critical flux (J_{ci}) to distinguish fouling with regard to its irreversibility. Above the critical flux for irreversibility, there are growing many-layers of irreversible fouling in the boundary layer while lower it only a concentration polarization layer occurs in all cases with an additional mono-layer of adsorbed species in some cases. When filtering colloidal or dispersion macromolecules, this critical flux is linked to the dispersed phase coagulation close to the surface of membrane, followed by precipitation upon it. Accumulative matter at the surface of membrane undertakes a phase transition from a concentration polarization (dispersed phase) to a multi-layer deposit (condensed phase). The critical flux of the irreversibility form can be defined by:

$$for\ J < J_{ci}: J = \frac{\Delta P - \Delta \pi}{\mu(R_m + R_{ads} + R_{rev})} \quad (2.24)$$

$$for\ J > J_{ci}: J = \frac{\Delta P - \Delta \pi}{\mu(R_m + R_{ads} + R_{rev} + R_{irrev})} \quad (2.25)$$

Here R_{ads} might involve monolayer adsorption or in-pore fouling.

The theoretical foundation for the critical flux for irreversibility in the work of **(Bacchin, et al., 1995)** accaunting for surface interaction of colloidal. This process can usually be found in the practical testes of **(Defrance and Jaffrin, 1999)** who known the critical flux as the flux below that transmembrane pressure continues stable and fouling is reversible.

2.9.3 Measurement Methods of Critical Flux

Determination of CF has basically been gained from trans membrane-flux measurements often by using transmembrane pressure or permeate flux stepping. Furthermore, observations have been deduced from immediate monitoring across the membrane, direct observation

through the membrane (DOTM) and by mass balance. Commonly, the critical flux for the cross flow filtration process can be measured by using one of the following methods.

2.9.4 Flux – Pressure Profile (Step by Step)

With suitable value of membrane permeability either fixed pressure or constant flux process can be used to estimate the critical flux. However, for ultrafilteration membranes of dilute feeds found that it was very difficult to control the transmembrane pressure at a low enough value to measure the critical flux of the strong from and therefore that constant flux operation was to be preferred. Constant permeate flux operation (with measurement of transmembrane pressure) is readily achieved by pumping the permeate. The transmembrane pressure should remain constant with time at each permeate flux, as any increase indicated fouling and therefore that the critical flux has been exceeded.

For both modes, the critical flux is the point where TMP-flux relation becomes non-linear. If TMP-flux gradient is lower than that of pure water but linear then this critical flux is often of the weak from. According to **(Harmant and Aimar, 1996)** study, the critical flux can be determined as two thirds of the limiting flux (see **Fig. 2.16**).

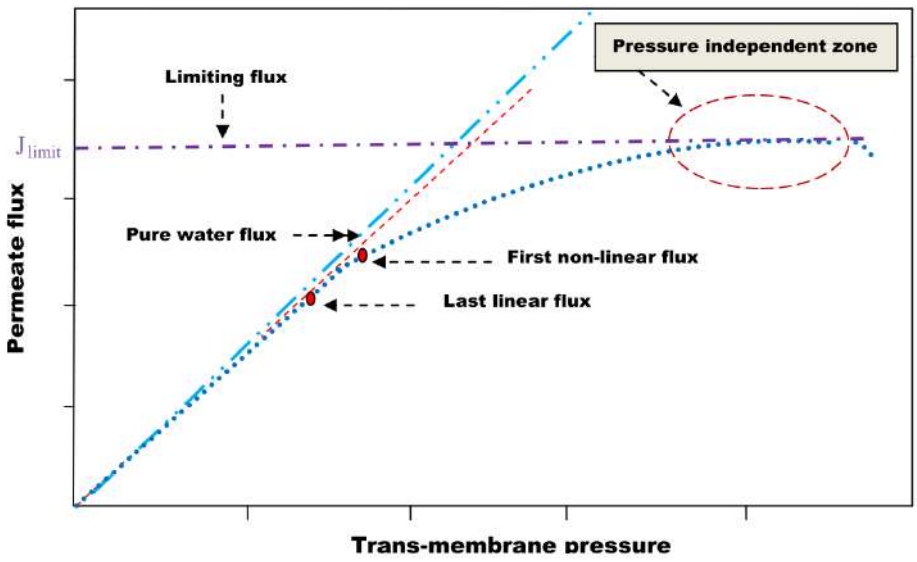

Figure 2.16 Schematic Representation of Flux-Pressure Linearity Method (Step Method) and the Limiting Flux Concept, Adopted from (Chiu and James, 2005).

2.9.5 Flux Stepping and Flux Cycling

The simplest form of this technique is a set of increasing TMP steps followed a set of decreasing steps **(Chen, et al., 1997).** They showed that above the critical flux a significant hysteresis occurred but when the magnitudes of permeate flux for increased and decreased pressure were the same, in this case the critical flux has not get been obtained. According to this (for each fixed pressure), the critical flux was exceeded when the increased pressure does not give the same flux magnitude has already been gained from decreased pressure. Both forms of the critical flux, strong and weak can be determined from this technique **(Patrice, et al., 2006)**.

Fig. 2.17, shows a schematic of a permeate flux- trans membrane pressure (TMP) technique.

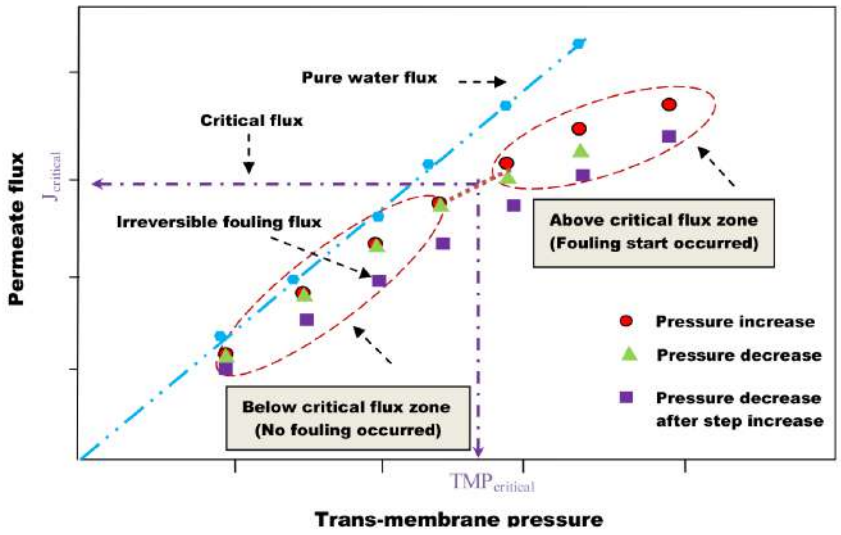

Figure 2.17 Schematic Representation of Flux-Pressure Standard Step Method (Standard Method) Adopted from (Bacchin, et al., 1995).

2.9.6 Critical Flux Determination from Mass Balance

Kwon, et al., (2000) measured critical flux according to a particle mass balance by watching the concentration of particles in the out let stream**.** The adsorption of particles in the system was determined by estimating the concentration when there was no flux. The concept is that any decreasing in concentration of particle outlet not caused by passive (adsorption / adhesion) is due to deposition. Once the rate of deposition at different fluxes was found a graph of deposition rate against permeate flux was plotted. Critical flux was then found by extrapolation; it is the flux at that the deposition rate is zero.

2.10 Zeta Potential and Electrokinetic Theory

Phenomena of electrokinetic **(Electric Double Layer EDL)** are resulted by the relative motion between a wall and the fluid, and they are immediately linked to the existence of an EDL, between the solid surface and the fluid.

When a liquid is in contact with a solid surface, an electric field is created vertical to the surface of NF membrane that attracts counterion

(commonly cations) and repulses coions (anions) in the vicinity of the interface of solid-liquid. This leads to distribution of the charge famous as the electric double layer. The electric double layer is consisted of the Gouy diffuse layer, where the ions are mobile and stern layer, where cations are adsorbed on the surface and are immobile due to the strong attraction of electrostatic. At the bulk liquid the number of anions and cations is equal so that it is electrically neutral. The nearer to the surface of NF membrane (solid) in the diffuse layer at that flow happens is termed the slipping plane or shear plane. The electric potential at the shear plane is known the electrokinetic (or zeta) potential. This potential is considerable and importance to surface and colloids science since the surface potential itself cannot be specified experimentally **(Glover and Jackson, 2010; Hunter, 1981).**

The basis of all models of the double layer is the idea of surface of the shear (slipping) plane. This plane surface separates the moving part of the electrical double layer from the fixed part. The characteristic length over that the electric double layer strongly exponentially decays is known as the Debye length, and it is of magnitude of a few nanometers for typical grain electrolyte combination **(Pride, 1994; Schoemaker, et al., 2012).**

Electrokinetic Potential (zeta) can be estimated from one of the following electrokinetic measurements. Streaming potential, electrophoresis potential, electroosmosis and sedimentation potential **(Hunter, 1981)**. The first two (Streaming potential and electrophoresis potential) are the base for the most common methods and the latter method may seldom be used. Inspections of the electrophoretic mobility of particles in suspension diagnose the particles net charge by measuring their velocity in an applied external electrical field (electrophoresis

measurements). Conversely, the streaming potential products from forcing fluid through a porous medium and its value can be provided a useful in situ characterization for solid charged surfaces **(Elimelech, et al., 1994; Herbig, 2003)**.

The streaming potential include measurement of electrical potential across the membrane under flow conditions. When the electrolyte solution is forced through the pores by the pressure gradient, the charges in the moving part of the double electrical layer are moved towards the ends of pores, producing in accumulation, it creates an electric field and a potential difference per pressure gradient that is usually known as streaming potential **(Szymczyk, et al., 1999)**.

2.11 Mechanism of Transport and Separation

The separation mechanism is usually demonstrated in terms of size and charge effects **(Peeters, 1997; Chaufer, et al., 1996)**. Transmission of uncharged solutes is obtained by diffusion due to a gradual difference of concentration and by convection due to a pressure variance a cross the membrane. A sieving mechanism is reliable for the rejection of uncharged solutes. For charged components an electrostatic reciprocal action (influence) happens between the membrane and the components, as almost nanofilteration membranes are charged (foremost negatively).

Several different theories linked with the attempts the mechanism of ion separation on NF membrane **(Anna, et al., 2016; Mukherjee, 2006)** have been studied. The transfer of mass across the nanofiltration membrane was depicted by many models Juchas Kedem-Katchalsky **(Kelewou, et al., 2011; Jarzyńska and Pietruszka, 2011)**, Spielgler-Kedem **(Chaudhari and Murthy, 2010; Mandale and Jones, 2010)** or Spiegler-Kedem-Katchalsky **(Hidalgo, et al., 2013; Koter, 2006)**. But, in these models don`t involve a membrane surface charge density that is one

of the major factors which evaluates the rejection of ions during NF membrane of salt solution **(Deon, et al., 2011; Nędzarek, et al., 2015).** Therefore, the partitioning of Donnan and steric model (DSPM), based on the extended Nernst-Plank equation, has been suggested for performance of ions separation from salt solutions on NF membranes **(Kowalik-Klimczak, et al., 2015)**.

The potential at the membrane-solution interface (Donnan potential) can happens as a result of the variance in concentrations of ionic in membrane pores and these in the bulk solution. Equilibrium happens between the solution and membrane due to the presence of the effective membrane particles charge density in order to attains electro neutrality (for each anion removed, one cation that must be removed). Repulsion of the ions at the surface of a charged membrane particles can be described by the Donnan potential **(Levenstein et al. 1996)**. When a charged particles of membrane is coming in contact with aqueous solution equilibrium happens between the solution and the membrane due to the presence of the effective membrane particles charge density, depending on the fact that the ionic concentrations in the bulk solution are not equal to those in the membrane particles.

The estimation of the Donnan potential for every membrane type, concentration of electrolyte and pH are very important particularly in modeling of the transport performance in nanofiltration membrane since all the obtainable partitioning models were depended on the magnitudes of the Donnan potential. Donnan distribution models belong to mechanistic models that are very interested in structure of membrane and the physical and chemical impacts of the electrolyte solutions and membrane. This kind of model can be used to predict the transportation of ion through the membrane based on diffuse, electric and convective

transport. In the meantime can also supply further information on charge of membrane, effective pore size and thickness, these kinds of models can a best understanding of the major mechanisms and parameter which could govern the transport in nanofiltration membrane.

A very good comprehensive survey by **(Hilal, et al., 2004)**. The distribution mechanisms of organic solutes and ionic species in aqueous media is described in detail. Today scientists accept that a combination of Donnan exclusion and steric hindrance forms the main of ion selectivity and partioning in nanofiltration membranes. The neutral solutes distribution at the interface nanofiltration of membranes depends on size or steric exclusion, in that shape and size of the solute are the predominant parameters **(Yacubowicz and Yacubowicz, 2005)**. Donnan equilibrium, for charged solutes, resulting from the charged nature of nanofiltration membranes serves as an additional partioning impact **(Timmer, 2001)**. A natural consequence of the Donnan equilibrium is which solutes with opposite charge (counter-ion) of the membrane charge are attracted while those with the same charge (co-ions) as the surface of the membrane are repelled. Furthermore, nanofiltration membrane display less rejection to multivalent of the different charge (counter-ion) than monovalent of the counter-ions, while those a higher rejection to multivalent of the same charge (co-ions) than monovalent co-ions **(Donnan, 1995)**.

2.12 Previous Study

Amy, (1996) inspected the influence of solution chemistry on the surface charge for (polymeric NF and RO) membrane using streaming potential analyzer for aqueous solutions of different composition with a range of pH values from 2 to 9. In the existence of a reference solution of sodium chloride (NaCl), the IEP of these membranes extent from (3 to

5.2). Results with salts including divalent ions calcium chloride ($CaCl_2$), sodium sulphate (Na_2SO_4) and magnesium sulphate ($MgSO_4$) indicate that the divalent anions less readily adsorb to the surface of membrane than the divalent cations, particularly in higher range of pH.

Johan, (1998) studied effect of charge and ion size for types of commercial NF membranes: one positively charged membrane (UTC20) and two negatively charged (NTR7450 and NF40). For the analysis of the results, the Spiegler-Kedem equation and steric hindrance pore model were used. Measurements of salt rejection were conducted for different salts at different concentration. For both nanofiltration UTC20 and NF40, the outcomes could not be depended to effects of charge only and the rejection sequence of salt solutions was inversely proportional to the diffusion coefficient of salt in water.

Szymczyk, et al., (1999); Chiu and James (2006); Narong, (2006) investigated the zeta potential of composite ceramic membranes (TiO_2, titanium oxide, Al_2O_3, aluminum oxide, and silica) and demonstrated this behavior in terms of proportion equilibrium that occurs on the surface of the ceramic membrane. The usual magnitude of zeta potential decreased as the concentration of electrolyte increased; this can be explained according to theory of electrical double layer, in that the effective thickness of diffuse layer (K^{-1}) reduces as the concentration ion increases.

Lee and Lee, (2000) investigated the effect of hydrodynamic operating conditions on $CaSO_4$ scale formation mechanisms using a film Tec (NF–45) polyamide and plate-and-frame membrane modules. The flux decline in that study was attributed to the formation of calcium sulphate scale which greatly influenced the crystallisation mechanism.

Puhlfurb, et al., (2000) investigated the surface charge of tubular ceramic titanium dioxide nanofiltration membrane had a main effect of the rejection efficiency of (Na_2SO_4 and NaCl) as a single salt at various pH magnitudes and TMP range (6-15) bar. The rejection of sulphate ions at pH above (6.0) is higher than 90%.

(Moritz et al. 2001) reported the effects of pH and NaCl concentration on the zeta potential. The results showed that the sign of the zeta potential can be significantly altered by changing the pH at constant NaCl concentration, whereas the changes in the concentration of salt did not have such a great influence under a constant pH.

Gouellec and Elimelech, (2002) inspected the calcium sulphate scaling mechanism compared to a calcium carbonate scaling mechanism by using a low pressure fully flat sheet aromatic polyamide NF membrane (NF –90, film Tec). The major finding from this work indicated that both calcium sulphate and calcium carbonate scales might result from particulate deposition rather than surface (wall) crystallization.

Van Gestel, et al., (2002) determined the zeta potential of a tubular ceramic TiO_2 NF membrane from measuring the electrophoretic mobility of the membrane (as powder). The results from this study confirmed the amphoteric behaviour of the Titania membrane. Also, salt rejection was investigated for five single salts (NaCl, KCl, LiCl, Na_2SO_4 and $CaCl_2$) at pH ranges from 2 to 11 and applied pressure of 5.0 bar.

Weber, et al., (2003) evaluated the salt rejection for (KCl, NaCl, $NaNO_3$ and Na_2SO_4) as a single salt at several pH magnitudes and TMP range from (4.0) to (15.0) bar using TiO_2 NF membrane. The results indicated that charge of membrane controls the rejection.

De Lint and Benes, (2005) estimated the ($CaCl_2$ - NaCl) double ionic solutions rejection using nanofiltration membrane. The experimental factors in inspection of rejection behaviour were TMP and pH. When rejection magnitudes of monovalent and divalent were compared, findings indicated the less rejection value of (Cl^- and Na^+) than (Ca^{+2}).

Lin, et al., (2006) reported the effects of pressure and flow velocity on cake formation of calcium sulphate by using a flat sheet polyamide and plate-and-frame membrane module. The major finding from this study indicated that the fouling of $CaSO_4$ was strongly dependent on operating parameters and the fouling of calcium sulphate was most sensitive to applied filtration pressure followed by cross flow velocity.

Narong and James, (2006) applied the method streaming potential to determine the charge of a ceramic TiO_2 ultrafiltration membrane by measuring the instantaneous potential deference per applied pressure because the observed potential changes quite rapidly due to the polarization of the electrodes. The results showed that IEP of UF membrane at pH value of (3.3).

Tzotzi, et al., (2007) studied the formation of calcium carbonate deposits on reverse osmosis membrane in relation with decline of permeate flux tests were conducted in a cross flow membrane cell in order to examine the scale characteristics. Many kinds of flat sheet membrane were used in the tests. In the absence of inhibitors, scaling occurred at supersaturation ratio more than 4 (nearly) at the surface of membrane.

Orecki and Maria, (2007) examined the treating of oily waste water using tubular nanofilteration membrane type (AFC30) with (MWCO) of 180 daltons and spiral wound nanofiltration membrane type (270) with (MWCO) of 250 Daltons. The feed of search was composed from permeate of ultrafilteration operation utilized to treat waste water from industry of metal working. The results shows that permeate from both of the selected membranes contain no oil and the rejection for the inorganic compounds exceeds 75% for all the cations (Na+, K+, Mg^{2+}, Ca^{2+}, Zn^{2+}**+** Cu^{2+}) with more than 95% and 65% for sulphates and total organic carbons respectively. The results of experimental show that the rejection and flux larger for the nanofilteration (270) than that of (AFC30) membrane. The workers suggested the permeate gained can be reused.

Mondal and Wickramasinghe, (2008) inspected the performance of nanofilteration and reverse osmosis membrane to treat produces water from oil production industry. The researchers used NF membrane types NF 270, NF 90 and RO membrane type BW 30. The NF 270 which had largest pore size and smoothest and most hydrophilic surface found to provide less reduction in flux., however, the permeate quality of BW30 seems to be highest.

Khedr, (2008) also compared the use of nanofiltration membranes and classical techniques, such as chelating ion exchange resins, for the trace heavy metal cations (Ag^{+2}, Hg^{+2} and Cd^{+2}) separation from mixture salt solutions.

Jawor and Hoek, (2009) was interested in the influence of feed water temperature on the inorganic fouling of ($CaSO_4$) in the brackish water desalination process by using a reverse osmosis flat sheet membrane module. This study suggested that the scale formation was

inhibited at high temperature but when the brine became super-saturated, gypsum formed rapidly.

Mazzoni, et al., (2009) studied polymeric TMMI non-impregnated nanofiltration membrane. When concentration of calcium chloride ($CaCl_2$) salt was (5 mol/m^3), rejection was approximately (50%). Rejection reduced (5%) rise of concentration to 10 mol/m^3.

Hajarat, (2010) investigated The zeta-potential for two different pore size tubular ceramic TiO_2 NF membranes at a pH range between 3-10 by using microelectophoresis method, then the iso-electric point (IEP) was found. The membrane zeta potential was measured by preparing NaCl at two different concentrations, which were 0.01M and 0.1M. Then the pH of each solution was changed to different values ranging between 3 and 10. For 0.01M concentration solution, the IEP was around 4.6. While for 0.1M concentration solution, the ISP was around 5.0.

Amer, (2013) used streaming potential method to evaluate the charge of a tubular ceramic TiO_2 nanofiltration membrane (1.0 nm) at 0.01M NaCl by measuring the changes of potential per applied (TMP). The findings from this study showed the amphoteric behaviour of TiO_2 membrane and IEP at pH of 4. Also, salt rejection was studied for four salts ($CaSO_4$, NaCl, Na_2SO_4, and $CaCl_2$) at pressure range (1-5) bar.

Mark, et al., (2014) investigated two NF membranes, a TriSep NF (TS 80) polyamide thin film and a Dow nanofiltration for the rejection of ionic species when filtering mine water effected at a range of pH magnitude. Both membranes showed alters in rejection at pH of (3.0).

Abadikahah, et al., (2014) studied the usage of response surface methodology prophetic models to optimization decline of Mg^{+2} ion rejection (%) and relative permeate flux decline (J/J_0) through the

treatment of wastewater by nanofiltration membrane. The workers researched the influence of many parameters on process of nanofilteration such as feed flow rate, transmembrane pressure (TMP), Mg^{+2} ion concentration, oil concentration and pH. Outcomes shows that Mg^{+2} ion and oil concentration and them interaction have effect on Mg^{+2} rejection and flux. Highest relative flux was found to be (0.86) which represent the lowest membrane fouling was obtained at transmembrane pressure TMP (3.4) bars, concentration of Mg (40 ppm) and pH of 4.

Safiye (2017) investigated tubular ceramic NF membranes for desalination of salt ($MgSO_4$) with 10^{-3}M at several values of pH. The highest Mg^{+2} and SO_4^{-2} ion rejections were gained 91% and 95% respectively.

Chapter Three
Experimental Work

This chapter included the experimental work that were conducted to study the behavior and performance of the ceramic titanium dioxide membrane with nominal pore size 0.9 nm to achieve the best operating conditions of the membrane, control of fouling and reduce the risk of fouling on the membrane. As a result, achieved an economic return by reducing the amount of materials used to regeneration the membrane due to the fouling. In order to achieve this purpose a system was set up and installation to conduct experiments of zeta potential measurements by using streaming potential method, (and the measurements of zeta potential in second method is the microelectrophoresis for purpose of comparing the results of two methods and verify the success of the use of the alternative electrodes manufactured locally) then to conduct rejection experiments and critical flux experiments using different (saline solutions, concentrations, transmembrane pressure, cross flow velocity and pH values). Finally, the produced water treatment experiments were carried out as a practical application. The experimental section is described in the following four stages.

Step 1. Zeta Potential Experiments.

Measurements of zeta potential for the ceramic 0.9 nm TiO_2 NF membrane were conducted using two basic and more common procedures microelectrophoresis potential and streaming potential methods. Microelectrophoresis method was used to measure the zeta potential of the membrane using sodium chloride as a reference salt at three different concentrations and calcium carbonate ($CaCO_3$) at two different concentrations. Second procedure was streaming potential by using alternative electrodes of (silver + 4% gold) for the first time instead of platinum, at two concentrations of reference salt NaCl and compare the results with the microelectrophoresis method in order to

examine the success of alternative electrodes in measuring the zeta potential and study the effect of concentration and pH on zeta potential value. Furthermore, the streaming potential method procedure was then used to measure the zeta potential for eight different saline solutions sodium chloride (NaCl), calcium chloride (KCl), sodium carbonate (Na_2CO_3), magnesium sulphate ($MgSO_4$), calcium chloride ($CaCl_2$), magnesium chloride ($MgCl_2$), sodium sulphate (Na_2SO_4) and sodium bicarbonate ($NaHCO_3$) at constant concentration (0.01 M) to study ion type and valency on zeta potential. In addition, study the effect of zeta potential on rejection and critical flux in the next two step.

Step 2. Rejection Experiments

Reject experiments were conducted for seven different salts (sodium chloride (NaCl), calcium carbonate ($CaCO_3$), magnesium sulphate ($MgSO_4$), calcium chloride ($CaCl_2$), magnesium chloride ($MgCl_2$), sodium sulphate (Na_2SO_4) and sodium bicarbonate ($NaHCO_3$) (neutral) at different concentrations and conditions to study the behavior of salts and estimate membrane performance efficiency. Other experiments were conducted for an uncharged solute (glucose). So it is possible to calculate the basic parameters of the membrane (effective radius (r_p), equivalent active layer thickness (Δx_e), surface charge density (σ^s), effective charge density (X^m) and Donnan potential (ψ_D)). Thus the nanofiltration membrane can be characterized.

Step 3. Critical Flux Experiments

The critical flux experiments were carried out for five different salts sodium chloride (NaCl), magnesium sulphate ($MgSO_4$), calcium chloride ($CaCl_2$), sodium sulphate (Na_2SO_4) and sodium bicarbonate ($NaHCO_3$) at different concentration and conditions to determine and predict when the fouling occurs for each saline solutions so that it can

be avoided. As a result, the membrane`s life is increased and no expensive chemicals are used for cleaning.

Step 4. Oilfield Produced Water Treatment

The produced water from oil tank dewatering of Bazargan oilfield in misan treated using polymer membranes (MF and UF) as a pretreatment and (the tubular ceramic TiO_2 NF membrane, polymer RO membrane) as a posttreatment.

3.1 Materials

Table A.1 in the appendix A shows all the chemicals used in these experiments (sodium chloride NaCl, calcium carbonate $CaCO_3$, calcium chloride $CaCl_2$, magnesium chloride $MgCl_2$, Magnesium sulphate $MgSO_4$, sodium carbonate Na_2CO_3, sodium sulphate Na_2SO_4, Nitric acid HNO_3, hydrochloric acid HCl and sodium hydroxide NaOH) with some of their properties.

3.2 Preparation of Alternative Silver Electrodes

The alternative silver electrodes have been prepared using silver with purity (98 %) and gold gauge 21 by melting the (silver and gold) at 1100 C^o. The first part of the molten was used in the manufacture of the outer electrode, by preparing a longitudinal sheet with a thickness of 0.2 mm, a width of 1.5 cm and a length of 30 cm. Then it is wrapped on a cylindrical iron rod with a diameter of 1.0 cm and length of 14 cm to obtain a cylindrical electrode with a same measurement as above. The outer electrode is perforated by a special mold. The second part of molten is poured into another mold longitudinal form as channel or (rough) and then pulled by a special pull device several times until the electrode is obtained with diameter of 4 mm and 50 cm length. **Fig. 3.1**

and **3.2** represent the outer electrode and the inner electrode respectively.

Figure 3.1 Represent the Outside Electrode form, it was Made from the (Silver and 4% Gold), Length = 14 cm, ID = 10.0 mm, OD = 10.4 mm.

Figure 3.2 Represents the Inside Electrode form, it was Made from Composite (Silver and 4% Gold), Length = 50 cm, D = 4 mm which Passed in the Center Line of Ceramic Membrane and the Outside Electrode was Warped around the Outer Wall of Tubular Ceramic Membrane.

The composite material used in the manufacturing of the two electrodes was analyzed in the (XRF: X-ray fluorescence), which works using different reagents and each reagent that determines a set of elements. **Table 3.1**, **Figs. 3.3** and **3.4** show the results of the electrodes analysis by X-ray fluorescence.

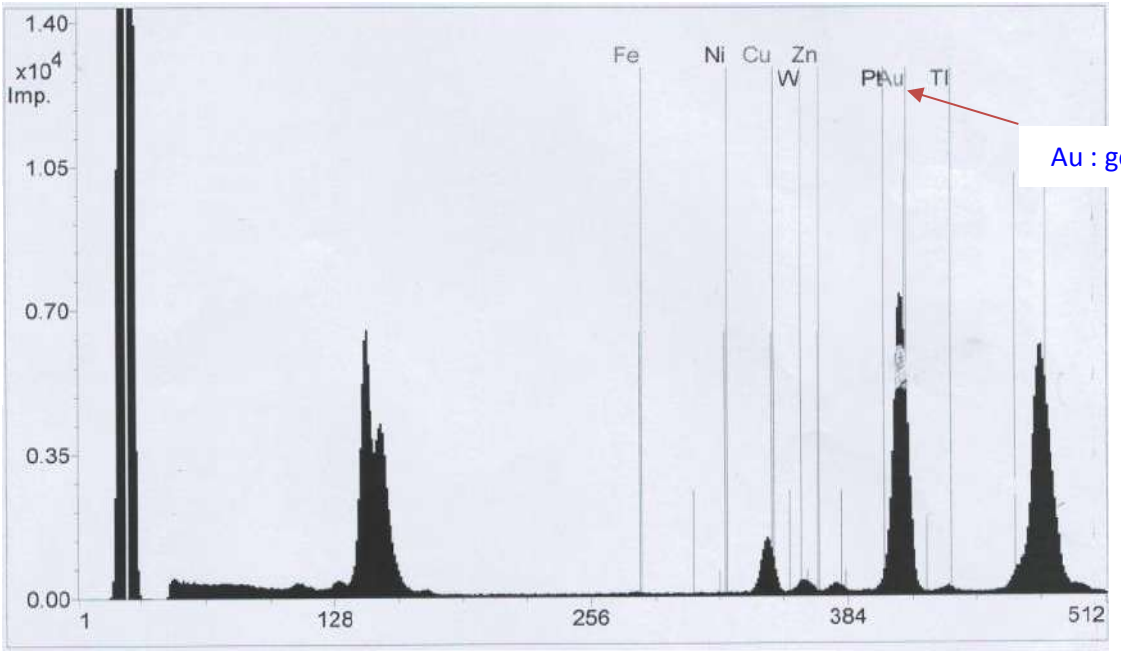

Impulses

Kilo Electron Volt (KeV)

Figure 3.3 Represents the Results of the X-ray Fluorescence Test using the First Detector, Which Showed the Presence of Gold Element.

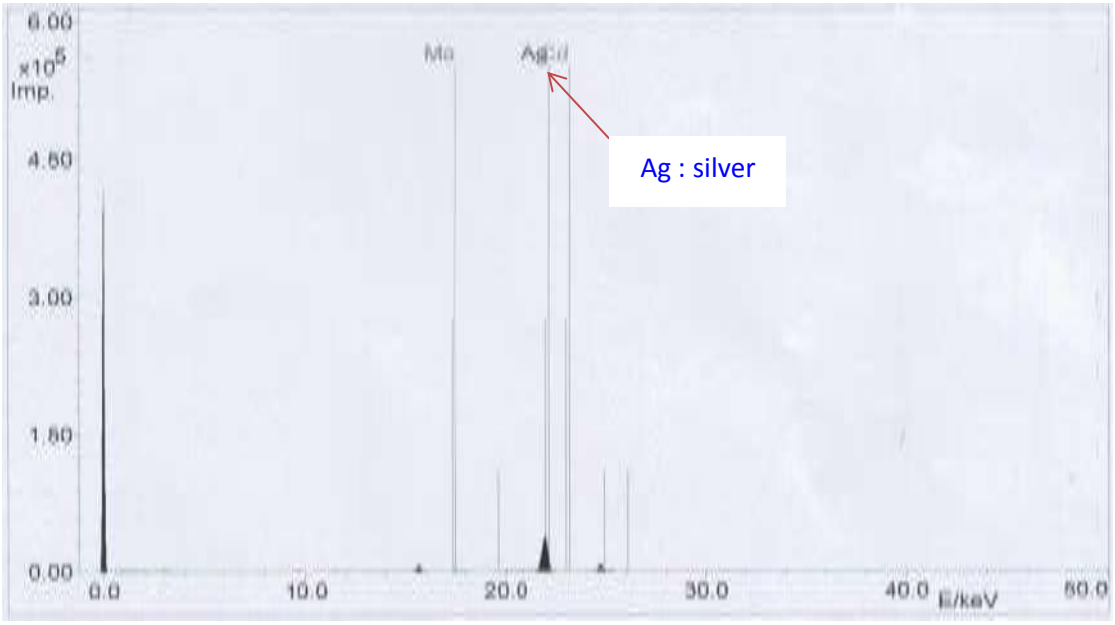

Impulses

Kilo Electron Volt (KeV)

Figure 3.4. Represents the Results of the X-ray Fluorescence Test using the Second Detector, Which Showed the Presence of Silver Element.

Table 3.1. Represents the Results of the X-ray Fluorescence Test for Two Electrodes

Symbol	Element	Concentration
Ag	Silver	94. 06 %
Au	Gold	4.2 %
Mg	Magnesium	0.041 %
Al	Aluminum	0.0069 %
Si	Silicon	0.0027 %
P	Phosphorus	0.14 %
S	Sulfur	0.00044 %
Ti	Titanium	0.0013 %
V	Vanadium	0.0014 %
Cr	Chromium	0.015 %
Mn	Manganese	0.0098 %
Fe	Iron	0.0241 %
Co	Cobalt	0.0048 %
Ni	Nickel	0.0054 %
Cu	Copper	0.3002 %
Zn	Zinc	0.0085 %
As	Arsenic	0.00051 %
Zr	Zirconium	0.050 %
Nb	Niobium	0.018 %
Mo	Molybdenum	0.134 %
Cd	Cadmium	0.0838 %
Sn	Tin	0.077 %
Sb	Antimony	0.0063 %
W	Tungsten	0.0172 %
Pb	Lead	0.0021 %

Silver was chosen because it has good properties of polarization and the addition of gold with percentage mentioned (Table 3.1) for improving the properties of silver electrode polarization and increase its resistance to the corrosion in the solutions of the base and acidic, therefore, its performance in the measurement of zeta potential of membrane such as performance of platinum electrodes.

3.3 Experiment Setup

A schematic diagram of a filtration rig experiments is illustrated in **Fig. 3.5**, used to characterize the surface charge magnitude and sign (by measurements of zeta potential) of the present ceramic titanium dioxide nanofiltration membrane. The filtration rig experiments setup used to investigate the behavior of rejection and fouling of different

salts and oilfield produced water **Fig. 3.5 (a,b)** for 0.9 nm titanium dioxide nanofiltration membrane. **Fig. 3.6** shows a picture of the bench scale for the experiment setup of rig.

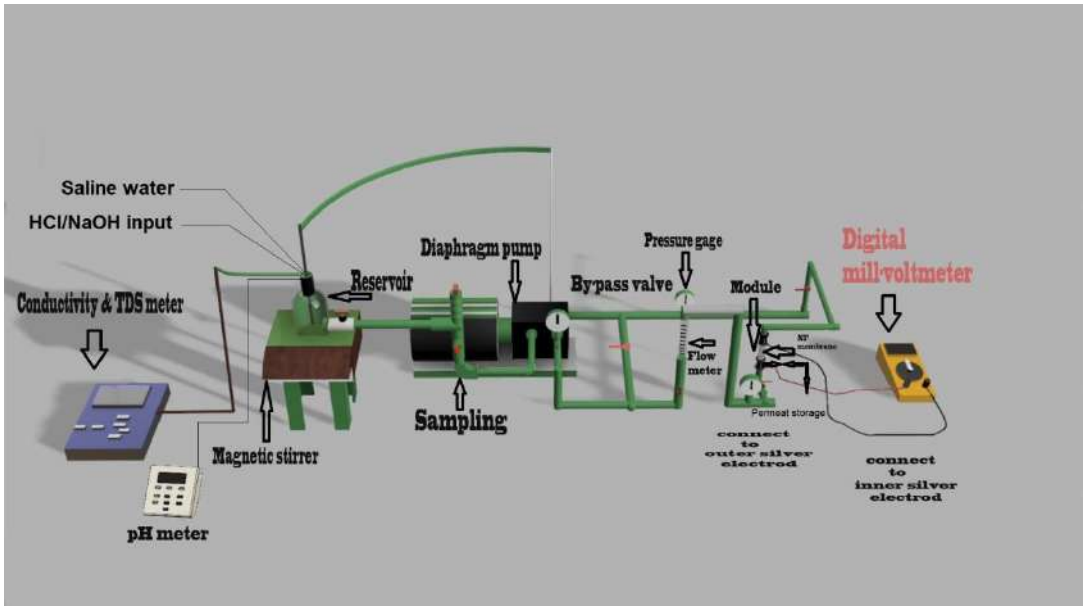

a

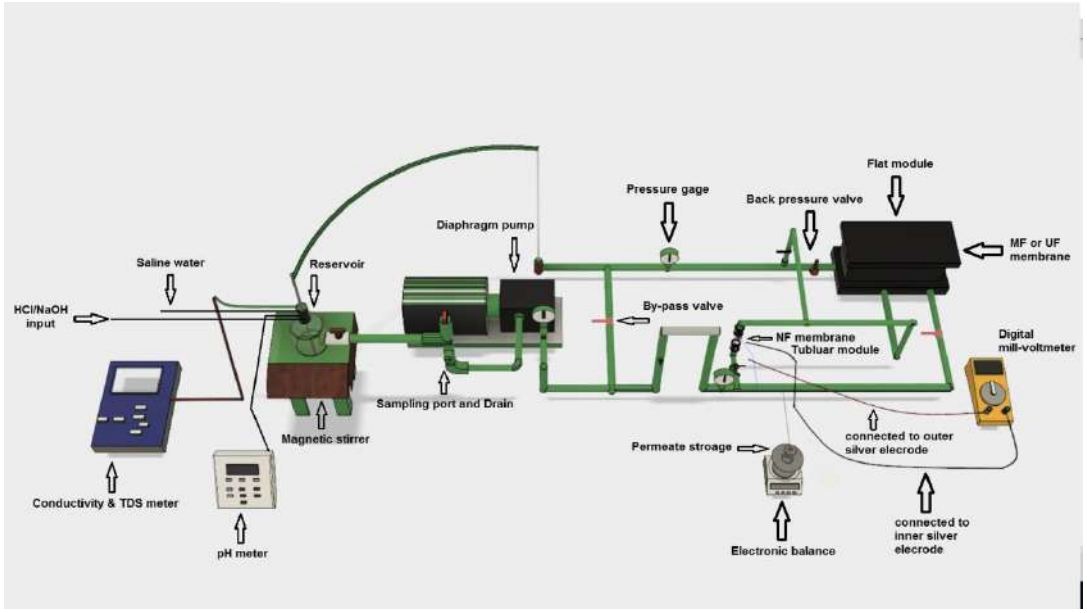

b

Figure 3.5 (a) Schematic Diagram of Tubular Ceramic Titanium Dioxide NF Membrane for Zeta Potential, Filtration Flux Rejection, Critical Flux and Fouling Installation, (b) Tubular Ceramic Titanium Dioxide NF Membrane and Flat Membrane (MF and UF) TOC and Oil Removal, Filtration Flux Rejection, Critical Flux and Fouling Installation for Oilfield Produced Water Treatment.

Figure 3.6 Bench Scale of Tubular Ceramic Titanium Dioxide NF Membrane and Flat Membrane Filtration Rig.

● MF Membrane

The MF membrane that was used is supplied by GE Osmonics, (dimension of 190 × 140 mm) USA. The specifications of membrane are listed in Table 3.2.

Table 3.2 Specification of MF Membrane

Manufacturer	Type	Pore size	Polymer	Feed	pH
GE Osmonics™	JX	0.3 µm	PVDF	Industrial/ Process Water	2-9

● UF Membrane

The UF membrane that was used is supplied by GE Osmonics, USA. The specifications of membrane are listed in Table 3.3.

Table 3.3 Specification of UF Membrane

Manufacturer	Type	Pore size	Polymer	Feed	pH
GE Osmonics™	MW	0.004 µm	Polyacrylonitrile (PAN)	Oil/Water	2-9

● MF and UF Membrane Cell

The membrane cell that was used is supplied by STERLITECH, GE Osmonics, (dimension of 190 × 140 mm) USA Flat and Frame (see **Fig. 3.7**). The specification of these parts are listed in Table 3.4.

Table 3.4 Technical Specification of UF and MF Membrane Cell

Specification	Value
Cell Type	Sepa CF, 316 Stainless Steel, 1000 psi
Number of Cells	1
Membrane Sample Size	7.5 in × 5.5 in (19 cm × 14 cm)
Effective Membrane Area	24 in^2 (140 cm^2)
Feed Flow Rate	1.8 GPM (6.8 LPM) Max

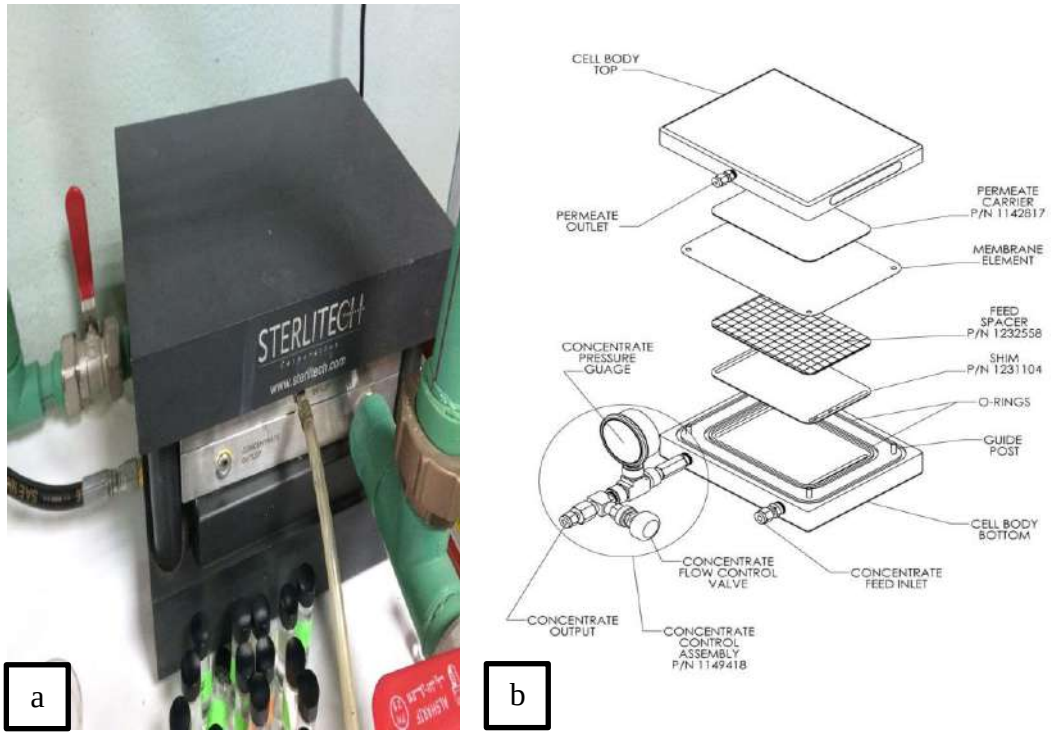

Figure 3.7 (a) Represents MF and UF Membrane Cell, (b) Typical Cell Body Assembly.

● **Feed Spacers and Permeate Carriers**

Users select from a variety of spacer configurations, identical to those used in large-scale operations, to help optimize flow characteristics for the particular solution being processed. Shim, mesh (diamond), or parallel feed spacers (along with the membrane and permeate carrier) are loaded into the cell body to simulate the actual flow characteristics of a wide variety of available spiral wound membranes. These shim/spacer combinations, in conjunction with the concentration flow control valve, allow the user to test laminar or turbulent flow conditions.

● **NF Membrane**

The filtration rig experiments installation consisted of one tubular ceramic TiO_2 NF membrane (See **Fig. 3.8**) supported by alumina sub layers supplied by (Inopor® single channel, produced by GmbH Veilsdrof – Germany). The technical specifications of nanofiltration membrane are listed in Table 3.5.

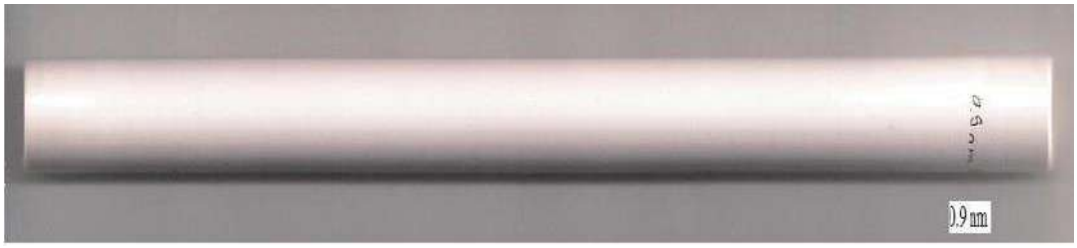

Figure 3.8 Vergin Ceramic Titanium Dioxide NF Membrane with Pore Size of 0.9 nm, Length = 19 cm, ID = 7 mm, OD = 10 mm.

Table 3.5 Specification of Tubular Ceramic TiO_2 NF Membrane (as Indicated by the Manufacturer: Inopor® single channel, GmbH Veilsdrof – Germany)

Specification	Value
Number of channel	1
External diameter	10 mm
Internal diameter	7 mm
Total length	190 mm
Surface area	4.18×10^{-8} m^2
Pore size	0.9 mm
Membrane surface material	TiO_2 / Al_2O_3
Cut-off	450 Da
Porosity	30-40 %
pH	0 – 14
Pressure	0 – 20 bar

● Housing of NF Membrane

The PVC-type (Housing of tubular membranes) was locally manufactured based on the **(Amer, 2013)** as shown in **Fig. 3.9**.

b

a

Figure 3.9. Schematic of Tubular Membrane Module that was used in the Experiments, a : Front View of the Module, b : Side View of the Basic Sections of the Module, c : Cross Section of Module with Fixing the Measurements of the Basic Sections and d : Cross Section of Module with Definition of the External and Internal Sections.

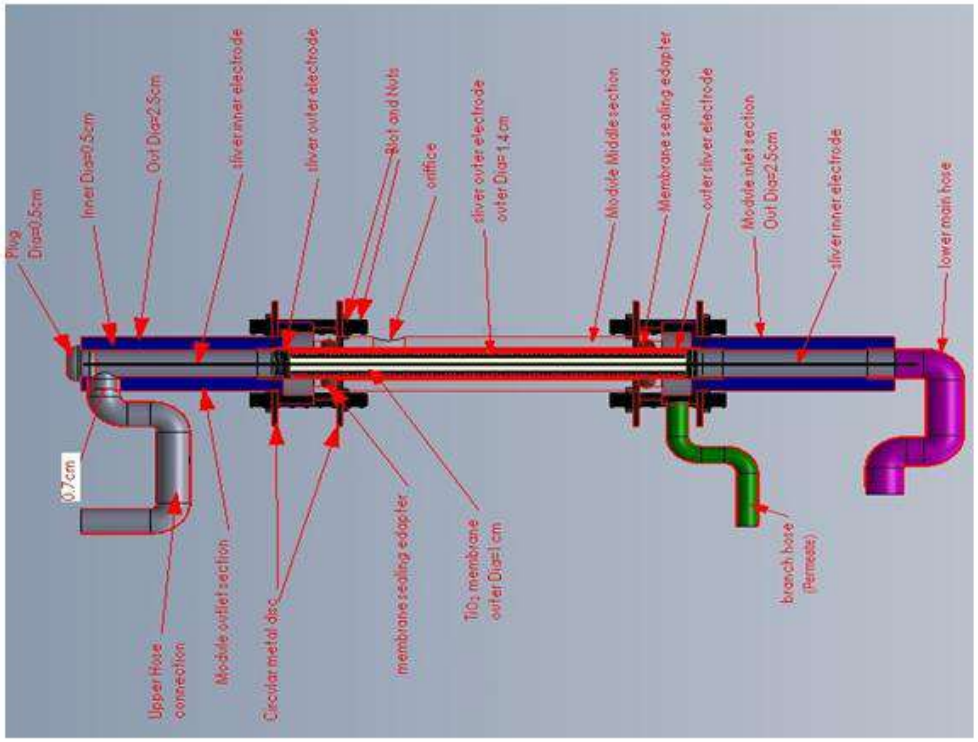

d

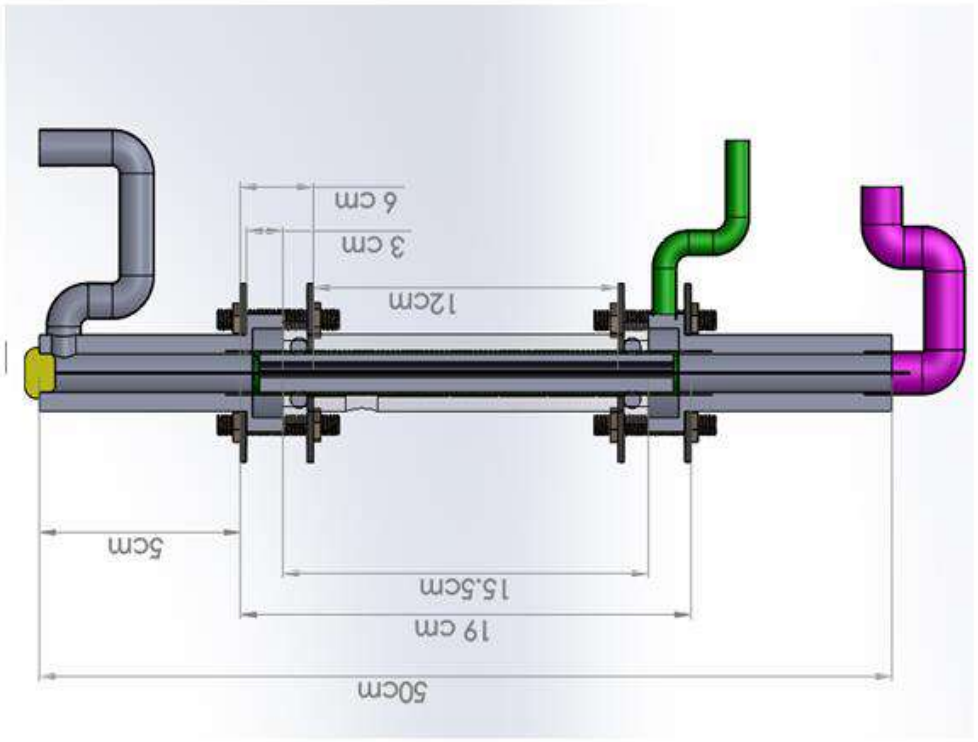

c

Continue Figure 3.9.

● RO Membrane

The RO membrane that was used is supplied by GE Osmonics, (dimension of 190 × 140 mm) USA. The specifications of membrane are listed in Table 3.6.

Table 3.6 Specification of RO Membrane

Manufacturer	Type	Pore size	Polymer	Feed	pH
GE Osmonics™	GE	0.3 nm	Composite Polyamide - TFC	Surface/ Chemical	1-11

● System of Reverse Osmosis (RO)

The reverse osmosis system that was used is supplied by STERLITECH, GE Osmonics, USA flat and frame type with flat sheet polyamide (PA) membrane. The specifications of RO system are listed in Table 3.7.

Table 3.7 Specification of RO System

Specification	Value
Cell Type	Sepa CF, 316 Stainless Steel, 1000 psi Rated
Number of Cells	1
Membrane Sample Size	7.5 in × 5.5 in (19 cm × 14 cm)
Effective Membrane Area	24 in^2 (140 cm^2)
Feed Flow Rate	1.8 GPM (6.8 LPM) Max
Feed Controls	Bypass Valve, Brine/Concentrate Control Valve, ON/OFF Switch
Data Display	Digital Display Max Flow: 1.8 GPM (6.8 LPM) Max Pressure: 1000 PSI (69 bar) Includes 1 Ethernet connection and 1 USB connection
Operating Pressure Range	0 - 1000 PSI (0-69 Bar)
Electrical Supply	230 V, 1 Phase, 50 Hz
Motor Rating	Leeson : 1.5 HP, 8.6 Amps, 1725 RPM 230 V 50 Hz 1 Ph
Pump	Hydra-Cell SS Diaphragm, Type M03SASGSNSCA
System Dimensions	67 in × 41 in × 59 in (170 cm × 104 cm × 150 cm)
Weight	650 lbs (295 Kg)
Optional Accessories :	
Chiller	Not Included
Variable Frequency Drive	Not Included

A sample of ceramic TiO_2 NF membrane was cut to a length of (2-3) mm to enable inspection of the membrane surface by using a scanning electron microscope (SEM). The (SEM) cross section image is shown in **Fig. (3.10)** and appendix A. The tubular ceramic NF TiO_2 membrane used in this work is an asymmetric (composite) membrane having effective side surface that is formed from a thin layer of TiO_2 which can be seen distinctly. A typical ceramic membrane pore was fixed and (3.0) various membrane support layers the outer of that is formed of sintered Al_2O_3 are seen. Furthermore, an elemental analysis was measured by using an energy dispersive X-ray spectrometer (EDXS). **Fig. (3.11)** shows the indicated spectrums of the effective surface of TiO_2 membrane gained by using EDXS.

It seen that the ceramic TiO_2 membrane used in this inspector contains the main elements, titanium, T, oxygen, O, aluminum, Al represent the indicated spectrums of the effective surface of TiO_2 membrane gained by using EDXS as shown in Table 3.8.

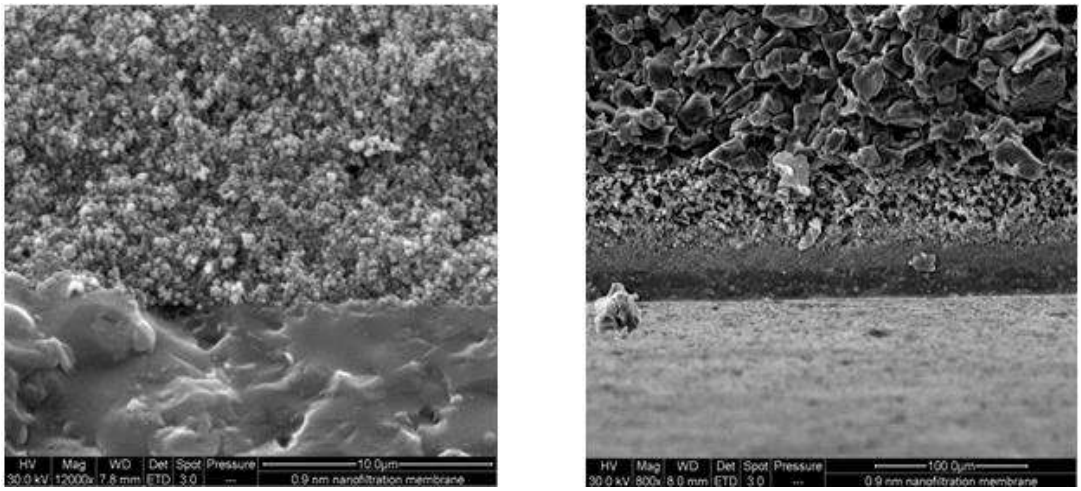

Figure 3.10 SEM Cross-Section Image of TiO_2 Nanofiltration Membrane

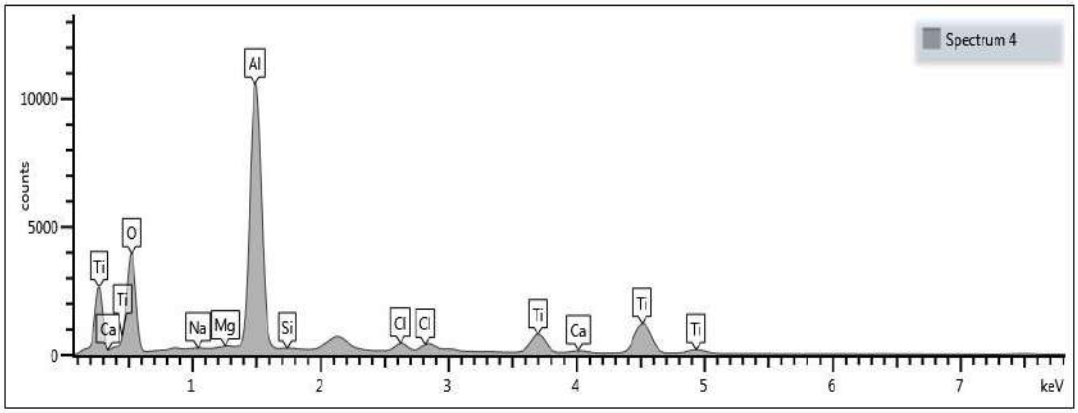

Figure 3.11 EDXS Spectrum of TiO_2 Nanofiltration Membrane.

Table 3.8 Represent Elemental Analysis using (EDXS)

Spectrum Label	O	Na	Mg	Al	Si	Cl	Ca	Ti	Total
Spectrum	46.74	0.15	0.19	35.58	0.18	1.72	1.39	14.06	100.00

● Pump

A diaphragm pump type BALDOR. RELIANCE SuperE Motor supplied by STERLITECH CO., U.S.A. was used as NF feed pump. The specification of the pump is listed in Table 3.9.

Table 3.9 Specification of Pump

Specification	Value
Model No.	M03SASGSNSCA
Serial No.	249807
Operating Pressure Range	0-1000 PSI (0-69 Bar)
Electrical Supply	230 V, 1 Phase, 50 Hz
Motor Rating	Leeson: 1.5 HP, 8.6 Amps, 1725 RPM, 230 V 50 Hz 1 Ph
Pump	Hydra-Cell SS Diaphragm, Type M03SASGSNSCA

● **Pressure Gauges**

Tow pressure gauges supplied by (WIKA, Pressure Range 0 – 16 bar, Germany) where installed at inlet and outlet of the membrane.

● **Feed Container**

One feed container QVF glass vessels with capacity of 5 liters was used as feeding vessels.

● **Flow Meter**

One calibrated rotameters produced by (Gemu Gebe Muler, Germany), where installed at charge section of the NF membrane module. The range of flow rate (0 -18) L/min was used for tubular ceramic NF membrane.

● **Valves Piping and Fittings**

Ball valves (st:st 316L), where installed at recycle line of the pump, inlet and outlet of the membrane in order to control on the transmembrane pressure (TMP). Reinforced PVC piping (Germany) and different fittings.

3.4 Experimental Procedure

The experimental work was carried out in four stages as follows.

3.4.1 Measurements of zeta potential using Microelectrophoresis Method

In order to estimate zeta potential of the membrane, sodium chloride (NaCl) salt was used. Three solution were prepared in the first step by using a solid (sodium chloride) with ultra-pure water at three different concentrations (0.001 M, 0.01 M and 0.1 M NaCl). Then the pH of each solution was altered to different magnitudes ranging from pH of 3 to pH of 9. The pH values of these three solutions were altered

by using 0.1 M (NaOH) solution and 0.1 M (HCl) solution. After the preparation of the saline solutions, 0.1gm of the powder of the crushed tubular ceramic titanium dioxide NF membrane was added for every 10 ml of prepared solutions for each pH value (3-9).This was done in order to investigate the effect concentration and pH on membrane zeta potential. In the second step, one salt was used (NaCl), in order to inspect the influences of solute ionic strength on the microelectrophoresis potential measurement, the membrane zeta potential magnitudes were also applied for 0.001, 0.005, 0.01, and 0.1 M (NaCl) solution at constant pH magnitude of 6.0 using exactly same manner for a background electrolyte of that used in the first step. 5×10^{-5} M and 10×10^{-5} M calcium carbonate ($CaCO_3$) solution was prepared by using a solids dried with ultra-pure deionized water. The other steps were followed by the same steps using a background electrolyte of sodium chloride (NaCl) as a reference salt. Microelectrophoresis measurements need powder particles of the membrane material that can only be achieved by destroying and crushing the (TiO_2) membrane using morter. The effective diameter of the membrane particles was measured by using measuring device of particle size and zeta potential approximately (515 nm) as shown in **Fig. (3.12).**

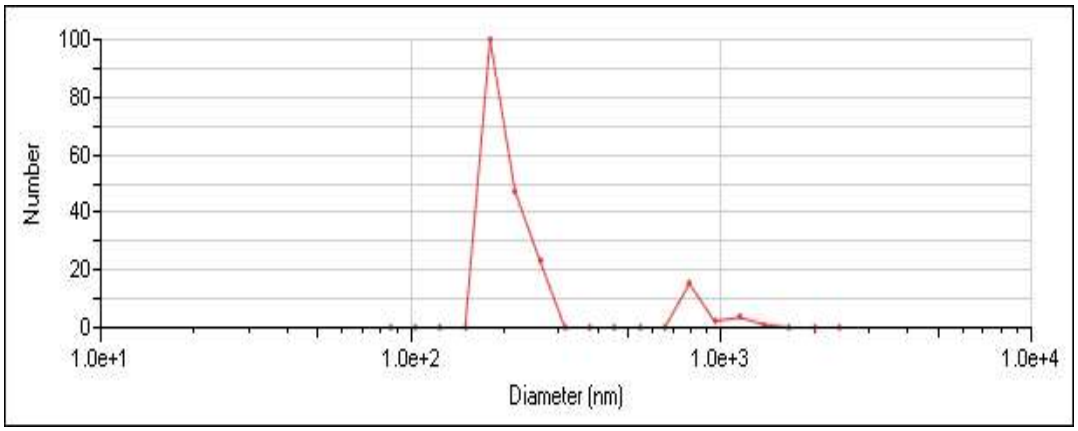

Fig. 3.12 Represents the Effective Diameter Measurement of the Tubular TiO_2 NF Membrane Particles with Effective Diameter : 515.65 nm.

3.4.2 Measurements of Zeta Potential using Streaming Potential Technique.

The streaming potential is the main for the most common methods used for researching the surface electrokinetic properties of the membrane. Conductivity and pH both permeate and retenate were continuously monitored at the beginning of the streaming potential experiments to assure that stable streaming potential was done.

The applied transmembrane pressure was monitored by using two pressure gauges at each ends of membrane module and controlled manually by gradually closing of the control valve (at discharge section of the membrane module) and by gradual manual opening of the control valve (at charge section of the membrane module) to obtain the needed back pressure and ensure that stable cross flow was achieved.

The pair (composite silver and 4% gold) electrodes were attached to the milli-voltemeter that recorded the potential variance which was produced by the electrolyte flow. The determining of the electrical potential variance (ΔE) started with the injections of 0.1 M sodium hydroxide (NaOH) to the electrolyte solution of NaCl for the groups of pH higher than 6 (pH at 7, 8 and 9). The same manner was repeated for injections of 0.1 M hydrochloric acid (HCl) for groups of pH lower than 6 (pH at 5, 4 and 3).

The streaming potential measurements were carried out at the across flow velocity of 1.0 m/s (at flow rate of 140 l/h) The applied pressure for the tubular membrane was increased in a gradual way with an interval of 0.25 bar and the matching electrical potential under every pressure were registered. The streaming potential represent the direct contact between active surface layer of the charged membrane and electrolyte solution (in situ method). In this investigation,

measurements of the streaming potential were done on the membrane through a range of pH (3-9), using NaCl as a reference salt at two concentrations (10^{-1},10^{-2} M) and for another salts, KCl, $MgSO_4$, $CaCl_2$, $MgCl_2$, Na_2SO_4, Na_2CO_3 and $NaHCO_3$ at fixed concentration (10^{-2} M). The electric potential variance through a range of applied transmembrane pressure driving forces ($0 \leq \text{TMP} \leq 2.0$ bar) was determined by using a pair of electrodes made from composite material consist of (silver and 4% gold 21 gauge) as an alternative to (platinum electrodes**)** connected to high impedance milli-voltemeter (Fluk corporation, 179 TRUE RMS MULTIMETER, U.S.A.). The first electrode was wrapped around the outer wall of the tubular ceramic membrane and the second was placed along the central line of the tubular membrane. The electrodes were linked to the voltmeter that recorded the potential variance created by the electrolyte flow. A detailed flow diagram presenting the main components of the cell for streaming potential were shown in **Fig. (3.13)**.

The streaming potential used in this work are known as the immediate potential variance per unit variance of applied pressure ($\frac{\Delta E}{\Delta TMP}$). This is because of the experimental potential variations very rapidly because polarization of the electrode if it is measured continuously and in the absence of the completely reversible electrodes the use of immediate potentials provides a suitable means of measuring streaming potentials and perfect reproducibility is accomplished using this methodology **(Toshio, 2002)**.

Figure 3.13 Represents the Basic Cell which Used in the Measurement of Zeta Potential, Consist of the Ceramic Membrane was Mounted in Transparent uPVC Module House, Outside Electrode and Inside Electrode were Connected to Nigh Impedance Milli-Voltmeter.

Experiment were conducted at room temperature (25^{o} C). The measurements of the streaming potential showed an excellent reproducibility and every filtration experiment was duplicated at least twice and the outcomes showed in the present study were mean magnitudes. The evaluated streaming potential in present study is explained as the instantaneous potential variance per applied pressure; that is due to the observed potential alters very rapidly because the polarization of the electrodes **(Narong, 2006; Chiu and James, 2006; Narong and James, 2006)**. Use of instantaneous potential supplies a helpful means of evaluating both filtration potential and streaming potential **(Le Gouellec and Elimelech, 2002)**.

3.4.3 Salts Rejection Experiments.

Experiments of rejection were conducted in order to study the factors affecting the performance NF membrane and the rejection efficiency of $CaCO_3$ (below, at the saturation and above the saturation concentration) as a single salt compared with the other neutral salts (NaCl, $NaHCO_3$, $CaCl_2$, $MgCl_2$, $MgSO_4$ and Na_2SO_4) by using 0.9 nm

ceramic TiO_2 nanofiltration membrane, that involves the major following steps:

Preparation of five liters of desired salt molar concentration in the 10 liters glass container by using a solid dried high purities with high pure deionized water with conductivity of 0.05 µs/cm and mix by magnetic stirrer for twenty minutes to achieve complete solubility of salt. Care should be given to calcium carbonate solutions because its low solubility in water. Experiments started when the diaphragm high pressure pump was worked on applied pressure was determined by regulating the tubular back pressure valve at 0.25 bar for approximate 15 minutes. During this period the permeate and rejection fluxes were monitored to assure that the system is steady after getting rid of the whole air bubbles which might occur in the filtration rig. Furthermore, pH and the conductivity of the feed solution were determined.

Flow rate of the system was monitored by the flowmeter and put to be at 140 l/h. The rejection was carried out for several applied transmembrane pressure (TMP) in the range from (1 to 15 bar). The applied pressure was monitored by the tow pressure gauges at each ends of the tubular ceramic membrane module and controlled by manual regulating the valves at charge and discharge parts of the membrane module to obtain the required pressure while maintaining the flow rate constant. In order to determine the highest salt rejection experiments were conducted by increasing the pressure up to (15) bars because the tubular ceramic membrane was not fouled yet, then the transmembrane pressure (TMP) was decreased in increments of (1) bar until to reach the least pressure that was obtained by (1) bar. Then, the filtration was continued by increasing the pressure in stages of 1 bar until it reaches the maximum pressure that was obtained by (15 bar).

The average of the ion rejection was accepted for any certain decreased or increased pressure. The filtration time was one hour for every applied trans membrane pressure and the sample of the permeate was assembled for analysis after the permeation of solute reached to the limits (15-20) ml. Experiments were conducted at a mean temperature of 25^{o} C (room temperature). Measurements of rejection were carried out at the cross flow velocities 1.0 m/s (140 l/h). The flux of permeate in m/s or ($m^3/m^2.s$) was determined by using a digital balance for any increased or decreased pressure stage. The conductivity of permeate usually measured in the average time. The measurements of the rejection showed a good reproducibility and every experiments of filtration were repeated at least twice for some non-matching experiment results.

3.4.4 Critical Flux Experiments

Experiments of the critical flux for the present titanium dioxide (TiO_2) nanofiltration membrane was carried out depending on flux – pressure profile (step by step method) using five different salts (sodium chloride (NaCl), magnesium sulphate ($MgSO_4$), calcium chloride ($CaCl_2$), sodium sulphate (Na_2SO_4) and sodium bicarbonate ($NaHCO_3$).

Before the beginning of any experiment, ensure the tightness of the exit and entrance junctions between the module and the membrane using flexible circular plastic rings and adapters tightened by the flanges to be well sealed for accurate flow measurement. Five liters (NaCl, $MgSO_4$, $CaCl_2$, Na_2SO_4 and $NaHCO_3$) salts were prepared with concentrations mentioned in 10 liters glass container by using dry solid salt and high purity (analytical grade) with ultra-pure deionized water.

The prepared salt solutions were lifted mixed by magnetic stirrer for a period of time up to 20 minutes to ensure complete solubility of

salt. Applied transmembrane pressure (TMP) was monitored by the pressure gauges at each ends of the ceramic membrane module and the pressure control was done manually by gradually closing the control valve at the discharge part of membrane module to the required limit and opening the control valve at the charge part to the required level to obtain the required transmembrane pressure (TMP) while maintaining a steady flow rate as required. Flow rate of the system was monitored by the flowmeter fixed at 140 l/h (1 m/s) by the manual regulating valves. The diaphragm high pressure pump was turned on and the required applied pressure was fixed by regulating the back pressure valve at (0.5) bar for about 15 minutes. During this period the permeate and rejection fluxes were constantly monitored to make sure that the system is steady after getting rid of all the air bubbles may have occurred inside the system. For every pressure step period, the flux of permeate was determined by using a digital balance.

In flux – pressure profile (step by step) method where the pressure was increased, associated flux of permeate was determined, the filtration period at every transmembrane pressure was 30 minutes as fixed intervals prior to the onset of nonlinearity in the increasing of permeate flux, that was indicate of critical flux (J_{crit}) after that (15 min) time steps were used **(Chiu and James, 2005)**, the critical flux was the average of the critical flux value of the first and the last time dependent step. When the period of filtration for the first pressure was finished, then the pressure was raised in increments of 1.0 bar until the maximum pressure of 15 bar was achieved. It is important to mention that the collected permeate flux was returned to the major glass container of process after any step. Flux measurements of the permeate showed a

good reproducibility after every experiment of filtration were repeated at least twice for somewhat non corresponding experiment results.

3.4.5 Produced Water From Bazargan Oilfield

A quantity of 15 liters of produced water from Bazargan oilfield in Misan southern Iraq were brought and a sample was analyzed before treatment as shown in the Table 3.10.

Table 3.10 Tests of Produced Water

Oil	TOC	TDS	Ca^{+2}	Mg^{+2}	Na^{+}
769 mg/l	3920 mg/l	63900 mg/l	5144.5 mg/l	711.45 mg/l	28637.6 mg/l

The experimental operation starts by filling the feed tank (reservoir) with ten liters of oilfield produced water and open circulation valve. The pump is run to start circulating the produced water around the tank. It must be insured that the permeate and rejection valves are open then after that the tubular module feed line was closed and the flat module feed line was opened (see **Fig. 3.5 b**).

Produced water was passed through the MF (0.3 µm) at flow rate 140 l/h and TMP 1 bar. After that the MF membrane was replaced with UF membrane (0.004 µm) and produced water out from MF membrane was passed across the UF membrane at flow rate 140 l/h and TMP 2 bar. Then, the flat module feed line was closed and tubular module feed line was opened. The produced water out from the UF membrane was passed through 0.9 nm TiO_2 NF membrane at flow rate 280 l/h and TMP (1-15) bar. The produced water out from NF membrane was treated with RO membrane. The applied pressure was 60 bar and flow rate 4.8 l/min. The permeates of MF, UF, NF and RO were collected and submitted to many tests such as: conductivity, TDS, TOC and oil content. The system of RO located at Ministry of Science and Technology/ Environmental and Water Directorate. Photo of RO system are shown in **Fig. (3.14)**.

Figure 3.14 Bench Scale of Flat Plate RO Membrane Filtration System.

3.4.6 Regeneration Procedure of Titanium Dioxide Membrane

The major approach that has been used in this work for regeneration and cleaning of the ceramic titanium dioxide membrane after every fouling (for rejection experiments and critical flux experiments) can be explained in this part. After the installation of the new tubular ceramic titanium dioxide nanofiltration membrane in the filtration rig, the ultra-pure water (deionized) was used as a feed solution and recirculate at applied transmembrane pressures of 1, 2, 3, 4, 5, 6, 7, 8, 9, 10, 11, 12, 13, 14 and 15 bar. The permeability of the pure water was determined for every pressure in order to estimate a relation (ordinarily linear) between the permeate flux of deionized water and the applied increment transmembrane pressure. Diaphragm regeneration pump in a low pressure was used to carry the regeneration process. After the completing of every fouling or rejection experiment, the sodium hydroxide solution (NaOH) 0.1% (w/v) and nitric acid

solution 0.1 % (v/v) were prepared to be used as the chemical cleaning agent for titanium dioxide membrane regeneration. Sodium hydroxide solution with a five-liter volume was used as a feed solution and recirculate in the filtration rig for two hours with the permeate line closed. Nitric acid solution with a five-liter volume was used as a feed solution and recirculate in the filtration rig for two hours with the permeate line closed.

Then the rig was rinsed with ultra-pure water until the value of the pH returned to 7.0. In order to ensure that the experiments have good reproducibility, the permeate flux was determined by using ultra-pure water after each cleaning operation. Measurement of each critical flux was repeated twice and the average value is reported her. Measurements of all critical flux showed good reproducibility. At the starting of the regeneration process the pressure was fixed to be 0.25 bar to assure that the system is steady after obtaining rid of air bubbles which may have existed within the system. Subsequently, the pressure was raised to 1.0 bar and the flux of permeate was monitored and determined every 20 minutes till reaching the same pure water flux of permeate at the pressure of 1.0 bar. The pH and conductivity of retenate and permeate of the ultra-pure water flux was checked and monitored to be cleaned from ions. The process of regeneration was carry out at room temperature at a steady flow rate of 140 l/hr. In order to evaluate the efficiency of regeneration, new ultra-pure water was used as a feed solution in the filtration rig and recirculate at applied transmembrane pressures of 1, 2, 3, 4, 5, 6, 7, 8, 9, 10, 11, 12, 13, 14 and 15 bar. The permeability of the pure water was determined for every pressure to estimate a relation (commonly linear) between the permeate flux of deionized water and the applied increment transmembrane pressure and

compare the permeation of deionized water before and after the process of regeneration. In this work changing in the flux of ultra-pure water cross the clean membranes were insignificant.

3.5 Instruments and Devices

● Zeta Potential Analyzer (Zeta Plus)

The Zeta Plus is an automatic instrument designed for using with suspensions of particles or solutions of macromolecules. Generally speaking particles with diameters from 10nm to 30μm (depending on particle density) can be measured. The software for instrument control and data analysis is written for use in the Microsoft Windows environment though a DOS version is also available. The technique employed - electrophoretic light scattering (ELS) - is based on reference beam (modulated) optics and a dip-in (Uzgiris type) electrode system. It is also known as Laser Doppler Velocimetry (LDV).

Zeta potential and particle size were measured using zeta potential analyzer model: zeta plus supplied by Brookhaven Instruments- USA. The specifications of device are listed in Table 3.11.

Table 3.11 Specification of Zeta Plus

Specifications	Value
Serial No.	21521
Zeta Potential Range	-150 to + 150 mV
Speed Typically	1 to 2 minutes
Accuracy	± 2%
Repeatability	± 2% with dust free samples
Laser	35 mW solid state laser, red (660 nm wavelength)
Complies with BRH 21CFR 1040	10 as applicable
Optional	50 mW green (532nm)laser, ~10x sensitivity incr
Temperature Control	6 °C to 74 °C in steps of 0.1 °C
Small Sample Volume	1.5 ml
Power	100 – 240 V 50/60 Hz

● Inductively Coupled Plasma (ICP)

Is used to measure ions (Na^{+}, Ca^{+2}, Mg^{+2}, K^{+}) even in small concentration, the method of measuring depends on addition of atoms of elements by shedding high thermal energy which formed as a result of ionize of Argon gas, which used as energy source. Argon gas ionized when it passed through inductive cell with heat generate called (plasma). The process summarizes by preparing clean standard solution that the elements which we want to measure in concentration as predicted of the concentration solution`s range, their amount was estimated by using inductively coupled plasma (ICP).

ICP (Inductively coupled plasma device from Agilent Technologies 700 Series ICP-OES-Company, U.S.A.). The specification of ICP device is listed in Table 3.12.

Table 3.12 Specification of ICP Device

Specifications	Value
Serial NO.	AUL3210072
Gas requirements	Argon Nitrogen
Purity	99.996%
Oxygen	<5 ppm
Nitrogen	<20 ppm
Water vapor	<4 ppm
Permissible pressure range	400-600 kPa (57 to 88 psi)
Recommended pressure	550 kPa (80 psi) regulated
Argon flow	12.75-21 L/min
N and Ar pressure range	410 kPa – 690 kPa (60 psi – 100 psi)
Max Ar flow	32 L/min (1.13 ft^3/min)
Voltage selector behind side panel	220/240 ±10% 50/60 Hz ±1Hz 5.0 KVA

● Ion Chromatography

The device which we used, is international, made by (metrohm Company) Model 883. Basic IC plus (Swiss origin). It was processed to environment department from Briatist Company (For middle copperchase company east). It was used to measure chloride ions (Cl^-) and sulphate ions (SO_4^{-2}). The specifications of IC are listed in Table 3.13.

Table 3.13 Specification of IC Device

Specifications	Value
Serial NO.	1883000123115
Type	1.883.0020
V	100-240 V
F	50-60 Hz
P	300 W

● X-Ray Fluorescence (XRF)

The device used to elemental analyze of alterative electrodes (silver and 4% gold) was X-ray florescence (XRF), SPECTRO Analytical instruments, model XEPOS, Germany. The specifications are listed in Table 3.14.

Table 3.14 Specification of (XRF) Device

Specifications	Value
Type	76004814 S/N 4L0058
Instr. Nr.	113443
Input	115/230 auto VAC 47-63 Hz
Power	100 VA

● SEM – EDXS

The device that was used to inspect the ceramic 0.9 nm TiO_2 NF was (SEM Vega 3, Czech Republic) worked at an accelerating voltage

of 20-30 KV. Furthermore an elemental analysis was measured by using an energy dispersive X-ray spectrometer (EDXS, Amertek Inc, Paoli, PA, USA).

The tests of (SEM – EDXS) were conducted at the Ministry of Science and Technology / Materials Research Center.

● **High-Performance Liquid Chromatography (HPLC)**

Device that was used to measure glucose (HPLC, model VQC1) supplied by SHIMADZU, Japan. HPLC device consists of four basic parts, which are (Degassing, pump, UV and system control) and contains three supplements (Ejector, Colum separator and Mixer). The specifications of HPLC device are listed in Tables 3.15.

Table 3.15 Specification of Basic Parts of HPLC Device

Item NO.	Name of part	Specification	Value
1	DEGASSING UNIT	Model	DGU-20A5R
		CAT. NO.	28-45019-42
		Serial NO.	L20705001931 IX
		Made in USA	
		Shimadzu Coporation Kyoto Japan	
2	Pump	Model	LC-20AD
		CAT. NO.	228-45000-38
		Serial NO.	L20105027316 AE
		220 – 240 V ~ 50 – 60 Hz 150 VA	
		Made in Japan	
		Shimadzu Coporation Kyoto Japan	
3	UV	Model	SPD-20A
		CAT. NO.	228-45003-38
		Serial NO.	L20135020277 AE
		220-230/240 V ~ 50-60 Hz 160 VA	
		Made in Japan	
		Shimadzu Coporation Kyoto Japan	
4	Control system	Model	CBM – 20A
		CAT. NO.	228-45012-38
		Serial NO.	L20235017865 CD
		220-240 V ~ 50-60 Hz 400 VA	
		Made in Japan	
		Shimadzu Coporation Kyoto Japan	

The tests were conducted at the Ministry of Industry and Minerals / Corporation of Research and Industrial Development / Veterinary Drugs Research and Production Center.

● pH meter

Measurement of the pH value was conducted by using bench pH meter type pp-203 by EZODO, Japan. The specifications of the pH meter are listed in Table 3.16.

Table 3.16 Specification of pH Meter Device

Specification	Value
Range	0~14.00 pH
Accuracy	± 0.01
Resolution	0.01 pH
Compensation	MTC: 0~100^{o} C
Battery	9 V (6F22)
Calibration	pH 4.00, 7.00, 10.00
Multi-function	Store/Recall, Min/Max
Dimensions	Meter: 96×120×46mm (folded)
Weight	Meter: 260 g (with battery)
Serial No.	023653
Made in Japan	

● Conductivity and Total Dissolve Solid (TDS)

A digital conductivity (µs/cm) and total dissolved solid (mg/L) were conducted by using bench meter type inoLab Cond 7110 supplied by WTW, Germany. The specifications of the meter are listed in Table 3.17.

Table 3.17 Specification of Conductivity and (TDS) Device

Specification	Value
TDS rang (ppm)	0 – 3000
Temperature ^{o}C	0 – 80
Accuracy (%)	±2
Power supply (Volts)	6

● Digital Balance

A digital balance type AZ214 supplied by Sartorius Weighing Technology Gm bH, Germany was used in preparation of salts solutions measurements and in the permeate flux measurements. The specifications of balance are listed in Table 3.18.

Table 3.18 Specification of Digital Balance

Specification	Value
Serial No.	28103699
Weighing range (g)	0.001-210
Operation Temperature (^{o}C)	0-40
Power supply (volts)	115/220

● Pre Treatment Cartridge

A filter cartridge BOECO 80910, type 50136990, Thermo Fisher, Germany was used to produce ultra-pure water with conductivity 0.05 μs/cm. Ultra-pure water was used for preparing salts solutions and cleaning the system and NF membrane. The specifications of filter cartridge are listed in Table 3.19.

Table 3.19 Specification of Treatment Cartridge

Specification	Value
Serial number :	41397207
Power :	60 W
Voltage :	110-240/5060 Hz
Pressure max :	6 bar
Performance l/h :	6 l/h
Manufactured by :	Thermo Fisher SCIENTIFIC

● **Magnetic Stirrer**

Mixing of solution was carried out by magnetic stirrer, model No. HS-30, supplied by HumanLab Instrument Company, Korea. The specifications of the magnetic stirrer are listed in Table 3.20.

Table 3.20 Specification of Magnetic Stirrer

Specification	**Value**
S/N	S05P2128-04-02
Power	22 VAC, 50 Hz

● **milli-voltemeter**

Measurement of the electrical potential variance (ΔE) value was conducted by using bench milli-voltemeter type (Fluk corporation, 179 TRUE RMS MULTIMETER, U.S.A.).

● **Measuring Oil in Water (Oil Content Analyzer)**

Oil content in water samples were measured using oil content analyzer of model OCMA-350-A, HGS NO. GOCDOINP, POWER 100-240V 50/60Hz HORIBA, JAPAN.

● **Measuring Total Organic Carbon (TOC) in Water**

TOC content in water samples were measured using TOC content analyzer of type LPG408.99.00012, Serial-No. 1300353, power AC 100-240 V, 50/60 Hz, HACH, USA. The tests were conducted at Ministry of Science and Technology / Environmental and Water Directorate.

3.6 Experimental Design and Operating Conditions

The experiments carried out in this work were conducted for zeta potential in both methods (microelectrophoresis potential method and streaming potential method), rejection and critical flux. The applied operating conditions for the work are explained in Table 3.21.

Table 3.21 Zeta Potential, Rejection and Critical Flux Process Operating Conditions

Variable	Value
Zeta potential	Microelectrophoresis and streaming potential measurements
Type of salts	($CaCO_3$), (NaCl), (KCl), (Na_2CO_3), ($MgSO_4$), ($CaCl_2$), ($MgCl_2$), (Na_2SO_4) and ($NaHCO_3$)
Transmembrane pressure (TMP)	(1, 2, 3, 4, 5, 6, 7, 8, 9, 10, 11, 12, 13, 14 and 15) bar for rejection and critical flux (0.25, 0.5, 0.75, 1.0, 1.25, 1.5, 1.75 and 2.0) bar for streaming potential measurements
Concentration of salts	0.001, 0.005, 0.01, 0.015 and 0.1 M for common salts (5, 10, 13 and 50) $\times 10^{-5}$ M for $CaCO_3$
pH	3, 4, 5, 6, 7, 8 and 9
Flow rate / cross flow velocity	140 $l/m^2.hr$ = 1 m/s 280 $l/m^2.hr$ = 2 m/s

The images of the equipment used in the measurements and analysis of the experimental work are showed in the appendix B.

Chapter Four
Modeling and Simulation

In this chapter, Donnan steric pore model (DSPM) was applied to study the effect of concentration and transmembrane pressure (TMP)/permeate flux on rejection (R%) of sodium chloride as a reference salt and comparing this model (DSPM) with experimental result. In order to apply the Donnan steric pore model and employing the model to optimize and predict the performance of nanofiltration membrane needs the calculation of many significant parameters, such as the zeta potential, surface charge density (σ^2), effective pore radius (r_p), active layer thickness ($\Delta X/A_k$), effective charge density (X_i^m) and Donnan potential (Ψ_D) of ceramic titanium dioxide nanofiltration membrane by using the basic equations.

Donnan steric pore model was chosen for being a reasonable hypothesis and is considered the best and newer among the other models. In addition, Donnan steric pore model assumption are close to our working conditions. Therefore, it can be used to calculate results theoretically and compare them with experimental results. Experimental results and the calculations of the process, theoretical results and program used are showed in appendices (C and D).

4.1 Determination of Zeta Potential

4.1.1 Microelectrophoresis Method

The charged particles suspended in the electrolyte (see **Fig. 4.1**) are attracted towards the electrode of apposite charge, when an electric field applied across an electrolyte. Forces of viscous working on the particles incline to oppose this movement. When equilibrium is achieved between these two opposing powers, the particles move with fixed speed.

The velocity of particle is dependent on the following factor:

- Voltage gradient.
- Strength of electric field.
- Viscosity of the medium.
- Dielectric constant of medium.
- Permittivity of free space and zeta potential.

The Velocity of a particle in an electric field is usually referred to as its electrophoretic mobility. With this information we can get the zeta potential of the particle by using the Henry equation.

The Henry equation is **(Israelachvili, 2007; Kirby, 2010)**:

$$U_E = \frac{2\varepsilon_r \varepsilon_o \zeta f(k_a)}{3\mu} \quad (4.1)$$

Where:

ζ is zeta potential (V).

ε_r is Dielectric constant for water (75.8) at temperature 25 ^{o}C.

ε_o is permittivity of free space (8.854×10^{-12} C/V.m).

μ is viscosity of the water (0.89×10^{-3} pa.s) at temperature 25 ^{o}C.

U_E is electrophoretic mobility ($\frac{u}{E}$).

u is velocity of particle (m/s) in electrical field of strength E (V/m) and $f(k_a)$ is Henry`s function.

Determinations of zeta potential from electrophoretic are most generally made in moderate electrolyte concentration and aqueous media. In this case $f(k_a)$ is 1.5, and is referred to as the Smolwchowski

approximation **(Narong and James, 2006; Chiu and James, 2006; Ernst, et al., 2000)**.

The Smolwchowski equation is:

$$\zeta = \frac{3\mu U_E}{2\varepsilon_r\varepsilon_o z f(k_a)} = \frac{3\mu U_E}{2\varepsilon_r\varepsilon_o \times 1.5} = \frac{3\mu U_E}{3\varepsilon_r\varepsilon_o} = \frac{\mu U_E}{\varepsilon_r\varepsilon_o} \quad (4.2)$$

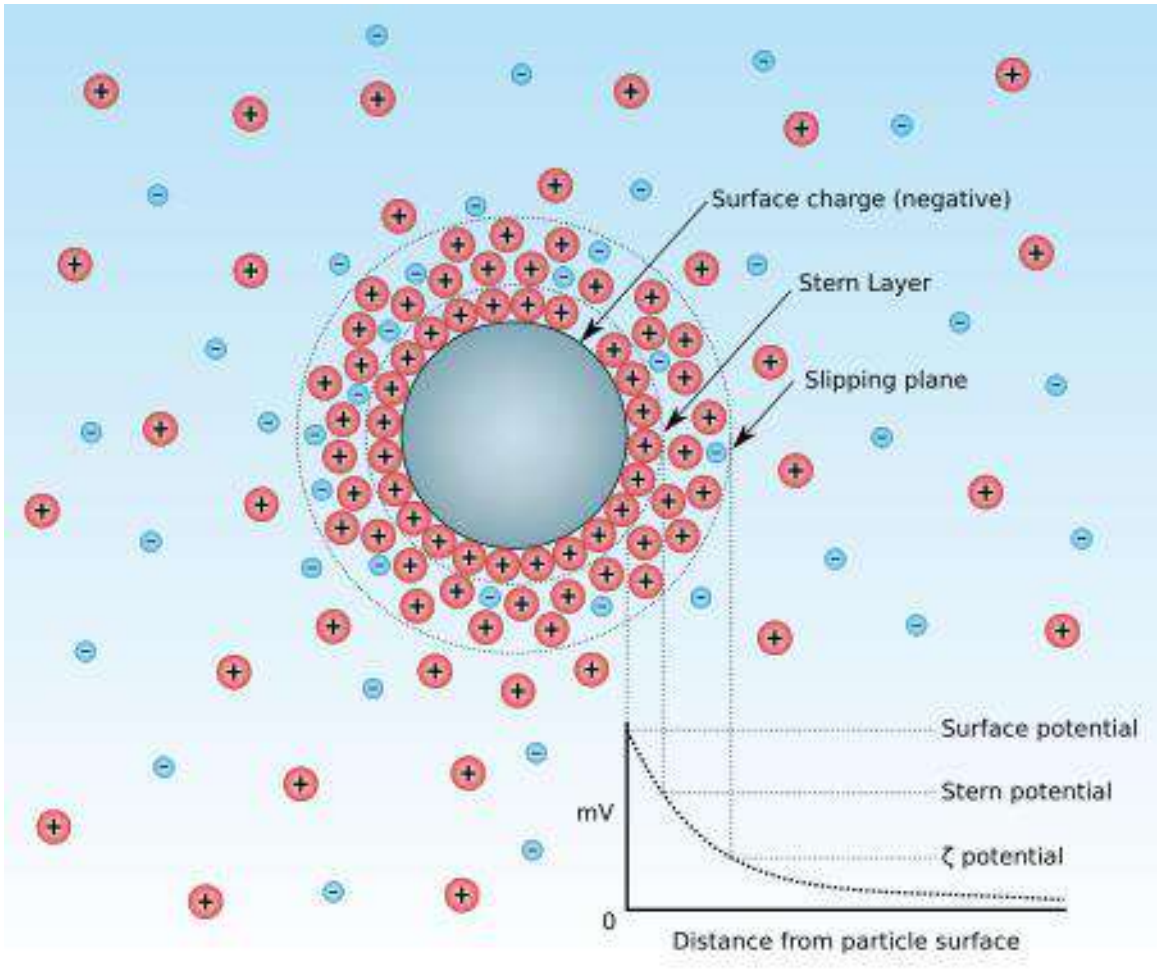

Figure 4.1. Diagram Showing the Potential Difference and Ionic Concentration Difference as a Function of Distance from the Charged Surface of a Particle Suspended in a Dispersion Medium (Kirby, 2010).

4.1.2 Streaming Potential Method.

The streaming current is generated by the motion of the diffuse layer with respect to the surface of solid produced by drop of a fluid pressure across the conduit. The current of conduction is then balanced by this

streaming potential. In a porous medium **(see Fig. 4.2 and Fig. 4.3)**, the fluid flux and the electric current density are coupled, so fluids moving across porous media create a streaming potential **(Jouniaux et al., 2000).**

The streaming potential rises linearly with the difference of fluid pressure which pushes the fluid flow, supplied that flow keeps laminar **(Boleve et al., 2007)**. The steady state coupling coefficient, C_s, of streaming potential is defined when the overall of current density is zero as flows:

$$C_s = \frac{\Delta E_{str}}{\Delta P_{TMP}} = \frac{\varepsilon_r \varepsilon_o \zeta}{\mu k} \quad (4.3)$$

With this knowledge we can obtain the zeta potential by application of Hilmholtz-Smoluchowski equation **(Afonso, 2006; Luong and Sprik, 2013; Peeters et al., 1999)**.

$$\zeta = \frac{\Delta E_{str}}{\Delta TMP} \frac{\mu k}{\varepsilon_r \varepsilon_o} \quad (4.4)$$

Here:

E_{str} is the streaming potential (V)

P is the applied transmembrane pressure (pa)

$(\frac{\Delta E_{str}}{\Delta P})$ is the slop of the streaming potential against applied transmembrane pressure $(\frac{V}{pa})$ and K is the solution conductivity (S/m).

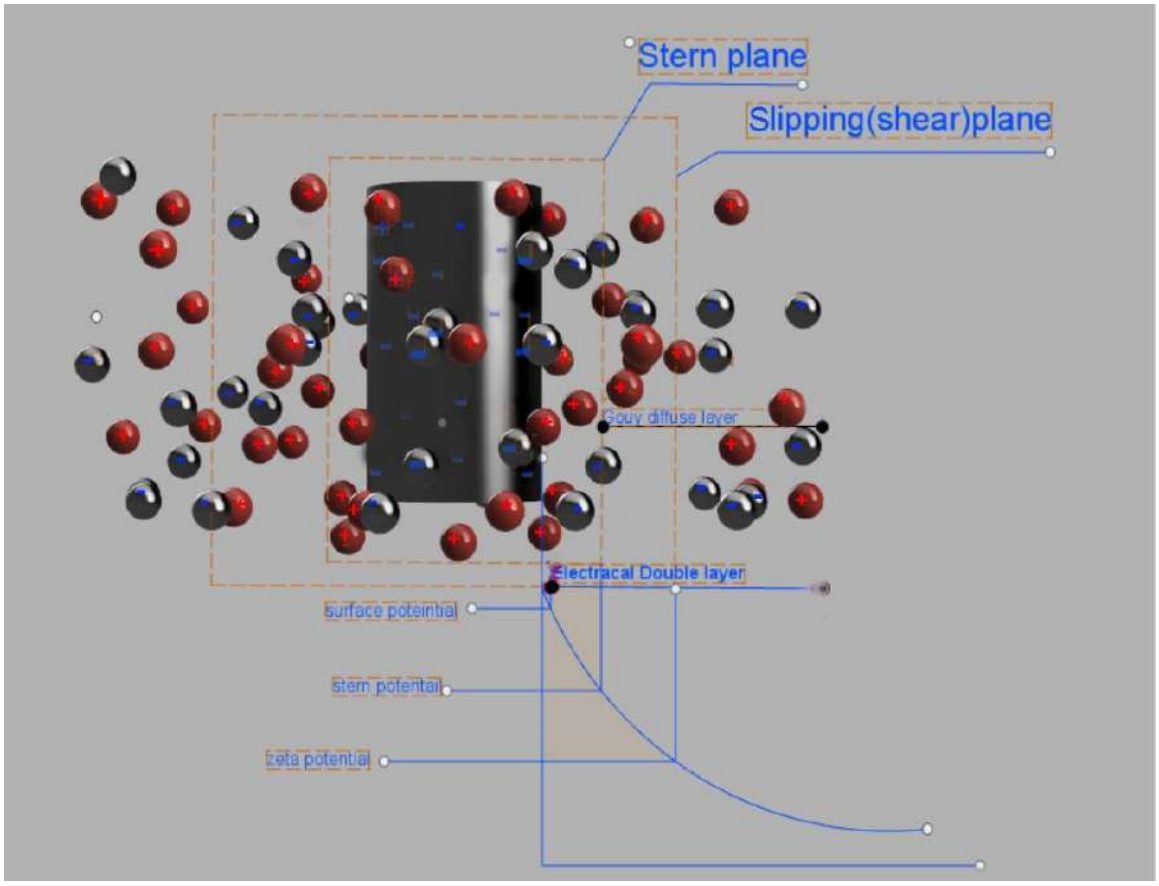

Figure 4.2 Schematic Representation of Electrical Double Layer (EDL) Formation in the Presence of Electrolytes.

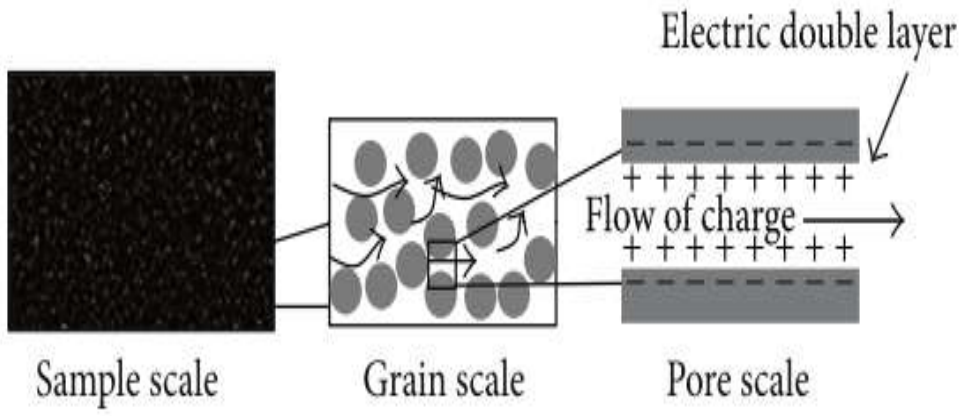

Figure 4.3 Represents the Porous Medium of the NF Membrane with Different Length Scales: Sample Scale, Grain Scale and Pore Scale (Luong and Sprik, 2013).

4.2 Donnan Steric Pore Model (DSPM)

The model is very significant in predicting the performance of membrane, understanding the mechanism of separation for different substances (for a certain NF membrane) can be described by using extended Nernst-Plank (ENP) equation, where it describes the change of solute concentration inside the membrane and the change between the permeate and feed concentrations, **(Ahmad, et al., 2005; Jesus and Jmaes, 2004; Serena, 2005).**

The extended Nernst-Planck equation can be represented as following **(Omar, et al., 2017)**.

$$J_i = -D_{i,p}\frac{dc_i^m}{dx} - \frac{z_i c_i^m D_{i,p}}{R_g T}F\frac{d\Psi^m}{dx} + K_{i,c}c_i V \qquad (4.5)$$

The first section of the right hand side of **Eq. (4.5)** represents transport due to diffusion, the second term represents the electric field, and the third term represents the convection respectively. The extend Nernst-Plank equation has been modified by coefficient of hydrodynamics in order to take the impact of limited pore size on both convection and diffusion into account. The nanofiltration membrane is usually considered as package of identical pores which diameter is much less than their length, so that both ions flux and volume flux can be considered as one dimensional. According to the approximation of no direct coupling between fluxes of ion and by using molar units for electrical potential, **(Garba, et al., 1999)** described the transport equation (ENP) for fluxes of ion across pores of nanofiltration membrane as determined in **Eq. (4.5)**.

$$D_{i,p} = D_{i,\infty}.K_{i,d} \qquad (4.6)$$

Where:

J_i is molar flux of species (mol/m^2s)

$K_{i,d}$ is hindrance factor of ionic diffusion (-)

$K_{i,c}$ is hindrance factor of ionic convection (-)

$D_{i,\infty}$ is molecular diffusion coefficient of ion i at infinite dilution (m^2/s)

$D_{i,p}$ is diffusion coefficient of ion (m^2/s)

c_i^m is ionic concentration inside pores of the NF membrane (mol/m^3)

V is solvent velocity (m/s)

x is axial position within the pore (m)

It must be noticed that ($K_{i,c}$ and $K_{i,d}$) are not dependent only on ratio of solute to pore size (λ_i), but usually on the radial location within pore. But, the impact of the finite pore size on both convection and diffusion can be perfect precisely evaluated by using the magnitudes of ($K_{i,c}$ and $K_{i,d}$) at the pore center only. The magnitude to that the finite pore size acts on the convection and diffusion fluxes of solute through pores depend essentially on geometry of pore. For a cylindrical geometry (supposing that they can be applied to charge species) the values of $K_{i,c}$ and $K_{i,d}$ can be determined as a function of ionic radius/ pore radius ratio for ($0 < \lambda_i \leq 0.8$) **(Bowen, et al., 2002)**.

$$K_{i,d} = 1.0 - 2.3\left(\frac{r_i}{r_p}\right) + 1.154\left(\frac{r_i}{r_p}\right)^2 + 0.224\left(\frac{r_i}{r_p}\right)^3 \quad (4.7)$$

$$K_{i,c} = (2 - \emptyset_i)(1.0 + 0.054\left(\frac{r_i}{r_p}\right) - 0.988\left(\frac{r_i}{r_p}\right)^2 + 0.441\left(\frac{r_i}{r_p}\right)^3 \quad (4.8)$$

$$\emptyset_i = (1 - \lambda_i)^2 \quad (4.9)$$

$$\lambda_i = \frac{r_i}{r_p} \quad (4.10)$$

Where:

$\emptyset_i$ is ionic steric partition coefficient (-)

r_i is ion radius (m)

r_p is pore radius (m)

Based on Boltzmann distribution the initial ion concentration inside NF membrane can be determined using following equation **(Davies and Rideal, 1961; Wahab, et al., 2002)**.

$$c^m_{i(x=0)} = \frac{\gamma_{i,sol}}{\gamma_{i,pore}} \phi_i C_i^{feed} exp\left(-\frac{z_i F}{R_g T} \Psi_{Don}\right) \quad (4.11)$$

The concentration of ion in permeate can be estimated from the following equation **(Omar, et al., 2017, Wahab, et al., 2002).**

$$C_i^{permeate} = \frac{\gamma_{i,pore}}{\gamma_{i,sol}} \frac{c^m_{i(x=\Delta x)}}{\phi_i exp\left(-\frac{z_i F}{R_g T} \Psi_{Don}\right)} \quad (4.12)$$

At x=0 → $C_i = C_i^{feed}$ at x=Δx → $C_i = C_i^{permeate}$

Where:

$C_i^{permeate}$ is ionic concentration of the permeate (mol/m^3)

T is temperature (K)

$\gamma_{i,sol}$ is activity coefficient of ion in the interface of solution side (-)

$\gamma_{i,pore}$ is pore activity coefficient of ion in the interface of pore side (-)

R_g is constant of universal gas (J/mol K)

$\Delta\psi_{Don}$ is Donnan potential (V)

To guess the effectives and the productivity of the ions separation from tested solutions it is required to collect mathematical model which described this process. The mathematical model was developed for one type of electrolyte system, i.e. charged solutes and a negatively charged membrane. The charged electrolyte system in the salt solution contains one cation and one anion species. The existence of an anion and action will cause the Donnan influence and consequently impact the separation performance together with the effect of steric.

The extended Nernst-Plank equation contains all three significant aspects in mechanisms of transport a cross the NF membrane: convection electro-migration and diffusion **(Garba, et al., 1999; Hilal, et al., 2004; Labbez, et al., 2003)**.

Four assumptions were made

- The solution is assumed ideal.
- All the ions that exist in the membrane are transportable.
- The membrane charge capacity is uniform.
- The Donnan equilibrium happens at the feed interface/ membrane and the membrane/ permeate interface.

The model development is based on two approaches: the hydrodynamic approach and the irreversible thermodynamic approach, that are governed by both charge influence and the steric effects is caused by the difference between the solute ion radius and the effective membrane pore radius, whereas the Donnan impact is actually the result of the charge polarities between the solute and the membrane. These combined impacts effect the selectivity of the membrane. The electrical potential gradient and

the concentration gradient cause ion diffusion through NF membrane **(Bowen and Mohammad, 1998, Bowen and Julian, 2002)**.

In order to depict the mass transport within the effective skin layer of nanofiltration membranes, the ENP equation is the more commonly and efficient used. Solving the ENP equation demands knowing the conditions of boundary at the feed side (pore inlet) and permeate side (exit). For a nanofiltration membrane, the present study discussed the most common model which has normally been used to estimate the conditions of boundary at membrane-interface partitioning. The rejection in NF membrane is often modelled by using the following three steps model (**Daniele and Serena, 2002**).

- The partitioning distribution between the pore entrance and bulk at the feed side.
- The transport inside the pore is described with the extended Nernst-Plank equation.
- The partitioning distribution between the bulk at permeate side and the pore existence.

The ion partitioning distribution between the bulk solution and the pore and the ion partitioning distribution at the side of permeate can be effected by different parameter such as steric partitioning and the Donnan equilibrium **(Oatley, et al., 2005; Richard and Wahab, 1998)**.

4.2.1 Determination of Effective Pore Size and Active Layer Thickness of NF Membrane

There are many suggested procedures in the literature to characterize the membrane effective pore radius (r_p). The present study will estimate the

effective pore radius of the ceramic nanofiltration membrane based on the one of best method consist of transport equations of solutes inside membrane pores, the Hagen-Poiseuille equation and permeation test of uncharged solute (glucose) **(Bowen and Mohammad, 1998; Lee et al., 2008).**

Pore size of the membrane is an important NF membrane characteristic to determine the effect of the solute size on its rejection. To calculate the membrane pore size, the Donnan steric pore partitioning model (DSPM) was used.

(Bowen et al., 1997) proved that the rejection evaluations of an uncharged solute gives the characterization of a membrane in terms of two factors : the effective ratio of membrane thickness to porosity ($\Delta x/A_k$) and the effective pore radius (r_p). The extended Nernst-Plank equation (ENP) composes the main for description transport of solute across NF membrane. It characterizes transport in terms of diffusion with the solute action flow or pressure gradient, migration with the effect of an instantaneously rising field of electric, and the action of the solute concentration.

The thickness divided by porosity and the pore size can be estimated by using the permeation test of the uncharged solute **(Ahmad, and Ooi, 2006**) For neutral or uncharged solutes (such as glucose), there will be no term of electrostatic thus, only diffusion and convection flows influence the transport of solutes through the NF membrane. So, the flux of solute may be written as follows:

$$J_i = -D_{i,p}\frac{dc_i^m}{dx} + K_{i,c}c_i^m V \qquad (4.13)$$

Rahi, et al., (2010) qualified glucose as the most considerable neutral sugar. While **(Bowen, and Mohammad, 1998**) showed that in such narrow

pores as these in NF membrane, the glucose has an acceptable range of rejection. Satisfactory to get an expression for the rejection of solute, **Eq. (4.13)** is combined through the membrane with concentrations of solute at (x=0) that is on the bulk side of the membrane and ($\Delta x = x$) that is on the permeate side of the membrane. **Eq. (4.13)** can be written in terms of rejection (R) as follows **(Labbez, et al., 2003)**

$$R_i = 1 - \frac{C_i^{permeat}}{C_i^{feed}} = 1 - \frac{K_{i,c}\emptyset}{1-\exp(-pe*)[1-\emptyset K_{i,c}]} \quad (4.14)$$

Here:

pe* is the number of peclet, that can be described as follows:

$$pe^* = \frac{K_{i,c}}{K_{i,d}} \frac{J_v \Delta x}{D_{i,\infty} A_K} \quad (4.15)$$

Where, A_K is the NF membrane porosity (dimensionless).

Moving of solute in free solution encounter a drag force extend by the solvent, so when solutes move in restricted spaces (pores of membrane), the drag is modified and the transport may be considered to be hindered **(Silva, et al., 2005)**. Stokes radius of ion (r_i) can be determined from the well-known Stocks-Einstein equation as follows **(Ahmad, and Ooi, 2006; Wang et al. 1995)**.

$$r_i = \frac{K_B T}{6\pi\mu D_{i,\infty}} \quad (4.16)$$

K_B is Boltzmann constant (1.3806×10^{-23})

Diffusion coefficient of the molecular of the glucose solute at infinite dilution equals to 0.69×10^{-9} (m^2/s) **(Omar, et al., 2017)**. Thus by applying **Eq. (4.16)**, the stocks radius of glucose solute equals to 0.31×10^{-9} (m) **(Wang et al. 1995)**.

The equation of Hagen-Poiseuille overs the connection between the applied pressure across the membrane and the pure water flux (J_w) as follows **(Ahmad and Ooi, 2006**):

$$J_w = VA_K = \frac{r_p^2 P}{8\mu(\frac{\Delta x}{A_K})} \quad (4.17)$$

The effective pore radius (r_p) and equivalent active membrane thickness ($\Delta x_e = \frac{\Delta x}{A_K}$) are calculated by using **(Eq. 4.14 and Eq. 4.17)** with the experimental results obtained from the permeate flux as function of (TMP/8μ). The transmembrane pressure TMP was determined as follows **(Ahmad and Mariadas, 2004; Avula et al., 2009; Blöcher et al., 2002; Oktay et al., 2007; Sarkar et al., 2009).**

$$TMP = \left(\frac{P_{inlet}+P_{outlet}}{2}\right) - P_{permeate} \quad (4.18)$$

Where the pressure at the side of permeate was supposed to be equal to zero, and as the result the transmembrane pressure (TMP) would be as follows:

$$TMP = \left(\frac{P_{inlet}+P_{outlet}}{2}\right) \quad (4.19)$$

4.2.2 Determination of Donnan Potential and Surface Charge Density

Based on **(Amer, 2013; Peeters, et al., 1999)** the correlation between the net charge density of surface (σ^s) for the NF membrane and the zeta potential of the membrane for low potentials (generally below 50 mV) can be estimated by using the simplified Grahame equation:

$$\sigma^s = \frac{\varepsilon_r \varepsilon_o \zeta}{K^{-1}} \quad (4.20)$$

Where:

σ^s is surface charge density, (C/m^2)

K^{-1} is the Debye length (m) **(Sema, et al., 2013)**

$$K^{-1} = \sqrt{\frac{\varepsilon_r \varepsilon_o K_B T}{2000 e^2 I N_A}} \quad (4.21)$$

Where:

N_A is Avogadro's number (6.02×10^{23} mol^{-1})

I is concentration (strength of ionic)

e is magnitude of the electron charge (1.6022×10^{-19} C) **(Jawor and Hoek, 2009**)

$$I = \frac{\Sigma z_i^2 c_i}{2} \quad (4.22)$$

Where**:**

z_i is ion valiancy

c_i is ion concentration.

For aqueous solution of NaCl, K^{-1}= 0.3 nm at 1.0 M and 30.4 nm at 10^{-4} M **(Israelachvili, 2007).**

The Donnan equilibrium must be obtained in order to achieve the conditions of electro-neutrality of the system (for cylindrical pores membrane **(Chein, et al., 2009)**); this can be written as follows:

$$z_f c_f + \sum_{i=1}^{N} z_i c_i = 0 \quad (4.23)$$

where (f) indicates the strongly bound on the pore wall. Based on the Boltzmann distribution, the ion concentration distribution c_i of valence z_i can be written as **(Davies, et al., 1961)**:

$$c_i = C_{i,bulk}\ exp\left(-\frac{z_i F}{R_g T}\Delta\psi_{Don}\right) \quad (4.24)$$

By selecting ion as the reference, the well-known expression for the Donnan potential of the membrane surface (in volt) can be determined based on the bulk concentration C_i,bulk of every ion and the effective membrane fixed charge concentration from substituting and solving of **Eq. (4.23)** and **Eq. (4.24)** as follow **(Amer, 2013; Chein, et al., 2009)**:

$$\Delta\psi_{Don} = \frac{R_g T}{F} sinh^{-1}\left(\frac{z_f X^m}{2C_{i,bulk}F}\right) \quad (4.25)$$

Eq. (4.25) applied only for 1:1 electrolytes with bulk concentration of C_i, bulk (mol/l) and valance z_f **(Chein, et al., 2009)** whereas the effective charge density X^m (mol/m^3) can be determined according to the value of the NF membrane surface charge density σ^s (C/m^2) as shown in following equation :

$$X^m = \frac{2\sigma^s}{r_p F} \quad (4.26)$$

Where:

X^m is electrical charged groups concentration on the surface of membrane (mol/m^3) and F is Faraday constant (964867 C/mol) **(Dukhin, et al., 2004)**.

4.3 Solution of Mathematical Model

The Runge-Kutta technique forth order was used to determine the difference inside the nanofiltration membrane. At the first, the initial concentration of permeate was assumed to be equal to concentration of feed (C_i^{feed}) in order to determine the initial value of the ion concentration inside the membrane (c_i^m). According to Boltzmann distribution the initial ion concentration inside NF membrane was determined by using **Eq. (4.11)** The

Substitution of **Equation, 4.6** in **Equation 4.5** and rearrangement yields concentration gradient **(Bowen and Mohammad, 1998)**.

$$\frac{dc_i^m}{dx} = \frac{J_v}{D_{i,p}A_k}\left(K_{i,c}c_i^m - C_i^{permeate}\right) - \frac{z_i c_i^m}{R_g T} F \frac{d\Psi^m}{dx} \quad (4.27)$$

Potential gradient can be estimated using the following equation **(Wahab, et al., 2002).**

$$\frac{d\psi^m}{dx} = \frac{\sum_i^{n=1}\frac{z_i J_v}{D_{i,p}}\left(K_{i,c}c_i^m - C_i^{permeate}\right)}{\frac{F}{R_g T}\sum_{i=1}^{n} z_i^2 c_i^m} \quad (2.28)$$

Eq. (4.28) was used to estimate potential gradient inside the membrane, where it was substituted into **Eq. (4.27)** to calculate concentration gradient (dc_i^m/dx) inside the membrane **(Bowen and Mukhtar, 1996; Palmeri, et al., 1999). Eq. (4.12)** was used to estimate $C_i^{permeate}$

This study concerned with the separation of solutes from solution solute (i) is given in the following equation **(Omar, et al., 2017)**.

$$R_i = \left(1 - \frac{C_i^{permeat}}{C_i^{feed}}\right)100\% \quad (4.29)$$

Here, C_i^{feed} ($C_{i,f}$) is the solute (i) concentration in the feed and $C_i^{permeat}$ ($C_{i,p|}$) is the solute (i) concentration in the permeate (mol/m^3).

For each ion, the difference ratio between the new concentration of permeate and assumed old permeate concentration at the first of the program was determined as follow:

$$ratio = \frac{C_{i,old}^{permeate} - C_{i,new}^{permeate}}{C_{i,old}^{permeate}} \quad (4.30)$$

If the error in the mentioned ratio was lower than or equal to (10^{-3}), then; end the program and determine the rejection of each ion for each flux according to its feed concentration from **Eq. (4.29)**.

In case of not obtaining the mentioned error condition, then; use the under relaxation factor for every ion to recalculate the new concentration of permeate in the following relationship and continue solving:

$$C_{i,new}^{permeate} = relax \times C_{i,old}^{permeate} + (1 - relax) \times C_{i,new}^{permeate} \quad (4.31)$$

The average calculation for integration the ordinary differential equation (ODE) model programmed using Fortran 95.

Ion permeation across NF membrane was described by **Eqs. (4.27), (4.28), (4.11) and (4.12)**. **Eqs. (4.27)** and **(4.28)** were integrated across the active layer thickness of the nanofiltration membrane and the interned solute concentrations ($C_{i,1}$) is linked to the bulk feed concentration ($C_{i,f}$) at the interface of feed/membrane and the internal solute concentration ($C_{i,N}$) is linked to the concentration of permeate ($C_{i,p}$) at the interface of membrane/permeate through **Eq. (4.27)**. The permeation of ions across the active layer of membrane is demonstrated in **Fig. (4.4)**.

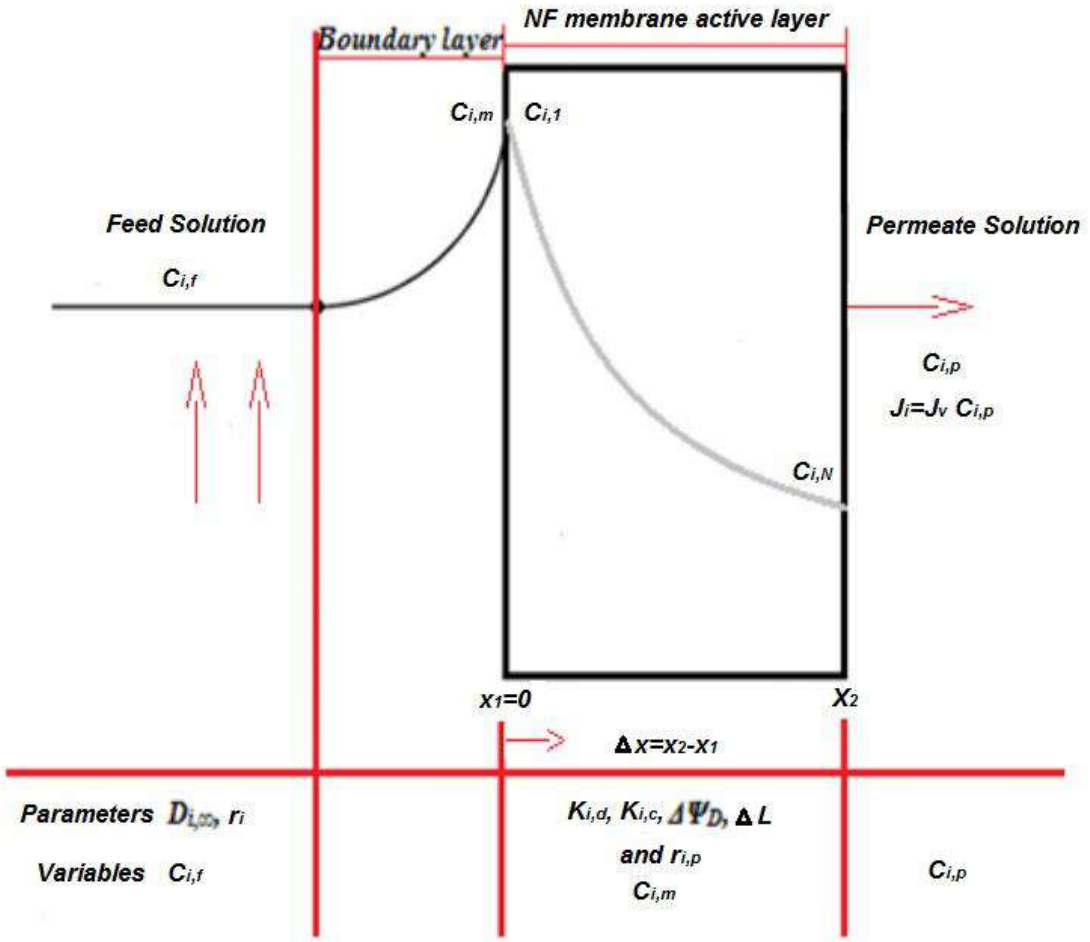

Figure 4.4 Ion Transport through Nanofiltration Membrane, (Vítor and Ana Maria, 2008).

The Runge-Kutta method can be used to integrate the ordinary differential equation (ODE) at highly reasonable accuracy **(Press, et al., 1992; Vetterling, 1992)**.

The step size (h) basically depend on equivalent membrane active layer thickness (Δx_e) and the chosen number of steps (n_{steps}) as represented in the following:

$$h = \frac{(X_2 - X_1)}{n_{step}} \tag{4.32}$$

Where, x_2 and x_1 represent the equivalent active layer thickness (Δx_e) at ($x = \Delta x$) and at ($x = 0$) respectively. Number of iteration (or step) 200, under relaxation factor of 0.8, with error ratio less than or equal to (10^{-3}).

Runge-Kutta method was used to integrate **Eqs. (4.27)** and **(4.28)**. The feed concentration ($C_{i,f}$) with **Eq. (4.11)** was used to determine the initial concentration inside the membrane ($c_{i,1}$) and the integrations of **Eqs. (4.27)** and **(4.28)** were used to determine of ($c_{i,N}$). Then from the determine of ($c_{i,N}$) and the application of **Eq. (4.12)** the evaluate of the permeate concentration ($C_{i,p}$) was determined. Then the ion rejection was determined using **Eq. (4.29)**. In order to integrate **Eq. (4.27)**, it need to have a value of $d\Psi/dx$, a calculation that demands a magnitude of the permeate concentration ($C_{i,p}$). Therefore it is logic to solve the model in an iterative function using an initial assumption for the value of the permeate concentration ($C_{i,p}$). Subsequently it was assumed to be equal to the initial feed concentration ($C_{i,f}$) that implied the rejection does not happen.

The hindered diffusivity ($K_{i,d}$), the hindrance factor for concentration ($K_{i,c}$) were calculated by using **Eqs. (4.7)** and **(4.8)** respectively. The solution was supposed to be dilute, as a result the activity coefficient to be calculated inside the membrane by effective charge density of membrane, would be equal to unity. The thickness of membrane and the pore size of membrane were determined experimentally.

The theory of Donnan steric pore partioning model (DSPM) has been presented in details by **(Bartels, et al., 2008; Lin, et al. 2006; Weber, et al., 2003)**. The basic equations used in the (DSPM) are summarized in **Table (4.1)**, allow for estimation of ions transport through the NF membrane taking

into account the selectivity of membranes evaluated by the rejection (equation).

In this study, a computer program has been suggested based on the Donnan steric pore model for describing the one dimensional transport for a sodium chloride 0.01 M as reference solution (the univalent single solute) across nanoporous media.

The program was run using (0.01 M) NaCl solutions as a feed concentration for changed permeate volume flux (m/s) at each pressure step from 1.0 to 15.0 bar. The FORTRAN/95 program codes used is given in Appendix (D).

Table 4.1 shows the main equations that have been used in the present work.

Table 4.1 Summary of the ion Transport Equations used for Modelling (DSPM) Model

The extender Nernst-Planck equation $J_i = -D_{i,p}\frac{dc_i^m}{dx} - \frac{z_i c_i^m D_{i,p}}{R_g T}F\frac{d\Psi^m}{dx} + K_{i,c}c_i V$ $D_{i,p} = D_{i,\infty}.K_{i,d}$	4.5 4.6
Sub **Equation 4.5** in **Equation 4.6** and rearrangement yields **Equation 4.27** Concentration gradient: $\frac{dc_i^m}{dx} = \frac{J_v}{D_{i,p}A_k}\left(K_{i,c}c_i^m - C_i^{permeate}\right) - \frac{z_i c_i^m}{R_g T}F\frac{d\Psi^m}{dx}$	4.27
potential gradient: $\frac{d\psi^m}{dx} = \frac{\sum_i^n = 1\frac{z_i J_v}{D_{i,p}}\left(K_{i,c}c_i^m - C_i^{permeate}\right)}{\frac{F}{R_g T}\sum_{i=1}^n z_i^2 c_i^m}$	4.28
Steric and Donnan effects: $c_{i(x=0)}^m = \frac{\gamma_{i,sol}}{\gamma_{i,pore}}\phi_i C_i^{feed} exp\left(-\frac{z_i F}{R_g T}\Psi_{Don}\right)$ $C_i^{permeate} = \frac{\gamma_{i,pore}}{\gamma_{i,sol}}\frac{c_{i(x=\Delta x)}^m}{\phi_i exp\left(-\frac{z_i F}{R_g T}\Psi_{Don}\right)}$ At x=0 → $C_i = C_i^{feed}$, at x=Δx → $C_i = C_i^{permeate}$	4.11 4.12
Hindrance factors: $K_{i,d} = 1.0 - 2.3\left(\frac{r_i}{r_p}\right) + 1.154\left(\frac{r_i}{r_p}\right)^2 + 0.224\left(\frac{r_i}{r_p}\right)^3$ $K_{i,c} = (2 - \emptyset_i)(1.0 + 0.054\left(\frac{r_i}{r_p}\right) - 0.988\left(\frac{r_i}{r_p}\right)^2 + 0.441\left(\frac{r_i}{r_p}\right)^3$	4.7 4.8
Steric partitioning: $\emptyset_i = (1 - \lambda_i)^2$	4.9
Where : $\lambda_i = \frac{r_i}{r_p}$	4.10
Electroneutrality conditions: $\sum_{i=1}^n z_i c_i^m = -X^m$ $\sum_{i=1}^n z_i c_i^b = 0$ $\sum_{i=1}^n z_i c_i^m + X^m = 0$ $\sum_{i=1}^n z_i C_i^{permeate} = 0$ $I_c = \sum_{i=1}^n F z_i J_i = 0$	4.23
Rejection of ion: $R_i = \left(1 - \frac{C_i^{permeat}}{C_i^{feed}}\right)100\%$	4.29

Where: c_i^b is concentration of ion in the bulk solution (mol/m^3)

I_c is current density (A/m^2)

Chapter Five
Results and Discussion

This chapter presents and discusses in detail all the results obtained experimentally from this work. Four major sets of experiments were carried out.

The first is experiments of zeta potential (electrokinetic). Measurements of the zeta potentials were obtained from microelectrophoresis and streaming potential techniques by using the Holmoholtz-Smluchowski equation.

The second set of experiments is the rejection behavior of the following salts found in nature on a large scale (sodium chloride, calcium carbonate, magnesium sulfate, magnesium chloride, sodium bicarbonate and sodium sulphate) as single salts solutions at different concentrations and applied transmembrane pressure (TMP) ranging from (1 to 15 bars). The rejection of uncharged solute (glucose) solution on 0.9 nm ceramic NF membrane was determined. The (DSPM) was fitted to the data of neutral solute (rejection and permeate flux as a function of applied transmembrane pressure) yielding effective pore radius and ratio of active membrane thickness/porosity ($\Delta X/A_k$).

The third set of experiments is the critical flux of (magnesium sulphate, calcium chloride, sodium chloride, sodium sulphate and sodium bicarbonate) solutes at different concentration. Flux – pressure profile (step by step method) was used to estimate the critical flux of 0.9 nm tubular ceramic NF membrane at applied transmembrane pressure ranging from (1 to 15 bars). The concept of critical flux was used under several operating conditions (ionic strength, pH, cross flow velocity and valency). The results of the experiments and calculations in the appendices (C and D).

The fourth set of experiments includes an applied aspect of using NF membrane in produced water treatment for reuse.

5.1 Zeta Potential

Measurements of microelectrophoresis potential and streaming potential have been conducted to estimate zeta potential in order to characterize the value and type of the surface charge for 0.9 nm ceramic titanium dioxide nanofiltration membrane.

5.1.1 Zeta Potential Measurements using Microelectrophoresis Method

Figs. 5.1, 5.2 and 5.3 and appendix (C) show the zeta potentials estimated from microelectrophoresis method at pH magnitudes (3- 9) respectively for a background sodium chloride 0.001, 0.01 ,0.1 M (NaCl)

Table (5.1) shows the measured ceramic (TiO_2) membrane zeta potential (mV) estimated from microelectrophoresis method through a range of pH magnitudes (3-9) for a background electrolyte of sodium chloride 0.001, 0.01 and 0.1 M (NaCl) respectively.

Fig. 5.4 shows a plot of the evaluated zeta potential (microelectrophoresis method) across a range of pH values form 3 to 9 using 0.001, 0.01 and 0.1 M sodium chloride as a background electrolyte.

The influence of pH on the zeta potential of the 0.9 nm NF TiO_2 membrane particles as a function of the increasing electrolyte concentration of NaCl and pH is shown in **Fig. 5.4** for the three NaCl concentrations (10^{-3}, 10^{-2} and 10^{-1} M). The zeta potential of the 0.9 nm NF membrane used in this research was positive at pH 3, which was equal to 8.52, 3.79 and 0.77 mV for 10^{-3}, 10^{-2} and 10^{-1} M NaCl, respectively. IEP was found between pH 3.6, 3.5 and 3.3; the interpretation of the observed related shifts in the IEP to the adsorption of cations and anions on the membrane surface **(Herbig, et al., 2003)**. This explanation can be applied to other results in this study.

The highest magnitudes, which were found at pH 9, were -35, −32.5 mV and −25.21 for10^{-3}, 10^{-2} and 10^{-1} M NaCl, respectively. This finding agreed with those of other workers **(Moritz et al. 2001).**

This finding agreed with those of other workers **(Chiu and James 2006; Narong and James 2006; Szymczyk, et al., 1999)**, This interpretation applies to the results for other similar experiments in this study. The result showed a reduction in the active thickness of the diffused layer as the electrolyte concentration (ionic strength) increased; thus a result which may be explained by the decrease in the effective thickness of the diffuse layer as the ionic strength increases so that in this system NaCl acts as an indifferent electrolyte **(Condom, et al., 2004)**. For the NaCl solution (1:1), the value of ionic strength was equal to its molarity (M) under 0.001, 0.01 and 0.1 M ionic strengths, respectively **(Petersen, 1993)**.

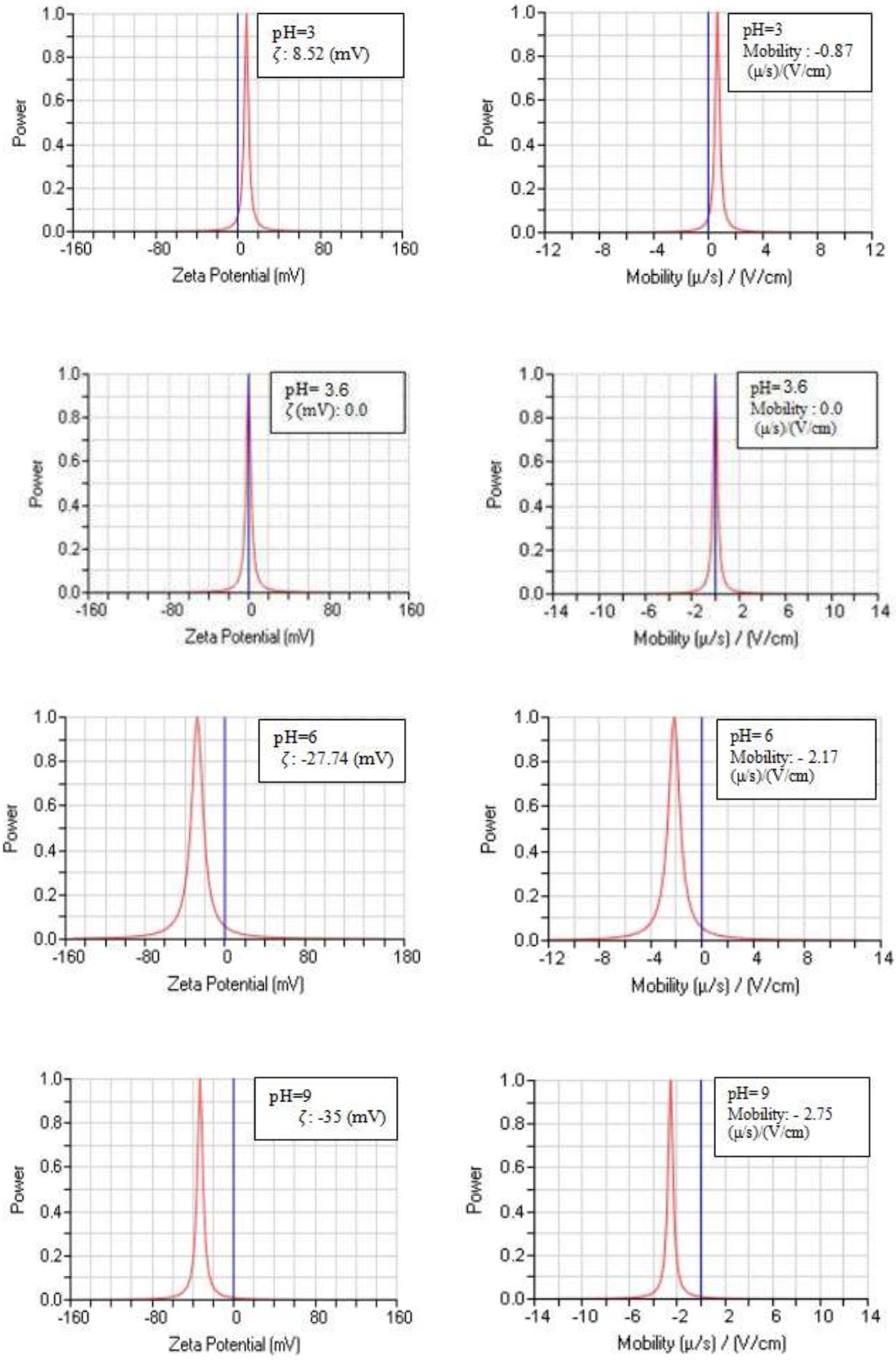

Fig. 5.1 Zeta Potential and Mobility (Microelectrophoresis Method) at 0.001 M NaCl Concentration for pH 3 – 9 and Temperature 25 ^{o}C.

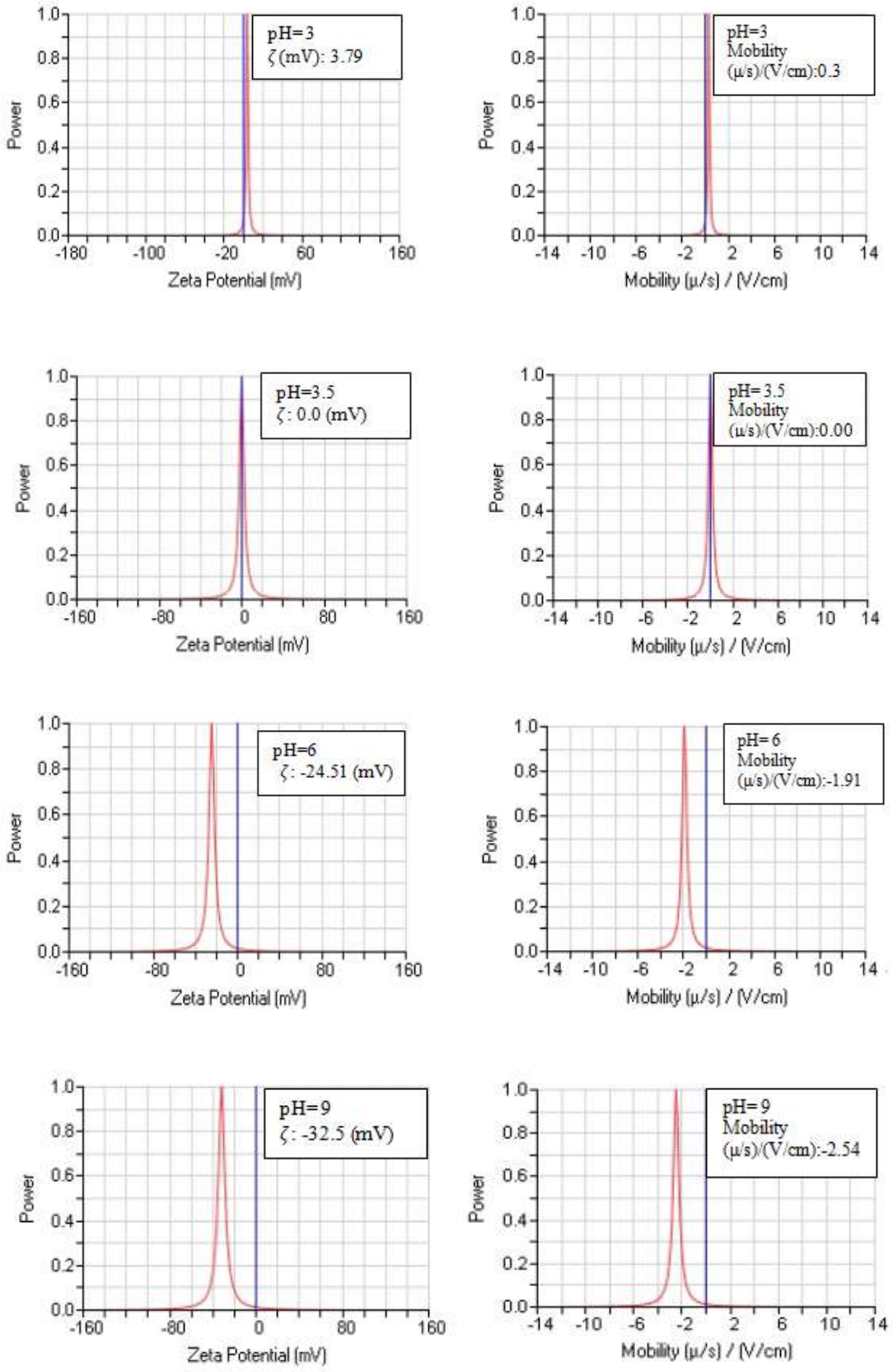

Fig. 5.2 Zeta Potential and Mobility (Microelectrophoresis Method) at 0.01 M NaCl Concentration for pH 3-9 and Temperature 25 ^{o}C.

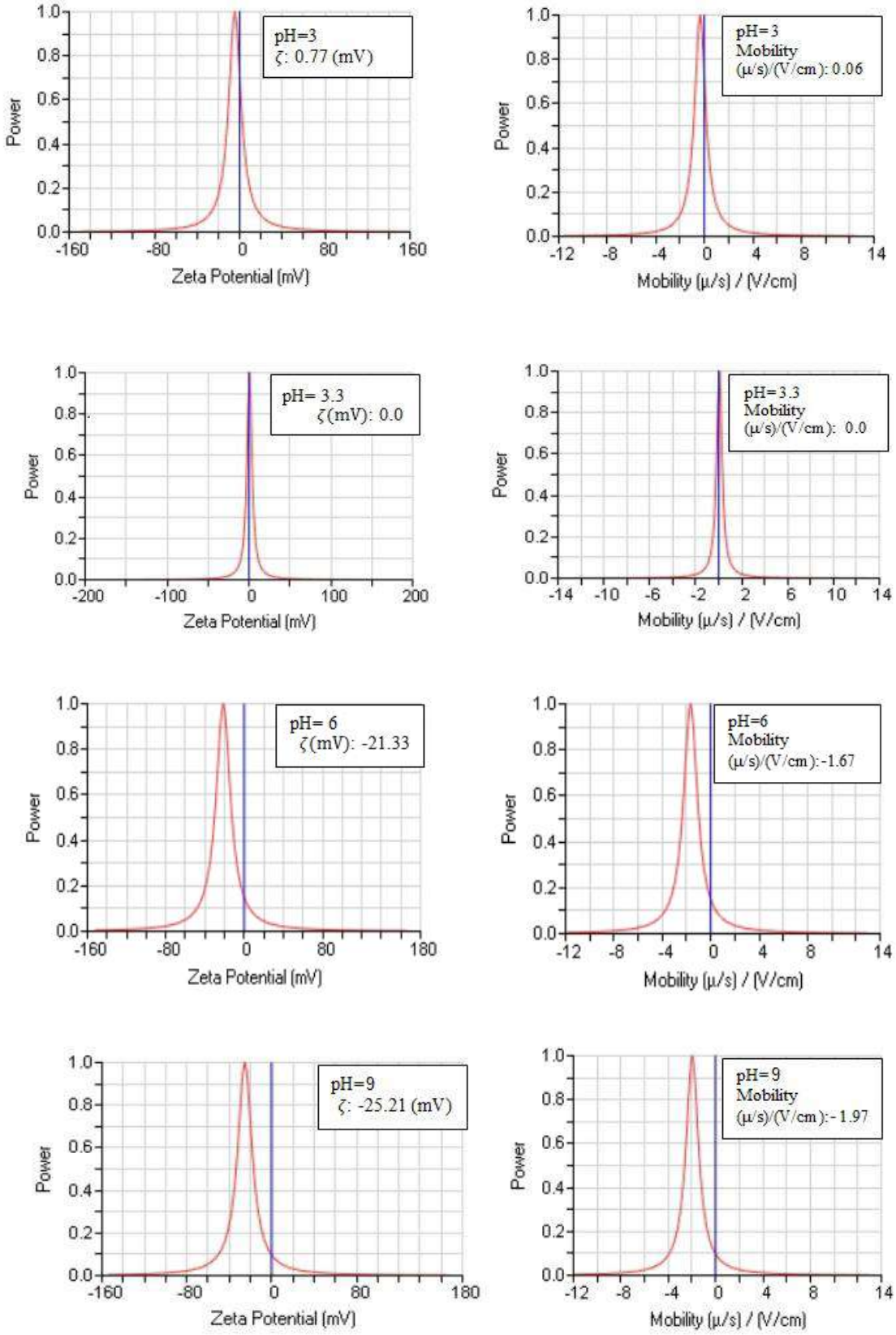

Fig. 5.3 Zeta Potential and Mobility (Microelectrophoresis Method) at 0.1 M NaCl Concentration for pH 3 – 9 and Temperature 25 ^{o}C.

Table 5.1. Evaluated Zeta Potential (mV) using Microelectrophoresis Method for Tubular Ceramic Titanium Dioxide NF across a Range of pH Magnitudes for Background Electrolyte Fixed at 0.001, 0.01 and 0.1 M NaCl and Temperature 25 ^{o}C.

pH	$\zeta\ (mV)$ 0.001 M	$\zeta\ (mV)$ 0.01 M	$\zeta\ (mV)$ 0.1 M
3	8.52	3.79	0.77
3.3	-	-	0.0
3.5	-	0	-
3.6	0	-	-
4	-15.08	-13.00	-10.58
4.5	-17.31	-	-
5	-20.55	-17.93	-15.08
6	-27.38	-24.51	-21.33
7	-31.5	-28.4	-22.88
8	-33	-30.6	-24.46
9	-35	-32.5	-25.21

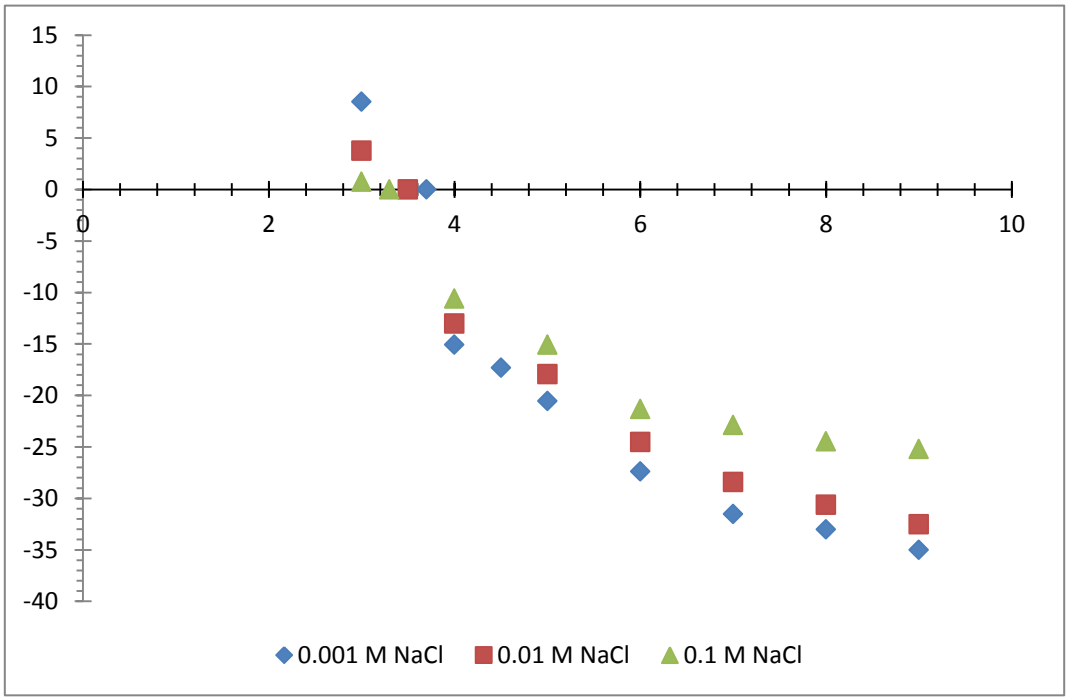

Fig. 5.4. Zeta Potential of 0.9 nm Titanium Dioxide NF Membrane Measured from Micro-Electrophoresis Potential Plotted versus pH for Background Electrolyte of 0.001 M, 0.01M and 0.1 M NaCl with (IEP) of 3.6, 3.5 and 3.3 Respectively and Temperature 25 ^{o}C.

Microelectrophoresis potential technique was used to investigate the effect of solution concentration (0.001, 0.005, 0.01 and 0.1 M) sodium chloride on the zeta potential of the membrane at constant pH of (9). **Fig. (5.5**) shows a plot of estimated zeta potential measured from microelectrophoresis potential at fixed pH of (9) by using 0.001, 0.01, 0.05 and 0.1 M NaCl as a background electrolyte for 0.9 nm ceramic NF titanium dioxide.

The microelectrophoresis potential measurement was carried out at pH of (9). The results showed that the value of zeta potential decreased with increasing concentration as shown in **Fig. (5.5)** the determined zeta potential values were -35, -32.5 and -24.46 mV at solute concentration 0.001, 0.01, 0.05 and 0.1 M respectively.

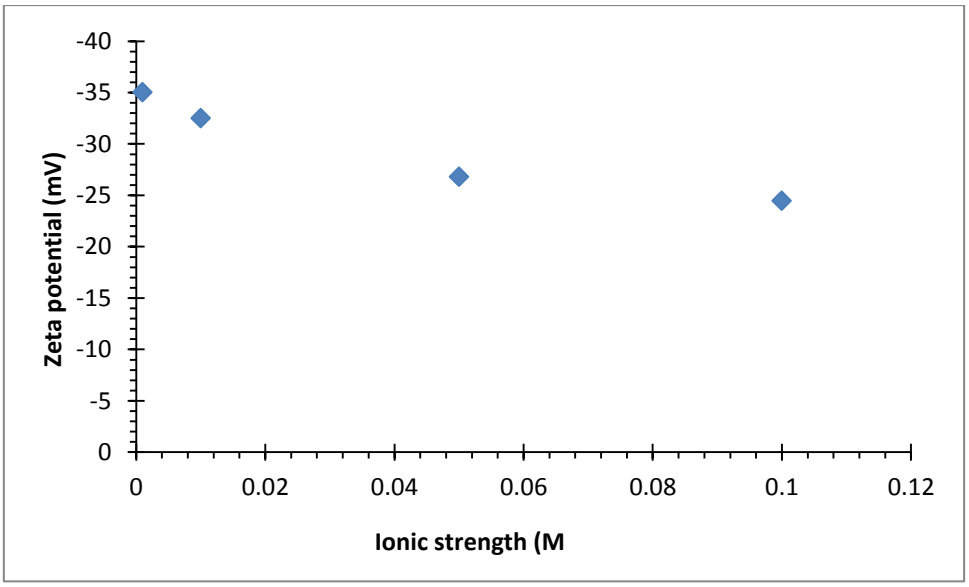

Figure. 5.5 Zeta Potential of 0.9 nm Ceramic Nanofiltration TiO_2 Measured from Electrophoresis Potential Plotted versus pH (Constant at 9) for Background Electrolyte of 0.001, 0.01, 0.05 and 0.1 M NaCl and Temperature 25 ^{o}C.

Figs. 5.6 and 5.7 show the zeta potentials estimated from microelectrophoresis method at pH magnitudes (3-9) for a background electrolyte of calcium carbonate 5×10^{-5} M and 10×10^{-5} M respectively ($CaCO_3$).

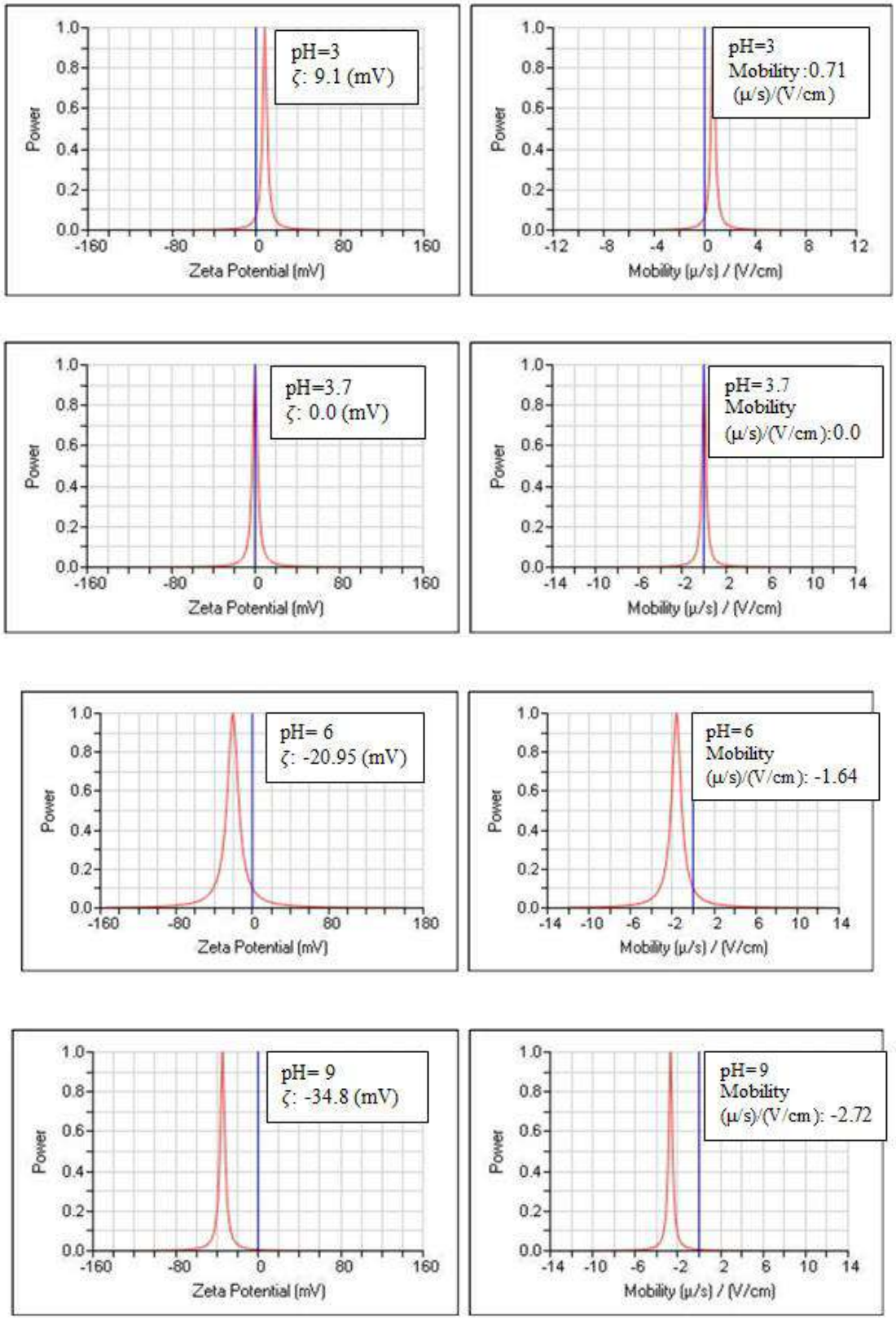

Fig. 5.6 Zeta Potential and Mobility (Microelectrophoresis Method) at 5×10^{-5} M $CaCO_3$ Concentration for pH 3 – 9 and Temperature 25 ^{o}C.

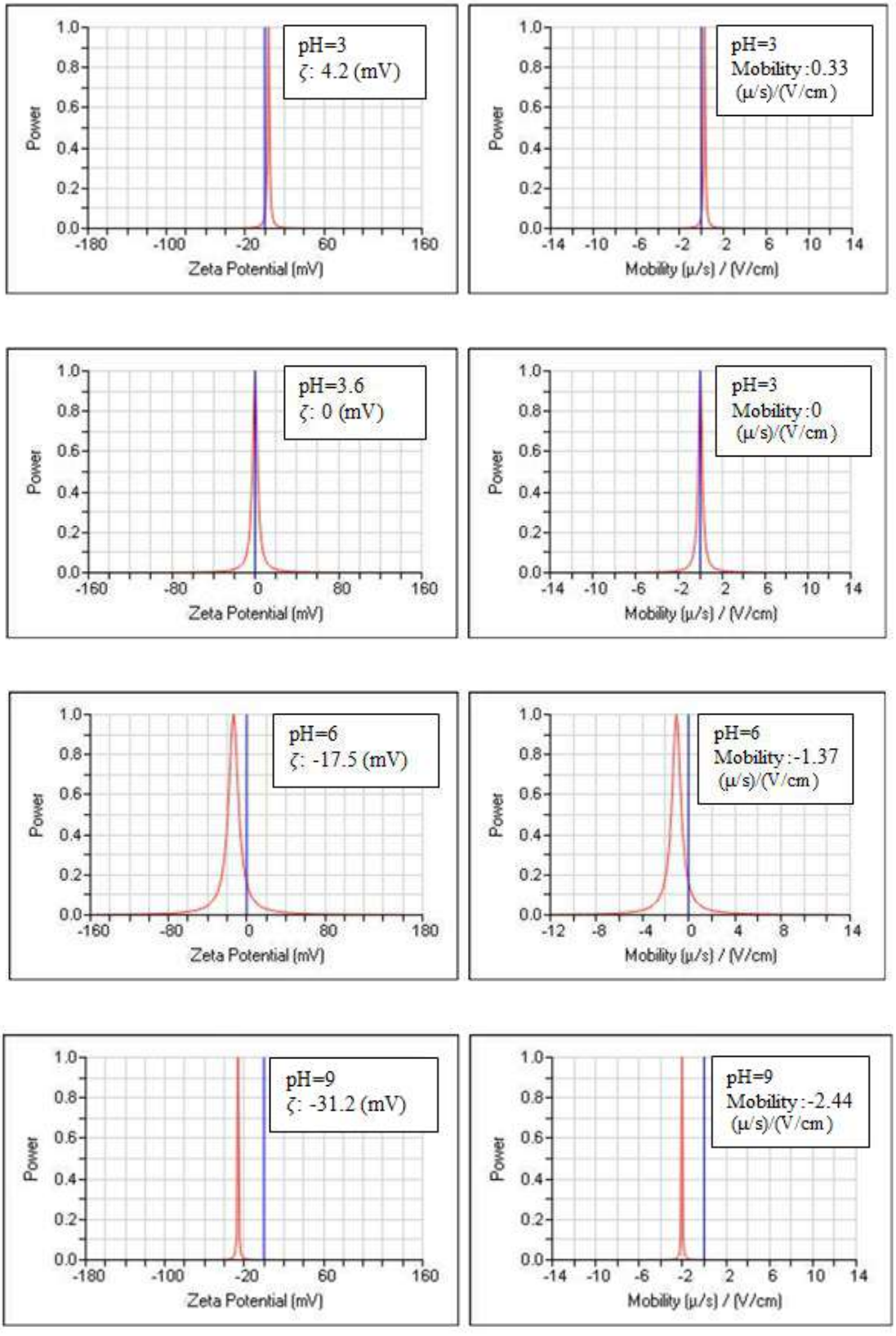

Fig. 5.7 Zeta Potential and Mobility (Microelectrophoresis Method) at 10×10^{-5} M $CaCO_3$ Concentration for pH 3 – 9 and Temperature 25 ^{o}C.

Table (5.2) shows the measured ceramic (TiO_2) membrane zeta potential (mV) estimated from microelectrophoresis method through a range of pH magnitudes (3-9) for a background electrolyte of calcium carbonate 5×10^{-5} M and 10×10^{-5} M respectively ($CaCO_3$).

Table 5.2 Evaluated Zeta Potential (mV) Using Microelectrophoresis Method for Tubular Ceramic Titanium Dioxide NF across a Range of pH Magnitudes for Background Electrolyte Fixed at (5×10^{-5} M and 10×10^{-5} M) $CaCO_3$ and Temperature 25 ^{o}C.

pH	$\zeta\ (mV)$ 5×10^{-5} M	$\zeta\ (mV)$ 10×10^{-5} M
3	9.1	4.2
3.6	-	0
3.7	0	-
4	-11.5	-7.8
5	-15.58	-12.8
6	-20.95	-17.5
7	-23.2	-19.2
8	-29.5	-25.8
9	-34.8	-31.2

Fig. 5.8 shows a plot of the estimate zeta potential (microelectrophoresis technique) across a range of pH (3-9) using (5×10^{-5} M and 10×10^{-5} M) $CaCO_3$ as a background electrolyte. The influence of (pH values and concentration) on the zeta (electrokinetic) potential of the TiO_2 NF membrane surface as a function of raising electrolyte pH and concentration of ($CaCO_3$) is shown in **Fig. 5.8** for two different concentrations (5×10^{-5} M and 10×10^{-5} M). The experiments results showed that the electrokinetic potentials of the NF membrane used in this investigate is positive at pH of 3 being 9.1 and 4.2 mV for 5×10^{-5} M and

10×10^{-5} M respectively. The isoelectric point IEP is found between pH value of 3.7 and 3.6 respectively. As the value of pH was increased the electrokinetic potential become higher negative, with the highest absolute values were found at pH 9 (-34.8 and -31.2) mV for (5×10^{-5} M and 10×10^{-5} M) calcium carbonate, respectively. From these outcomes, it is showed that at fixed calcium carbonate concentration the sign of the electrokinetic potential can be significantly changed by changing pH, whilst at the fixed value of pH, the changes in concentration of salt do not have such a big influence can be significantly changed by varying magnitude of pH.

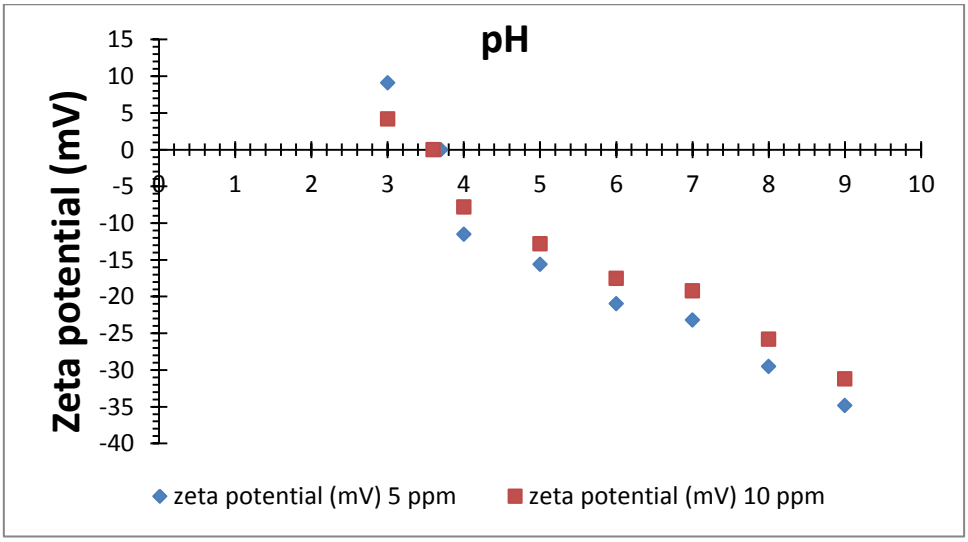

Fig. 5.8 Zeta Potential of TiO_2 NF Membrane Measured using Microelectrophoresis Potential Method Plotted against pH for Background Electrolyte of Calcium Carbonate 5×10^{-5} M and 10×10^{-5} M with IEP of 3.7 and 3.6 Respectively and Temperature 25 ^{o}C.

5.1.2 Zeta Potential Measurements using Streaming Potential Method

The measurements of zeta potential were estimated by using streaming potential technique for a background electrolyte concentration 0.01 M sodium chloride through a range of pH magnitudes from 3 to 9.

Streaming potential was calculated from the transmembrane pressure increment (ΔP_{TMP}) of (0.25, 0.5, 0.75, 1, 1.25, 1.5, 1.75 and 2.0

bar) at every pH value to inside tube membrane and by determining the difference of the resulting instantaneous electrical potential variation (ΔE) for nanofiltration membrane.

This electrical potential variation per unit of applied transmembrane pressure is the streaming potential coupling coefficient, ($C_s = \frac{\Delta E_{str}}{\Delta P_{TMP}} = \frac{\varepsilon_r \varepsilon_o \zeta}{\mu K}$ see **Equation 4. 3**). The measured streaming potential (ΔE_{str}) changes linearly versus the applied transmembrane pressure increments.

The coupling coefficient can be deduced from the slope of **Eq. 4.3** ($C_s = slope = \frac{\Delta E_{str}}{\Delta P_{TMP}} = \frac{\varepsilon_r \varepsilon_o \zeta}{\mu K}$).

The electrical (zeta) potential can be determined from the Helmoholtz-Smoluchowski equation; based on the correlation between the measurable streaming potential coupling coefficient (V/pa) and the zeta potential (V) then:

$\zeta = slope \ \frac{\mu K}{\varepsilon_r \varepsilon_o}$ (see **Equation 4.4**)

The conductivity of circulating electrolyte 0.01 M NaCl ($S.m^{-1}$) and the dynamic viscosity (pa.s) according to the results of experiment are equal to (0.104) and 8.9×10^{-4} respectively for water at temperature 25 ^{o}C.

5.1.2.1 Effect of pH and Type of Salt

Figs. (5.9 and 5.10) show the streaming potential measurements against the applied pressure increments at pH of 3- 9 for 0.01 and 0.1 M (NaCl) respectively.

The **Figs. (5.9 and 5.10)** show an increase in streaming potential with increasing transmembrane pressure at each pH value due to

increased forcing of ions to push towards the ends of the pores, leading to greater density of ions and thus greater streaming potential. An increased streaming potential was also observed with increasing pH values and this explains the reason for the increased zeta potential due to the proportional relationship between streaming potential and zeta potential. This result corresponds to the result obtained by **(Narong and James, 2006)**. This interpretation can be applied to other results in this study.

Table (5.3) Explains the estimated TiO_2 ceramic membrane zeta potential (mV) determined from streaming potential and microelectrophoresis potential techniques over a range of pH values for background electrolyte constant at (0.01 M) NaCl.

The streaming potential was an in-situ (direct surface membrane) measurement that was helpful in detecting the sign of membranes' electrokinetic (zeta) potential and the IEP. The zeta potential could be measured using the streaming potential method, which potentials were zero at the IEP (3.6 and 3.5 for 10^{-2} and 10^{-1} M respectively), which could readily be determined from streaming potential data (as shown in **Fig. 5.11**). **Fig. 5.12** shows the zeta potential measurements by streaming potential and microelectrophoresis with pH for 10^{-2} M NaCl. When pH was raised, zeta potentials became highly negative, and a highest value was found at pH 9 (−31.35 mV) and (-32.5 mV) respectively for 10^{-2} M NaCl. The zeta potential measurements by using microelectrophoresis potential method in good agreement with values obtained by using streaming potential method. This is a promising indication of the success (silver and 4% gold electrodes) in measuring the zeta potential (and used as an alternative to platinum electrodes).

The IEP for the streaming and electrophoresis potentials depended on the electrolyte (ionic strength) concentration and changed slightly

between (3.5–3.6) and (3.3–3.5), respectively for 10^{-1} and10^{-2} M NaCl, that varies slightly due to changes in properties of surface of the constituent material of membrane to the requirements of the technique of measuring used (streaming potential and microelectrophoresis potential methods). The decrease in IEP with increasing salt concentration was demonstrated clearly in terms of the particular adsorption of weakly hydrated chlorine (Cl^-) ions **(Herbig, et al., 2003)**, and the reduction in the thickness of the effective layer (diffuse layer) as the concentration increased.

The estimated result of the zeta potential is in agreement with the result stated by the workers **(Amer, 2013; Narong and James, 2006).** The IEP of 0.01 M NaCl was 3.6 according to the streaming potential method and 3.5 through microelectrophoresis, as shown in **Fig. 5.12**. The results show that the zeta potential values of the TiO_2 NF membrane were increased with increasing pH values.

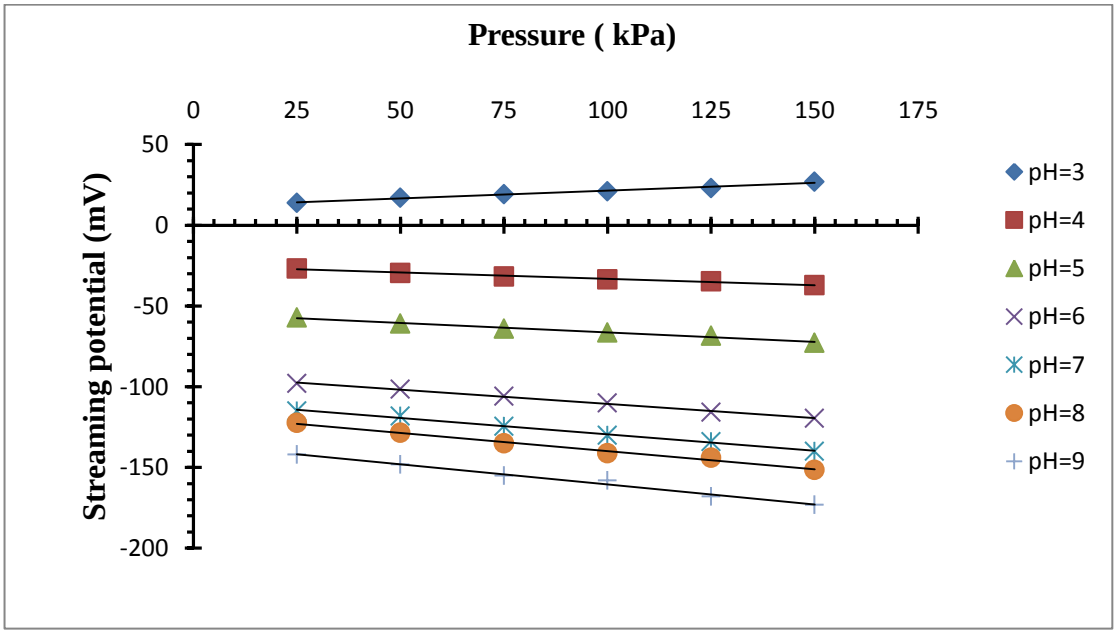

Fig. 5.9 The Streaming Potential Measurements of 0.9 nm Titanium Dioxide NF Membrane versus Applied Pressure Increment over a Range of pH Values for Backgrounded Electrolyte Fixed at 0.01 M NaCl and Temperature 25 ^{o}C.

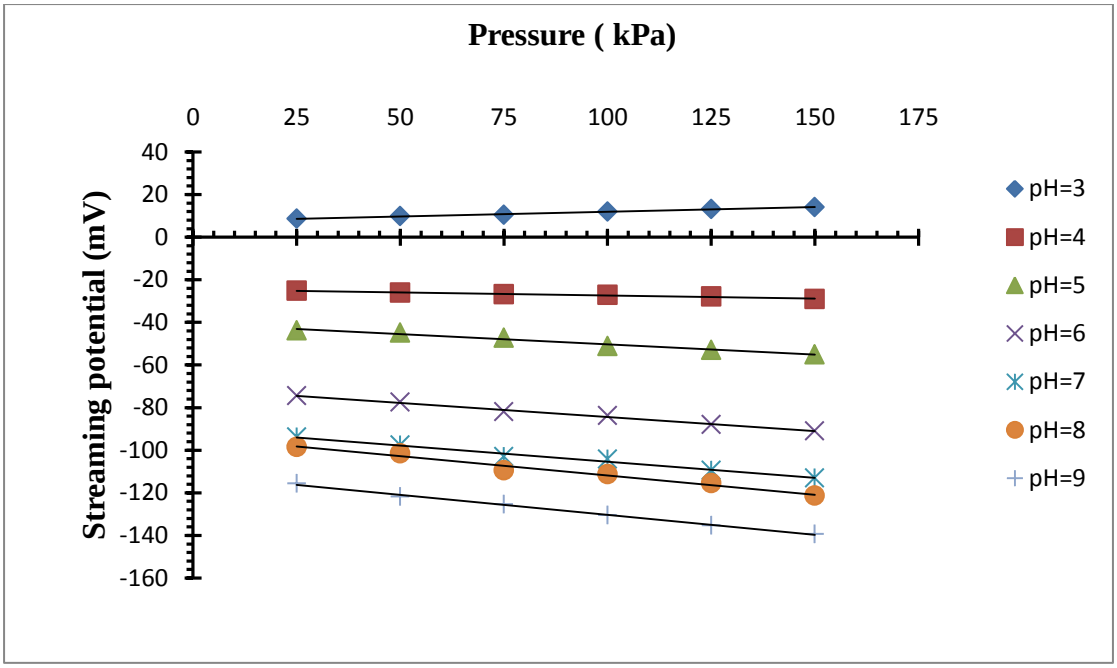

Figure 5.10 The Streaming Potential Measurements of 0.9 nm Titanium Dioxide NF Membrane versus Applied Pressure Increment over a Range of pH Values for Backgrounded Electrolyte Fixed at 0.1 M NaCl and Temperature 25 ^{o}C.

Fig. (5.11) shows the streaming potential coupling coefficient (mV/bar) at pH of 3,4,5,6,7,8 and 9 for 0.01 and 0.1 M NaCl.

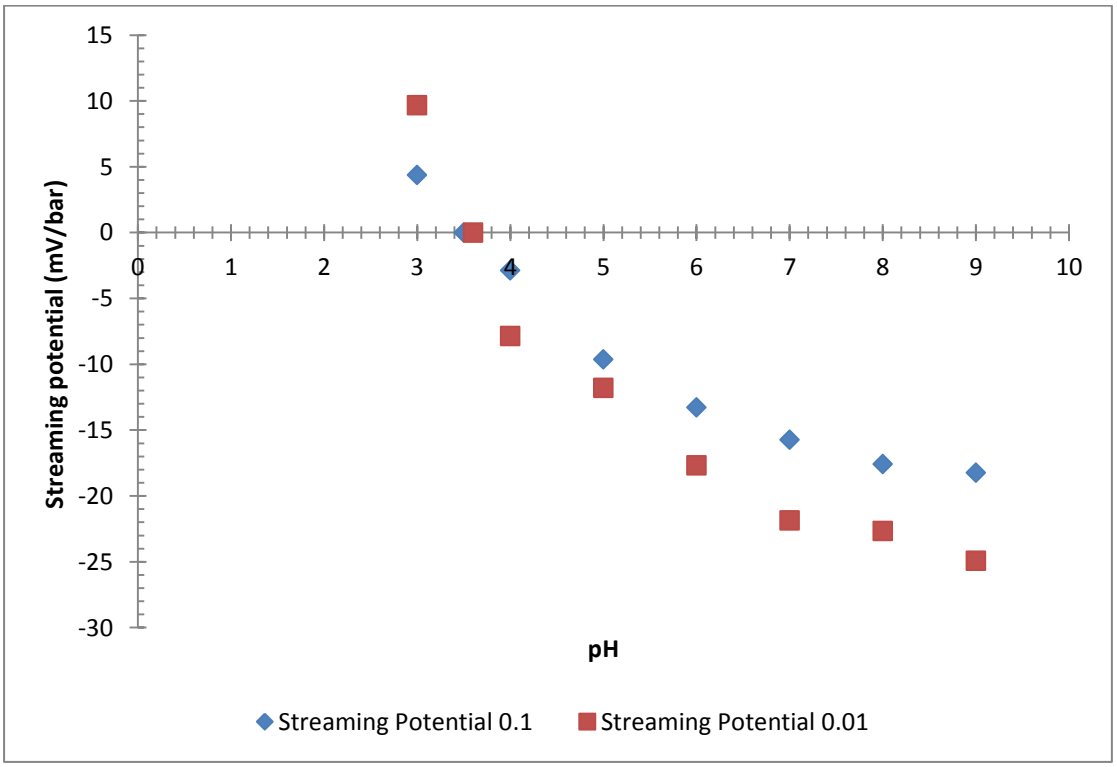

Figure 5.11 The Streaming Potential of 0.9 nm Titanium Dioxide NF Membrane Measured Plotted Versus pH for Background Electrolyte of 0.01M and 0.1 M NaCl with (IEP) of 3.6 and 3.5 Respectively and Temperature 25 ^{o}C.

Table 5.3 Estimated Zeta Potential of 0.9 nm Titanium Dioxide NF Membrane from Streaming Potential and Microelectrophoresis Potential Techniques over a Range of pH Values for Background Electrolyte Fixed at 0.01 M NaCl.

pH	ζ (mv) Streaming potential	$\zeta\ (mV)$ Microelectrophoresis potential
3	10.3412	3.79
3.5	-	0
3.6	0	-
4	-6.73	-13.00
5	-15.64	-17.93
6	-21.44	-24.51
7	-27.43	-28.4
8	-29.23	-30.6
9	-31.35	-32.5

Fig. 5.12 shows a plot of the measured zeta potential (for two methods streaming and microelectrophoresis) with a range of pH values for a background electrolyte from 3 to 9 by using 0.01 M (NaCl) respectively. Given the increasing pH value, the zeta potentials of the TiO_2 NF membrane slightly increased to pH values of approximately 7, 8, and 9 for both techniques, as shown in **5.12.** The IEP of 0.01 M NaCl was 3.6 according to the streaming potential method and 3.5 through microelectrophoresis, as shown in **Fig. 5.12.**

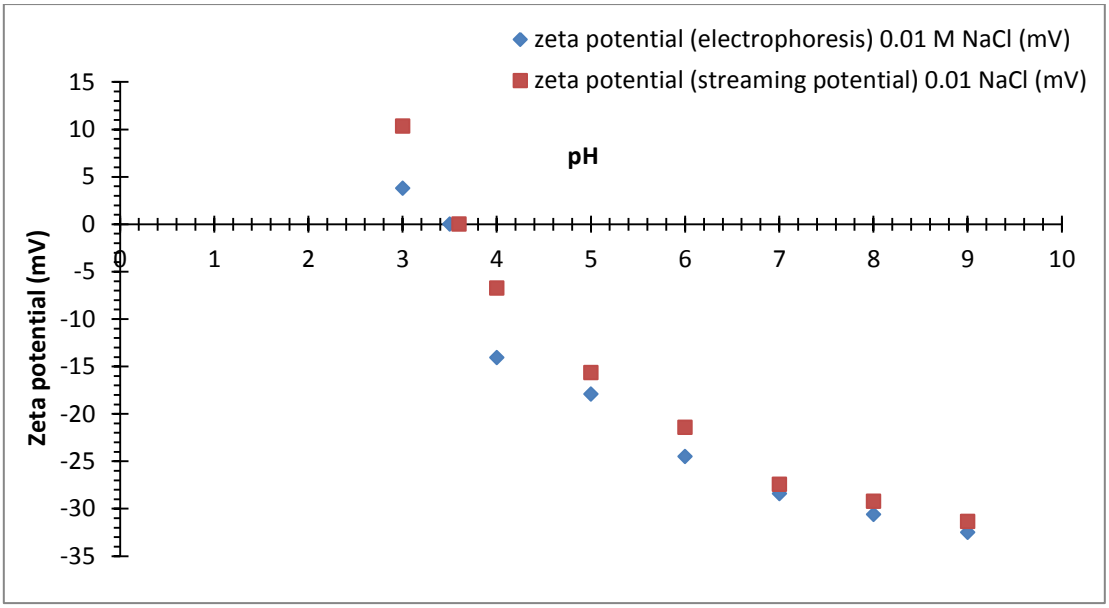

Fig. 5.12 The Zeta Potential of 0.9 nm Ceramic Titanium Dioxide Nanofiltration Membrane Determined from Streaming Potential and Microelectrophoresis Potential Techniques Plotted against pH for Background Electrolyte Fixed at 0.01 M NaCl and Temperature 25 ^{o}C.

Table (5.4) Explains the estimated TiO_2 ceramic membrane zeta potential (mV) over a range of pH values for background electrolyte constant at 0.01 M (KCl, $NaHCO_3$, $CaCl_2$, $MgCl_2$, Na_2CO_3, $MgSO_4$ and Na_2SO_4) respectively.

Table 5.4 Estimated Zeta Potential of 0.9 nm Titanium Dioxide NF Membrane from Streaming Potential Technique over a Range of pH Values (3-9) for Background Electrolyte Fixed at 0.01 M (NaCl, KCl, $NaHCO_3$, $CaCl_2$, $MgCl_2$, Na_2CO_3, $MgSO_4$ and Na_2SO_4) and Temperature 25 ^{o}C.

pH	ζ (mv) NaCl	ζ (mv) KCl	ζ (mv) $NaHCO_3$	ζ (mv) $CaCl_2$	ζ (mv) $MgCl_2$	ζ (mv) Na_2CO_3	ζ (mv) $MgSO_4$	ζ (mv) Na_2SO_4
3	10.3412	10.2	9.3	4	5.6	9.3	12.7	15.53
4	-6.73	-4.88	-6.59	-3	-3.7	-6.59	-13.99	-17.7
5	-15.64	-9.05	-13	-5.75	-6.5	-13	-18.65	-23.36
6	-21.44	-16.2	-19.8	-9.5	-10.8	-19.8	-23.73	-28.5
7	-27.43	-21.7	-22.2	-15.3	-17	-22.2	-27.2	-34.6
8	-29.23	-25.82	-26.2	-18.9	-21	-26.2	-31.82	-38
9	-31.35	-27.18	-29.1	-22.84	-24.3	-29.1	-36.82	-40.62

5.1.2.2 Effect of Anion on Zeta Potential of TiO_2 NF Membrane

Fig. (5.13) shows a plot of the measured zeta potential with a range of pH values for a background electrolyte from 3 to 9 by using 0.01 M (NaCl, $NaHCO_3$, Na_2CO_3, and Na_2SO_4).

The zeta potential variations of the TiO_2 NF membrane in salt solutions (NaCl, $NaHCO_3$, Na_2CO_3, and Na_2SO_4) as a function of pH magnitude are shown in **Fig. (5.13)**. The zeta potential of the TiO_2 NF membrane was decreased in the following order: $SO^{2-}_4 > CO_3^{2-} > Cl^- > HCO^-_3$, that the SO^-_4 anion was more active and had more zeta potential with the studied pH extent. **Fig. (5.13)** shows that the zeta potentials of the TiO_2 NF membrane were monitored with monovalent cations and divalent anions (1:2) and were more than which monitored with monovalent cations and anions (1:1).

All salt solutions had a concentration of 0.01 M (electrolyte). The determined ionic strength using **Eq. (4.26)** for the monovalent cation and monovalent anion electrolyte solutions was 0.01 M, and that for monovalent cation and divalent anion electrolyte solutions was 0.03 M. An increase in the ionic strength of the electrolyte solution reduces EDL thickness, which decreases the zeta potential. The EDL thicknesses determined using **Eq. (4.21)** were 3.02 and 1.72 nm for 0.01 and 0.03 M ionic strengths, respectively. The potential of TiO_2 NF membrane had more divalent anion electrolyte solution (SO_4^{2-}) with more ionic strength (had more zeta potential) in noticeable contrast to classical electrical double layer (EDL) theories. The increase in zeta potential for the divalent anion (SO_4^{-2}) was possible because of the particular anion adsorption on the ceramic membrane. The performance was similar to that reported by **(Zhao, et al., 2005)**. This explanation can be applied to other results in this study.

The adsorption of anions to the TiO_2 NF surface of the membrane caused the negative zeta potential measured using streaming potential and microelectrophoresis. Anions imposed a powerful effect on the TiO_2 NF membrane zeta potential from at a pH range of 4–9. The pH value less than 4 was monitored, and the adsorption of the Na^+ cation as a counterion was increased. Thus, a less negative zeta potential was obtained, and IEP appeared at pH 3.6–3.8. Furthermore, a reduce pH value less than 3.6–3.8, the zeta potential was gained positive.

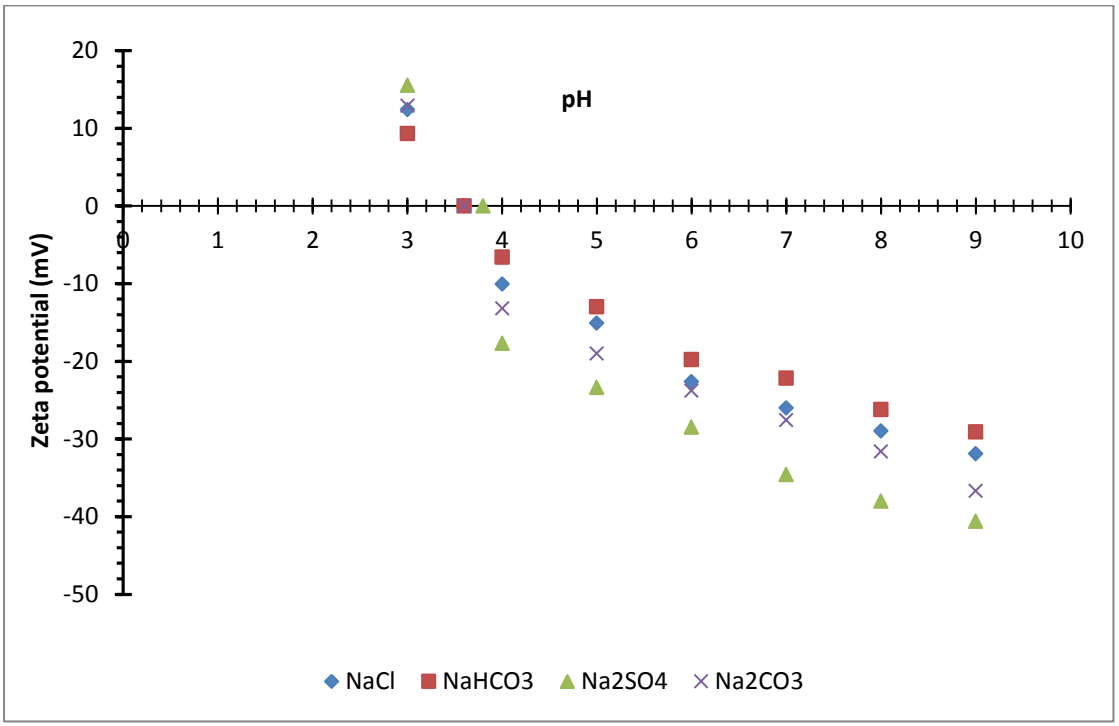

Figure 5.13 The Zeta Potential of 0.9 nm Ceramic Titanium Dioxide Nanofiltration Membrane Determined from Streaming Potential Plotted against pH (3-9) for Background Electrolyte Fixed at 0.01 M (NaCl, $NaHCO_3$, Na_2CO_3, and Na_2SO_4) and Temperature 25 ^oC.

5.1.2.3 Effect of Cation on Zeta Potential of TiO_2 NF Membrane

To study the influence of different cations on the zeta potential of the TiO_2 NF membrane, chloride salts (NaCl, KCl, $MgCl_2$, and $CaCl_2$) were used in the experiments of streaming potential. In **Fig. (5.14)**, plotted changes in zeta potential for the TiO_2 NF membrane at the 0.01 M salt solutions existed as a function of pH values of 3–9. For the Na^+, K^+,

Mg^{2+}, and Ca^{2+} cation electrolyte solutions, the zeta potential of the TiO_2 NF membrane was reduced with decreased pH values, the adsorption of monovalent and divalent cation electrolyte solutions (Na^+, K^+, Mg^{2+}, and Ca^{2+}) increased. Thus, a less negative surface charge was obtained. IEP appeared at pH 3.4–3.6, and a reduced pH value less than of 3.4–3.6 positive zeta potential was obtained.

From pH 3 to 9, the TiO_2 NF membrane zeta potential was compatible and agreed with EDL theory. The zeta potential of the TiO_2 NF membrane showed an increased zeta potential with reduced ionic strength (0.01 M) for NaCl and KCl and a decreased zeta potential with increased ionic strength (0.03 M) for $MgCl_2$ and $CaCl_2$. Similar results were gained by membranes under various ionic strength, and agreement with results were obtained by **(AWWA, 1992 ; Baticle, et al., 1997 ; Elimelech, et al.,1994).**

The zeta potential reductions were in the following order: $Na^+ > K^+ > Mg^{2+} \geq Ca^{2+}$ within pH 3–9. The adsorption of cations on the TiO_2 NF membrane surface became highly significant in gaining a higher positive zeta potential at a low pH range for the monovalent and divalent cations.

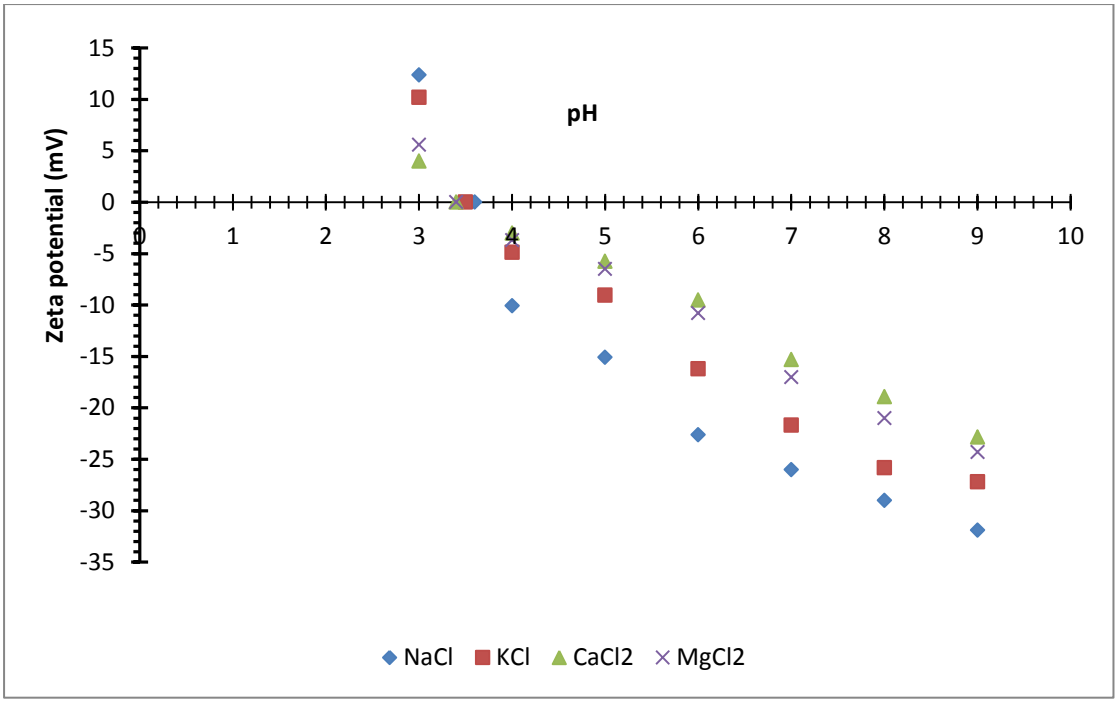

Figure 5.14 The Zeta Potential of 0.9 nm Ceramic Titanium Dioxide Nanofiltration Membrane Determined from Streaming Potential Plotted against pH (3-9) for Background electrolyte Fixed at 0.01 M (NaCl, KCl, $MgCl_2$ and $CaCl_2$) and Temperature 25 ^oC.

$MgSO_4$ and Na_2SO_4 were used in the experiments of streaming potential to study the influence of two cations (Mg^{2+} and Na^+) on the zeta potential of the ceramic NF membrane salts.

Fig. (5.15) plots the changes in the ceramic TiO_2 NF membrane in the 0.01 M salt solutions of $MgSO_4$ and Na_2SO_4 solutions produced IEP at pH 3.7 and 3.8, respectively.

The zeta potential of the TiO_2 membrane changed linearly with the electrolyte solution under a pH range of 4–9 for the Na^+ and Mg^{2+} cations. Positive zeta potentials were gained at pH values less than 3.7 and 3.8. The zeta potential of the TiO_2 NF membrane was decreased in this order $Na^+ > Mg^{2+}$ because the thicknesses of the EDL that were determined using **Equation (4.21)** were 1.72 and 1.51 nm for concentrations of 0.03 and 0.04 M, respectively.

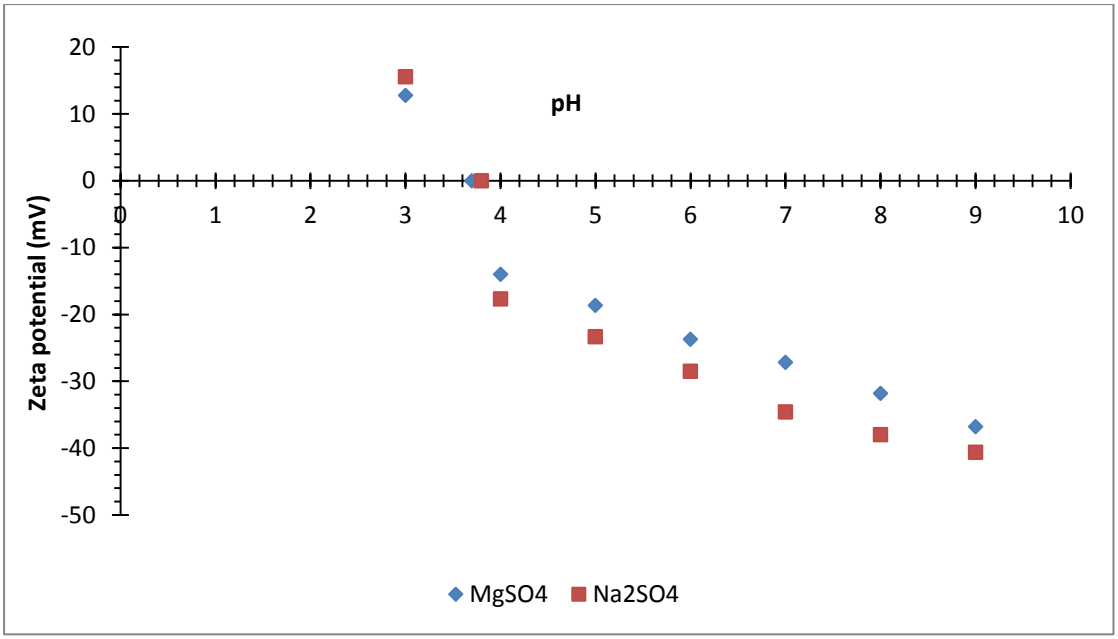

Figure 5.15 The Zeta Potential of 0.9 nm TiO_2 NF Membrane Determined from Streaming Potential Plotted against pH (3-9) for Background Electrolyte Fixed at 0.01 M ($MgSO_4$ and Na_2SO_4) and Temperature 25 ^oC.

5.2 Rejection Measurements of Membrane

Many factors influence on the ion rejection, such as ion concentration, membrane charge and ion charge density. Therefore, ions rejection would differ, where the rejection of monovalent ions should be lower than divalent ions. The counter ions (have an opposite charge of the TiO_2 NF membrane) with small valences would have more rejection due to shield would be weak. The coions (have the same charge as the membrane) with higher valences would have a more rejection due to the repulsion interaction with charge of membrane would be more effective. Higher concentration would cause counter ions to shield the surface charge of membrane, thus reducing rejection with the charge membrane is known as the Donnan effect. Exclusion of Donna has higher of an effect on coions. Because the effect of Donna exclusion, the membrane would reject counter ions to maintain electro neutrality in the solution

In addition, Acid-base transformation impacts the rejection of membrane, where the rejection of membrane is effected by the behavior

of the solute acid-base. As well the complexity is the interaction between anionic and cationic species in the electrolyte solution, that would result in the formation of a many of soluble species beside the actual species, the formed complex's rejection is influenced by its charge and size. Complexity depends on concentrate and pH. Deposition has an impact on rejection of ion. If species of solid precipitate, its rejection would increase, but this would be associated by concentration polarization.

5.2.1 Rejection of Salts (NaCl, Na_2SO_4, $MgSO_4$, $MgCl_2$, $CaCl_2$, and $NaHCO_3$).

The rejection of NaCl as a single electrolyte in the 0.9 nm circular tube ceramic titanium dioxide nanofilteration membrane as a function of (TMP) with confirmation on the influence of feed concentration has been investigated experimentally. **Figs. (5.16, 5.17 and 5.18)** show the rejection of NaCl at 0.001, 0.01, 0.1 M respectively versus of applied (TMP). Form these figures, it can be concluded that the rejection so (Na^+) and (Cl^-) were gradually raised as the applied (TMP) raised.

In all three concentrations the rejection of (Na^+) was a little higher than the rejection of chloride ions (Cl^-), this due to the fact that the sodium ion (Na^+) hydrate radius, which is equal to (0.36 nm) **(Narong and James, 2006; Israelachvili, 2007; Schaep, et al., 1998)** larger than the radius of the chloride ion, which is equal to (0.33 nm) **(Bowen and Welfoot, 2002; Schaep, and Vandecasteele, 2001)**. In addition, the diffusion coefficient to sodium ion (1.33×10^{-9} $m^2.s^{-1}$) (**Bowen, et al., 2002; Shih, et al., 2005)** is less than the diffusion coefficient of the chloride ion (2.03×10^{-9} $m^2.s^{-1}$) **(Alfonso and Pinho, 2000; Gutman, 1987; Wąsik, et al., 2005)**. The rejection of sodium ions at the lowest applied (TMP) was 6.3 %, 3.2 % and 1.6%. While, the rejection of

chloride ions at same concentration was 5.5 %, 2 % and 1.4 % respectively.

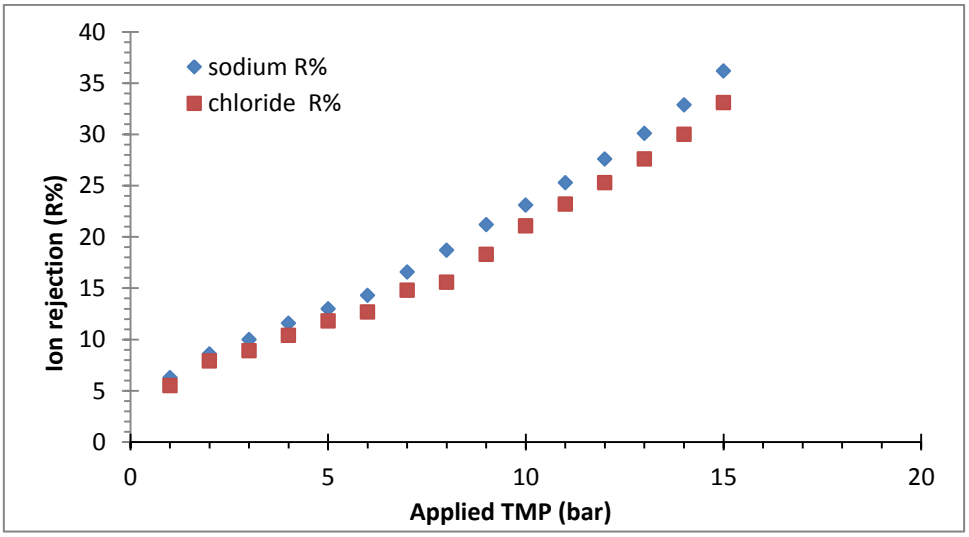

Figure (5.16) Sodium Chloride Rejection at (0.001 M) versus TMP (1-15 bar), Cross Flow Velocity 1 m/s, pH 6 and Temperature 25 ^{o}C.

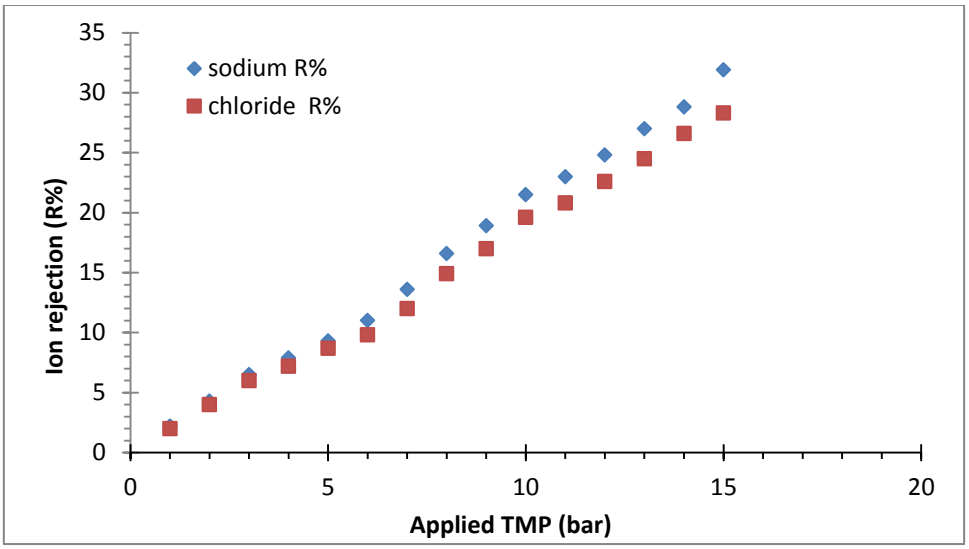

Figure (5.17) Sodium Chloride Rejection at (0.01 M) versus TMP (1-15 bar), Cross Flow Velocity 1 m/s, pH 6 and Temperature 25 ^{o}C.

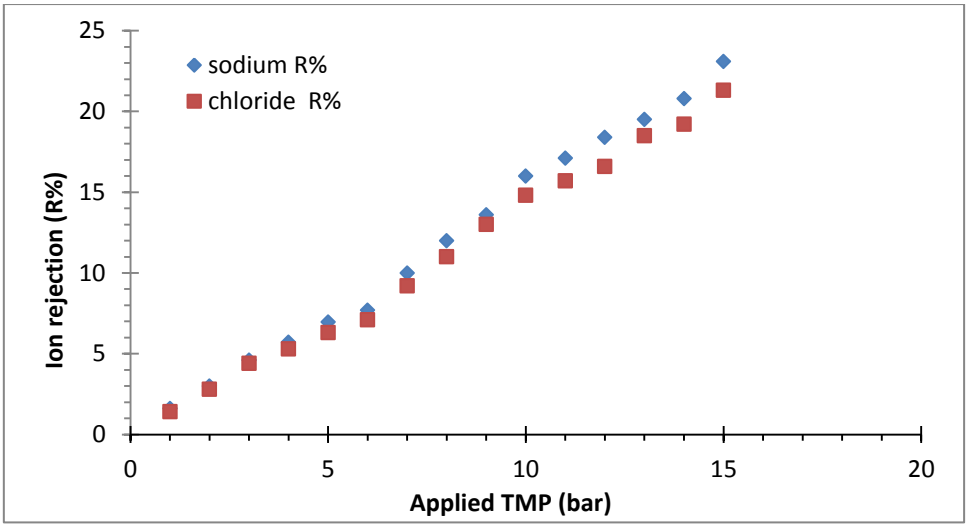

Figure (5.18) Sodium Chloride Rejection at (0.1 M) versus TMP (1-15 bar), Cross Flow Velocity 1 m/s, pH 6 and Temperature 25 ^{o}C.

Fig. (5.19) shows the rejection of NaCl solutes at 0.001, 0.01 and 0.1 M against applied (TMP). From this figure it can noticed that for any of three concentrations there was an increased progressive in the rejection of sodium chloride salt related to the applied (TMP). At the lowest applied (TMP) of 1.0 bar; the rejection of NaCl salt was 5.9 %, 2.1 % and 1.5 % for sodium chloride feed concentration of 0.001, 0.01 and 0.1 M respectively. On the other hand, at the largest applied (TMP) of 15.0 bar, the rejection of NaCl salts was 34.7 %, 30.1 % and 22.5 % for sodium chloride feed concentration of 0.001, 0.01 and 0.1 M respectively. Increased rejection with increased pressure is due to increasing permeate flux. This explanation applies to the results of other experiments in this study.

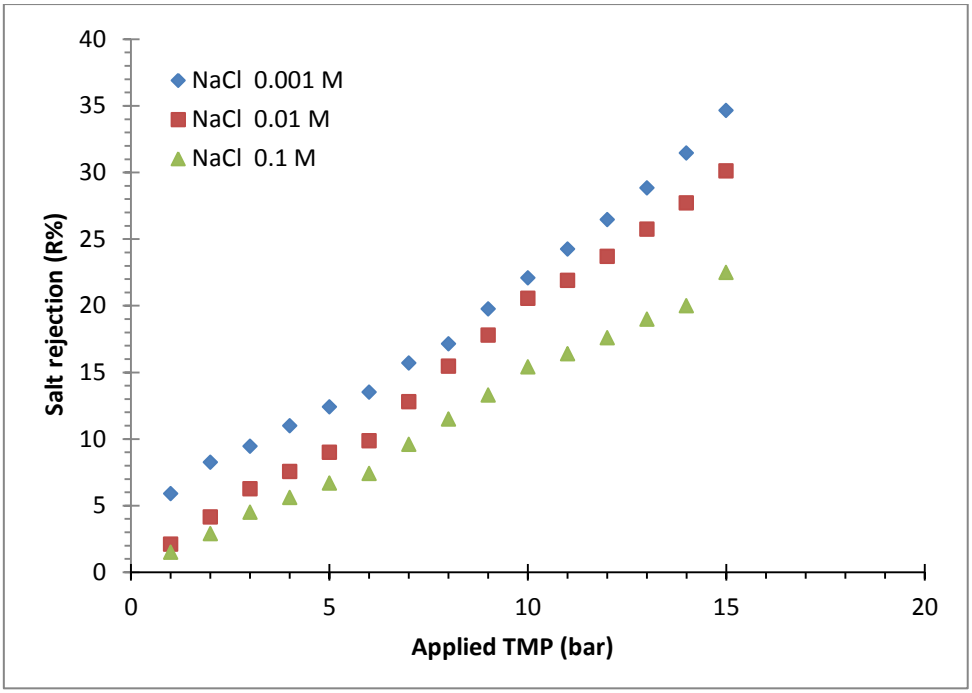

Figure (5.19) Sodium Chloride Rejection at (0.001, 0.01 and 0.1 M) versus TMP (1-15 bar), Cross Flow Velocity 1 m/s, pH 6 and Temperature 25 ^{o}C.

Magnesium sulphate rejection as a single electrolyte in the 0.9 nm circular tube ceramic titanium dioxide NF membrane as a function of applied transmembrane pressure with focus on the impact of feed concentration has been investigated experimentally.

Figs. (5.20, 5.21 and 5.22) show the rejection of magnesium sulphate at 0.001, 0.005 and 0.01 M respectively as a function of applied (TMP). It can be seen from these figures, the rejections of (Mg^{+2}) ions and (SO_4^{-2}) ions were continually increased as the applied (TMP) increased at concentration 0.001 M $MgSO_4$.

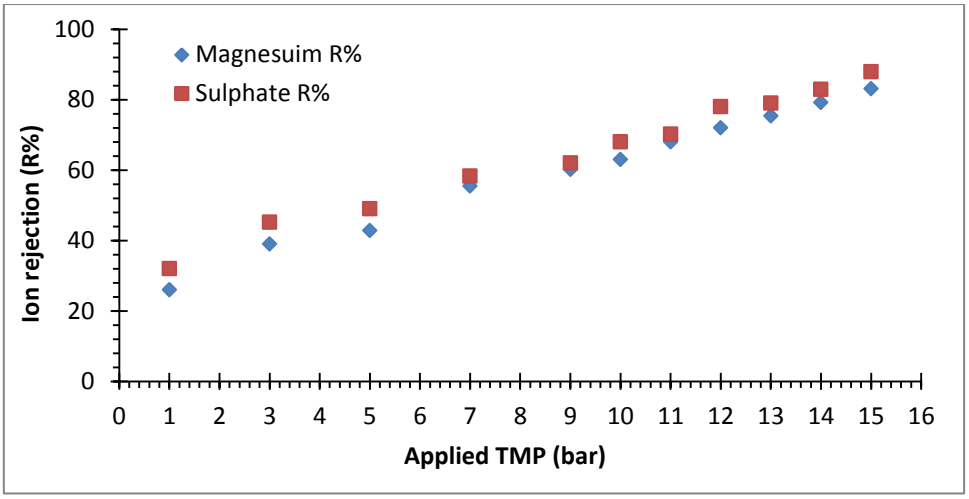

Figure (5.20) Magnesium Sulphate Rejection at (0.001 M) versus TMP (1-15 bar), Cross Flow Velocity 1 m/s, pH 6 and Temperature 25 ^{o}C.

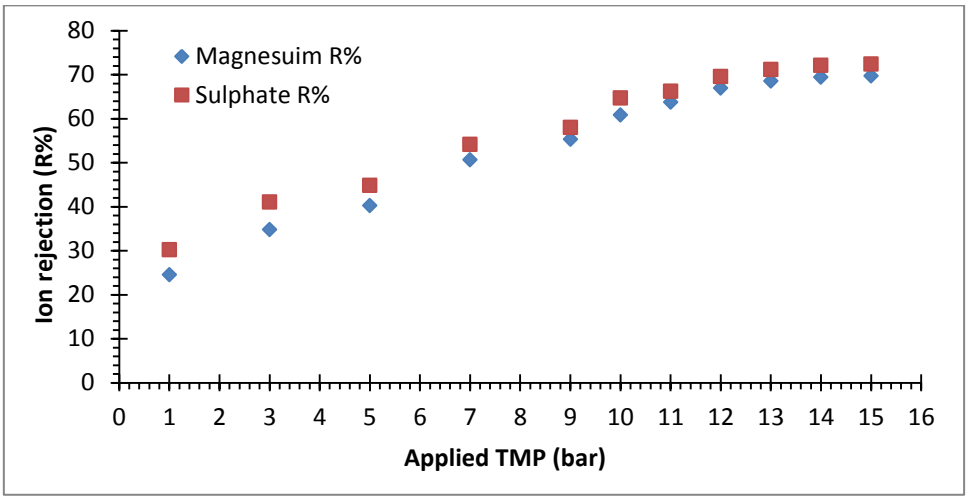

Figure (5.21) Magnesium Sulphate Rejection at (0.005 M) versus TMP (1-15 bar), Cross Flow Velocity 1 m/s, pH 6 and Temperature 25 ^{o}C.

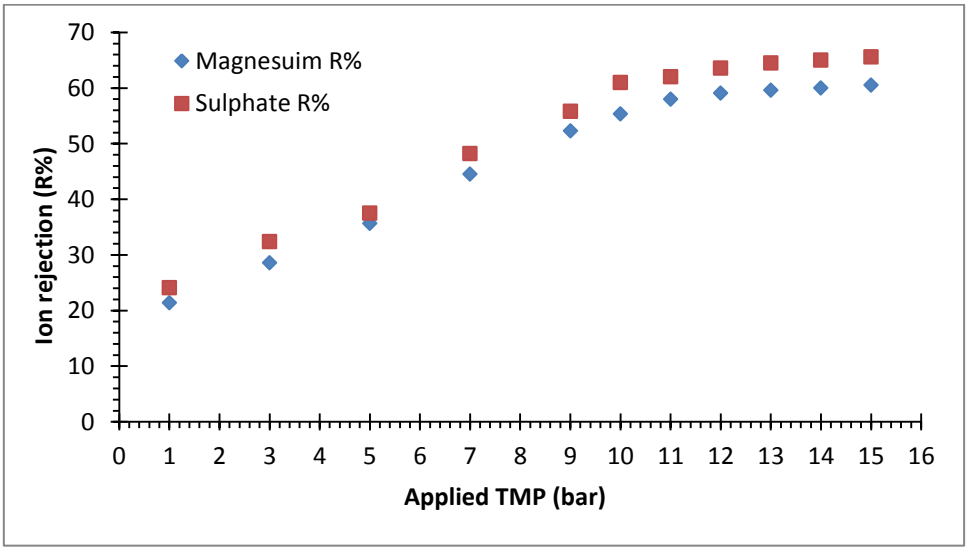

Figure (5.22) Magnesium Sulphate Rejection at (0.01 M) versus TMP (1-15 bar), Cross Flow Velocity 1 m/s, pH 6 and Temperature 25 ^{o}C.

On the other hand at (0.005 and 0.01 M) $MgSO_4$ the rejection of (Mg^{+2}) and (SO_4^{-2}) ions were constantly increased as increasing the applied (TMP) until the (TMP) of 13 and 10 bar respectively, after that the rejection stabilized gradually inspite of the continues increasing in the applied TMP. This due to the critical flux was reached the limit critical flux, in which the permeate flux begins to stabile approximately with the continuation increasing of applied transmembrane pressure. Critical flux process happened as a result of three factors which caused to decrease permeate flux gradually, until it reached to stabilization, these factors are : adsorption, pore blockage (partial closure of pores) and deposit of particles and grow layer by layer at the membrane surface **(Chiu and James, 2005; Mänttäri and Nyström., 2000; Patrice, et al., 2006)** all this explanation can be applied on the other gained results.

All three figures show that the rejections of sulphate ions (SO_4^{-2}) was a little higher than the rejection of calcium ion (Mg^{+2}). This attributed to the fact that the ionic radius of magnesium ion (0.086 nm) is lower than the ionic radius of the sulphate (0.29 nm) **(Hussain, et al., 2007)**, whereas the nominal pore size of ceramic titanium dioxide nanofiltration membrane 0.9 nm. This means that the transport by ion convective across the membrane pore can be hindered for both magnesium and sulphate ions and the hindered impact of sulphate ion is higher than the magnesium.

The rejection of magnesium ions at lowest applied (TMP) was (26%, 24.5 % and 21.4 %) Whereas the rejection of sulphate ions (SO_4^{-2}) at similar concentration was (32 %, 30.2 % and 24.1 %) respectively, for $MgSO_4$ feed concentration of (0.001, 0.005 and 0.01 M) respectively.

At the highest applied (TMP), 15 bar the rejection of calcium ions was (83.1 %, 59.65 %, and 60.5 %) for $MgSO_4$ feed concentration of

(0.001, 0.005 and 0.01 M) respectively. Whereas the rejection of sulphate ions (SO_4^{-2}) at similar concentration was (87.9 %, 72.4 % and 65.6 %) respectively.

Fig. (5.23) Shows the rejection of magnesium sulphate solutes at (0.001, 0.005 and 0.01 M) as a function of applied (TMP) It can be seen from **Fig. (5.23)**, that the rejection of $MgSO_4$ salt solutions by the titanium dioxide membrane reduced with increasing of salt concentration. This due to decrease in the diffusion layer with increased concentration. It can be concluded from this figure that the rejection of magnesium sulphate was similar to the rejection behavior of ions previously mentioned.

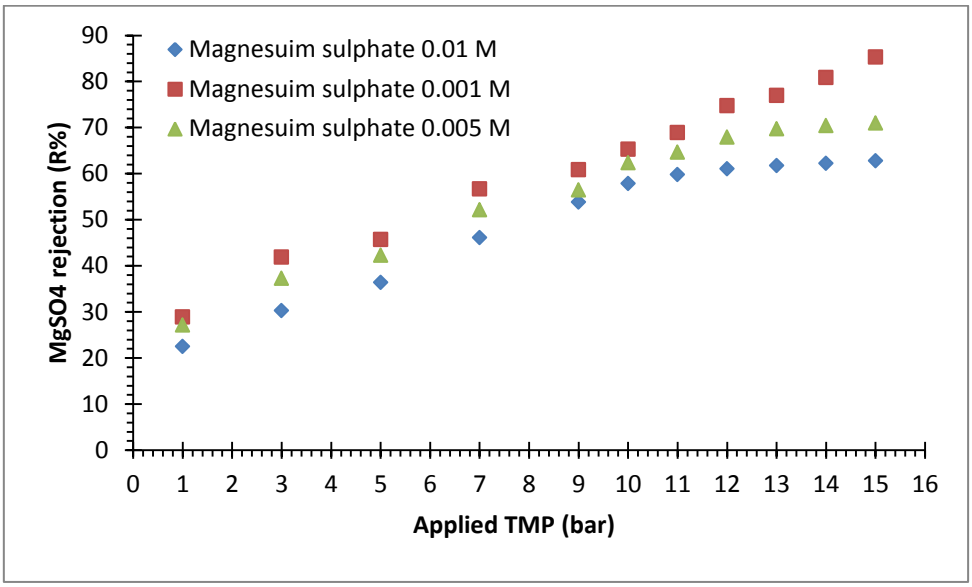

Figure 5.23 Magnesium Sulphate Rejection at (0.001, 0.005 and 0.01 M) versus TMP (1-15 bar), Cross Flow Velocity 1 m/s, pH 6 and Temperature 25 ^{o}C.

At the applied (TMP) of 1 bar, the rejection of magnesium sulphate salts was (28.9 %, 27.1 % and 22.5 %) for $MgSO_4$ feed concentration of (0.001, 0.005 and 0.01 M) respectively. At maximum applied (TMP) of 15.0 bars, the rejection of magnesium sulphate salt was (85.25 %, 80 % and 62.75 %) for feed concentration of (0.001, 0.005 and 0.01 M) respectively.

The calcium chloride rejection as a single electrolyte in the 0.9 nm circular tube ceramic titanium dioxide NF membrane as a function of applied (TMP) with focus on the influence of feed concentration has been studied experimentally.

Figs. (5.24, 5.25, 5.26 and 5.27) show the rejection of $CaCl_2$ at 0.001, 0.005, 0.01 and 0.015 M respectively as a function of applied (TMP). From these figures, it can be deduced that the rejections of (Ca^{+2}) ions was little higher than the rejection of (Cl^-) ions. At the lowest applied TMP of 1bar, the rejection of (Ca^{+2}) was 24.6 %, 20.8 %, 14 % and 7.5% for calcium chloride ($CaCl_2$) feed concentration of 0.001, 0.005, 0.01 and 0.015 M respectively, whereas the rejection of (Cl^-) ions at the same concentrations was 22.3 %, 18.5, 13.2 % and 5.2 % respectively.

At the highest applied (TMP) 15.0 bar, the rejection of (Ca^{+2}) was 75 %, 72.8 %, 54 % and 34. % for calcium chloride ($CaCl_2$) feed concentration 0.001, 0.005 and 0.01 M respectively, whereas the rejection of (Cl^-) ions at the same concentrations was 72.3 %, 69.7 %, 51.5 %, and 32%.

This can be explained by two essential reasons. The first is the calcium hydrate radius equal to (0.41 nm) **(Hassan, et al., 2007)** which is higher than the hydrate radius of chloride ion which is equal to (0.36 nm) **(Narong and James, 2006; Israelachvili, 2007)**.

The second reason is the most important because the both radius of ions are smaller than the nominal pore size of the membrane (0.9 nm) is that the calcium ion diffusion coefficient is equal to (0.9×10^{-9} m^2/s) **(Ko and Chen, 2007)** smaller than the chloride ion diffusion coefficient which is equals (2.03×10^{-9} m^2/s) **(Maria and Maria, 2000)**.

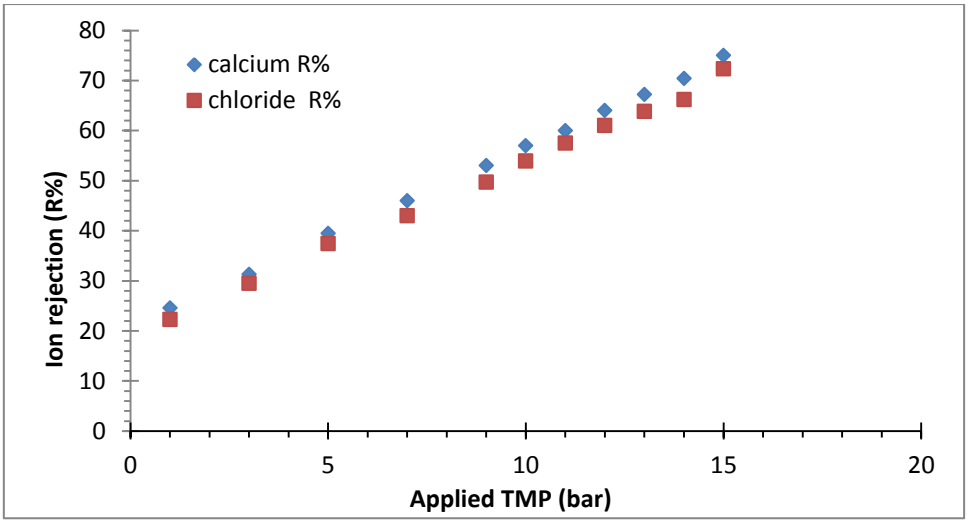

Figure 5.24 Calcium Chloride Rejection at (0.001 M) versus TMP (1-15 bar), Cross Flow Velocity 1 m/s, pH 6 and Temperature 25 ^{o}C.

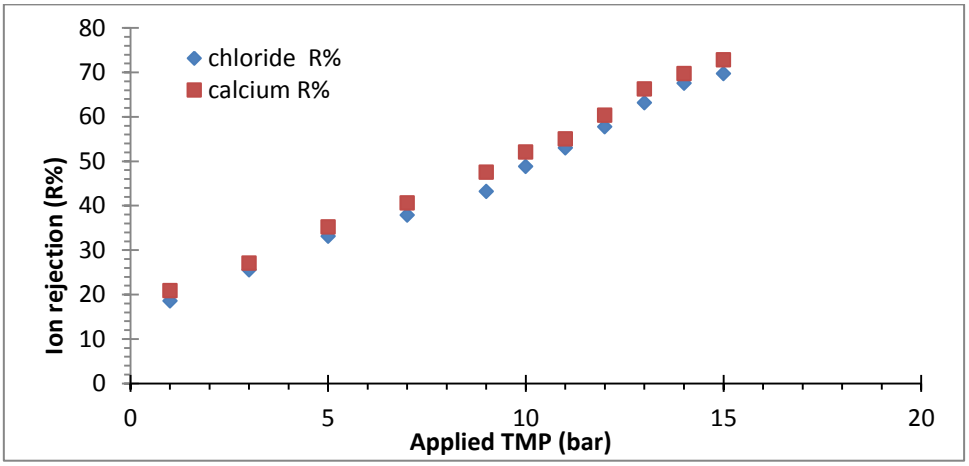

Figure 5.25 Calcium Chloride Rejection at (0.005 M) versus TMP (1-15 bar), Cross Flow Velocity 1 m/s, pH 6 and Temperature 25 ^{o}C.

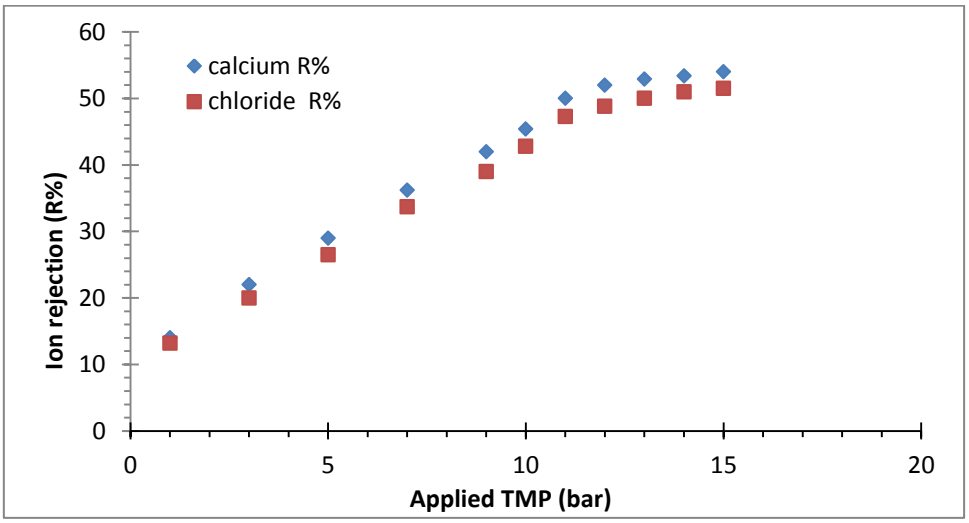

Figure 5.26 Calcium Chloride Rejection at (0.01 M) versus TMP (1-15 bar), Cross Flow Velocity 1 m/s, pH 6 and Temperature 25 ^{o}C.

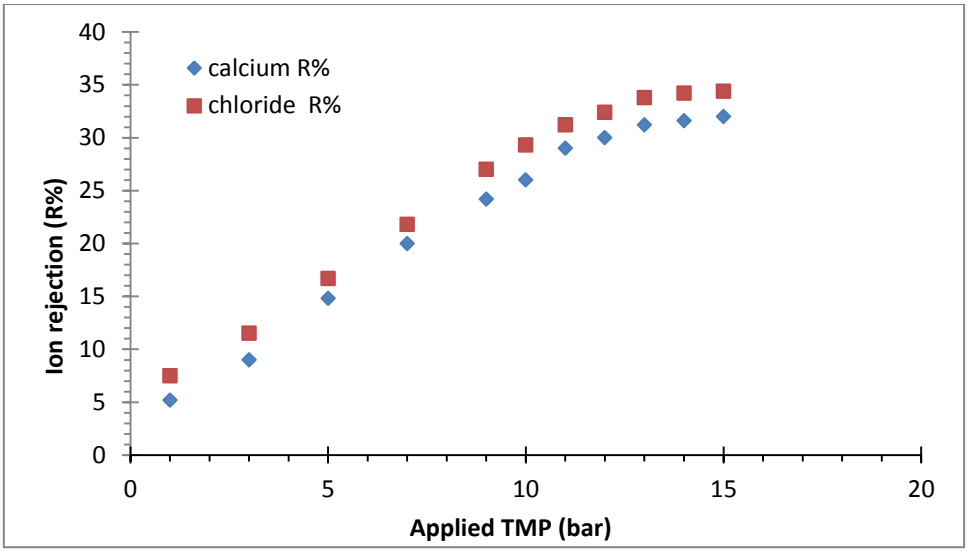

Figure 5.27 Calcium Chloride Rejection at (0.015 M) versus TMP (1-15 bar), Cross Flow Velocity 1 m/s, pH 6 and Temperature 25 ^{o}C.

Fig. (5.28) shows the rejection of $CaCl_2$ solutes at (0.001, 0.005, 0.01 and 0.015 M) as a function of applied (TMP). From this figure it can be seen that for any used concentration there was a gradual increasing in the rejection of calcium chloride related to the increasing applied (TMP).

At the applied (TMP) of (1 bar), the rejection of $CaCl_2$ salt was (23.75 %, 20.8 %, 14 % and 6.6 %) for the feed concentration of (0.001 M, 0.005 M 0.01 M and 0.015 M) respectively.

On the other hand, at largest applied (TMP) of (15 bar), the rejection of $CaCl_2$ salts was (74 %, 71.6 %, 53 % 33.4 %) for calcium chloride feed concentration of (0.001, 0.005, 0.01 and 0.015 M) respectively.

From **Figs. (5.28)**, it can be seen that the rejection of calcium chloride salt solutions by the titanium dioxide (TiO_2) nanofiltration membrane decreased with increasing of salt concentrations.

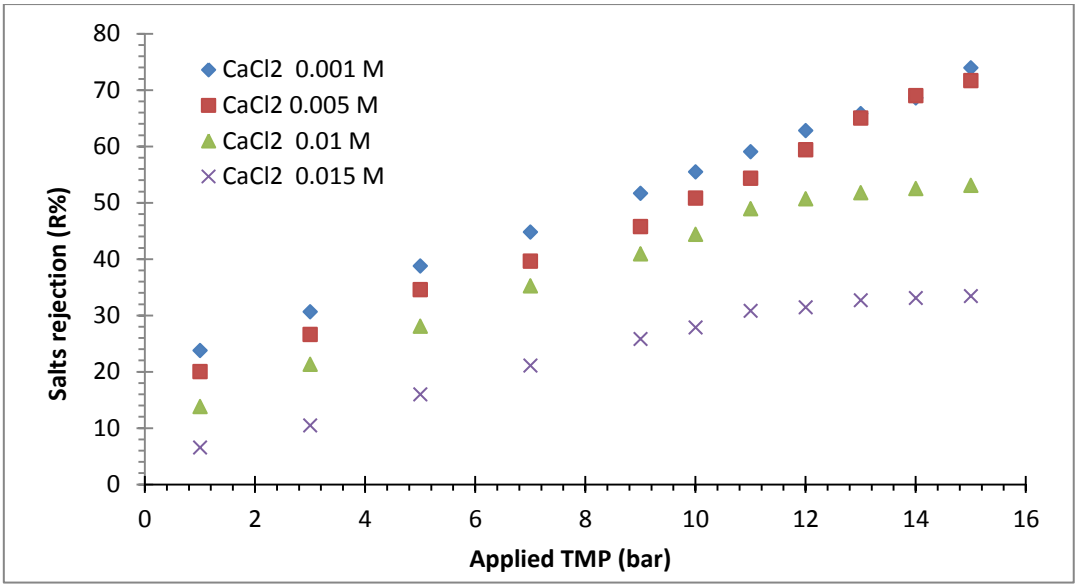

Figure (5.28) Calcium Chloride Rejection at (0.001, 0.005, 0.01, 0.015 M) Versus TMP (1-15 bar), Cross Flow Velocity 1 m/s, pH 6 and Temperature 25 ^{o}C.

Fig. (5.29) shows the rejection of Sodium Sulphate, Magnesium Chloride and Sodium Bicarbonate at 0.01 M as a function of applied (TMP). From this figure, it can be deduced that the rejections of Sodium Sulphate was higher than the rejection of Magnesium Chloride and Sodium Bicarbonate (Na_2SO_4 > MgCl2 > $NaHCO_3$). At the lowest applied (TMP) of 1 bar, the rejection of (Sodium Sulphate) was (24.45%), whereas the rejections of ($MgCl_2$ and $NaHCO_3$) at the same concentrations were (16 %) and (13%) respectively.

At the highest applied (TMP) 15 bar, the rejections of Sodium Sulphate, Magnesium Chloride and Sodium Bicarbonate were (82.2%, 60% and 57%) respectively.

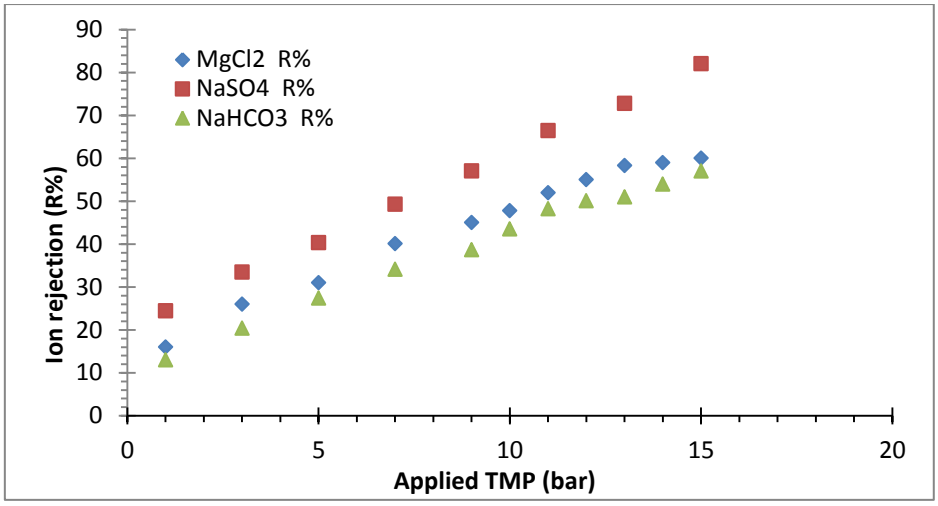

Figure 5.29 Sodium Sulphate, Magnesium Chloride and Sodium Bicarbonate Rejection at Constant Concentration (0.01 M) versus TMP (1-15 bar), Cross Flow Velocity 1 m/s, pH 6 and Temperature 25 ^{o}C.

5.2.2 Rejection of Salt ($CaCO_3$)

The impact of concentration and (TMP) on the rejection of calcium carbonate as a single electrolyte in the 0.9 nm circular tube has been investigated experimentally. The experiments of rejection were carried out at fifteen different feed pressures in the extent from 1 to 15 bar with solute feed concentrations of 5×10^{-5} M, 10×10^{-5} M (below saturation), 13×10^{-5} M (saturation) and 50×10^{-5} M supersaturation concentration at constant pH (6).

Fig. 5.30 shows that the rejection of calcium carbonate at 5×10^{-5} M, 10×10^{-5} M and 13×10^{-5} M as a function of applied transmembrane pressure TMP at pH (6) and velocity 1 m/s. It can be deduced, from this figure that the rejections of calcium carbonate were increased with increasing TMP in a noticeable jump when increasing the TMP from 1bar to 2 bar. After that, the increase of rejection is gradually and slightly with increasing pressure until it reaches the highest rejection at a certain pressure and according to the concentration. The highest rejection of the calcium carbonate at constant pH (6) and applied transmembrane

pressures (6, 4 and 2 bar), was (61.2%, 56.8% and 50%) for $CaCO_3$ feed concentration of 5×10^{-5} M, 10×10^{-5} M and 13×10^{-5} M respectively.

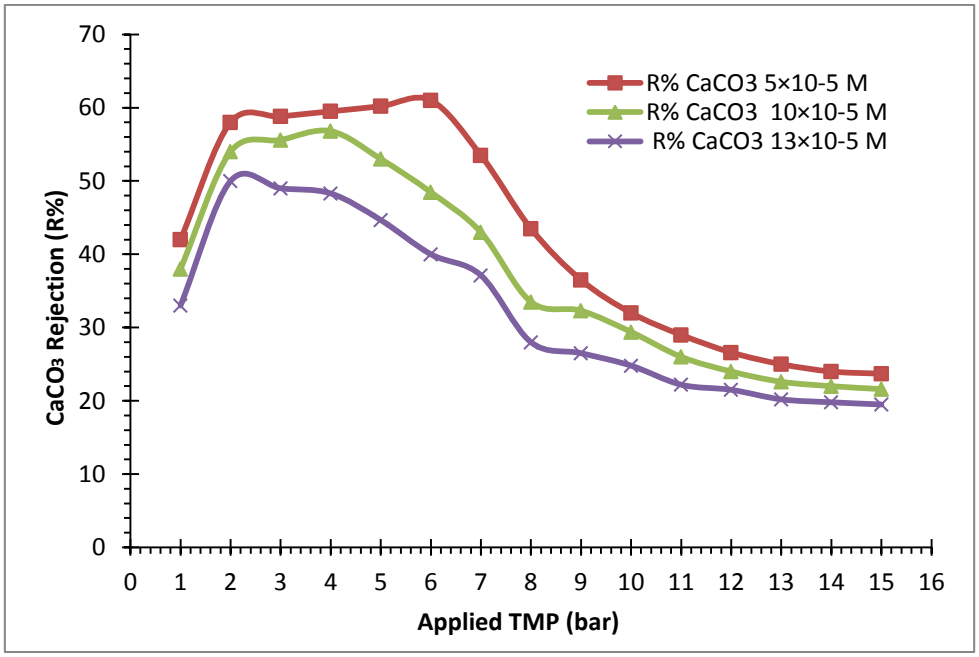

Figure 5.30 Calcium Carbonate Rejection as a Function of Applied (TMP) for the NF TiO_2 Membrane (1-15 bar) at three Concentration (5.0×10^{-5}, 10.0×10^{-5} and 13.0×10^{-5} M $CaCO_3$), Constant pH (6), Cross Flow Velocity 1 m/s and Temperature 25 ^oC.

After pressures 6,4 and 2 bar the rejections of calcium carbonate gradually decreases to the lowest rejection of (23.7%, 22% and 20%) for feed concentration (5×10^{-5}, 10×10^{-5} and 13×10^{-5} M) respectively, at 15 bar.

The rejection behavior of salt solutions of calcium carbonate is rare and differs from other salts. Although calcium carbonate salt ($CaCO_3$) has very low solubility in water (13×10^{-5} - 15×10^{-5} M at 25^o C), but its solubility increase with increasing pressure. All waters in contact with atmospheres absorb carbon dioxide. However, with increased applied transmembrane pressure (TMP), the pressure in the small nanopores of membrane will increase. Thus, the ratio of carbon dioxide solubility increased, carbonated water is formed by dissolving CO_2, reacts with lime

stone calcium carbonate ($CaCO_3$) to form soluble calcium carbonate ($Ca(HCO_3)_2$) **(Gill, 1996)**, as shown in the following chemical equations.

$$H_2O + CO_2 \rightarrow H_2CO_3 \quad (5.1)$$

$$H_2CO_3 + CaCO_3 \rightarrow Ca(HCO_3)_2 \quad (5.2)$$

The first reaction produces carbonic acid and the second reaction produces calcium bicarbonate.

A demonstration for the experimentally estimated rejection order can be found by matching the diffusion coefficients of the two different ions (CO_3^{-2} and HCO_3^-). The diffusion coefficient of HCO_3^- ion (1.19×10^{-9} m^2/s) is greater than CO_3^- ion (0.92×10^{-9} m^2/s) **(Li and Gregory 1974; Robinson and Stokes 1959)**. It is supposed that the coefficients of diffusion in the membrane can be similar by those in electrolyte solutions. The rejection of salts does not depend on the coefficient of diffusion of the salt, but on the ratio of coefficients of diffusion for the co-ions (HCO_3^- and CO_3^{-2}) and counter ion (Ca^{+2}) as previously fixed for another salts by **(Dresner, 1972)** in explanation the perfect exclusion theory. Rejection raises with lowering coefficient of diffusion of the salt if the ratio of diffusion coefficients of the ions is fixed **(Bowen, et al., 1997)**. Based on those determines diffusion coefficient of ($Ca(HCO_3)_2$) higher than the diffusion coefficient of ($CaCO_3$) and decreases the rejection with rising diffusion coefficient of the co-ion (HCO_3^-) and increases with rising coefficient of diffusion of counter-ion (Ca^{+2}). The order of the rejection sequence is inversely reflected in diffusion coefficients, so that diffusion shows to be a significant transport mechanism **(Johan, 1998)**.

Solubility of calcium carbonate ($CaCO_3$) increases due to the formation of more soluble calcium bicarbonate. This explains why the

rejection is reduced with increasing pressure to a certain rang, based on the calcium carbonate concentration.

Fig. 5.31 shows that the rejection calcium carbonate at 50×10^{-5} M (supersaturation) as a function of applied (TMP). Form this figure it can be deduced that the rejections of calcium carbonate decreased with increasing the applied (TMP).

The rejection of the calcium carbonate at applied (TMP) 1 bar was (34 %) for $CaCO_3$ concentration 50×10^{-5} M while the rejection at 10 bar was (-37.6 %). This explained by the reasons mentioned above in the case of concentrations 13×10^{-5} M and less. Add to that precipitation (or scaling) outcomes from the raised concentration of scale forming species behind their solubility limits and their scaling onto the membrane. A raised concentration of scale creating species in the bulk distinctly happens because withdrawal of permeate, that is further enhanced in the zone next to the permeate surface by superimposed influence of concentration polarization: in fact, as permeate of water through the membrane, the concentration of rejections ions in a layer of boundary near the membrane becomes significantly higher than which prevailing in the bulk. This impact is more pronounced at high fluxes of permeate and at low cross flow velocities **(Faller, 1999; Rautenbach and Albrecht, 1989)**. The nucleation and the growth of the crystal stages of the scale creation process based mainly on the ratio of supersaturation of a salt in the concentrate **(Tzotzi, et al., 2007)**.

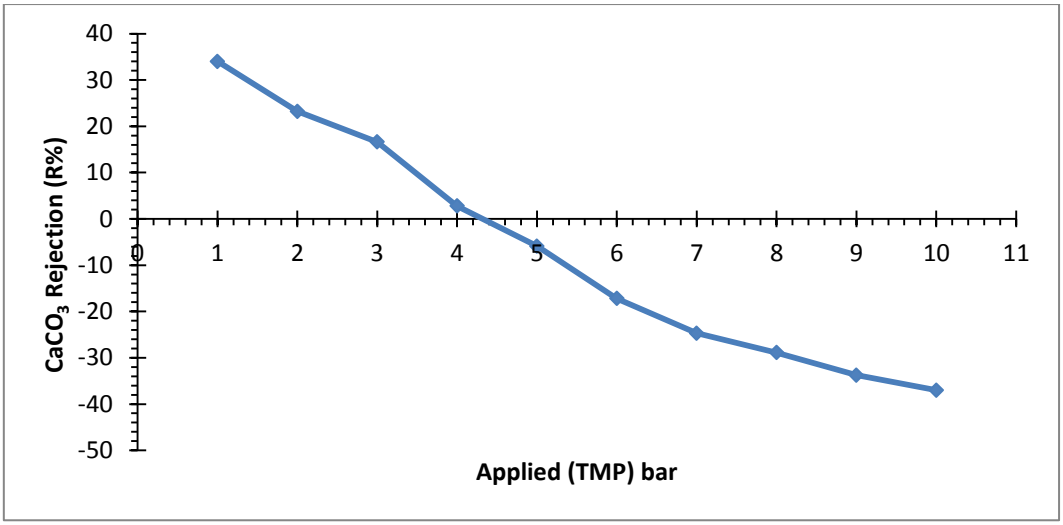

Figure 5.31 Calcium Carbonate Rejection as a Function of Applied (TMP) for the NF TiO_2 Membrane (1-10 bar) at Supersaturation Concentration (50×10^{-5} M $CaCO_3$), Cross Flow Velocity 1 m/s, pH 6 and Temperature 25 ^oC.

5.2.3 Effect of Zeta Potentials on salts rejection

In the present research the isoelectric point is about pH (3.3 – 3.5) (microelectrophoresis method) at concentration 0.1 and 0.01 M NaCl respectively and pH (3.6) for streaming potential method at 0.01 M NaCl, so a lower in salt rejection is predicted between pH 3.5 and 4. **Fig. 5.32** shows the rejection of NaCl as a function of pH at two various concentrations of NaCl, this explains the succession of the electrokinetic interactions developed between the ions and the ceramic membrane charge.

The lowest in the salt rejection is found at around pH 3.8 which is mainly in agreement with the isoelectric point fixed using streaming potentials. It appears that the isoelectric point found in situ form streaming potentials is a better predictor of the pH of lower rejection in a nanofiltration ceramic membrane. Since the lower rejection is still around 17% close to the isoelectric point, it is probable that repulsion of electrostatic is not the only mechanism included. These results are in consistent with the result obtained by **(Narong and James, 2006)**.

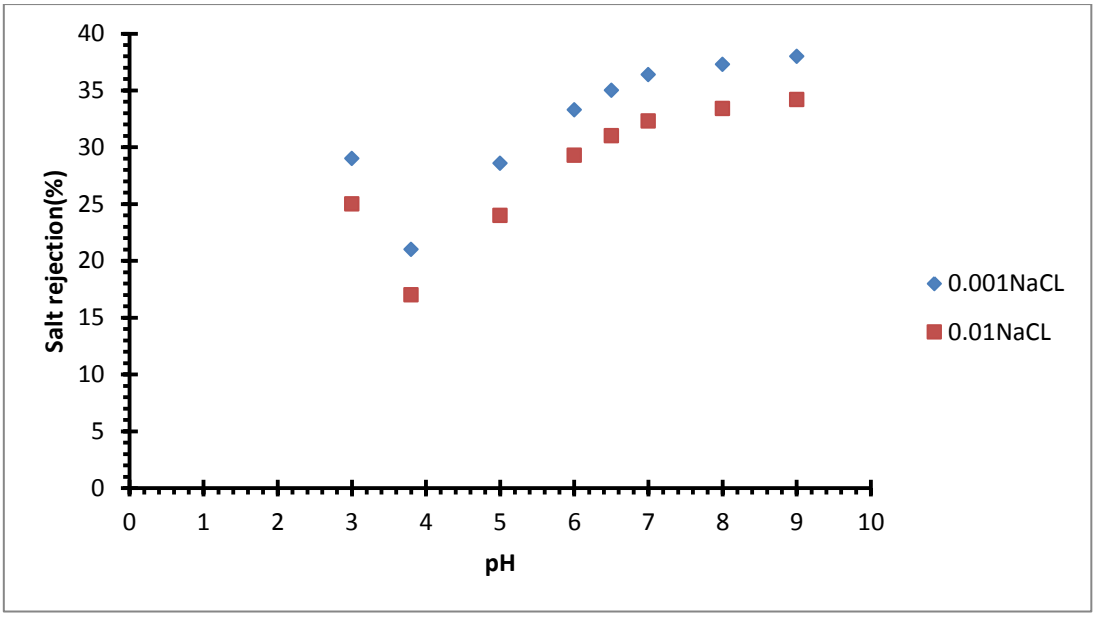

Figure 5.32 Percentage of Salt (Sodium Chloride) Rejection versus pH (3-9) in two Concentrations (0.01 M NaCl; 0.001 M NaCl), Constant Pressure (12 bar) , Cross Flow Velocity 1 m/s and Temperature 25 ^{o}C.

Nanofiltration membranes are commonly negatively charged and their negative charge rises with increased pH. The surface charge of the ceramic membrane, that rely on the pH of the solution, is a significant parameter inquiring the performance efficiency of a membrane separation process, exceptionally when eliminating ionic species. It must be conserved in mind that that Cl^- anion has a smaller hydrated radius 0.33 nm than Na^+ cation hydrated radius 0.36 nm **(Narong and James, 2006)** and that both of them are smaller than the pore size ceramic membrane used (0.9 nm). Subsequently, since the radius of ceramic membrane pore is large contrasted to the ionic radii, the rejection of electrolyte is not predominated by the impact of size and the major mechanism dependable for the rejection of salt is the electrostatic influence between the ceramic membrane surface and ions. The zeta potentials which are connected to its surface charge can be helpful significance of the ceramic membrane`s tendency for salt rejection. It shown that for the composite ceramic membrane (TiO_2 / Al_2O_3) used in the present research, the surface of ceramic membrane has charge with positive sign at low pH of (3), so that

the adsorption of H^+ ions from water must be still taken into consideration and this may assistance to excess the rejection rate **(Santos, et al., 2001)**. While, one of the operators ruling ion rejection by the NF ceramic membrane is the electrostatic repulsion between membrane and ions consequently changes in the streaming potential and zeta potential must be reflected by differences in salt rejection.

In this work, the zeta potential and the related streaming potential are shown to be functions of salt concentration (ionic strength) and pH. Raised salt concentration decreases the zeta potential by the compression the electrical double layer (EDL) while alter in pH changes the zeta potential of amphoteric metal oxide (ceramic membranes) through reactions of the type **(Ricq, et al., 1998)**:

$$MOH + H^+ \rightleftharpoons MOH^+ \rightleftharpoons M^+ + H_2O \quad (5.3)$$

$$MOH + OH^- \rightleftharpoons M(OH)_2^- \rightleftharpoons MO^- + H_2O \quad (5.4)$$

The first reaction produced positively charged surface and the second produce negatively charged surface. Therefor the isoelectric point matches to the point where is no net charge (zero) on the surfaces of membrane. In addition to separate from the amphoteric oxide surface dissociation the hydronium groups may be physically adsorbed thus changing the membrane surface charge. Accordingly, there is no electrostatic repulsion between the ions and the ceramic membrane surface. As there is no surface charge a ceramic membrane will be most inactive at its isoelectric point and this will be recorded as a lower in the salt rejection. This explanation can be applied to other results.

Fig. 5.33 shows the magnesium sulphate ($MgSO_4$) rejection as a function of (TMP) at pH (3.5, 6 and 9) at concentration (0.01 M), this

represents the sequence of zeta potential interactions developed between the membrane surface charge and the ions.

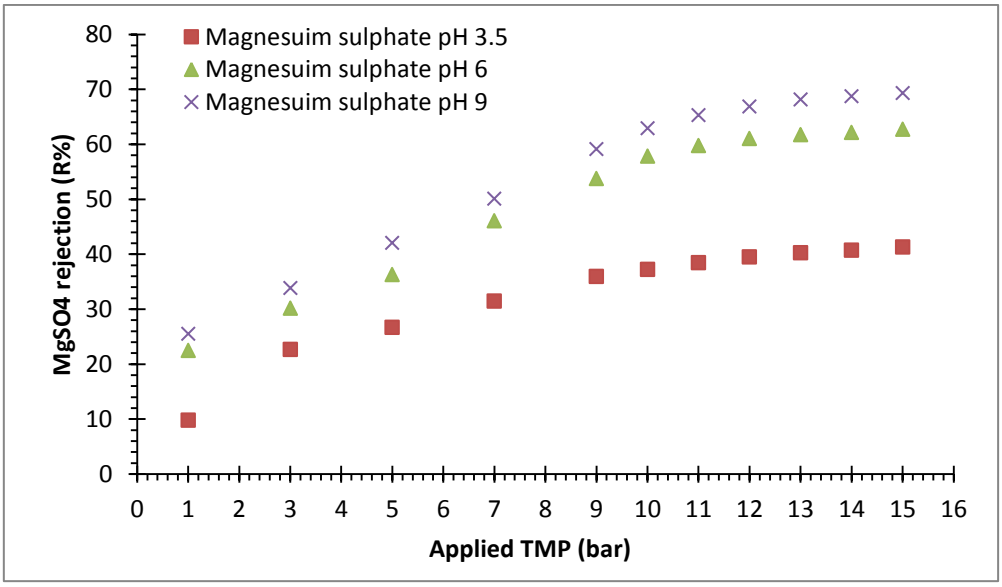

Figure 5.33 $MgSO_4$ Rejection at pH (3.5, 6.0 and 9.0) and Constant Concentration (0.01 M) versus TMP (1-15 bar), Cross Flow Velocity 1 m/s and Temperature 25 ^{o}C.

At the applied (TMP) of (1 bar), the rejection of (0.01 M $MgSO_4$) was (9.8 %, 22.5 % and 25.55 %) for pH value of (3.5, 6 and 9) respectively.

On the other hand, at highest applied (TMP) of (15 bar), the rejection of $MgSO_4$ salts was (41.3 %, 62.75 % and 69.35 %) for pH value of (3.5, 6 and 9) respectively, at constant feed concentration 0.01 M $MgSO_4$.This is due to the increased zeta potential with increasing of the pH which leads to the expansion of the double layer and Donnan potential, as a result, there is an increased repulsion between the membrane charge and ions.

The charge of material surface, that depends on the values of pH of the electrolyte solution, is an essential measurable factor inquiring the efficiency of a tubular ceramic NF membrane separation process. It should be saved in memory that the Ca^{+2} cation has a lesser ionic radius

(0.099) nm **(Hassan, et al., 2007)** than the CO_3^{-2} anion (0.178) nm **(Dasent, 1979)** and which both of them are smallest than the pore radius of NF membrane used 0.9 nm. Therefore, the interaction of the (zeta) potential that are connected to surface charge of membrane can be a helpful designation of a membrane`s propensity for rejection of salt.

The rejection of calcium carbonate at different pH (3,6 and 9) as a function of applied TMP is equal to (58%, 61% and 70%) respectively, for zeta potential (9.1, -20.95 and -34.8 mV) respectively at fixed concentration 5×10^{-5} M and velocity 1 m/s as shown in **Fig. 5.34**. It is shown that, for asymmetric titanium dioxide (TiO_2)/ Alumina (Al_2O_3) membrane used in the present research, the surface of membrane has positive charge at a value of pH lower than the pH value of isoelectric point (3.6 – 3.7), so that the cations adsorption, at least the ions of (H^+) from electrolyte solution must be taken into considerable and this may help to raise the rate of rejection and in addition the rate of rejection of the neutral salts combining a divalent cation and an anion could be predicted to reduction when the a values of pH rises to the IEP and then increase the percentage of rejection with increasing pH values more than IEP **(Santos, et al., 2001)**.

However, one of the essential parameters governing rejection of ions by the ceramic NF membrane is the repulsion of electrostatic between TiO_2 membrane and ions and thus alters in the zeta potential should be reflected by alters in rejection of salt. In this search, is seen to be functions of pH values and concentration of salt. Increased concentration of salt decreased the (zeta) potential by reducing thickness of the electrical double layer (EDL) whereas alter in values of pH changes the zeta potential of amphoteric titanium dioxide nanofiltration ceramic membrane. In the existent search the isoelectric point is about pH

of (3.6 – 3.7) (electrophoresis), thus a lower in the rejection of salt is predicted between pH of (3.5 – 4). **Fig. 5.34** shows the calcium carbonate ($CaCO_3$) rejection as a function of (TMP/permeate flux) at pH of (3 ,6 and 9) for concentration (5×10^{-5} M) calcium carbonate respectively, this represents the sequence of zeta potential interactions created between the membrane surface charge and the ions.

The least rejection of salt was found at pH of (3) equals to (58%) that is broadly in correspond with the determined of rejection (for different salt) by using streaming potential method **(Jacobasch, et al., 1996)**.

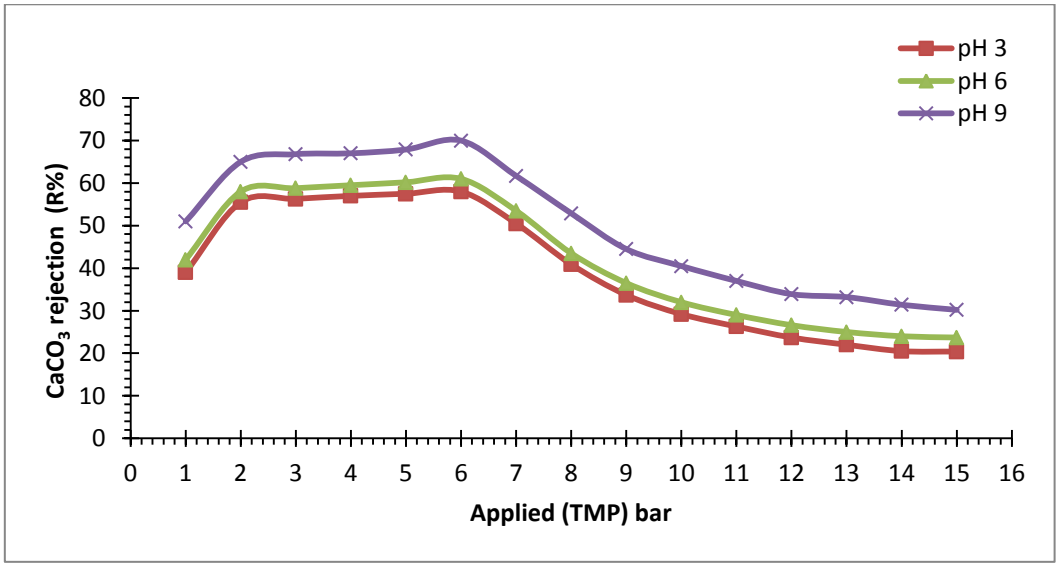

Fig. 5.34 Calcium Carbonate Rejection as a Function of Applied (TMP) for the NF TiO_2 Membrane (1-15 bar) at three Different pH (3, 6 and 9) and Fixed Concentration (5×10^{-5} M), Cross Flow Velocity 1 m/s and Temperature 25 ^{o}C.

5.2.4 Effect of Velocity on the Rejection

The cross flow velocity is an important factor in membrane filtration. **Fig. 5. 35** Shows the rejection of $CaCl_2$ at 0.01 M as a function of TMP for two different velocities (1 m/s and 2 m/s) respectively. Increasing the velocity from 1 m/s to 2 m/s led to an increase in rejections from (13.8%) to (16.4%) respectively at the lowest (TMP) 1.0 bar.

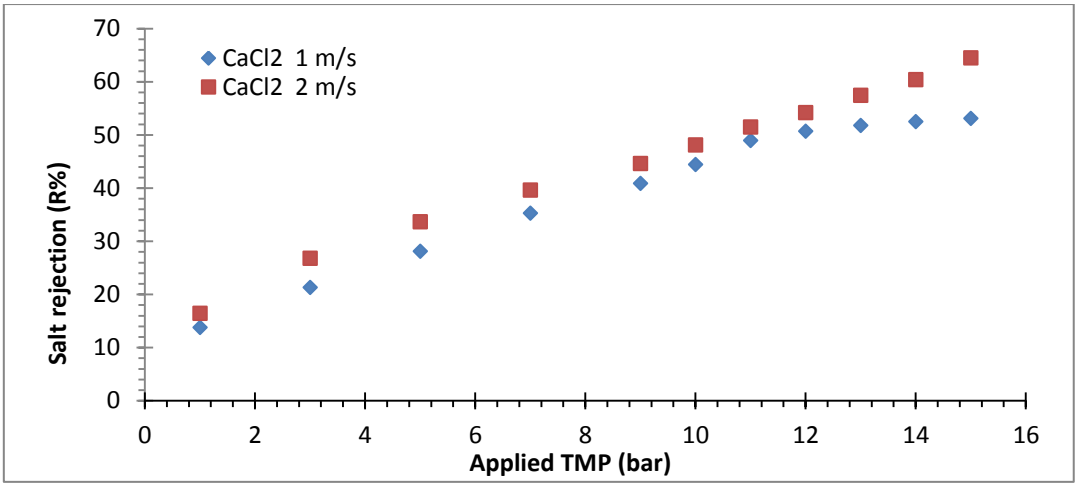

Figure 5.35 Calcium Chloride Rejection at (0.01 M) versus TMP (1-15 bar) at Cross Flow Velocity (1 and 2 m/s), Constant pH 6 and Temperature 25 ^{o}C.

On the other hand, at highest applied (TMP) of (15 bar), the rejection of $CaCl_2$ salts increased from (53.1%) to (64.5%). This results can be explained due to increase turbulence and thus reduce the make-up of polarization layer **(Broussous, et al., 1998; Faller, 1999; Johan, 1998; Rautenbach, and Albrecht, 1989 ; Stopka, et al., 2001)**. This explanation applies to the results of other experiments in this study.

The effect of across flow velocity on the rejection of ($CaCO_3$) as a function of (TMP) / flux of permeate has been studied. The experiments of rejection were conducted at average of feed pressures (1-15 bar) with solute feed concentration of 10 $\times 10^{-5}$ M and pH (6). **Fig. 5.36** shows that the rejection of ($CaCO_3$) was increased with increasing cross flow velocity as the maximum rejection (56.8 %) at 1 m/s has become (60.7 %) at 2 m/s and increase ratio was approximately (6%) and interpretation of the result is that increased across flow velocity leads to minimize concentration polarization.

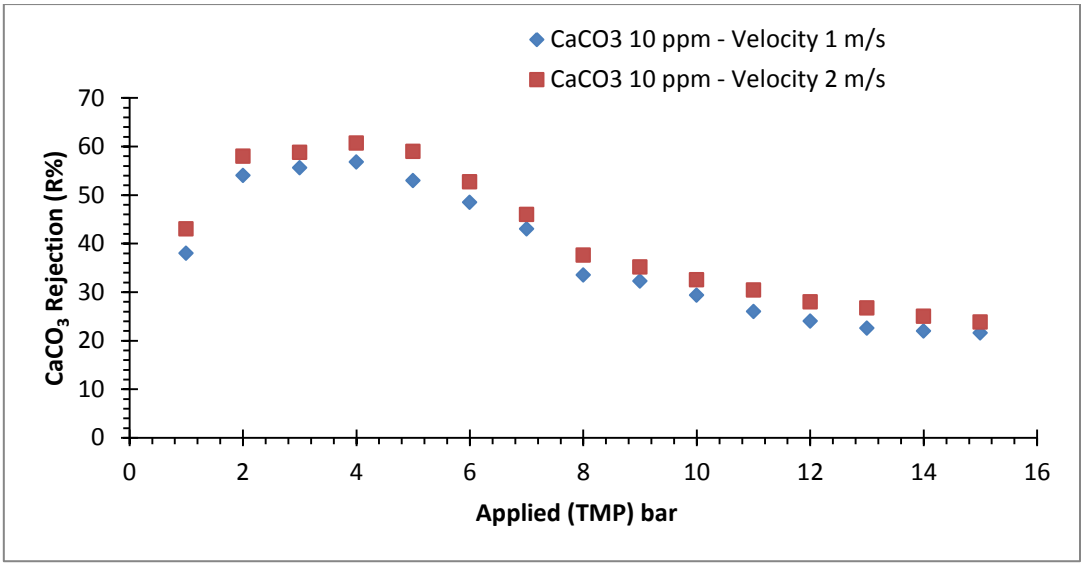

Figure 5.36 Calcium Carbonate Rejection as a Function of Applied (TMP) for the NF TiO_2 Membrane (1-15 bar) at Cross Flow Velocity (1 and 2 m/s), Fixed Concentration (10×10^{-5} M), pH 6 and Temperature 25 ^{o}C.

5.2.5 Effect of Anion on the Rejection

Fig. (5.37) shows the rejection of Sodium Sulphate, Sodium Bicarbonate and Sodium Chloride at 0.01 M as a function of applied (TMP). From this figure, it can be deduced that the rejections of Sodium Sulphate was higher than the rejection of ($NaHCO_3$ and NaCl). At the lowest applied (TMP) of 1.0 bar, the rejections were (24.5%, 13% and 2.1%) respectively. At the highest applied (TMP) 15 bar, the rejections of Sodium Sulphate, Sodium Bicarbonate and Sodium Chloride were (82,2% 57% and 30.1%) respectively. The sequence of rejection as the following: R % (Na_2SO_4 > $NaHCO_3$ > NaCl). This can be explained on the basis of diffusion coefficient of salphate ion (SO_4^{-2}) equal to 1.06×10^{-9} m^2/s **(Maria and Maria, 2000)** less than the diffusion coefficient of bicarbonate ion 1.19×10^{-9} m^2/s **(Li and Gregory 1974 ; Robinson and Stokes 1959)** and the latter less than the diffusion coefficient of chloride ion 2.03×10^{-9} m^2/s **(Maria, et al., 2000)**.

It is important to mention that the sequence of rejection is consistent with zeta potential sequence observed (see Section 5.1.2.2) and

another reason is the hydrated ionic radius of sulphate ion equal to 0.38 **(Hussain, et al., 2007)** nm is greater than the hydrated ionic radius of chloride ion 0.33 nm **(Schaep, et al., 1998)**.

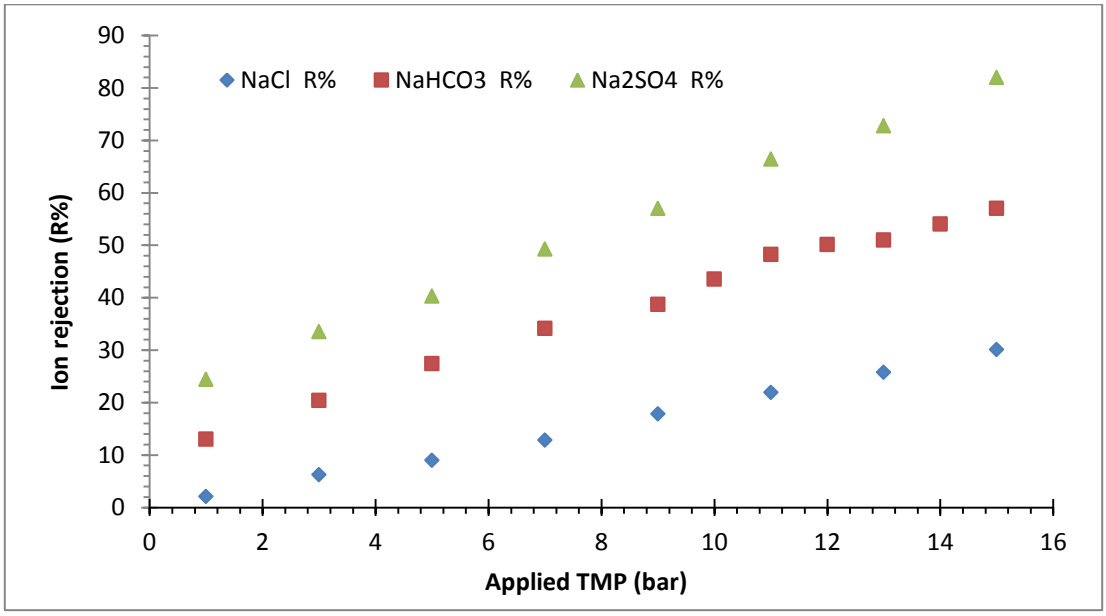

Figure 5.37 NaCl, $NaHCO_3$ and Na_2SO_4 Rejection at Constant Concentration (0.01 M), pH 6, Cross Flow Velocity 1 m/s and Temperature 25 ^oC versus TMP (1-15 bar).

5.2.6 Effect of Cation on the Rejection

The rejection behavior of ($CaCl_2$, $MgCl_2$ and NaCl) as a single salt at concentration (0.01 M) will be discussed.

Fig. (5.38) shows the following salt rejection sequence: R ($MgCl_2$> $CaCl_2$ > NaCl). This due to diffusion coefficient of calcium ion 0.92×10^{-9} m^2/s **(Newman, 1991)** less than the diffusion coefficient of sodium ion 1.33×10^{-9} m^2/s **(Shih, et al., 2005)**.

The behavior of rejection of salt ($MgCl_2$) is greater than ($CaCl_2$) because the zeta potential of ($MgCl_2$) larger than the zeta potential of ($CaCl_2$) (see Section 5.1.2.3). In addition, the rejection of ($CaCl_2$) is greater than (NaCl) because hydrated ionic radius of calcium ion equal to

0.41 nm **(Hassan, et al., 2007)** is greater than the hydrated ionic radius of sodium ion 0.36 nm **(Israelachvili, 2007)**.

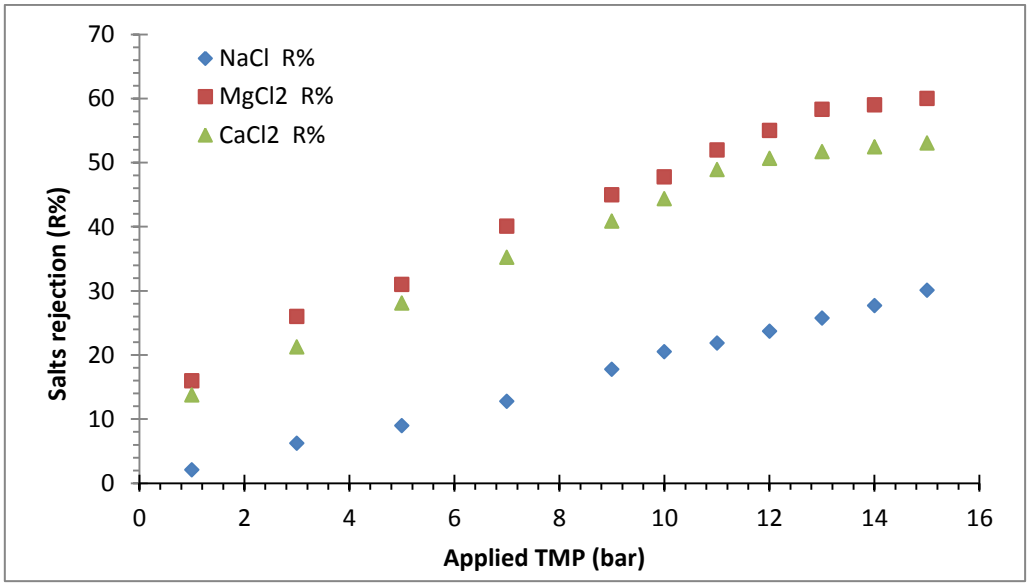

Figure 5.38 NaCl, $MgCl_2$ and $CaCl_2$ Rejection at Constant Concentration (0.01 M) pH 6, Cross Flow Velocity 1 m/s and Temperature 25 ^{o}C versus TMP (1-15 bar).

Fig. (5.39) shows the sodium sulphate rejection and magnesium sulphate rejection at concentration of 0.01 M. It can be seen from this figure the rejection of sodium sulphate larger than the rejection of magnesium sulphate. This due to the zeta potential of sodium sulphate at pH 6.0 equal to (-28.5) larger than the zeta potential of magnesium sulphate (-23.7) see Section (5.1.2.3). The mechanism of Donnan exclusion influence increase with increasing of the zeta potential **(Bandini, 2005)** and the separation mechanism in nanofiltration membranes is ordinarily demonstrated in terms of electrokinetic (zeta) potential **(Bandini, et al., 2005)**.

The meek consequence of the Donnan equilibrium is that solutes with opposite charge (counterions) of the NF TiO_2 membrane (Na^{+} and Mg^{+2}) are attracted whereas those with the same charge (coions) as the TiO_2 NF membrane are repelled **(Farah, 2013)**.

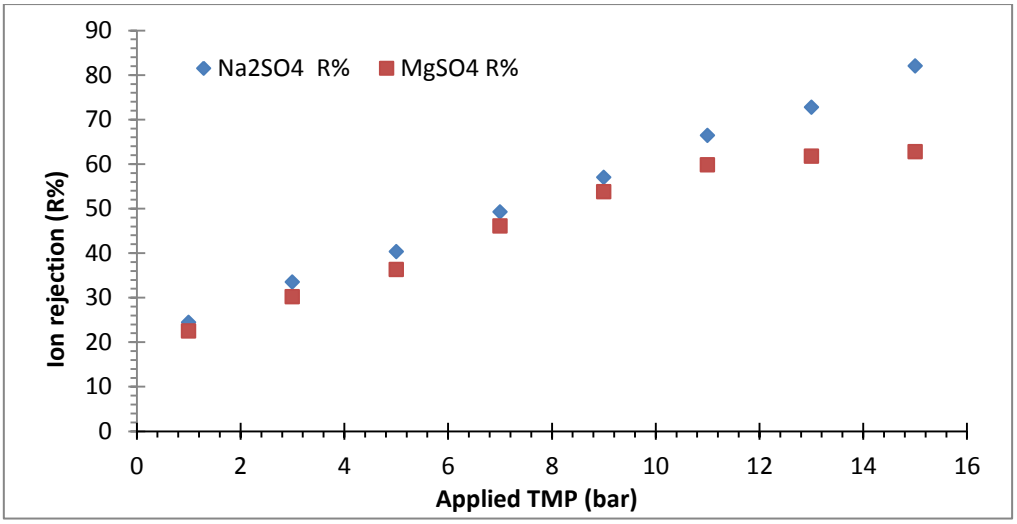

Figure 5.39 Na_2SO_4 and $MgSO_4$ Rejection at Constant Concentration (0.01 M), pH 6, Cross Flow Velocity 1 m/s and Temperature 25 ^oC versus TMP (1.0-15.0 bar).

The rejection behavior of (Na_2SO_4, $MgSO_4$, $MgCl_2$, $CaCl_2$, $NaHCO_3$ and NaCl) as a single salt at concentration (0.01 M) as shown in **Fig. (5.40)**.

Fig. (5.40) shows the following salt rejection sequence:

R (Na_2SO_4 > $MgSO_4$ > $MgCl_2$ > $CaCl_2$ ≥ $NaHCO_3$ > NaCl)

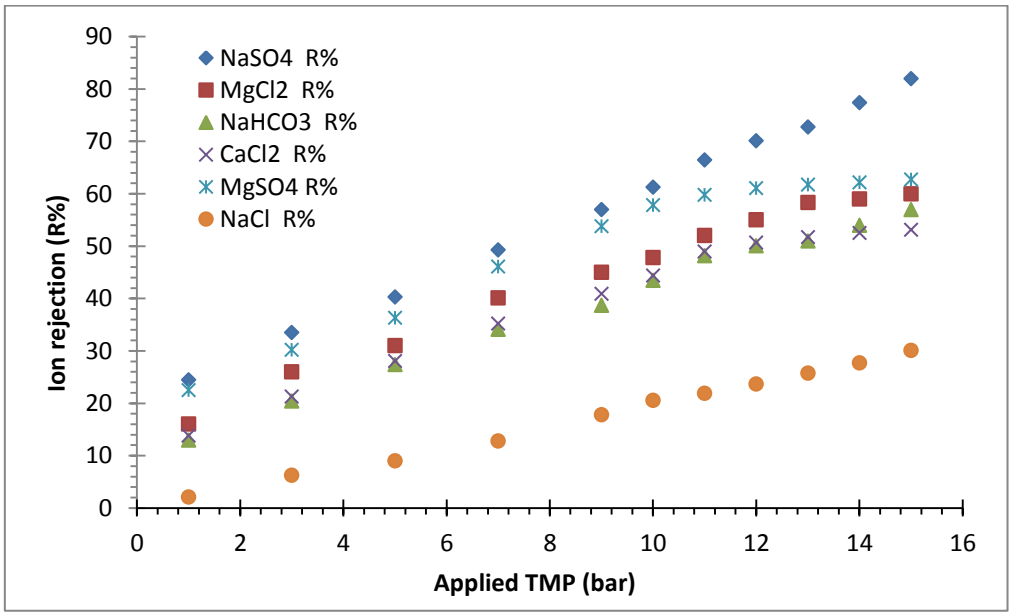

Figure 5. 40 $NaSO_4$, $MgCl_2$, $NaHCO_3$ $CaCl_2$, $MgSO_4$ and NaCl Rejection at Constant Concentration (0.01 M), pH 6, Cross Flow Velocity 1 m/s and Temperature 25 ^oC versus TMP (1-15 bar).

5.3 Critical Flux Determines

Basic reasons for the decline of permeate flux are fouling and concentration polarization is a reversible phenomenon which can be managed by adjusting the conditions of filtration. In several cases, concentration polarization encourages fouling. Therefore, lowering concentration polarization also reduces fouling significantly. Based on **(Field, et al., 1995)**, the concept of critical permeate flux is that, start up, there occurs a permeate flux lower position that a decline of permeate flux with time does not occur.

The concept of critical flux was inserted in this study based on cross flow filtration tests in order to characterize the fouling (scaling) behavior of magnesium sulphate at concentration (0.001, 0.005, 0.01 M), calcium chloride (0.001, 0.005, 0.01 and 0.015M), sodium chloride (0.001, 0.01, 0.1 M), sodium bicarbonate (0.01 M) and sodium sulphate (0.01 M).

5.3.1 Effect of Concentration on the Critical Flux using Flux – Pressure Profile (Step by Step Method)

To determine the critical flux, step by step method has been used for ($MgSO_4$, $CaCl_2$, NaCl, $NaHCO_3$ and Na_2SO_4) using a 0.9 ceramic titanium NF membrane. The measurements result from critical flux in this study by using the mention method for different salts solutions were discussed and compared.

For any of the above concentrations, there were fifteen step heights covered applied transmembrane pressure extent from 1 to 15 bars. For every setting. The average applied pressure or transmembrane pressure through the NF membrane (see **Eq. 4.19**) was determined based on the

recorded inlet and outlet pressure of the tubular NF membrane module whereas the pressure of permeate side was ignored.

In this technique, the permeate flux pressure of magnesium sulphate, calcium chloride solutions and other salts were compared to that flux of pure water, the solid line represents a tangent to the permeate flux pressure profile that is used ordinary for indicating the point that the profile diverges from linearity. **Fig. (5.41)** Shows the permeate flux of both pure water and magnesium sulphate (0.001, 0.005 and 0.01 M) versus transmembrane pressure for 0.9 nm TiO_2 NF membrane by using a step by step method.

It was observed from **Fig. (5.41)** that the critical flux was arrived and exceeded where the $MgSO_4$ solution permeate flux begins to deviate from linearity. Other significant factors that have an impact on estimating the critical flux as the temperature and cross flow velocity were fixed for each magnesium sulphate concentration. The effect of pH factor was studied. Results of experiments indicated that the critical flux magnitudes in titanium dioxide membrane depend basically on the ionic strength of magnesium sulphate. This study showed that the critical flux magnitudes resulted from step by step method were decreased as the ionic strengths (concentrations) of the $MgSO_4$ solution was increased.

Permeate flux of the strong form has occurred only in 0.001 M magnesium sulphate solution. Since all permeate fluxes do not deviate from tangential straight line, this form represents the conditions in which there is no deposition. Although the permeate flux of $MgSO_4$ solution diverted from pure water but, it was very little after TMP (11) bar, it does not deviate from permeate flux line of $MgSO_4$ with increased (TMP). In other word all permeate fluxes with increasig pressures are located on one tangential line and this indicates that there is no critical flux at

concentration (0.001 M $MgSO_4$) and the flux of strong form. Critical flux of the weak form was occurred in 0.005 and 0.01 M magnesium sulphate solutions. It can be seen from the obtained results using step by step method that the estimated critical flux magnitudes were 55 and 26 ($l/m^2.hr$) for magnesium sulphate solutions 0.005 and 0.01 M respectively.

It can be seen from **Fig. (5.41)**, permeate flux of magnesium sulphate (0.005M) was not identical to that of pure water. Flux even at lowest (TMP). Based on this, the critical flux considered weak form. The critical flux was exceeded at TMP higher than (12) bar where the solute permeate flux no longer linearly dependent. According to the method of step by step, the critical flux ($J_{crit.}$) of magnesium sulphats (0.005 M) in a 0.9 nm membrane equals to 55 ($l/m^2.hr$) at TMP (12) bar.

The permeate flux of magnesium sulphate at (0.01M) concentration was remarkably lower than which of pure water flux at the identical (TMP), subsequently, the critical flux is weak form. This figure showed that the critical flux value exceeded at TMP higher than (9) bar where the permeate flux of solute solution was no longer linearly dependent. The critical flux of (0.01M $MgSO_4$) 26.2 ($l/m^2.hr$) at TMP (9) bar. It can be seen from the figure that the magnesium sulphate permeate flux at 0.01M concentration was greatly lower than that of pure water flux beginning from the lowest (TMP). Therefore, the critical flux at this concentration was clearly weak form. According to these results, it can be seen that the values of critical flux were decreased up to (50 %) when the concentrations of magnesium sulphate increased from (0.005 M) to (0.01 M). Thus, a raise in concentration reduces the critical flux. The results of this study consistent with findings of researchers **(Chiu and James, 2005; Mänttäri and Nyström, 2000)**.

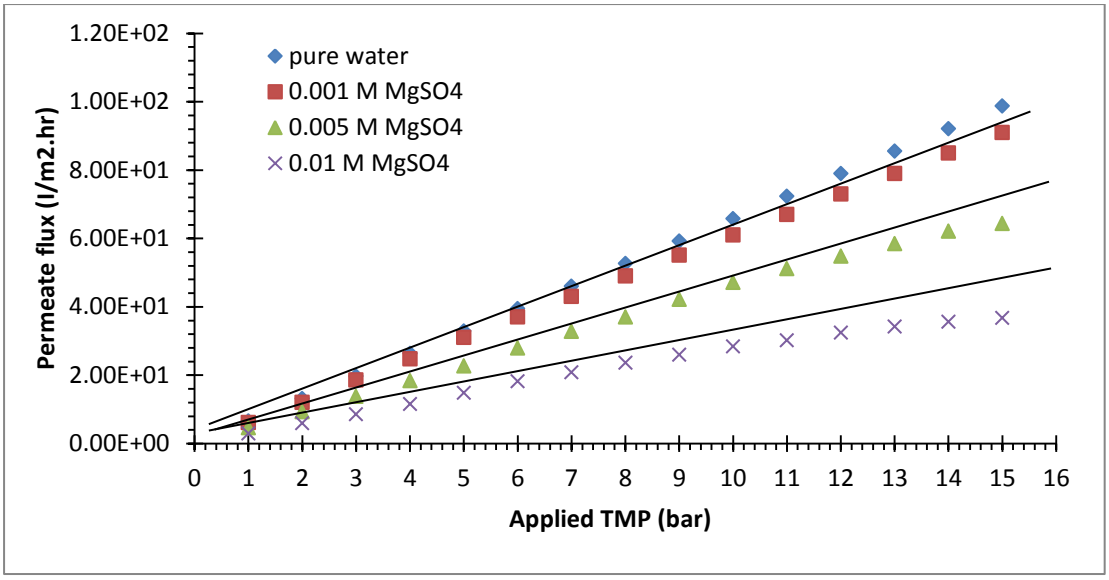

Figure (5.41) Critical Flux of (0.001, 0.005, 0.01M) $MgSO_4$ at Constant pH 6, Cross Flow Velocity 1 m/s and Temperature 25 ^oC.

Fig. (5.42) Shows the permeate flux of both pure water and calcium chloride at (0.001, 0.005, 0.01 and 0.015 M) and pure water versus (TMP) by using step by step method for 0.9 nm TiO_2 NF membrane. It can be shown from **Fig. (5.42)** that at comparable pressures reach to 15 bar the profile of (0.001 M) $CaCl_2$ was nearly similar as that of pure water. At transmembrane pressure slightly lower than 13.0 bar, $CaCl_2$ solution permeate flux was started to deviate very little but all permeate fluxes increased pressures are located on one tangential line and this indicate that there is no critical flux at concentration (0.001M $CaCl_2$) and flux of strong form.

According to **Fig. (5.42)** the permeate flux of calcium chloride (0.005M) was not comparable to that of pure water flux at TMP more than 6 bar and in which permeate flux equals to 34.92 ($l/m^2.hr$). This indicates, that the permeate flux is strong form the beginning up to TMP 6 bar after that its form is weak. The critical flux was exceeded above TMP of (14 bar) when the permeate flux was no longer linearly dependent.

Fig. (5.42) Shows differences in the permeate flux of calcium chloride (0.01M) and pure water with trans membrane pressure even at the lower TMP. It can be seen from **Fig. (5.42)** that the critical flux was exceeded above the TMP of 12 bar in which permeate flux equals to 57.5 ($1/m^2$.hr). based on this, the observed critical flux form was weak from the beginning. **Fig. (5.42)** shows differences in the permeate flux of calcium chloride (0.015M) and pure water even at the minimum (TMP). According to this the critical flux can be observed of the weak form. It can be seen from this figure the critical flux was exceeded above the (TMP) of 11 bar where the $CaCl_2$ solution permeate flux was no longer linearly dependent. Based on the determination of the step by step technique, the critical flux of calcium chloride (0.015M) in a 0.9 nm ceramic titanium dioxide equals to 43.3 (l/m^2.hr). It was observed from **Fig. (5.42)** that the critical flux arrived and exceeded where the calcium chloride ($CaCl_2$) permeate flux begins to deviate from linearity.

Strong permeate flux has occurred only in 0.001 M ($CaCl_2$) solution. Although the permeate flux of ($CaCl_2$) diverted from pure water but, it was very little after (TMP) 13 bar, it does not deviate from permeate flux line with increased (TMP). Critical flux of weak form was occurred in 0.005, 0.01 and 0.015 M ($CaCl_2$).

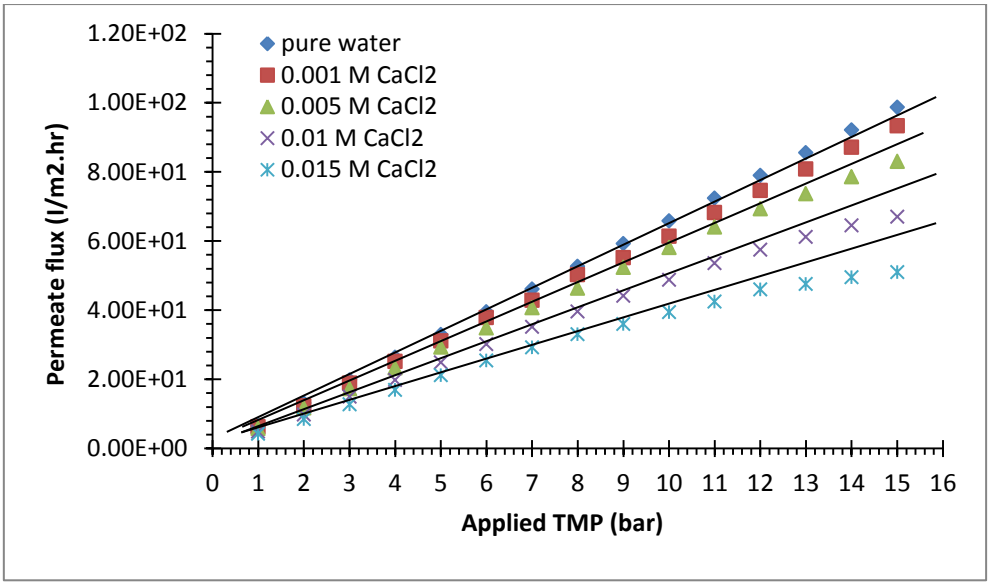

Figure 5.42 Critical Flux of (0.001, 0.005, 0.01, 0.015 M) $CaCl_2$ at Constant pH 6, Cross Flow Velocity 1 m/s and Temperature 25 ^oC.

Fig. (5.43) shows the volume flux of permeate for sodium chloride at 0.001, 0.01 and 0.1 M (NaCl) as a function of applied (TMP). It can be noticed from **Fig. (5.43)** that there is a steady and linear increasing of permeate flux of NaCl salts solutions connected to the increased applied (TMP). There was a little change in permeate flux, for each sodium chloride concentration as a function of the applied (TMP). At the applied (TMP) of 1.0 bar, permeate volume flux of NaCl salt was 6.46, 6.08 and 4.31($1/m^2$.hr) for feed concentration of 0.001, 0.01 and 0.1 M respectively.

While at the largest applied TMP of 15 bar, permeate volume flux of NaCl salt was 96.89, 91.15 and 64.59 ($1/m^2$.hr) for feed concentration of 0.001, 0.01 and 0.1 M respectively. Whereas the permeate flux of pure water was 98.87 ($1/m^2$.hr). According to **Fig. (5.43)** and for each NaCl concentration, it can be deduced that the volume flux of permeate increased with increasing applied TMP, while the volume flux of permeate reduced with the increasing of feed concentration. It can be seen from this figure that the permeate flux of sodium chloride (0.001 M) and

pure water was similar and this means no critical flux occurs. At (0.01 M) NaCl the profile was nearly similar at identical pressures reach to 11 bar, then permeate flux of NaCl started to deviate very little, however, all permeate fluxes-increased pressures are located on one tangential line and this indicate there is no critical flux at concentration (0.01 M) NaCl and flux strong form until pressure 12 bar.

Fig. (5.43) Shows that permeate fluxes of NaCl solution at concentration (0.1 M) were not identical to pure water fluxes, accordingly, the flux was weak form, all permeate fluxes-increasing pressures are located on one tangential line and this indicate there is no critical flux at concentration (0.1 M) NaCl and flux weak form until pressure 15 bar.

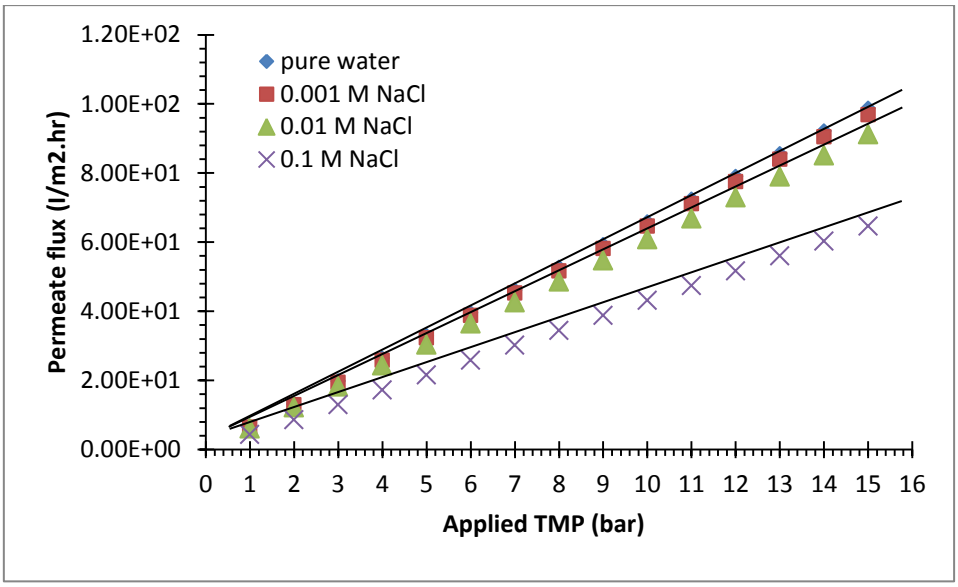

Figure 5.43 Critical Flux of (0.001, 0.01 and 0.1 M) NaCl at Constant pH 6, Cross Flow Velocity 1 m/s and Temperature 25 ^{o}C.

Fig (5.44) shows the volume flux of permeate for sodium sulphate and sodium bicarbonate at concentration (0.01 M) as a function of applied (TMP).It can be seen from this figure that the permeate fluxes of (Na_2SO_4 and $NaHCO_3$) at (0.01 M) were not identical to pure water fluxes and accordingly, the fluxes were weak form, all permeate fluxes with

increasing pressure are located on one tangential line for each of the salt and this indicate there is no critical flux at concentration (0.01 M) and flux weak form until pressure 15 bar.

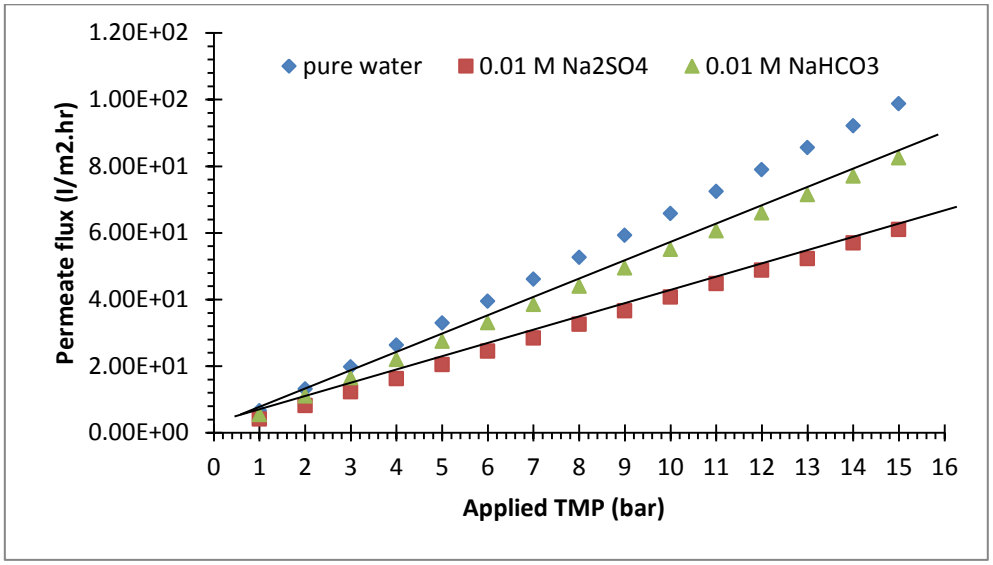

Figure 5.44 Critical Flux 0.01M Na2SO4 and $NaHCO_3$ at Constant pH 6, Cross Flow Velocity 1 m/s and Temperature 25 ^{o}C.

5.3.2 Effect of pH on the Critical Flux

The critical flux increased with increasing in the zeta potential (or pH) as shown in **Fig. (5.45)**. At pH of 6 and 9 the values of zeta potentials for (0.01 M) $MgSO_4$ equals to (-23.73 mV) and (-36.82 mV) respectively (see Section 5.1.2.3).

When the pH increased, the interface repulsion between the ions and the membrane was increasing also, due to the changes in zeta potential (increased) of the membrane. As the result, the similar effect found when reducing concentration (ionic strength) is monitored. The rising interface repulsion prohibits particles from deposing on the surface of TiO_2 NF membrane creating a rising critical flux. These results are consistent with result obtained by **(Elzo, et al., 1998; Huisman, et al., 2000; Jönsson, et al., 1988)**. One enjoyable mark is that the extra alkaline conditions, an apparent rise is monitored in the critical flux, then

the rises in the electrokinetic potential **(Elzo, et al., 1998; Huisman, et al., 2000)** shown in this figure. This interpretation can be applied to the other salts.

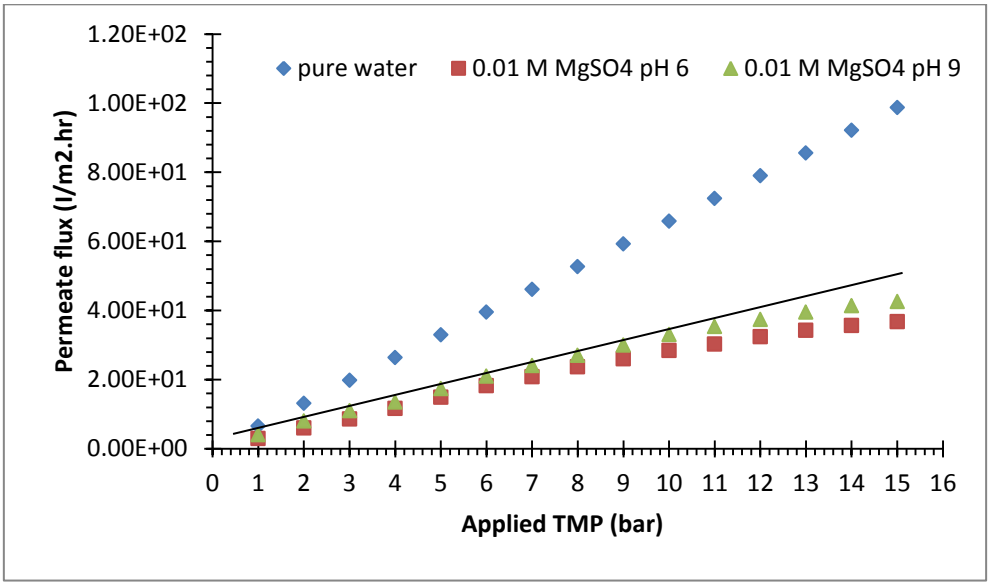

Figure 5.45 Critical Flux of 0.01 M $MgSO_4$ at pH (6 and 9), Cross Flow Velocity 1 m/s and Temperature 25 ^oC.

It can be seen from **Fig. (5.45)** that the critical flux for of 0.01 M ($MgSO_4$) at pH of 9 was noticeably higher than which of 0.01 M ($MgSO_4$) at pH of 6.

5.3.3 Influence of Valency

The gained critical fluxes by using various background electrolytes have different valences, it is appeared that valiancy raises from (+1) to (+2), the critical flux reduces as shown in **Fig. (5.46).**

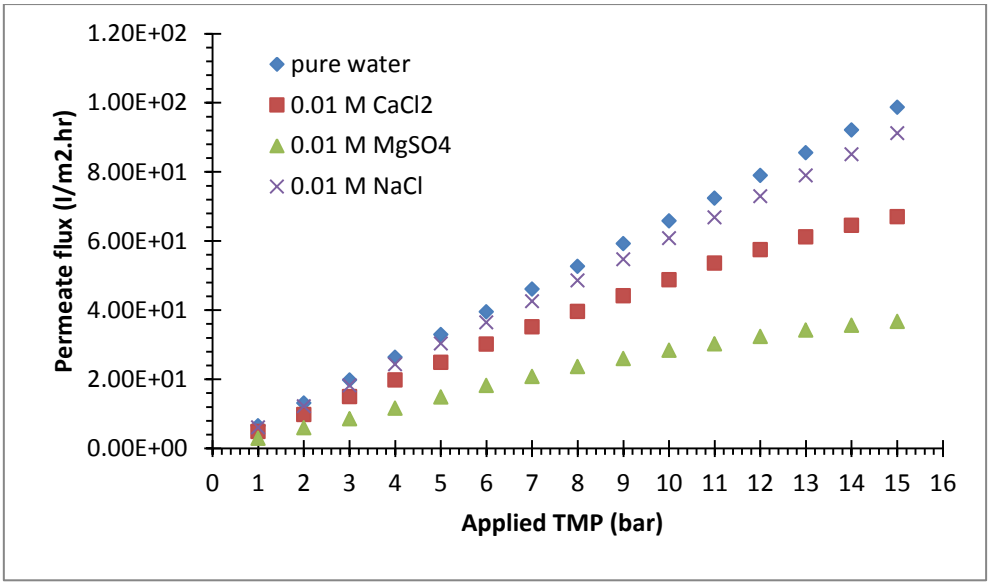

Figure 5.46 Critical Flux of 0.01 M $CaCl_2$, $MgSO_4$ and NaCl at Constant pH 6, Cross Flow Velocity 1 m/s and Temperature 25 ^oC.

The outcomes gained are the same to trends stated by other investigators **(Elzo, et al., 1998)** who inspected interactions of inter particle during membrane filtration less fluxes by using ions of higher valiancy.

Divalent magnesium and calcium ions are particularly adsorbed, rising a reduction in the value of electrokinetic potential (zeta) as shown in section (5.1.2.3), that is associated with a less charge on the TiO_2 NF membrane and thus it leads to a reduce in energy of repulsive interaction. In that case, the forces of attractive becomes controlling and enhance fouling.

5.3.4 Comparison Critical Flux of Salts

The Table 5.5 Shows the influences of increasing concentration on critical flux**.** The maximum flux was occurred in the absence of salt (ultra-pure water) of approximately 98.87 ($l/m^2.h$). A decreased flux (14.6 %), (27.22%) and (40.2 %) was obtained for 0.005, 0.01 and 0.015 M $CaCl_2$ respectively.

As for the magnesium sulphate salt ($MgSO_4$) a decreased flux (30.4 %), (44 %) was obtained for 0.005 and 0.01 M respectively. At the presence of ($CaCl_2$) ions and ($MgSO_4$) ions, the charges of the TiO_2 NF membrane are screened. This induces between the membrane and the particles. Therefore, the buildup of a cake deposit happens most rapidly generating in a decreased critical flux when contrast to the situation where ($CaCl_2$) and ($MgSO_4$) ions are absent.

The similar conclusion and direction has been stated by researchers **(Chiu and James, 2005; Espinasse, et al., 2002; Kwon, et al., 2000; Riley,1990)** though both groups of workers used latex particles.

Table (5.5). Impact of Changing Electrolyte Type, Concentration of Electrolyte and Ion Valency

Type of electrolyte	Form of flux	Concentration of electrolyte (M)	Valency	Critical flux J_{crit} ($l/m^2.hr$)	Permeate of pure water ($l/m^2.h$)	(TMP) bar
$MgSO_4$	Strong	0.001	2 : 2	no critical flux (91)	98.87	15
	Weak	0.005		55	79	12
	Weak	0.01		26	59	9
$CaCl_2$	Strong	0.001	2 : 1	no critical flux (93.3)	98.87	15
	Weak	0.005		78.6	92	14
	Weak	0.01		57.5	79	12
	Weak	0.015		43.3	72.4	11
Sodium chloride	Strong	0.001	1 : 1	no critical flux (96.89)	98.87	15
	Strong	0.01		no critical flux (91.15)	98.87	15
	Weak	0.1		no critical flux (64.59)	98.87	15
$Na(HCO_3)$	Weak	0.01	1 : 1	no critical flux (82.5)	98.87	15
Na_2SO_4	Weak	0.01	1 : 2	no critical flux (61)	98.87	15

5.4 Effective Pore Radius (r_p) Determination of 0.9 nm Ceramic TiO_2 NF Membrane

There are several approaches proposed in the literature to characterize the membrane effective pore radius (r_p). The present study will determine the effective pore radius of the ceramic nanofiltration

membrane based on the one best method consist of transport equations of solutes inside membrane pores, the Hagen-Poiseuille equation and permeation test of uncharged solute (glucose) **(Bowen et al., 1997; Bowen and Mohammad, 1998; Lee et al., 2008)**.

Pore size of the membrane is an important NF membrane characteristic to determine the effect of the solute size on its rejection. To calculate the membrane pore size, the Donnan steric pore partitioning model (DSPM) was used.

The rejection of solutes was determined as a function of the flux. For 0.9 nm NF ceramic membrane the results are shown in **Fig. (5.47)** The hindered nature of solute (glucose) transport in the extended Nernst-Plank equation (ENP) gives the ability of estimated (r) of the ceramic NF (TiO_2) membrane.

The Hagen-Poiseuille equation provides the relationship between the applied pressure across the membrane and the pure water flux (J_w) as follows **(Ahmad and Ooi, 2006**):

$$J_w = VA_K = \frac{r_p^2 P}{8\mu(\frac{\Delta x}{A_K})} \quad (4.17)$$

P is the applied pressure (pa) and μ is the dynamic viscosity of solution (pa.s).The rejection of solutes was determined as a function of the flux. For 0.9 nm NF ceramic membrane the results are shown in **Fig. (5.48).**

Experiment of rejection for an uncharged solute (glucose) at concentration of 200 (ppm) **(Johan, et al., 1998**) was conducted by using the present study tubular ceramic titanium dioxide NF membrane at various applied pressure limited from 1 to 8 bars. The glucose rejection was determined based on its bulk permeate concentrations **Equation (4.12)**. **Fig. (5.47)** shows the flux of permeate (m/s) versus the applied

pressure/ 8 μ (s^{-1}). The resulting slop ($\frac{r_p^2}{\Delta x/A_k}$) from **Fig. (5.47)** equals to 1.5×10^{-13}. Subsequently, the active membrane thickness (Δx) can be easily measured from the determined slope as function of the measured effective pore radius $\Delta x = (r_p^2 A_K / slope)$.

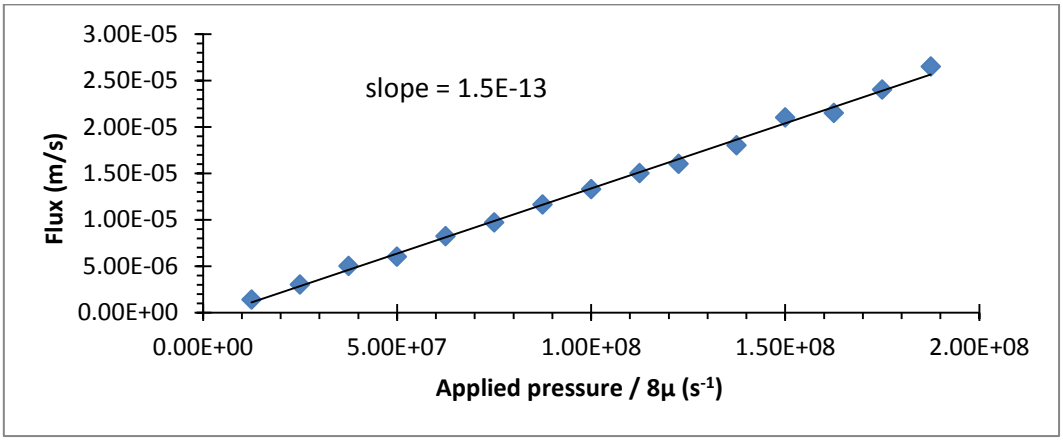

Figure 5.47 Permeate Flux of Glucose as a Function of Applied Pressure for NF Membrane.

Fig. 5.48 shows the rejection of glucose with the permeate flux of glucose (m/s) in the present study for ceramic NF titanium dioxide membrane. Data of the glucose rejection show, as predictable, that the rejection increases with permeate flux increase. By using (Microsoft`s spreadsheet solver™ add in, Microsoft Excel™) and substituting **Equations (4.15), (4.9), (4.10), (4.16), (4.7) and (4.8) into Equation (4.14)**, and solved to evaluate the effective membrane pore radius of the NF titanium dioxide membrane according to the result rejection value of the glucose. The active layer thickness of the effective membrane surface can be substituted in terms of effective pore radius of membrane surface that was also stated in the slope of **Fig. (5.47).**

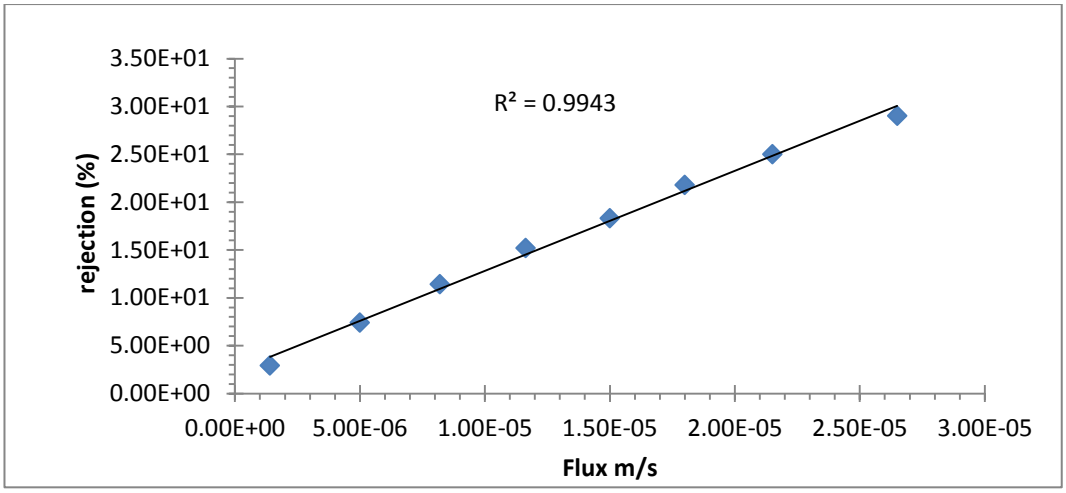

Figure 5.48 Rejection of Glucose as a Function of Permeate Flux for 0.9 nm (TiO_2) NF Membrane.

The determined result of the effective pore radius for the existent tubular ceramic titanium dioxide membrane from using the Donnan steric pore model showed that the effective pore radius of the present tubular NF ceramic titanium membrane was found equal to 0.56 nm.

After knowing the value of effective pore radius, the active layer of the membrane can then be easily determined from the slope equation declared in **Fig. (5.47)**, the determined effective layer thickness (Δx) of the ceramic membrane titanium dioxide based on the Donnan steric pore model was equal to 0.8×10^{-6} (m) and the ratio of effective membrane length (thickness) to porosity ($\Delta x_e = \Delta x/A_k$) was approximately equal to 2×10^{-6} m. The effective estimated results of the effective ceramic (TiO_2) radius and active membrane thickness from applying this model are in agreement with the result stated by **(Bowen and Mukhtar, 1996)**.

The determination effective pore radius (r_p) of membrane was used to estimate the basic physicochemical parameters of membrane whereas the evaluation of the active layer thickness (Δx) of membrane based on the Donnan steric pore model was used to estimate the equivalent active layer thickness (Δx_e) of membrane that can be defined as the ratio of

active layer thickness to the membrane surface porosity **(Geraldes and Brites, 2008; Bowen, et al., 1997)**.

5.5 Donnan Potential Determination

This part consists of three main parts; the first one is correlated to the evaluation surface charge density of the membrane particles surface whereas the second part and third part are correlated to the evaluation of the effective fixed charge density of membrane particles and the Donnan potential.

5.5.1 Surface Charge Density Determination

The net particle surface charge density or the electrokinetic particles surface charge density (σ^s) at the plane shear (slipping) can be determined from the electrokinetic (zeta) potential data depending on the Gouy-Chapmman theory. In the case of relatively low potential which less than 50 mV **(Pessarakli, 1999)**, and depending on the electrical double layer, the correlation between the zeta potential and the surface charge density at the hydrodynamic shear plane is given in Graham Eq. (4.20).

The magnitude of the Debye length (K^{-1}) for (1:1) electrolytes (for example NaCl) can be estimated from the equation (4.21). The membrane particles surface charge density can be calculated from Graham equation by substituting the magnitudes of zeta potential which were previously evaluated for each (pH) value (see appendix (C), Tables (C.5.1), (C.5.2) and (C.5.3)) at 0.001,0.01 and 0.1 M NaCl respectively.

The membrane zeta potentials that can be evaluated from electrokinetic measurements gives information concerning the net charge of the particles surface and thereby, membrane charge density (X^m) can be determined from data of zeta potential depending on the theory of

Gouy-Chapman and Graham equations. **Fig. (5.49)** shows a plot of the estimated surface charge density (mC/m^2) across a range of pH magnitudes from (3 to 9) using 0.001 ,0.01 and 0.1 M (NaCl) respectively, as a background electrolyte.

The results from **Fig. (5.49)** shows as the pH magnitudes increase, the particles surface charge density begins to be more negative found at pH (9) that is equal to (-2.53 mC/m^2), (-7.46 mC/m^2) and (-17.67 mC/m^2) at 0.001, 0.01 and 0.1 M NaCl respectively, while, at a pH of 3 the particles surface density becomes positive with a value of (0.62 mC/m^2), (0.87 mC/m^2) and (0.55) for 0.001, 0.01 and 0.1 M NaCl respectively that quite the same behavior of related zeta potential.

The outcomes also show that the (pH) magnitudes for 4 to 9, there is significant jump in the net particles surface charge magnitudes from (-0.98 mC/m^2 to -2.53 mC/m^2), (-2.52 mC/m^2 to -7.46 mC/m^2) and (-3.2 to -18.21) for 0.001, 0.01 and 0.1 M NaCl respectively, that would reflect the influence of (pH) on the outcomes of the particles surface charge density. The evaluated membrane particles surface charge density determined from the present study is compatible with study done by **(Hurwitz, et al., 2010)**, their results showed that for (zeta) potential of (-20.6 mV), the related surface charge was equal to (-5.0 mC/m^2) for 0.01 M NaCl, while in the present study, for a measured membrane zeta potential of (-24.51) mV, (-21.44) mV the related evaluated membrane surface charge (-5.6 mC/m^2), (-4.9 mC/m^2) by using microelectrophoresis method and streaming method respectively (see Appendix C, Tables C.5.2 and C.5.4) and which can prove the uniformity the outcomes between the determined outcomes of this study compared with Hurwitz et al. study. This consistence in outcomes between the above two works means that there were usually compatible in other important determined

factors such as the Debye length (K^{-1}) magnitude for (1:1) electrolytes, that was original evaluated in this study depending on a simplified Graham formula which represents the diffuse layer thickness in the electrical double layer theory.

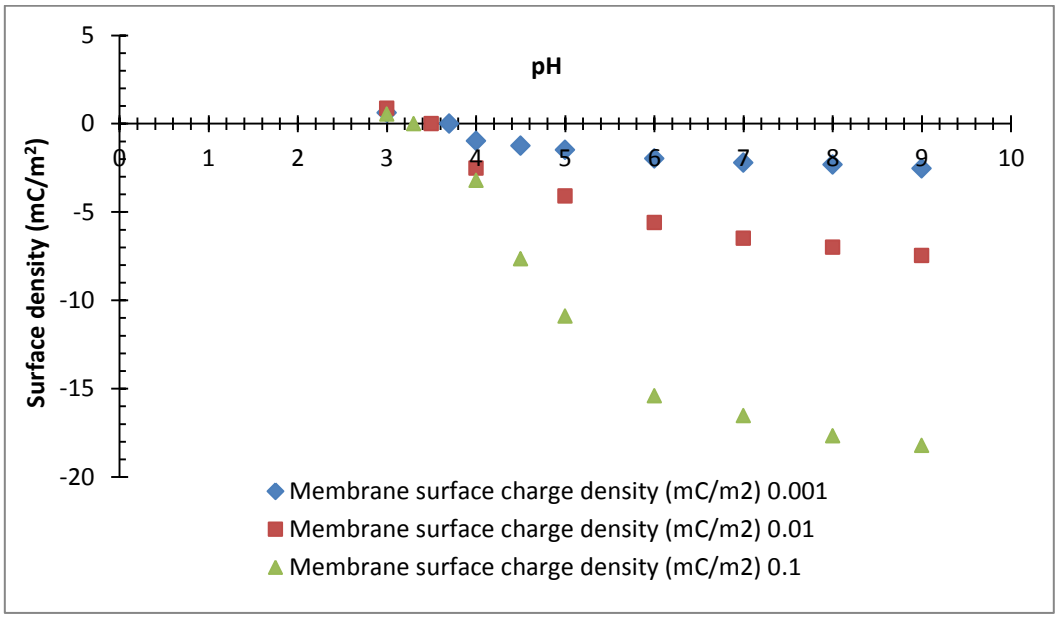

Figure 5.49 Surface Charge Density (mC/m^2) of 0.9 nm Tubular Ceramic Titanium Dioxide NF Membrane Estimated from Micro-Electrophoresis Potential Plotted versus pH (3-9) for Background Electrolyte (Concentration) Fixed at 0.001, 0.01 M and 0.1 M Sodium Chloride and Temperature 25 ^{o}C.

Fig. (5.50) shows surface charge density (mC/m^2) for NF TiO_2 membrane determined from two method streaming and microelectrophoresis potential method plotted versus pH values from (3-9) at constant concentration 0.01 M NaCl. It can be seen from **Fig. (5.50)** that the results of the surface charge for both methods are identical to a large degree.

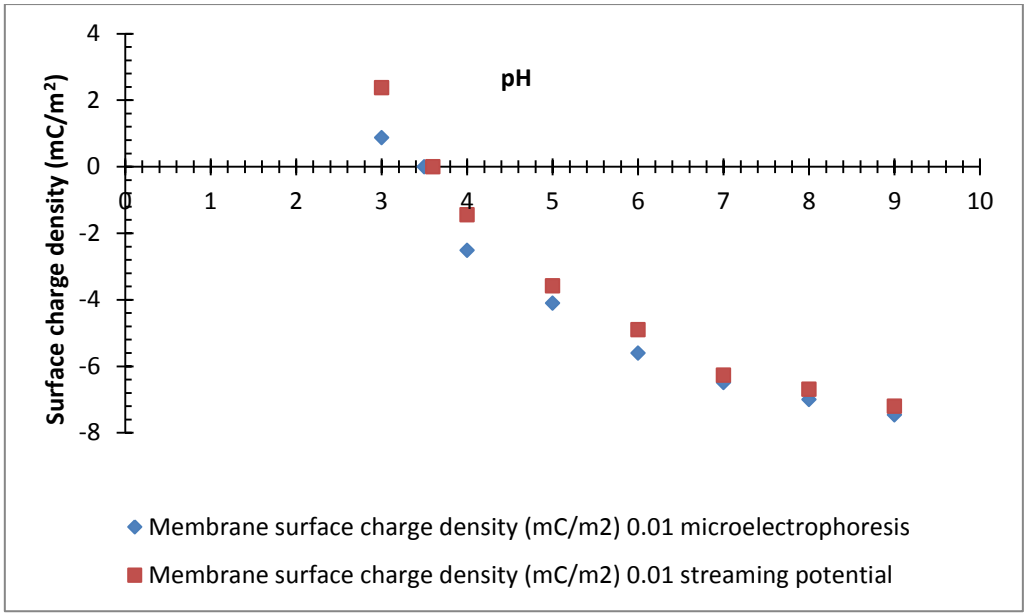

Figure 5.50 Surface Charge Density (mC/m^2) of 0.9 nm Tubular Ceramic Titanium Dioxide NF Membrane Estimated from Two Methods (Streaming and Micro-Electrophoresis Potential) Plotted versus pH (3-9) for Background Electrolyte (Concentration) Fixed at 0.01 M Sodium Chloride and Temperature 25 ^{o}C.

5.5.2 Effective Charge Density Determination

Net charge density of the membrane (X^m) at the shear plane was estimated depending on (the Gouy-Chapman and Graham equations). So, the evaluated surface charge of membrane particles can be then transformed to concentration units by using equation 4.26 The fixed charge density (X^m) of the membrane particles represents the concentration of electrical charged on the membrane particle surface in (mol/m^3).

Eq. (4.26) assumes that the surface charge of the membrane particles is uniformly distributed in the void volume of pores. It is important to mention that in this equation, the effective membrane surface pore radius (r_p) for the tubular ceramic titanium dioxide membrane used in this study is equal to 0.56nm (depending) on pore radius evaluated from (DSPM) model, (see Section 5.4).

Fig. (5.51) shows a plot of the estimated membrane effective charge density (X^m) in (mol / m^3) over a range of (pH) magnitudes from 3 to 9 using (0.001, 0.01 and 0.1 M NaCl) respectively as a background electrolyte for a 0.9 nm tubular ceramic titanium dioxide nanofiltration membrane. In order to determine the effective charge density (X^m) for membrane in (mol/m^3), the estimated membrane particles surface charge (σ^s), (mC/m^2) should be subsequently transformed to concentration unites (X^m), (mol/m^3). It is important to mention this can be done with the assumption that the surface charge of membrane particles is uniformly distributed in the void volume of the pores.

The effective charge of the membrane particles is really representing the electrical charge groups concentration on the membrane particles in (mol/m^3), The results from appendix (C), Tables (C.5.1), (C.5.2) and (C.5.3)) show that at (pH=3), the effective membrane particles charge was equal to (22.95 mol/m^3), (32.2 mol/m^3) and (20.36 mol/m^3) related to surface charge density (0.62 mC/m^2), (0.87 mC/m^2) and (0.55 mC/m^2) for (0.001. 0.01and 0.1 M NaCl) respectively, while at pH (9), the effective of the membrane charge particles was equal to (-93.67 mol/m^3), (-276.18 mol/m^3) and (-719.56 mol/m^3) related to the surface charge density (-2.53 mC/m^2), (-7.46 mC/m^2) and (-18.21 mC/m^2) for (0.001. 0.01and 0.1 M NaCl) respectively. It can be readily realized this factor is also dependent on (pH) value.

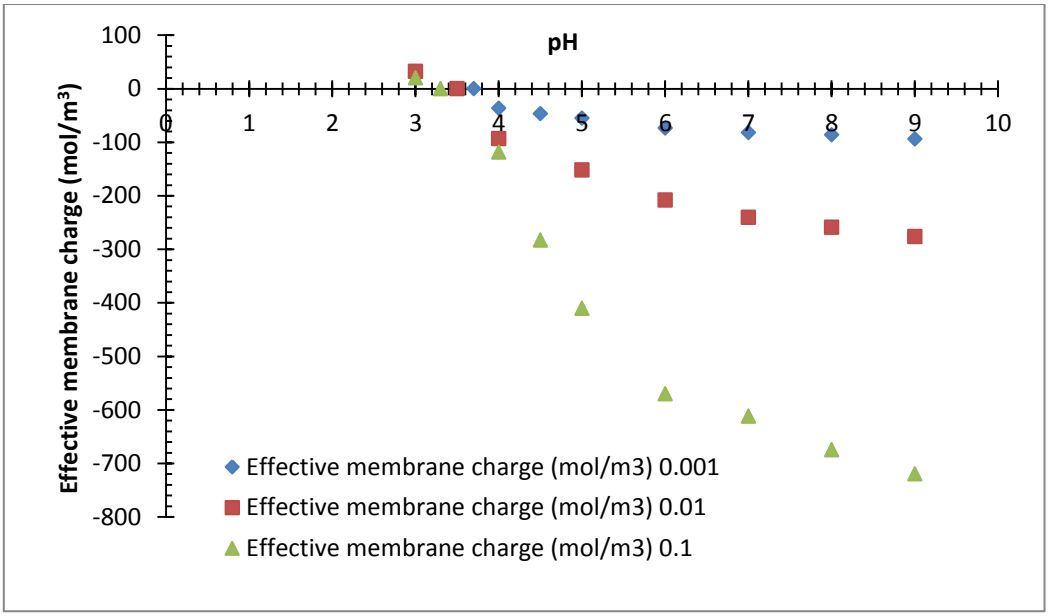

Figure 5.51 Effective Membrane Charge (mol/m^3) of 0.9 nm Tubular Ceramic Titanium Dioxide NF Membrane Estimated from Micro-Electrophoresis Potential Plotted versus pH (3-9) for Background Electrolyte (Concentration) Fixed at 0.001, 0.01 M and 0.1 M NaCl and Temperature 25 ^{o}C.

Fig. (5.52) shows effective charge density (mC/m^3) for NF TiO_2 membrane determined from streaming and microelectrophoresis method plotted versus pH values from (3-9) at constant concentration 0.01 M NaCl. The results of the effective membrane charge for both methods are identical as the membrane surface charge density σ^s.

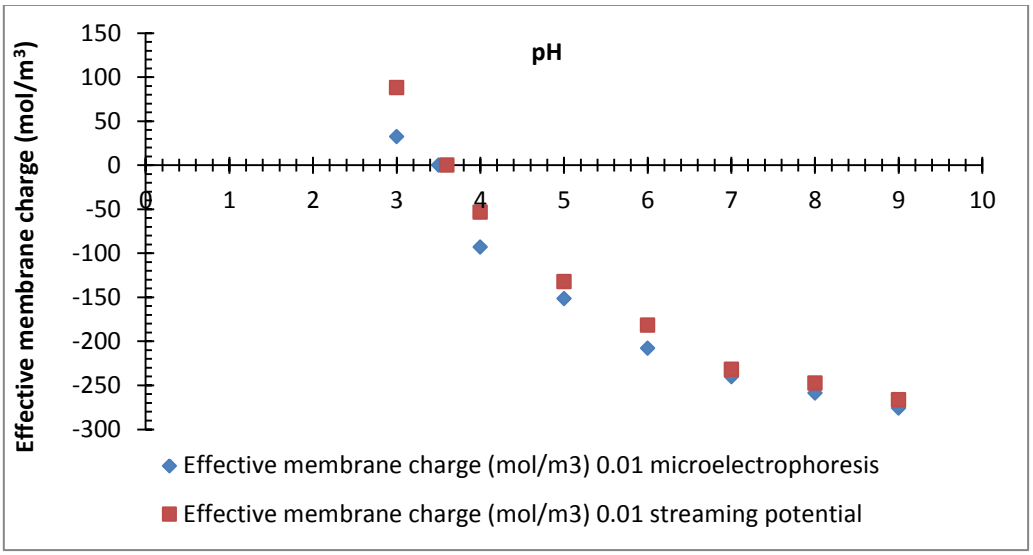

Figure 5.52 Effective Membrane Charge (mol/m^3) of 0.9 nm Tubular Ceramic Titanium Dioxide NF Membrane Estimated from (Streaming and Micro-Electrophoresis Potential) Plotted versus pH (3-9) for Background Electrolyte (Concentration) Fixed at 0.01 M NaCl and Temperature 25 ^{o}C.

5.5.3 Donnan Potential of NF Membrane

In the present study, the Donnan potential magnitudes in (mV) were calculated from Chein formalism (see equation 4.25) depending on the magnitudes of the effective membrane particles charge (x^m) in (mol/m^3) for bulk concentration $C_{i,bulk}$ of 0.001, 0.01 and 0.1 M sodium chloride solution.

Fig. (5.53) shows a plot of the estimated Donnan potential (mV) across a range of pH magnitudes from (3 to 9) using 0.001 ,0.01and 0.1 M (NaCl), as a background electrolyte. Results from (appendix (C), Tables (C.5.1), (C.5.2) and (C.5.3)) show that as (pH) magnitudes increase, the potential of Donnan becomes more negative at pH(9) is equal to (-12.3 mV) ,(-3.66 mV) and (-0.897 mV) for 0.001 ,0.01 and 0.1M sodium chloride respectively, while at a (pH) of 3 the potential of Donnan becomes positive with a values of (2.95 mV), (0.58 mV) and (0.03 mV) for 0.001 ,0.01 and 0.1M sodium chloride respectively, obviously, the lower the concentration, the greater the Donnan potential at the same (pH).

Also, the outcomes show that for the (pH) magnitudes from 4 to 9, there is a significant jump in the determined Donnan potential magnitudes from (-4.57 mV), (-1.19 mV) and (-0.174 mV) to (-12.3 mV), (-3.66 mV) and (-0.897 mV) for 0.001, 0.01 and 0.1M sodium chloride respectively. The determined Donnan potential magnitudes achieved is in agreement with the results of study worked by **(Pivonka, et al., 2005)**. The outcomes from this study show that's at the same background electrolyte concentrations of 0.01M NaCl and at normal pH; the Donnan potential magnitude is equal to (-2.96 mV), while the Donnan potential value from the present work is equal to (-3.19 mV), (-3.12 mV) by using

microelectrophoresis method and streaming potential method respectively.

The Donnan potential is basically dependent on salt bulk concentration of feed, concentration of effective fixed charge in the membrane (x^m), and valence of both co-ions and counter ions. All those factors exist in equation (4.25), therefore by applying this equation, a direct magnitude for Donnan potential can be determined.

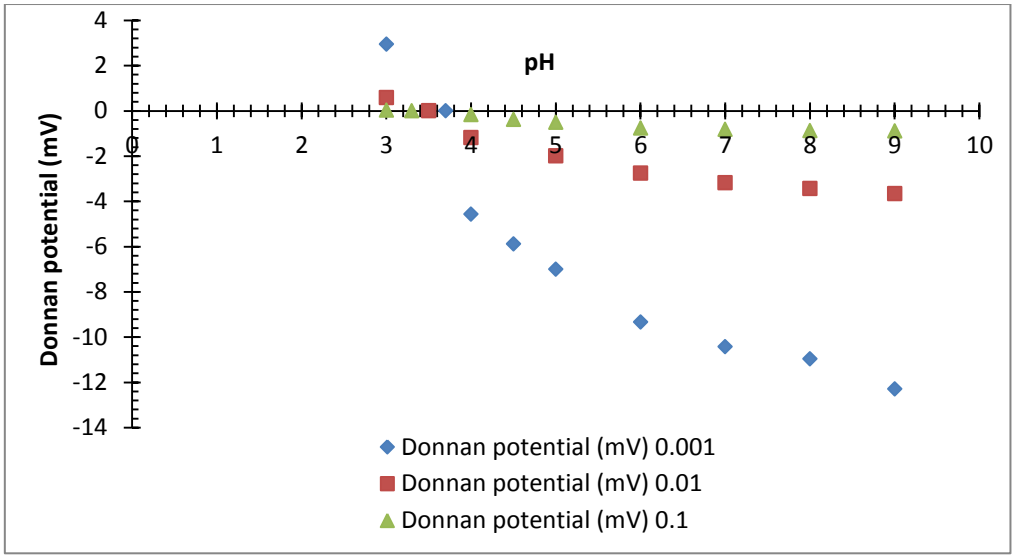

Figure 5.53 Donnan Potential of 0.9 nm Tubular Ceramic Titanium Dioxide NF Membrane Estimated from Micro-Electrophoresis Potential Plotted versus pH (3-9) for Background Electrolyte (Concentration) Fixed at 0.001, 0.01 M and 0.1 M NaCl and Temperature 25 ^{o}C.

Fig. (5.54) shows Donnan potential (mV) for NF TiO_2 membrane determined from streaming and microelectrophoresis potential method plotted versus pH value (3-9) at constant concentration (0.01 M NaCl).

It can be seen from **Fig. (5.54)** that the results of the Donnan potential for both methods are identical as the membrane effective charge density. The Donnan potential (ψ_D) created by the microelectrophoresis method is higher than (ψ_D) created by streaming potential method with a very small percentage (3.5%) approximately. This is due to the difference in technique used in both methods. This gives a strong and sure indication

of the success of the alternative silver electrodes used to measure the zeta potential by using streaming potential.

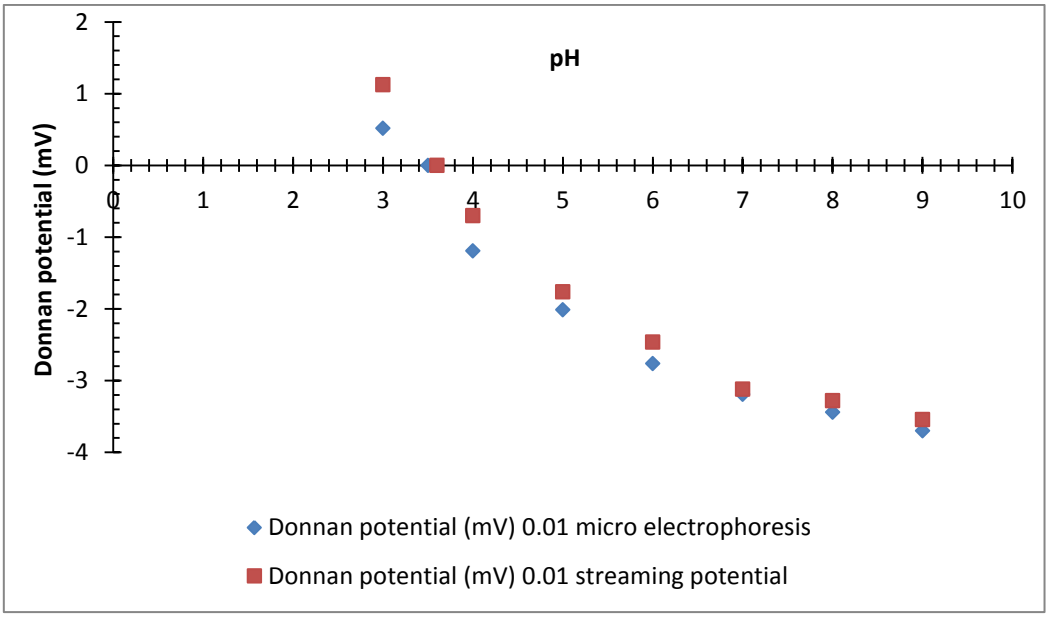

Figure 5.54 Donnan potential of 0. 9 nm Tubular Ceramic Titanium Dioxide NF Membrane Estimated from (Streaming and Micro-Electrophoresis Potential) Plotted versus pH (3-9) for Background Electrolyte (Concentration) Fixed at 0.01 M NaCl and Temperature 25 ^{o}C.

5.6 Oilfield Produced Water

The produced water from Bazargam oilfield was treated by using flat plate polymer membranes (MF, UF) and (tubular ceramic TiO_2 NF membrane, flat plate polymer RO membrane).

Table 5.6 shows the values of oil, TOC and TDS before and after treatment of four membranes.

Table 5.6 Testes of Oil, TOC and TDS for Produced Water before and after Treatment

Test	Before Treat. (PPM)	After Treat. MF at 1 bar, Flow Rate 140 l/h (mg/l)	Removal	After Treat. UF at 2 bar, Flow Rate 140 l/h (mg/l)	Removal	After Treat. NF at 12 bar, Flow Rate 140 l/h (mg/l)	Removal	After Treat. RO at 60 bar Flow Rate 288 l/h (mg/l)	Removal
TOC	3920	626	84 %	483.3	87.7 %	164.4	95.8 %	0.406	99.99 ≈ 100 %
Oil	769	73.5	90.44 %	24.8	96.77%	4.5	99.4 %	0	100 %
TDS	63900	not measure	not measure	not measure	not measure	44730	30 %	359	99.44 %

The **Figs. (5.55)** and **(5.56)** show rejection of ions (Ca^{+2}, Mg^{+2}, Na^{+1}) and the total dissolved solid plotted versus TMP (1 - 12 bar). The **Figs. (5.55)** and **(5.56)** also show that the rejection increased with increasing of TMP and decreasing TDS respectively. The highest rejection and removal of TDS obtained at TMP 12 bar by using the best conditions obtained from pervious experiments.

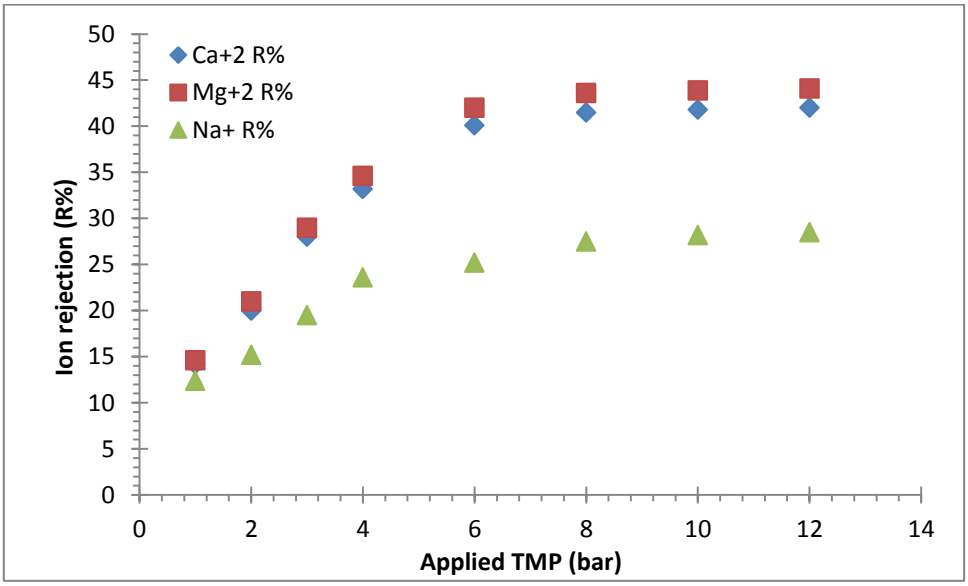

Figure 5.55 Rejection of Calcium ion 51.445 gm/l, Magnesium ion 7.1145 gm/l and Sodium ion 28.6376 gm/l Concentration versus TMP (1-12 bar) at pH 6, Cross Flow Velocity 2 m/s and Temperature 25 ^{o}C.

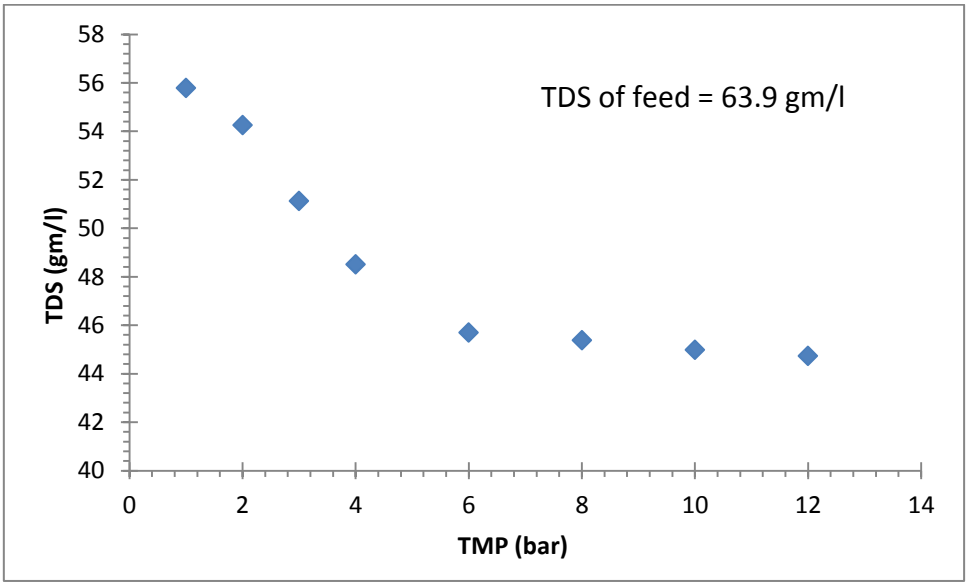

Figure 5.56 TDS of Oilfield Produced Water versus TMP 1-12 bar at pH 6, Cross Flow Velocity 2 m/s and Temperature 25 ^{o}C.

Fig. (5.57) shows the permeate flux of both pure water and oilfield produced water (63.9 gm/l) versus transmembrane pressure by using step by step method. It was observed from **Fig. (5.57)** that the critical flux of produced water started to deviate from pure water linear flux at TMP just below 6 bar. Above this pressure the critical flux was exceeded since the produced water permeate flux was clearly deviate from linearity.

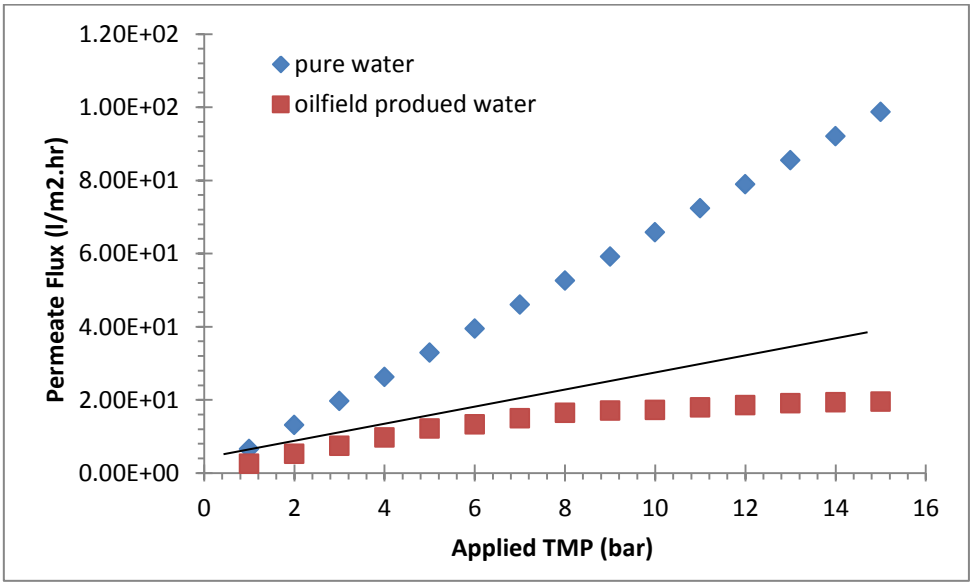

Figure 5.57 Critical Flux of Oilfield Produced Water at Concentration 63.9 gm/l, pH 6, Cross Flow Velocity 2 m/s and Temperature 25 ^{o}C.

5.7 Theoretical Results of Donnan Steric Pore Model (DSMP): Numerical Solution

The program has been used for one feed concentration of sodium chloride (as a reference solution) at a various volume of permeate flux based on the area of the membrane ($m^3/m^2.s$) values. Value of the concentration used was the similar as the value used in the experiments. It is important to note that the model has only been turned for sodium chloride (NaCl) due to the presence some limitations for being solved for other kinds of ions.

The Runge-Kutta method was used in this program to solve equations (4.11), (4.28), (4.27) and (4.12), to determine the change of

ions concentration across the membrane (inside membrane) and concentrations of ions in the permeate solution. After estimating the concentration of ions in the permeate, the ions rejection was determined (using Equation 4.29). The determination of ion rejection would help in attempting to understand the conditions which would impact the ion rejection and which factor can be adjusted in the experiments.

The program used the step-size (h) which is given as follows:

$$h = \frac{x_2 - x_1}{n\ step}$$

Here, $(x_2 - x_1)$ is the membrane thickness and (n step) is the number of step. The Nernst-Planck was solved for one feed ion concentration across different volume of permeate fluxes. The initial ion concentration of feed was 10 mol/m^3. The volume of permeate fluxes based on the area of membrane that was extended between (1.5×10^{-6} and 2.5×10^{-5} m^3/m^2.s). Effective thickness of membrane was estimated equals to 2.0×10^{-6} m.

The ionic properties of sodium (Na^+) and chloride ion (Cl^-) are shown as follows:

- Diffusion coefficient of sodium ion is equal to 1.33×10^{-9} m^2/s **(Bowen, et al., 2002; Shih, et al., 2005).**
- Diffusion coefficient of chloride ion is equal to 2.031×10^{-9} m^2/s **(Alfonso and Pinho, 2000; Gutman, 1987; Wąsik, et al., 2005)**.
- Stockes radius of sodium equal to 0.184×10^{-9} m. **(Bowen, et al., 2002)**
- Stockes radius of chloride equal to 0.121×10^{-9} m. **(Peeters, et al., 1998)**

Based on the ionic properties of both ions (Na^+ and Cl^-) the hindrance and steric coefficients which used in the present study were calculated as shown in the Table 5.7.

Table 5.7 The Steric Coefficients and Hindrance (for a Determined Effective Pore Radius 0.56 nm).

Ionic type	Hindered coefficient for diffusion ($K_{i,d}$) (dimensionless)	Hindered coefficient for convection ($K_{i,c}$) (dimensionless)	Steric coefficient (ϕ_i) (dimensionless)	Hindered diffusivity ($D_{i,p}$) (m^2/s) × 10^{-9}
Na^{+1}	0.377	1.436	0.45	0.503
Cl^{-1}	0.562	1.343	0.615	1.141

At pH value of (6), temperature 298 Kº and porosity 0.4 with some assumption as shown below.

- The activity coefficients = (1)
- Ignored the osmotic pressure.
- Effective charge density is constant.

The basic parameters of the Donnan steric pore model (DSPM) which have been used in the present study, the membrane surface charge density and Donnan potential (ψ_{Don}) were estimated which equal to (-5 mC/m^2) and (-2.76 mV).

The concentration of ions (Na^{+1} and Cl^{-}) inside the membrane reduced as the ions moved across the active layer of membrane from feed side to the permeate side. See **Fig. (5.58)**. It was observed that the concentration of (Na^{+1}) ion inside effective layer of membrane was lower than the concentration of (Cl^{-1}) ion inside the membrane. These results are linked to the transmembrane pressure (TMP), where the theory proposes that the rejection of the ions would rise as the transmembrane pressure rises **(Bowen and Mukhtar, 1996; Koyuncu, 2000)**.

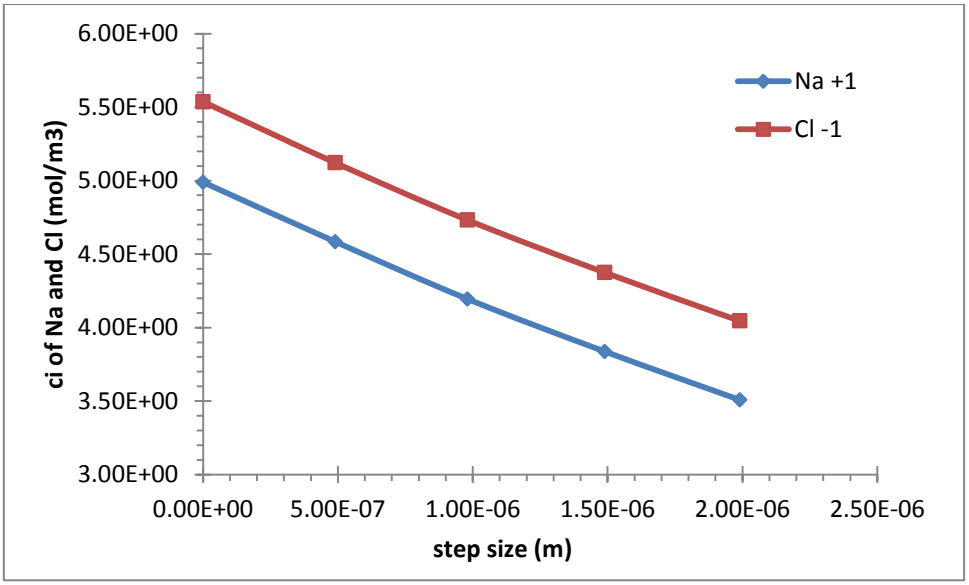

Figure 5.58 Na^{+1} and Cl^{-1} Ions Concentration Inside the Membrane Active Layer against the Step Size.

The rejection of (Na^{+1}) was slightly higher than the rejection of (Cl^{-1}), that corresponds with the result gained from the experiments. Such rejection behavior is related to the diffusion coefficient for sodium (Na^{+}) ion equal to (1.33×10^{-9} m^2/s) less than the diffusion coefficient for chloride (Cl^{-}) ion which equal to (2.0310^{-9} m^2/s), in addition the hydrate radius of (Na^{+}) equal to (0.36 nm), that is higher than hydrate radius of (Cl^{-}) ion (0.33 nm).

Fig. (5.59) shows the theoretically simulated results of the rejection of ions in the present titanium dioxide NF membrane based on the (DSPM) as a function (TMP – permeate volume flux). The rejection of (Na^{+1}) and (Cl^{-}) ions raised as the permeate flux raised. See **Fig. (5.59)**.

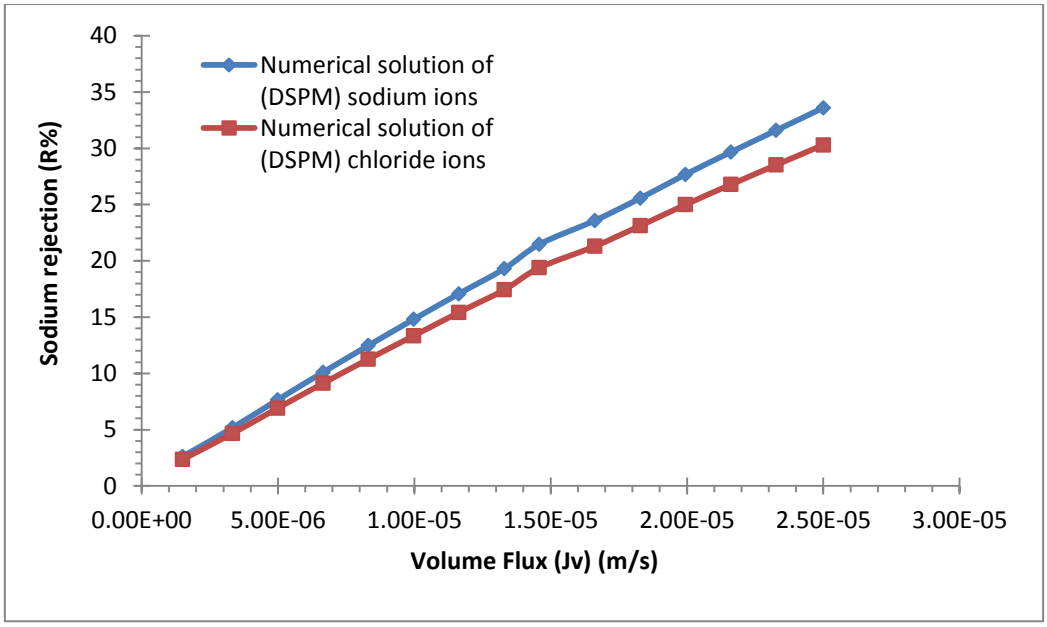

Figure 5.59 Rejection of Na^{+1} and Cl^{-1} verses J_v ($m^3/m^2.s$).

It can be seen from **Fig. (5.60)** that the rejection of sodium chloride (NaCl) by using the numerical solution of the (DSPM) model was steadily raised as the (transmembrane pressure-volume flux of permeate) raised. The rejection of sodium chloride solute at the highest volume flux of permeate (at applied transmembrane pressure of 15 bar) was (33.6%) whilst the results of experimental indicated that the rejection of sodium chloride at the highest volume flux of permeate was (30.3%). It can be noticed that the prediction of the present theoretical model was found to be almost in agreement with data of experimental.

The gained linear relationship results of theoretical (mathematical) work from the present study model are consistent with the results stated by **(Bowen and Mukhtar, 1996; Bowen, et al., 1997; Bowen and Mohammad, 1998)**.

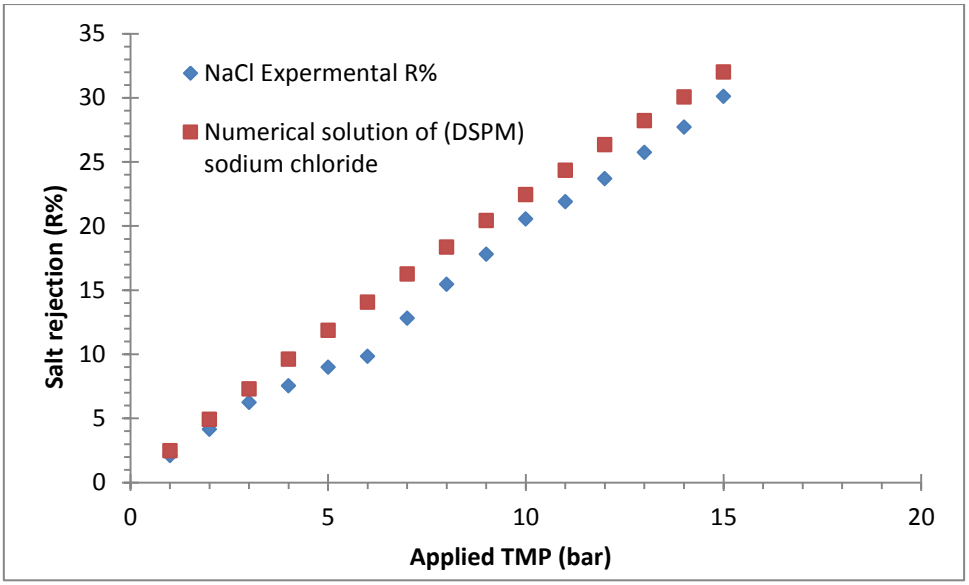

Figure (5.60) Sodium Chloride Rejection (Experimental and Theoretical) verses Applied Transmembrane Pressure (TMP) bar.

Although, the experimental results in agreement with the prediction of theoretical results, but not exactly, this can be explained to some assumptions in the Donnan steric pore model (DSPM) in this study that are shown as follows:

- The activity coefficients at the pore and at the solution were assumed as unity, since the solution were considered to be very diluted.

- Ignored the influence of osmotic pressure, since the (DSPM) of the pressure study conducted at very low concentration less than 0.1 M NaCl **(Bowen and Mukhtar, 1996)**.

- Neglected the effect of concentration polarization with the surface of NF membrane **(Hussain, et al., 2007)**.

- The effective charge density was assumed constant across the nanofiltration membrane. When the results of the present study compared with **Amer, (2013)** study, the basic differences shown as flows:

- It can be seen that the sodium concentration at the membrane permeate interface reduced to (5.42 mol/m^3) in Amer`s study compared to (4.37

mol/m^3) in the present study, while the concentration of chloride ion reduced to (5.85 mol/m^3) in Amer`s study compared to (4.9) in this work at the same condition (for transmembrane pressure 5 bar and feed concentration of 10 mol/m^3).

- Amer`s study used the highest transmembrane pressure (5 bar) while in the present study used (15 bar) and the result of sodium concentration at the membrane interface reduced to (3.51 mol/m^3), and the concertation of chloride ion reduced to (4.05 mol/m^3).
- Amer`s study obtained the highest rejection of sodium chloride (6%) at 5.0 bar and feed concentration 10 mol/m^3, while the highest rejection of sodium chloride obtained (32%) at 15 bar and feed concentration 10 mol/m^3.

Chapter six
Conclusions and Recommendations

6.1 Conclusions

● Measuring the zeta potential of the tubular ceramic TiO_2 NF membrane using locally produced electrodes (streaming potential method) consisting of silver and 4% gold which showed similar results with standard method of microelectrophoresis.

● For NaCl, the isoelectric point is found at around pH of 3.5 and concentration of 0.01 M NaCl using microelectrophoresis method, while IEP at around pH of 3.6 with concentration 0.01 M NaCl using streaming potential method. The IEP using streaming potential for the other salts (KCl, $NaHCO_3$, $CaCl_2$, $MgCl_2$, Na_2CO_3, Na_2SO_4, $CaCO_3$ and $MgSO_4$) were between pH value of 3.4 to 3.8.

● Zeta potential reduces with increasing of electrolyte concentration, while, it increases with increasing pH. So the effect of the pH more than the effect of concentration.

● The lowest value of the NaCl rejection at (pH of IEP) for the composite TiO_2 NF membrane because the membrane at the IEP does not have an electrostatic mechanism thus, only diffusion and convection flows influence the transport of solutes through the NF membrane.

● The critical flux has been obtained for 0.01 M $MgSO_4$ and $CaCl_2$ at applied TMP 9 and 12 bar respectively. Other salts NaCl, $NaHCO_3$ and Na_2SO_4 have not critical flux.

● The critical flux decreases with the increasing of the ionic valence to the salt so that it is (2:2 > 2:1 > 1:1) and increases with value of pH and cross flow velocity.

● In general, rejection increases with increasing transmembrane pressure, but salts $MgSO_4$ and $CaCl_2$ after the critical flux begins the rejection and permeate flux start to be constant with increased TMP.

● The rejection of SO_4^{-2} ions was remarkably higher than the rejection of Na^{+1} and Mg^{+2} ions for all concentration. While, the rejection of calcium ions was noticeably larger than the rejection of chloride ions for each concentrations.

● Measurements of the salts rejection found to have the following sequence: R (Na_2SO_4 > ($MgSO_4$) > $CaCl_2$) ≥ $NaHCO_3$ > (NaCl). The highest rejection of sodium sulphate (Na_2SO_4) salt is approximately equal to (82.2%).

● The treatment of produced water showed that the removal ratio of oil 99.4%, TOC 95.8% and TDS 30% (after treatment by using ceramic NF membrane).

● The obtained results of Donnan and steric partitioning pore model (DSPM) showed satisfying agreement between data of modeling and experimental for the applied transmembrane pressure from 1 to 15 bar and 0.01 M NaCl concentration.

6.2 Recommendations:

● Study NF and UF made of other ceramic materials such as zirconia ZrO_2 and silica SiO_2 and another polymeric membranes.

● Using other feed such as sea water and brackish water on the same membrane tubular ceramic NF TiO_2 membrane.

● Study the rejection of salts using the same type of NF TiO_2 membrane with nominal pore size less than 0.9 nm.

● Apply other model such as the Donnan steric pore and dielectric exclusion model (DSPM-DE) and compare it with Donnan steric pore model (DSPM).

● Study the effect of temperature of contaminated water flowing from different factories on zeta potential and rejection.

References

References

A1-Amoudi, A.S. , and A.M. Farooque, (2005), Performance restoration and autopsy of NF membranes used in seawater pretreatment, Desalination 178: 261-271.

Abadikhah, Hamidreza, Farzin Zokaee Ashtiani, and Amir Fouladitajar. 2014. "Nanofiltration of Oily Wastewater Containing Salt; Experimental Studies and Optimization Using Response Surface Methodology." Desalination and Water Treatment: 1–14.

Afonso, M. D., 2006, Surface charge on loose nanofiltration membranes. Desalination. 191(1–3): 262-272.

Agoudjil N., N. Benmouhoub, A. Larbot: (2005) Synthesis and characterization of inorganic membranes and applications. Desalination 184, 1-2:65 – 69.

Ahmad A. L., and A. Mariadas. (2004), Baffled micro filtration membrane and its fouling control for feed water of desalination. Desalination 168: 223–230.

Ahmad, A. and B. Ooi, 2006, Optimization of composite nanofiltration membrane through pH control: Application in CuSO4 removal. Separation and Purification Technology, 47(3): 162-172.

Ahmad, A. L., Chong, M. F. and Bhatia, S., (2005), Mathematical modelling and simulation of the multiple solutes system for Nanofiltration process. Journal of membrane science, 253: 103-115.

Alfonso Maria D. , and Maria N. de Pinho, 2000, Transport of $MgSO_4$, $MgCl_2$, and Na_2SO_4 across an amphoteric nanofiltration membrane. Journal of membrane science. 179: 137-154.

Alventosa-deLara E., S. Barredo-Damas, M.I. Alcaina-Miranda, M.I. Iborra-Clar, (2014) Study and optimization of the ultrasound-enhanced cleaning of an ultrafiltration ceramic membrane through a combined experimental-statistical approach. Ultrasonics Sonochemistry, 21: 1222–1234.

Amer Naji Ahmed, Al-Naemi, 2013, Rejection and Critical Flux of Calcium Sulphate in a Ceramic Titanium Dioxide Nanofiltration Membrane. phD thesis, The University of Manchester.

Amy E. Childress, Menachem Elimelech, (1996), Effect of solution chemistry on the surface charge of polymeric reverse osmosis and nanofiltration membranes, Journal of Membrane Science 119: 253-268.

Andrea Schafer and Tony Fane. 2018. Nanofiltration Principles and Applications, Second Edition (Elsevier).

Andritsos, N., Kontopoulou, M., Karabelas, A.J., Koutsoukos, P.G., (1996), $CaCO_3$ deposit formation under isothermal conditions, Can. J. Chem. Eng. 74: 911–919.

Anna Kowalik-Klimczak, Mariusz Zalewski, Paweł Gierycz, 2016, Prediction of The Chromium (III) Separation From Acidic Salt Solutions on Nanofiltration Membranes using Donnan and Steric Partitioning Pore (DSP) Model, Architecture Civil Engineering Environment, The Silesian University of Technology, 3: 135-140.

Anna Rosell, 2015, Purification of radioactive waste water using a ceramic membrane, Master of Science thesis in Nuclear Engineering, Department of Chemical and Biological Engineering, Chalmers University of Technology, Gothenburg, Sweden.

ASTM procedure, Designation: D 4194 – 03. 2008. Standard Test Method for Operating Characteristics of Reverse Osmosis and Nanofiltration Devices1.

Avula, R.Y.; Nelson, H.M. & Singh, R.K. (2009). Recycling of Poultry Process Wastewater by Ultrafiltration. Innovative Food Science and Emerging Technologies, 10, 1:1-8, ISSN 14668564.

AWWA Manual, 1999, "Reverse Osmosis and Nanofiltration", American Water Works Association.

AWWA, (1992), Membrane Technology Research Committee, Committee report: membrane processes in potable water treatment, J. Am. Water Works Assoc., 84(1) :59.

Bacchin, P., P. Aimar, and V. Sanchez, 1995. Model for colloidal fouling of membranes. AIChE journal, 41(2): 368-376.

Balabel, A. and H. Kotbb. 2013. "Analysis of a Hybrid Renewable Energy Stand-Alone Unit for Simultaneously Producing Hydrogen and Fresh Water from Sea Water." Int. J. of Thermal & Environmental Engineering.

Bandini, S., 2005, Modelling the mechanism of charge formation in NF membranes: Theory and application. Journal of membrane science. 264(1–2):75-86.

Bandini, S., J. Drei, and D. Vezzani, 2005, The role of pH and concentration on the ion rejection in polyamide nanofiltration membranes. Journal of membrane science. 264(1): 65-74.

Bartels, C., Wilf, M., Casey, W. and Campbell, J., 2008, New generation of low fouling nanofiltration membranes. Desalination. 221(1-3): 158-167.

Baticle P., C. Kiefer, N. Lakchaf, A. Larbot, O. Leclerc, M. Persin, J. Sarrazin, (1997), Salt filtration on gamma alumina nanofiltration membranes fired at two different temper- atures, J. Membrane Sci. 135,1.

Benfer, S., P. Arki and G. Tomandl, (2004) Ceramic membranes for filtration applications – preparation and characterization, Advanced Engineering Materials 6: 495-500.

Benfer, S., U. Popp, H. Richter, C. Siewert and G. Tomandl, (2001), Development and characterization of ceramic nanofiltration membranes, Separation and Purification Technology 22-23: 231–237.

Blöcher, C.; Noronha, M.; Fünfrockcn, L.; Dorda, J.; Mavrov, V.; Janke, H.D. & Chmiel, H. (2002). Recycling of Spent Process Water in the Food Industry by an Integrated Process of Biological Treatment and Membrane Separation. Desalination, 144, 1-3: 143-150, ISSN 00119164.

Boerlage, S.F.E., Kennedy, M.D., Bremere, I., Witkamp, G.J., van der Hoek, J.P., Schippers, J.C., (2000), Stable barium sulphate supersaturation in reverse osmosis, J. Membr. Sci. 179: 53–68.

Boussu, K. 2007. Influence of membrane characteristics on flux decline and retention in nanofiltration. PhD dissertation, Katholieke Universiteit Leuven.

Bowen, R. and W. Mohammad, 1998, Diafiltration by nanofiltration: prediction and optimization. AIChE journal. 44(8):1799-1852.

Bowen, W. R., Julian S. Welfoot. (2002), Modelling the performance of membrane nanofiltration - critical assessment and model development. Chemical engineering science 57: 1121–1137.

Bowen, W. and A. W. Mohammad, 1998, Characterization and prediction of nanofiltration membrane performance—a general assessment. Chemical Engineering Research and Design, 76(8): 885-893.

Bowen, W. R. , and H. Mukhtar, (1996), Characterisation and prediction of separation performance of nanofiltration membranes, J. Membr. Sci. 112: 263-274.

Bowen, W. R., A. W. Mohammad, and N. Hilal, 1997, Characterisation of nanofiltration membranes for predictive purposes—use of salts, uncharged solutes and atomic force microscopy. Journal of membrane science. 126(1):91-105.

Broussous L., J.C. Ruiz, A. Larbot, L. Cot, (1998), Stamped ceramic porous tubes for tangential filtration, Sep. Purif. Technol. 14: 53–57.

Cabassud C., S. Laborie, L. Durand-Bourlier, J.M. Lainé, (2001) Air sparging in ultrafiltration hollow fibers: Relationship between flux enhancement, cake characteristics and hydrodynamic parameters. Journal of Membrane Science, 181 (1): 57–69.

Çakmakcı M., N. Kayaalp and I. Koyuncu, (2008), Desalination of produced water from oil production fields by membrane processes, Desalination 222: 176–186.

Chandan Das and Sujoy Bose. 2017. Advanced Ceramic Membranes and Applications.

Chapman D (Ed.) (1992), Water Quality Assessments, A Guideto the Use of Biota, Sediments & Water in Environmental Monitoring. Chapman Hall, UK.

Chaudhari L.B., Murthy Z.V.P.; 2010, Separation of Cd and Ni from multicomponent aqueous solutions by nanofiltration and characterization of membrane using IT model. Journal of Hazardous Materials, 180:309-315.

Chaufer B., M. Rabiller-Baudry, L. Guihard, G. Daufin, (1996), Retention of ions in nanofiltration at various ionic strength, Desalination 104, 37.

Chein, R., H. Chen, and C. Liao, 2009, Investigation of ion concentration and electric potential distributions in charged membrane/electrolyte systems Journal of membrane science. 342(1–2): 121-130.

Chen J.P., S.L. Kim, Y.P. Ting, (2003) Optimization of membrane physical and chemical cleaning by a statistically designed approach. Journal of Membrane Science, 219 (1–2): 27–45.

Chen V., A.G. Fane, S. Madaeni and I.G. Wenten, (1997), Particle deposition during membrane filtration of colloids: Transition between concentration polarization and cake formation, Journal of Membrane Science, 125: 109-122.

Chen X., H. Deng, (2013) Effects of electric fields on the removal of ultraviolet filters by ultrafiltration membranes. Journal of Colloid and Interface Science, 393: 429–437.

Cheremisinoff, Nicholas P. 2002. Handbook of Water and Wastewater Treatment Techonologies.

Chiu T.Y., A.E. James, (2005), Critical flux determination of non-circular multi-channel ceramic membranes using TiO_2 suspensions, Journal of Membrane Science 254: 295–301.

Chiu T.Y., A.E. James, (2006), Electrokinetic characterisation of cleaned non-circular multi-channelled membranes, Desalination 189: 13–20.

Condom S., A. Larbot, S.A. Younssi, M. Persin, (2004), Use of ultra- and nanofiltration ceramic membranes for desalination, Desalination 168: 207–213.

Cui Z., T. Taha, (2003) Enhancement of ultrafiltration using gas sparging: A comparison of different membrane modules. Journal of Chemical Technology and Biotechnology, 78 (2–3): 249–253.

Daniele Vezzani and Serena Bandini, 2002, Donnan equilibrium and dielectric exclusion for characterization of nanofiltration membranes. Desalination. 149(1-3): 477-483.

Dasent, (1979); H.D.B. Jenkins and K.P. Thakur, J. Chem. Educ., 56, (9):576-577.

Davies J. T., E. K. Rideal, ed., 1961, Electrostatic Phenomena. , Academic Press, Inc., New York and London.

De Lint, W. B. S., & Benes, N. E. (2005). Separation properties of γ-alumina nanofiltration membranes compared to charge regulation model predictions. Journal of Membrane Science, 248(1-2): 149-159.

Defrance L., M.Y. Jaffrin, (1999), Reversibility of fouling formed in activated sludge filtration, Journal of Membrane Science, 157:73-84.

DeLara E.A-., S.B-. Damas, M.I.A-. Miranda, M.I.I-. Clar, (2014) Study and optimization of the ultrasound-enhanced cleaning of an ultrafiltration ceramic membrane through a combined experimental statistical approach. Ultrasonics Sonochemistry, 21:1222–1234.

Deon S., A. Escoda, P. Fievet. (2011) . "A transport model considering charge adsorption inside pores to describe salts rejection by nanofiltration membranes", Chemical Engineering Science, 66: 2823–2832..

Donnan, F.G., (1995), Theory of membrane equilibria and membrane potentials in the presence of non-dialysing electrolytes. A contribution to physical-chemical physiology, Journal of Membrane Science 100: 45-55.

Drak, A., Glucina, K., Busch, M., Hasson, D., Laˆıne, J.-M., Semiat, R., (2000), Lab-oratory technique for predicting the scaling propensity of RO feed waters, Desalination 132: 233–242.

Dresner L., (1972), Some remarks on the integration of the extended Nernst-Planck equations in the hyperfiltration of multicomponent solutions, Desalination 10: 27-46.

Ducom G., C. Cabassud, (2003) Possible effects of air sparging for nanofiltration of salted solutions. Desalination, 156 (1–3) :267–274.

Dukhin, S. S., R. Zimmermann, and C. Werner, 2004, Intrinsic charge and Donnan potentials of grafted polyelectrolyte layers determined by surface conductivity data. Journal of Colloid and Interface Science, 274(1): 309-318.

Ebrahim S., (1994) Cleaning and regeneration of membranes in desalination and wastewater applications: State of the art. Desalination, 96 (1–3) :225–238.

Ebrahimi M, K Shams Ashaghi, L Engel, P Czermak: 2008, Characterization and Application of Different Ceramic Membranes For the Oil-Field Produced Water Treatment, Proceedings Engineering with Membranes: 231-232, Vale do Lobo, Portugal.

Elimelech M., W.H. Chen and J.J. Waypa, (1994), Measuring the zeta (electrokinetie) potential of reverse osmosis membranes by a streaming potential analyzer, Desalination, 95: 269.

Elimelech, M., Gregory, J., Jia, X. and Williams, R.A., 1995, Particle Deposition and Aggregation: Measurement, Modelling, and Simulation, Butterworth-Heinemann, Oxford.

Elzo D., I. Huisman, E. Middelink, V. Gekas, (1998), Charge effects on inorganic membrane performance in a cross-flow microfiltration process, Colloids Surf. A: Physicochem. Eng. Aspects 138: 145-159.

Eriksson P., U. Bharwada, Q. Niu, R. Reddy, P.R. Dontula, Y. Tayalia, (2010), "Nanofiltration for Seawater Softening: An Emerging and Economically Viable Process", IDA journal – Desalination and Water Reuse, 2: 26 – 33.

Ernst M., A. Bismarck, J. Springer, M. Jekel, (2000), Zeta-potential and rejection rate of a polyethersulfone nanofiltration membrane in single salt solution, J. Membr. Sci. 165: 251–259.

Evans, P. and Robinson, K.: 1999, "Produced Water Management-Reservoir and Facilities Engineering Aspects, paper SPE 53254 presented at the SPE Middle East Oil Show, Bahrain.

Faller, K.A. (Technical Editor), 1999, AWWA Manual M46 Reverse Osmosis and Nanofiltration, AWWA.

Farah Naz Ahmed, (2013), Modified Spiegler-Kedem Model to Predict the Rejection and Flux of Nanofiltration Processes at High NaCl Concentrations.

Field R.W., D. Wu, J.A. Howell and B.B. Gupta, (1995), Critical flux concept for microfiltration fouling, Journal of Membrane Science, 100: 259-272.

Fouladitajar A., F.Z. Ashtiani, H. Rezaei, A. Haghmoradi, A. Kargari, (2014) Gas sparging to enhance permeate flux and reduce fouling resistances in cross flow microfiltration. Journal of Industrial and Engineering Chemistry, 20 (2): 624–632.

Garba Y., S. Taha, N. Gondrexon, G. Dorange. (1999), Ion transport modelling through nanofiltration membranes. Journal of Membrane Science 160: 187–200.

Geraldes, V. and A. M .Brites Alves, 2008, Computer program for simulation of mass transport in nanofiltration membranes. Journal of membrane science. 321(2): 172-182.

Geraldes, V. , and M. de Pinho, (1995), Process water recovery from pulp bleaching effluents by an NF/ED hybrid process, J. Membr. Sci. 102: 209-221.

Ghadimkhani A., W. Zhang, T. Marhaba, (2016) Ceramic membrane defouling (cleaning) by air nano bubbles. Chemosphere, 146: 379–384.

Gilbert T., Tellez et al., (1995), Water. Res. 29: 1711-1718.

Gill, J.S., 1996, Development of scale inhibitors, in: Proceedings of the Corrosion, NACE Conference, Paper 229: 18.

Gilron, J., N. Daltrophe, O. Kedem. (2006), Trans-membrane pressure in nanofiltration. Journal of Membrane Science 286: 69–76.

Glover, P.W.J. and M.D.Jackson, 2010, "Boreholeelectrokinetic," he Leading Edge, 29, 6:724–728.

Gouellec Le, Y. A. and M. Elimelech, 2002, Calcium sulfate (gypsum) scaling in nanofiltration of agricultural drainage water. Journal of membrane science. 205(1): 279-291.

Gryta M., (2011) The influence of magnetic water treatment on $CaCO_3$ scale formation in membrane distillation process. Separation and Purification Technology, 80 (2): 293–299.

Gulde C.M., (2003), Water Res. 37: 705–713.

Gupta, Vineet K. 2003. "Experimental and Theoretical Studies in Reverse Osmosis and Nanofiltration." University of Cincinnati.

Gutman, R. G., 1987, Membrane Filtration, The technology of pressure-driven crossflow processes, Bristol, UK: IOP publishing Ltd.

Haghighi, Leila Safazadeh. 2011. "Determination of Fouling Mechanisms for Ultrafiltration of Oily Wastewater." University of Cincinnati.

Hajarat, R. A., 2010, The use of nanofiltration in desalinating brackish water, in School of Chemical Engineering and Analytical Science. phD thesis, The University of Manchester.

Harmant P., P. Aimar, (1996) Coagulation of colloids retained by porous wall, Aiche Journal, 42: 3523-3532.

Hassan A., (2012), "Time to upgrade Carlsbad SWRO design to NF-SWRO Hybrid", IDA journal – Desalination and Water Reuse: 17 – 21.

Hassan, A., Ali, N., Abdull, N. and Ismail, A., 2007, A theoretical approach on membrane characterization: the deduction of fine structural details of asymmetric nanofiltration membranes. Desalination, 206(1): 107-126.

Hassan, A., A. Farooque, A. Jamaluddin, A. A1-Amoudi, M. A1-Sofi, A. AI-Rubaian, N. Kither, I. Al.-Tisan and A. Rowaili, (2000), A demonstration plant based on the new NF-SWRO process, Desalination 131: 157-171.

Hassan, A., M. A1-Sofi, A. A1-Amoudi, A. Jamaluddin, A. Farooque, A. Rowaili, A. Dalvi, N. Kither, G. Mustafa and I. AI-Tisan, (1998), A new approach to thermal seawater desalination processes using nanofiltration membranes (Part 1), Desalination 118: 35-51.

Herbig R., P. Arki, G. Tomandl, R.E. Br¨aunig, (2003), Comparison of electrokinetic properties of ceramic powders and membranes, Sep. Purif. Technol. 32: 363–369.

Hidalgo A.M., Leon G., Gomez M., Murcia M.D., Gomez E. Gomez J.L.; 2013, Application of the Spiegler-Kedem-Kachalsky model to the removal of 4-chlorophenol by different nanofiltration membranes. Desalination, 315:70-75.

Hilal N., H. Al-Zoubi, N. A. Darwish, A. W. Mohammad and M. Abu Arabi. (2004), A comprehensive review of Nanofiltration membranes: Treatment, pre-treatment, modelling, and atomic force microscopy. Desalination 170: 281–308.

Howard, K., (2003). OSMOSIS (A self-instructional package)", Department of Molecular Physiology and Biological Physics, University of Virginia School of Medicine.

Hua FL, Tsang F, Wang FJ et al. (2007), Chem. Eng. J. 128: 169-175

Hubbard, A.T., 2002, Encyclopedia of Surface and Colloid Science, New York: Marcel Dekker.

Huisman I.H., P. Pradanos, A. Hern´ andez, (2000),The effect of protein–protein and protein–membrane interactions on membrane fouling in ultrafiltration, J. Membr. Sci. 179: 79–90.

Hunter R. J., 1981, Zeta Potential in Colloid Science, Academic Press, New York, NY, USA.

Hurwitz, G., G. R. Guillen, and E. M. Hoek, 2010, Probing polyamide membrane surface charge, zeta potential, wettability, and hydrophilicity with contact angle measurements. Journal of membrane science ,2252. 343 (5–2:): 349-357.

Hussain, A. A., M. E. E. Abashar, and I. S. Al-Mutaz, 2007, Influence of ion size on the prediction of nanofiltration membrane systems. Desalination. 214(1-3) : 150-166.

IAEA. 2004. Application of Membrane Technologies for Liquid Radioactive Waste Processing.

IDA Desalination Year Book, 2014, Media Analytics Ltd, Oxford.

Israelachvili, J. N., 2007, Intermolecular and surface forces : Academic press.

Jacobasch, H.J., Simon, F., Werner, C., Bellmann, C., (1996), Technisches Messen. 63: 439–446.

Jaffrin, Michel Y., Lu H. Ding, Omar Akoum, and Ambroise Brou. 2004. "A Hydrodynamic Comparison between Rotating Disk and Vibratory Dynamic Filtration Systems." Journal of Membrane Science 242(1–2): 155–167.

Jagannadh S.N., H.S. Muralidhara, (2006) Electrokinetics methods to control membrane fouling. Industrial Engineering & Chemistry Research, 35 (4) :1133–1140.

Jarzyńska M., Pietruszka M.; 2011, The application of the Kedem-Katchalsky equations to membrane transport of ethylalcohol and glucose. Desalination, 280:14-19.

Jawor, A. and E. Hoek, 2009, Effects of feed water temperature on inorganic fouling of brackish water RO membranes. Desalination, 235(1-3): 44-57.

Jesus Garcia-Aleman and Jmaes M. Dickson. (2004), Mathematical modelling of Nanofiltration membranes with mixed electrolyte solutions. Journal of membrane science 235: 1-13.

Johan Schaep, Bart Van der Bruggen, Carlo Vandecasteele, Dirk Wilms, (1998), Influence of ion size and charge in nanofiltration, Separation and Purification Technology 14:155–162.

Jönsson A.-S., Y. Blomberg, E. Petersson, (1988), Influence of pH and surfactants on ultrafiltration membranes during treatment of bleach plant effluent, Nordic Pulp Paper Res. J. 4:159–165.

Jouniaux, M. L. Bernard, M. Zamora, and J. P. Pozzi, L., 2000, "Streaming potential in volcanic rocks from Mount Pelee," Journal of Geophysical Research B, 105, 4:8391–8401.

Judd, S and Jefferson, B. 2003. Membranes for Industrial Wastewater Recovery and Re-use. Elsevier, U.K.

Kelewou H., Lhassani A., Merzouki M., Drogui P., Sellamuthu B.; 2011, Salts retention by nanofiltration membranes: Physicochemical and hydrodynamic approaches and modeling. Desalination, 277:106-112.

Kharaka, Y.K., Leong, L.Y.C., Doran, G. and Breit, G.N. (1998) Can produced water be Reclaimed? Experience with placerita oil field, California. In Enviromental issues and solutions in petroleum exploration, production and refining Sublette, K.L., Ed., Proceedings of the 5th international petroleum environmental conference, Albuquerque, NM.

Khedr ,M.G., (2008), Membrane methods in tailoring simpler, more efficient, and cost effective wastewater treatment alternatives, Desalination 222: 135–145.

Khudair W. N., (2011). Concentration Poisonous Metallic Radicals from Industrial Water by Forward and / or Reverse Osmosis. M.Sc. thesis, Baghdad University.

Kim H.-S., K. Wright, D.J. Cho, Y.I. Cho, (2015) Self-cleaning filtration with spark discharge in produced water. International Journal of Heat and Mass Transfer, 88: 527–537.

Kim, Jae-Jin, A. Chinen, and H. Ohya. 1997. "Membrane Microfiltration of Oily Water." in Macromolecular Symposia, 118: 413–18. Wiley Online Library.

Kim, Jaeshin, Zhenxiao Cai, and Mark M. Benjamin. 2008. "Effects of Adsorbents on Membrane Fouling by Natural Organic Matter." Journal of Membrane Science 310(1–2):356–64.

Kimura, K., G. Amy, J. E. Drewes, T. Heberer, T.-U. Kim and Y. Watanabe, (2003), Rejection of organic micropollutants (disinfection by-products, endocrine disrupting compounds, and pharmaceutically active compounds) by NF/RO membranes, Journal of Membrane Science 227:113–121.

Kirby, B.J. (2010). Micro- and Nanoscale Fluid Mechanics: Transport in Microfluidic Devices. Cambridge University Press. ISBN 978-0-521-11903-0.

Ko, Y. W. and R. M. Chen, 2007, Ion Rejection in Single and Binary Mixed Electrolyte Systems by Nanofiltration: Effect of Feed Concentration. Separation science and technology. 42(14): 3071-3084.

Košutić, K., D. Dolar, D. Ašperger and B. Kunst, (2007), Removal of antibiotics from a model wastewater by RO/NF membranes, Separation and Purification Technology 53: 244–249.

Koter S.; 2006, Determination of the parameters of the Spiegler-Kedem-Katchalsky model for nanofiltration of single electrolyte solutions. Desalination,.198: 335-345.

Kowalik-Klimczak A., Zalewski M., Gierycz P.; 2015, Experimental and modelling analysis of the separation of ionic salts solution in nanofiltration process. Challenges of Modern Technology,6,.2:.24-29.

Koyuncu, I., M. Turan, D. Topacik and A. Ates, (2000), Application of low pressure nanofiltration membranes for the recovery and reuse of dairy industry effluents, Water Science and Technology 41: 213-221.

Kullab, A. 2011. Desalination using membrane distillation. Royal institute of Technology, Stockholm, Sweden.

Kumar, S.Mahesh and Sukumar Roy. 2008. "Recovery of Water from Sewage Effluents Using Alumina Ceramic Microfiltration Membranes." Separation Science and Technology 43(5):1034–64.

Kwon D.Y., S. Vigneswaran, A.G. Fane, R.B. Aim, (2000), Experimental determination of critical flux in cross-flow microfiltration, Sep. Purif. Technol. 19: 169–181.

Labbez C., P. Fievet, F. Thomas, A. Szymczyk, A. Vidonne, A. Foissy, and P. Pagetti. (2003), Evaluation of the "DSPM" model on a titania membrane: measurements of charged and uncharged solute retention, electrokinetic charge, pore size, and water permeability. Journal of colloid and interface science 262: 200–211.

Le Gouellec, Y. A. and M. Elimelech, 2002 Calcium sulfate (gypsum) scaling in nanofiltration of agricultural drainage water. Journal of membrane science. 205(1): 279-291.

Lee, H. S., Im, S. J., Kim, J. H., Kim, H. J., Kim, J. P., and Min, B. R,. 2008. Polyamide thin-film nanofiltration membranes containing TiO_2 nanoparticles. Desalination, 219(1-3): 48-56.

Lee, S. and C. H. Lee, 2000, Effect of operating conditions on $CaSO_4$ scale formation mechanism in nanofiltration for water softening. Water research, 34(15):3854-3866.

Leo Choe Peng. 2008. Bimodal Porous Ceramic Membrane via Nanosized Polystyrene Templating: Synthesis, Characterization and Performance Evaluation, Ph.D. thesis.

Levenstein, R., D. Hasson, and R. Semiat, 1996, Utilization of the Donnan effect for improving electrolyte separation with nanofiltration membranes. Journal of membrane science, 116(1): 77-92.

Li J., R.D. Sanderson, E.P. Jacobs, (2002) Non-invasive visualization of the fouling of microfiltration membranes by ultrasonic time-domain reflectometry. Journal of Membrane Science, 201 (1–2): 17–29.

Li Y.-H. and Gregory S. (1974) Diffusion of ions in sea water and in deep-sea sediments. Geochim. Cosmochim. Acta 38: 703–714.

Li, Yu Shui, Lu Yan, Chai Bao Xiang, and Liu Jiang Hong. 2006. "Treatment of Oily Wastewater by Organic–inorganic Composite Tubular Ultrafiltration (UF) Membranes." Desalination 196(1):76–83.

Liikanen R., J. Yli-Kuivila, R. Laukkanen, (2002) Efficiency of various chemical cleanings for nanofiltration membrane fouled by conventionally treated surface water. Journal of Membrane Science, 195 (2) :265–276.

Lin, C., Shirazi, S., Rao, P. and Agarwal, S., 2006, Effects of operational parameters on cake formation of $CaSO_4$ in nanofiltration. Water research. 40(4):806-816.

Lu J.Y., X. Du, G. Lipscomb, 2009, Cleaning membranes with focused ultrasound beams for drinking water treatment, Proceedings of IEEE International Ultrasonics Symposium Proceedings: 1195–1198, Rome, September.

Luong, D. T., and R. Sprik, 2013, "Streaming Potential and Electroosmosis Measurements to Characterize Porous Materials", Volume, Article ID 496352, 8 :http://dx.doi.org/10.1155/2013/496352.

Mandale S., Jones M.; 2010, Membrane transport theory and the interactions between electrolytes and nonelectrolytes. Desalination,.252:17-26.

Mänttäri M., M. Nyström, (2000), Critical flux in NF of high molar mass polysaccharides and effluents from the paper industry, Journal of Membrane Science 170: 257–273.

Maria D. Alfonso, and Maria N. de Pinho, 2000. Transport of $MgSO_4$, $MgCl_2$, and $Na2SO_4$ across an amphoteric nanofiltration membrane. Journal of membrane science 179: 137-154.

Mark Mullett, Roberta Fornarelli, and David Ralph, 2014, Nanofiltration of Mine Water: Impact of Feed pH and Membrane Charge on Resource Recovery and Water Discharge, Membranes, 4: 163-180.

Mazzoni, C., Orlandini, F., & Bandini, S. (2009). Role of electrolyte type on TiO_2– ZrO_2 nanofiltration membranes performances. Desalination, 240(1-3): 227-235.

Mondal, S. and S.Ranil Wickramasinghe. 2008. "Produced Water Treatment by Nanofiltration and Reverse Osmosis Membranes." Journal of Membrane Science 322(1):162–70.

Moritz, T., S. Benfer, P. Arki, G. Tomandl, 2001, Influence of the surface charge on the permeate flux in the dead-end filtration with ceramic membranes, Sep. Purif. Technol. 25: 501–508.

Mukherjee P., 2006, Some observations about electrolyte permeation mechanism through reverse osmosis and nanofiltration membranes. Journal of Membrane Science,.278:301-307.

Nada, Tariq (2014) Characterisation of nanofiltration membranes for sulphate rejection.PhD thesis. The University of Glasgow.

Narong P., A.E. James, (2006) Sodium chloride rejection by a UF ceramic membrane in relation to its surface electrical properties, Separation and Purification Technology 49: 122–129.

Narong, P., 2006, The influence of electrokientics on membrane MICRO/ULTRA filtration of colloidal systems, in School of Chemical Engineering and Analytical Science, PhD thesis, The University of Manchester: Manchester,UK.

Nędzarek A., Drost A., Harasimiuk F.B., Tórz A.; 2015, The influence of pH and BSA on the retention of selected heavy metals in the nanofiltration process using ceramic membrane. Desalination,.369:62-67.

Newman, J. S., 1992, Electrochemical Systems. 2nd edition ed. : Prentice Hall,USA.

Nicolaisen B., (2002), Desalination 153: 355–360.

Oatley, D. L., Cassey, B., Jones, P., and Richard Bowen, W., 2005, Modelling the performance of membrane nanofiltration-recovery of a high-value product from a process waste stream. Chemical engineering science. 60(7): 1953-1964.

Oktay, S.; Iskender, G.; Babuna, F.; Kutluay, G. & Orhon D. (2007). Improving the Wastewater Management for A Beverage Industry With In-Plant Control. Desalination,.211,. 1-3:138-143 ISSN 00119164.

Omar Labban, Chang Liu, Tzyy Haur Chong, John H. Lienhard V, (2017), Fundamentals of Low-Pressure Nanofiltration: Membrane Characterization, Modeling, and Understanding the Multi-Ionic Interactions in Water Softening, Journal of Membrane Science 521: 18-32.

Orecki, Aleksander and Maria Tomaszewska. 2007. "The Oily Wastewater Treatment Using the Nanofiltration Process." Polish Journal of Chemical Technology 9(4):40–42.

Palmeri J., Blanc, P., Larbot, A. and David, P., 1999, Theory of pressure-driven transport of neutral solutes and ions in porous ceramic nanofiltration membranes. Journal of membrane science. 160(2): 141-170.

Patrice Bacchin, Pierre Aimar, Robert Field. 2006, Critical and sustainable luxes: theory, experiments and applications. Journal of Membrane Science, Elsevier, 281 (1-2):42-69.

Peeters, J. M. M., Boom, J. P., Mulder, M. H. V. and Strathmann, H., 1998, Retention measurements of nanofiltration membranes with electrolyte solutions. Journal of membrane science. 145(2): 199-209.

Peeters, J. M. M., M. H. V. Mulder, and H. Strathmann, 1999, Streaming potential measurements as a characterization method for nanofiltration membranes. Colloids and Surfaces A: Physicochemical and Engineering Aspects, 150(1–3): p. 247-259.

Peeters, J.M.M. , 1997, Characterization of nanofiltration membranes, Ph.D. Thesis, University of Twente, Enschede, The Netherlands.

Pessarakli, M., 1999, Handbook of plant and crop stress : CRC.

Petersen R.J., (1993), Composite reverse osmosis and nanofiltration membranes, J. Membrane Sci., 83, 81.

Pivonka P., D. Smith, and B. Gardiner, 2005 Modelling of Donnan equilibrium in charge porous materials – a scale transition analysis, in VIII International Conference on Computations Plasticity: Barcelona.

Popovic S., M. Djuric, S. Milanovic, M.N. Tekic, N. Lukic, (2010) Application of an ultrasound field in chemical cleaning of ceramic tubular membrane fouled with whey proteins. Journal of Food Engineering, 101: 296–302.

Press, W., Teukolsky, S., Vetterling, W., and Flannery, B., 1992, Numerical recipes in Fortran 77: the art of scientific computing,. 1. Fortran Numer. Recipes. 994.

Pride S., 1994, "Governing equations for the coupled electromagnetics and acoustics of porous media," Physical Review B, 50, 21: 15678–15696.

Psoch C., S. Schiewer, (2006) Direct filtration of natural and simulated river water with air sparging and sponge ball for fouling control. Desalination, 197 (1–3): 190–204.

Puhlfürß, P., A. Voigt, R. Weber and M. Morbé, (2000), Microporous TiO_2 membranes with a cut off <500 Da, Journal of Membrane Science 174: 123–133.

Qdaisa, H.A., and H. Moussa, (2004), Removal of heavy metals from wastewater by membrane processes: a comparative study, Desalination 164: 105-110.

Rahi, K. A. and T. Halihan, 2010, Changes in the salinity of the Euphrates River system in Iraq. Regional Environmental Change, 10(1):27-35.

Rautenbach and A. Gröschl. (1990), Separation Potential of Nanofiltration Membranes. Desalination 77: 73–84.

Rautenbach, R., Albrecht, T., 1989, Membrane Processes, John Wiley & Sons, New York.

Rautenbach, R., and Th. Linn, (1996), High pressure reverse osmosis and nanofiltration, a "zero discharge" process combination for the treatment of waste water with severe fouling/sealing potential, Desalination, 105: 63-70.

Rautenbach, R., Th. Linn and L. Eilers, 2000, Treatment of severely contaminated waste water by a combination of RO, high-pressure RO and NF-potential and limits of the process, J. Membr. Sci. 174:231-241.

Richard Bowen, W. and Wahab Mohammad, A., 1998, A theoretical basis for specifying nanofiltration membranes-Dye/salt/water streams. Desalination. 117(1-3): 257-264.

Ricq, L., Pierre, A., Reggiani, J.-C. , Pagetti, J., Foissy, A. (1998), Use of the electrophoretic mobility and streaming potential measurements to characterize electrokinetic properties of ultrafiltration and microfiltration membranes, Colloids Surf. A Physicochem. Eng. Aspects 138:301–308.

Riley R.L., 1990, Reverse osmosis, in: Membrane Separation Processes —A Research & Development Needs Assessment, DOE-report, Under Contract No. DE-AC01-88ER30133, US Department of Energy.

Robinson R. A. and Stokes R. H. (1959) Electrolyte Solutions, second ed. Butterworth's, London, :559.

Safiye YALDIZ, 2017, Application of Tubular Ceramic Nanofiltration Membranes for Textile Wastewater Desalination, M.Sc. Thesis.

Sagiv A., R. Semiat, (2010), Parameters affecting backwash variables of RO membranes.Desalination, 261 (3): 347–353.

Salahi, Abdolhamid, Ali Gheshlaghi, Toraj Mohammadi, and Sayed Siavash Madaeni. 2010. "Experimental Performance Evaluation of Polymeric Membranes for Treatment of an Industrial Oily Wastewater." Desalination 262(1–3):235–42.

Santafé-Moros, A., J. M. Gozálvez-Zafrilla, J. Lora-García. (2008), Applicability of the DSPM with dielectric exclusion to a high rejection nanofiltration membrane in the separation of nitrate solutions. Desalination 221: 268–276.

Santos, L.R.B. , Santilli, C.V. , Larbot, A., Persin, M., Pulcinelli, S.H. (2001), Influence of membrane-solution interface on the selectivity of SnO_2 ultrafiltration membranes, Sep. Purif. Technol. 22–23: 17– 22.

Sarkar, B.; Chakrabarti, P.P.; Vijaykumar, A. & Kale, V., (2009), Wastewater Treatment in Dairy Industries-Possibility of Reuse. Desalination,.195,3-4:141-152, ISSN 00119164.

Saxena A., B.P. Tripathi, M. Kumar, V.K. Shahi, (2009), Membrane-based techniques for the separation and purification of proteins: An overview. Advances in Colloid and Interface Science, 145 (1–2): 1–22.

Schaep, J. and C. Vandecasteele, 2001, Evaluating the charge of nanofiltration membranes. Journal of membrane science. 188(1): 129-136.

Schaep, J., Van der Bruggen, B., Vandecasteele, C. and Wilms, D., 1998, Influence of ion size and charge in nanofiltration. Separation and Purification Technology. 14(1–3): 155-162.

Schafer, A., Andritsos, N., Karabelas, A.J., Hoek, E.M.V., Scheider, R., Nystrom, M., 2004, Fouling in nanofiltration, in: A. Sch¨ afer, D. Waite, A. Fane (Eds.), Nanofiltration Principles and Applications, Elsevier, Oxford, UK: 169–239.

Schoemaker F. C., N. Grobbe, M. D. Schakel, S. A. L. de Ridder, E. C. Slob, and D. M. J. Smeulders, 2012, "Experimental validation of the electrokinetic theory and development of seismoelectric interferometry by cross-correlation," International Journal of Geophysics, Article ID 514242:23.

Seader, J.D and Henley, E.J. 2006. Separation Process Principles. 2 Ed. John Wiley & Sons, U.S.A.

Sema Salgın, Uğur Salgın and Nagihan Soyer, (2013), Streaming Potential Measurements of Polyethersulfone Ultrafiltration Membranes to Determine Salt Effects on Membrane Zeta Potential, Int. J. Electrochem. Sci., 8: 4073 - 4084.

Serena Bandini, Daniele Vezzani. (2003), Nanofiltration modeling: the role of dielectric exclusion in membrane characterization. Chemical Engineering Science 58: 3303-3326.

Serena Bandini. (2005), Modelling the mechanism of charge formation in NF membranes: Theory and application. Journal of membrane science 264: 75–86.

Shams Ashaghi K., M. Ebrahimi, P. Czermak. (2007), Open Env. J. 1, 1-8.

Shih, W. Y., Rahardianto, A., Lee, R. W. and Cohen, Y., 2005, Morphometric characterization of calcium sulfate dihydrate (gypsum) scale on reverse osmosis membranes. Journal of membrane science, 252(1): 253-263.

Silva, P., S.J. Han and A.G. Livingston, (2005), Solvent transport in organic solvent nanofiltration membranes, Journal of Membrane Science 262: 49.

Song L., and M. Elimelech, (1995), Particle deposition onto a permeable

Stefan Duscher. 2014. Ceramic membranes for the filtration of liquids: An actual overview, F & S International Edition,14: (13-21).

Stopka J., S.G. Bugan, L. Broussous, S. Schlosser, A. Larbot, (2001), Microfiltration of beer yeast suspensions through stamped ceramic membranes, Sep. Purif. Technol. 25: 535–543.

Susanto, Heru, Yu Feng, and Mathias Ulbricht. 2009. "Fouling Behavior of Aqueous Solutions of Polyphenolic Compounds during Ultrafiltration." Journal of Food Engineering 91(2):333–40.

Szymczyk A., B. Aoubiza, P. Fievet and J. Pagetti, (1999), Electrokinetic phenomena in homogenous cylindrical pores, J. Colloid Interf. Sci., 216: 285–296.

Tellez, G.T., N. Nirmalakhandan and J.L. Gardea-Torresdey, (1995), Evaluation of biokinetic coefficients in degradation of oilfield produced water under varying salt concentrations, Water Research 29: 1711–1718.

Timmer, J.M.K., 2001, Properties of nanofiltration membranes; model development and industrial application, Eindhoven: Technische Universiteit Eindhoven.

Tzotzi Ch., T. Pahiadaki, S.G. Yiantsios, A.J. Karabelas, N. Andritsos, (2007), A study of $CaCO_3$ scale formation and inhibition in RO and NF membrane processes, Journal of Membrane Science 296: 171–184.

van der Meer, W., C. Aeijelts Averink, J. van Dijk. (1995). "Mathematical model of nanofiltration systems", Desalination, 105 : 25-31.

Van Gestel, T., C. Vandecasteele, A. Buekenhoudt, C. Dotremont, J. Luyten, R. Leysen , B. Van der Bruggen and G. Maes, (2002), Salt retention in nanofiltration with multilayer ceramic TiO_2 membranes, Journal of Membrane Science 209: 379–389.

Van Gestel, T., H. Kruidhof, D.H.A. Blank and H.J.M. Bouwmeester, (2006), ZrO_2 and TiO_2 membranes for nanofiltration and pervaporation: Part 1. Preparation and characterization of a corrosion-resistant ZrO_2 nanofiltration membrane with a MWCO < 300, Journal of Membrane Science 284: 128–136.

Vela, M.Cinta Vincent, Silvia Álvarez Blanco, Jaime Lora García, and Enrique Bergantiños Rodríguez. 2008. "Analysis of Membrane Pore Blocking Models Applied to the Ultrafiltration of PEG." Separation and Purification Technology 62(3):489–98.

Vetterling, W. T., S. A. Teukolsky, and H. William, Press, 1992, Numerical Recipes: Example Book (FORTRAN), Cambridge University Press, New York, NY, USA.

Vitaly Gitis and Gadi Rothenberg. 2016. Ceramic Membranes, New Opportunities and Practical Applications.

Vítor Geraldes, Ana Maria Brites Alves. (2008), Computer program for simulation of mass transport in nanofiltration membranes. Journal of Membrane Science 321: 172-182.

Wahab Mohammad, Lim Ying Pei, A. Amir H. Kadhum, (2002), Characterization and identification of rejection mechanisms in nanofiltration membranes using extended Nernst–Planck model, Clean Techn Environ Policy 4: 151–156.

Wang, X.L., T. Tsuru, M. Togoh, S. Nakao and S. Kimura, (1995), Transport of organic electrolytes with electrostatic and steric- hindrance effects through nanofiltration membranes, J. Chem. Eng. Japan 28: 372-380.

Wąsik, E., J. Bohdziewicz, and K. Ćwiklak, 2005, Ion balance in NF-treated well water for drinking water production. Desalination: (1):186 81-87.

Weber, R., H. Chmiel and V. Mavrov, (2003), Characteristics and application of new ceramic nanofiltration membranes, Desalination 157: 113-125.

Williams, Ceri and Richard Wakeman. 2000. "Membrane Fouling and Alternative Techniques for Its Alleviation." Membrane Technology 2000(124):4–10.

Wu D.X., J.A. Howell and R.W. Field, (1999), Critical flux measurement for model colloids, Journal of Membrane Science, 152: 89-98.

Yacubowicz, H., and J. Yacubowicz, (2005), Nanofiltration: properties and uses, Filtration & Separation, 42: 16-21.

Zhao, Y., Xing, W., Xu, N. and Wong, F.S., (2005), Sep. Purif. Technol., 42: 117-121.

Appendices

Appendix-A

The Chemicals used and SEM Section Image

Table A.1.1 Represent the Chemicals used with Some their Properties

Calcium Chloride $CaCl_2$	
Manufacture	RIEDEL-DE HAEN AG SELZE-HANNOVER Chem. Rein. Ph. Eur. L, B. P. Ph. France. IX. U. S. P. XX
Assay (%)	99.5 %
HCl	0.002 %
CaO	0.002 %
(As)	0.0001 %
(Fe)	0.0005 %
Magnesium (Mg)	0.03 %
(Na)	0.005 %
(Pb)	0.0005 %
(SO_4)	0.01 %
Molecular Weight	147.02 g/mol
Magnesium Chloride $MgCl_2$	
Manufacture	BDH Chemicals Ltd Poole England
Assay (%)	99.5 %
Molecular Weight	95.22 g/mol
Magnesium Sulfate $MgSO_4$	
Manufacture	Fluka-Garantie Made in Switzerland
Assay (%)	99 %
Chloride (Cl)	0.01 %
(Cu)	0.005 %
(Pb)	0.005 %
(Fe)	0.005 %
Zink (Zn)	0.005 %
Cadmium (Cd)	0.005 %
Molecular Weight	120.37
Sodium Carbonate Na_2CO_3	
Manufacture	BDH Chemicals Ltd Poole England
Assay (%)	99.5 %
Chloride (Cl)	0.002
Sulphate (SO_4)	0.005
Nitrate (NO_4)	0.002
Phosphate (PO_4)	0.001
Silicate (SiO_2)	0.005
Heavy Metals (Pb)	0.002
Molecular Weight	106 g/mol

Sodium Sulfate Na_2SO_4	
Manufacture	Fluka-Garantie Made in Switzerland
Assay (%)	99.0 %
Chloride (Cl)	0.005 %
(S_2O_3)	0.02 %
(Cu)	0.0005 %
(Pb)	0.0005 %
Cadmium (Cd)	0.0005 %
Zink (Zn)	0.0005 %
(Fe)	0.0005 %
(Co)	0.0005 %
Nickel (Ni)	0.0005 %
Calcium (Ca)	0.005 %
Arisen (As)	0.00001 %
Molecular Weight	142.04
Nitric Acid HNO_3	
Manufacture	GAINLAND CHEMICAL COMPANY (GCC), ENGLAND
Assay (%)	71 %
Non Volatile Matter	0.001 %
Chloride	0.00005 %
Sulphate	0.0002 %
Arsenic	0.000001 %
Cu	0.00001 %
Fe	0.00002 %
Pb	0.00001 %
Mn	0.00004 %
Molecular Weight	63.01
Hydrochloric Acid HCl	
Manufacture	Gainland Chemical Company, UK
Assay (%)	35.4 %
Non Volatile Matter	0.001 %
Free Chlorine	0.0002 %
Sulphate	0.0005 %
Arsenic	0.000002 %
Sulphite	0.0001 %
Ammonium	0.0003 %
Iron	0.00004 %
Lead	0.00005 %
Copper	0.00001 %
Molecular Weight	36.46

Sodium hydroxide NaOH	
Manufacture	Fluka AG Chemische Febrik CH- 9470 Made in Switzerland
Assay	99%
Chloride (Cl)	0.005%
Iron (Fe)	0.001%
Sulphate (SO_4)	0.005%
Phosphate (PO_4)	0.001%
Molecular Weight	40.00 g/mol
Calcium Carbonate $CaCO_3$	
Manufacture	BDH Chemicals Ltd, England
Assay (%)	99.5 %
Acid-insoluble matter	0.003 %
Soluble alkali	0.25 ml N/1 %
Chloride (Cl)	0.001 %
Nitrate (NO_3)	0.01 %
Phosphate (PO_4)	0.001 %
Silicate (SiO_2)	0.01 %
Sulphate (SO_4)	0.005 %
Ammonium (NH_4)	0.1 %
Molecular Weight	100.09
Sodium Chloride NaCl	
Manufacture	BDH Chemicals Ltd poole Engalnd
Assay (%)	99.9 %
pH (5% solution)	5.0 – 8.0
Water-insoluble matter	0.003 %
Bromide (Br)	0.005 %
Ferrocyanide [$Fe(CN)_6$]	0.0001 %
Iodide (I)	0.001 %
Nitrogen Compounds (N)	0.0005 %
Phosphate (PO_4)	0.0005 %
Sulphate (SO_4)	0.002 %
Barium (Ba)	0.001 %
Calcium (Ca)	0.002 %
Copper (Cu)	0.0002 %
Iron (Fe)	0.0002 %
Lead (pb)	0.0002 %
Magnesium (Mg)	0.002 %
Potassium (K)	0.005 %
Molecular Weight	58.44

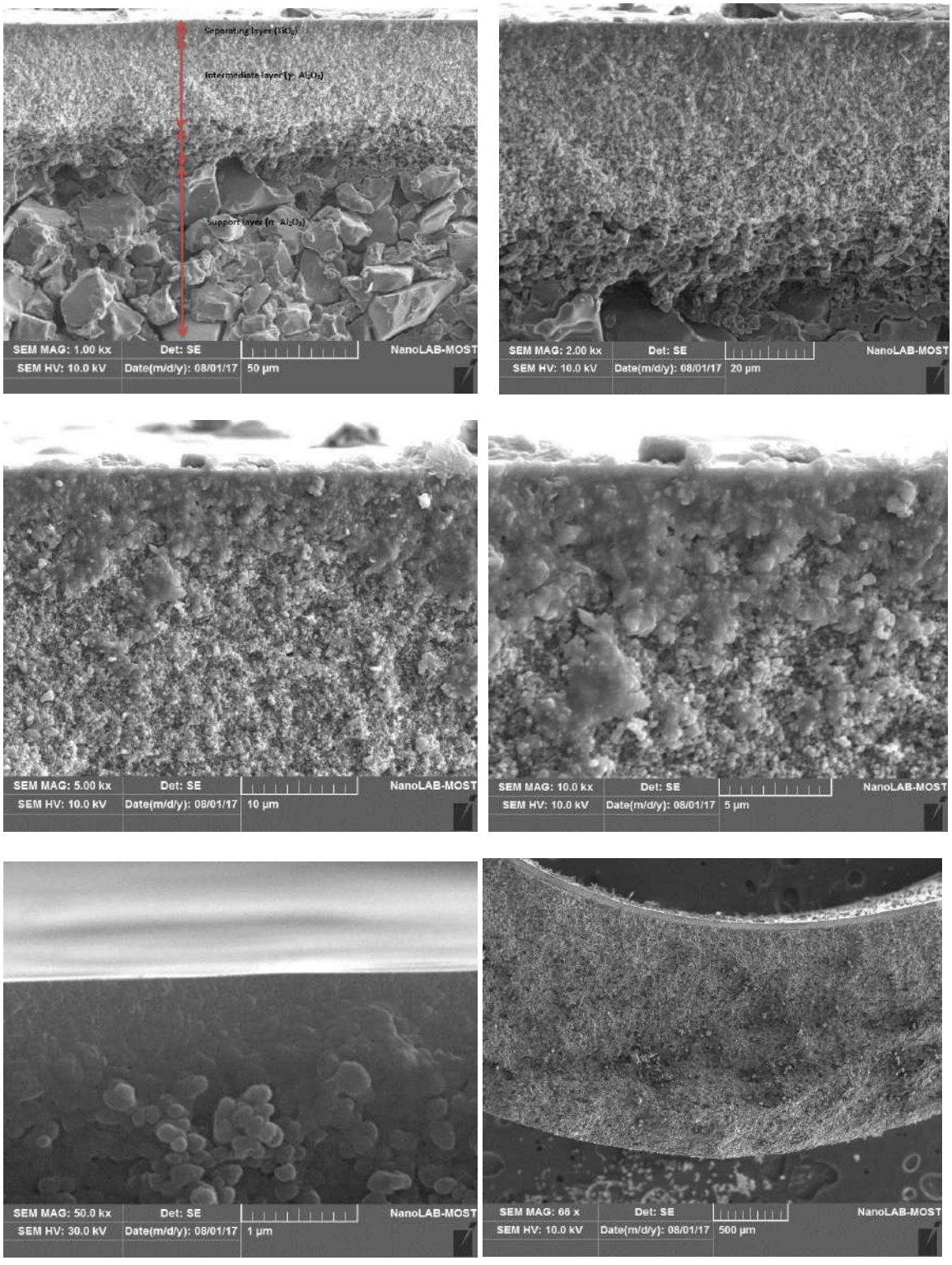

Figure A.1.1 SEM Section Image of Ceramic TiO_2 NF Membrane (0.9 nm)

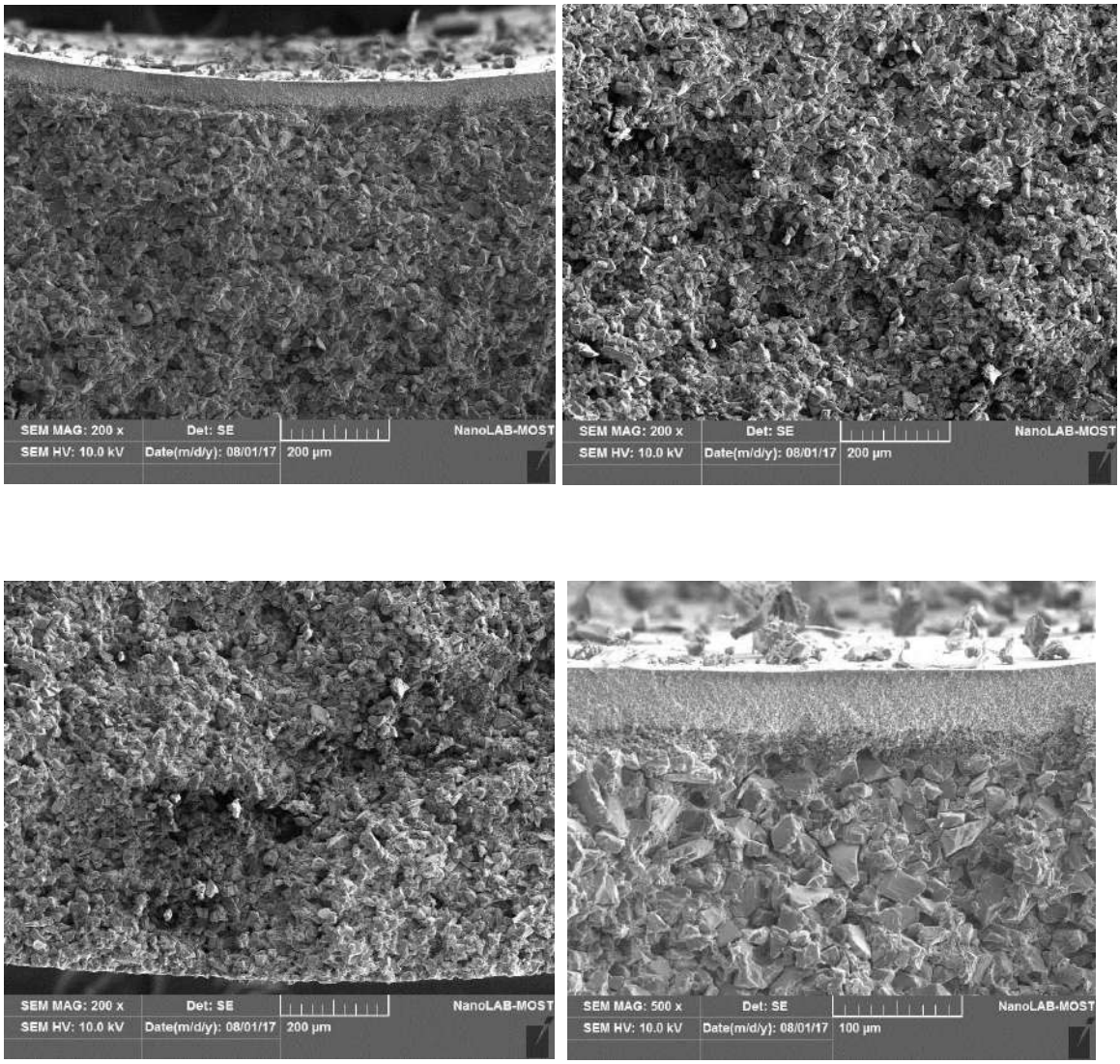

Continue Figure A.1.1

Appendix-B

B.1 Equipment used during the Experiments

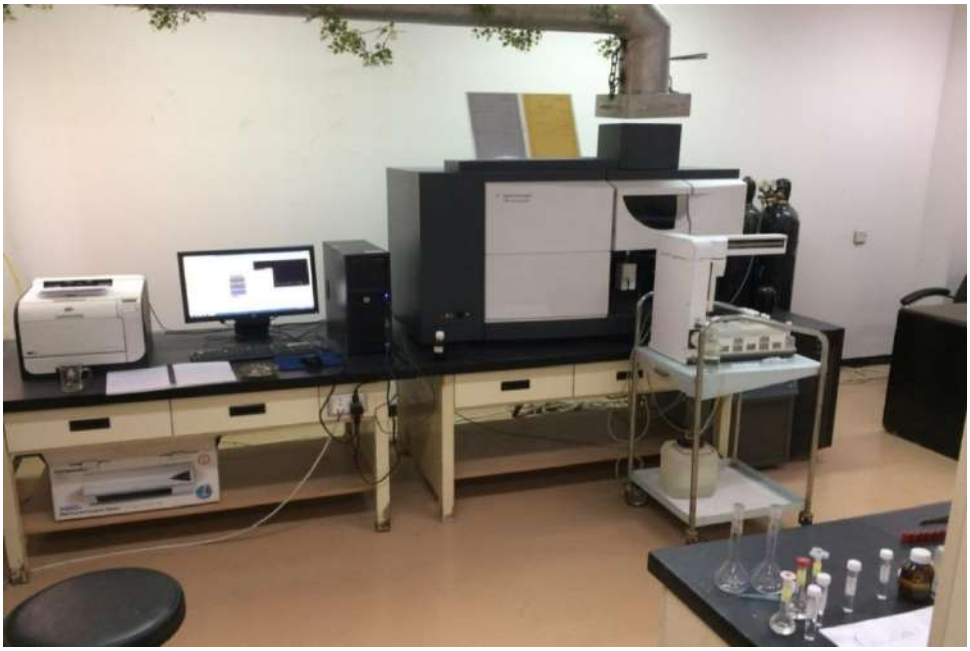

Figure B.1.1 Inductively Coupled Plasma ICP (Device from Agilent Technologies 700 Series ICP-OES-Company, U.S.A.)

Figure B.1.2 Zeta Potential Analyzer (Zeta Plus, Supplied by Brookhaven Instruments- USA)

Figure B.1.3 SEM – EDXS (SEM Vega 3, Czech Republic, EDXS, Amertek Inc, Paoli, PA, USA)

Figure B.1.4 Ion Chromatography (Metrohm Company, Model 883. Basic IC Plus, Swiss Origin)

Figure B.1.5 X-ray Fluorescence XRF (SPECTRO Analytical instruments, model XEPOS, Germany)

Figure B.1.6 High-Performance Liquid Chromatography (HPLC) (HPLC, model VQC1 supplied by SHIMADZU, Japan)

Figure B.1.7 Pre Treatment Cartridge (BOECO 80910, type 50136990, Thermo Fisher, Germany)

Figure B.1.8 pH meter (pp-203 by EZ0DO, Japan)

Figure B.1.9 Conductivity and Total Dissolve Solid TDS (InoLab Cond 7110 Supplied by WTW, Germany)

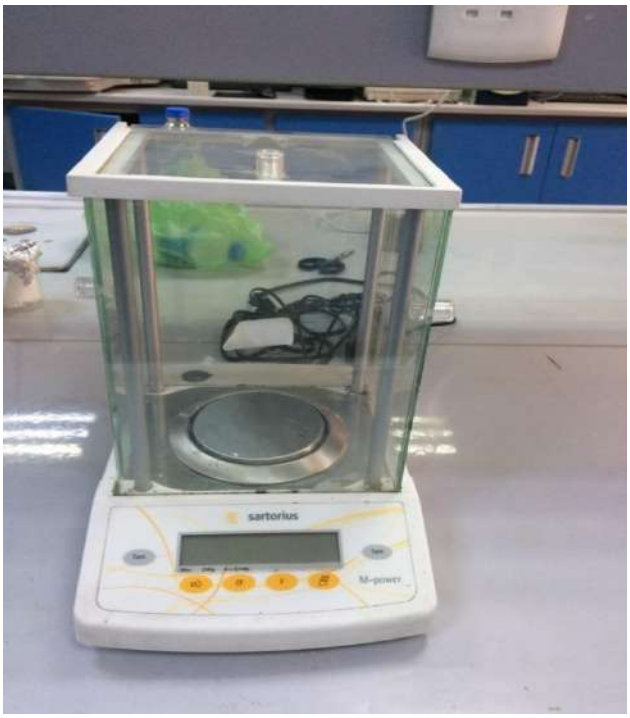

Figure B.1.10 Digital Balance (AZ214 supplied by Sartorius Weighing Technology GmbH, Germany)

Figure B.1.11 Oil Content Analyzer

Figure B.1.12 TOC Analyzer

Figure B.1.13 Milli-Voltemeter (Fluk corporation, 179 TRUE RMS MULTIMETER, U.S.A.)

Appendix C

Experimental Results

C.1 Zeta Potential Measurements

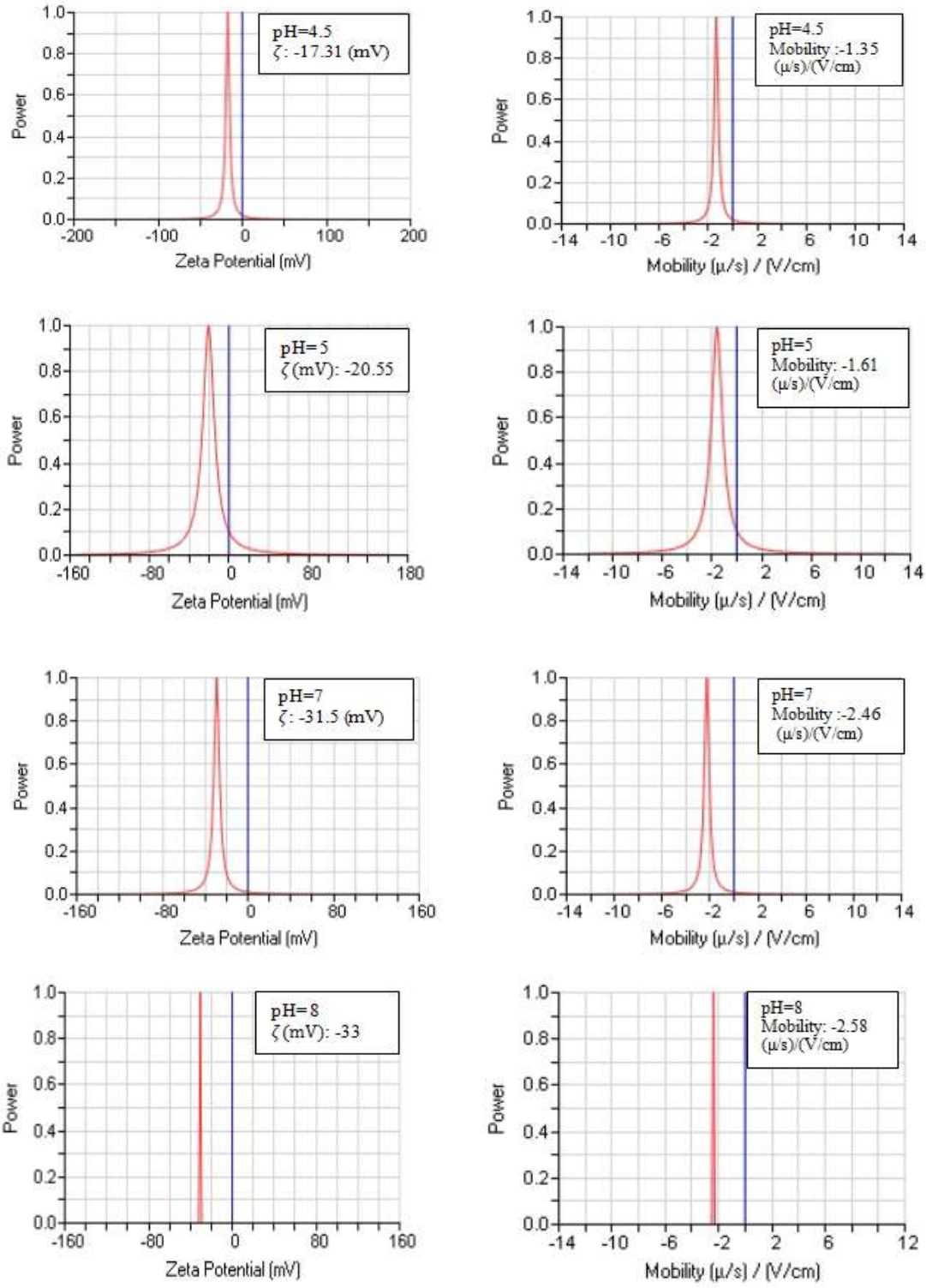

Fig. C.1.1 Zeta potential and mobility (microelectrophoresis method) at 0.001 M NaCl concentration for pH 4.5, 5, 7 and 8

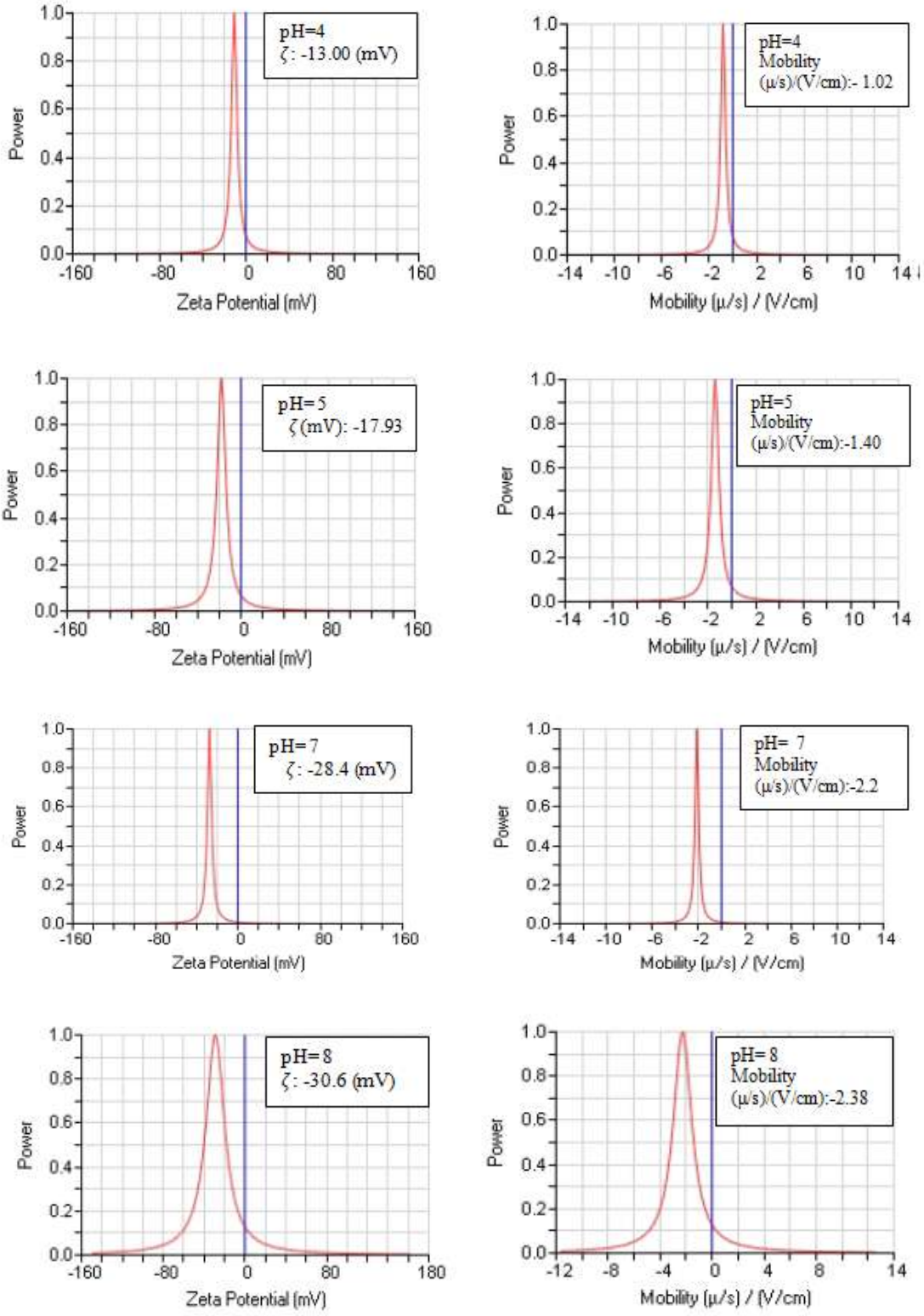

Fig. C.1.2 Zeta potential and mobility (microelectrophoresis method) at 0.01 M NaCl concentration for pH 4, 5, 7 and 8

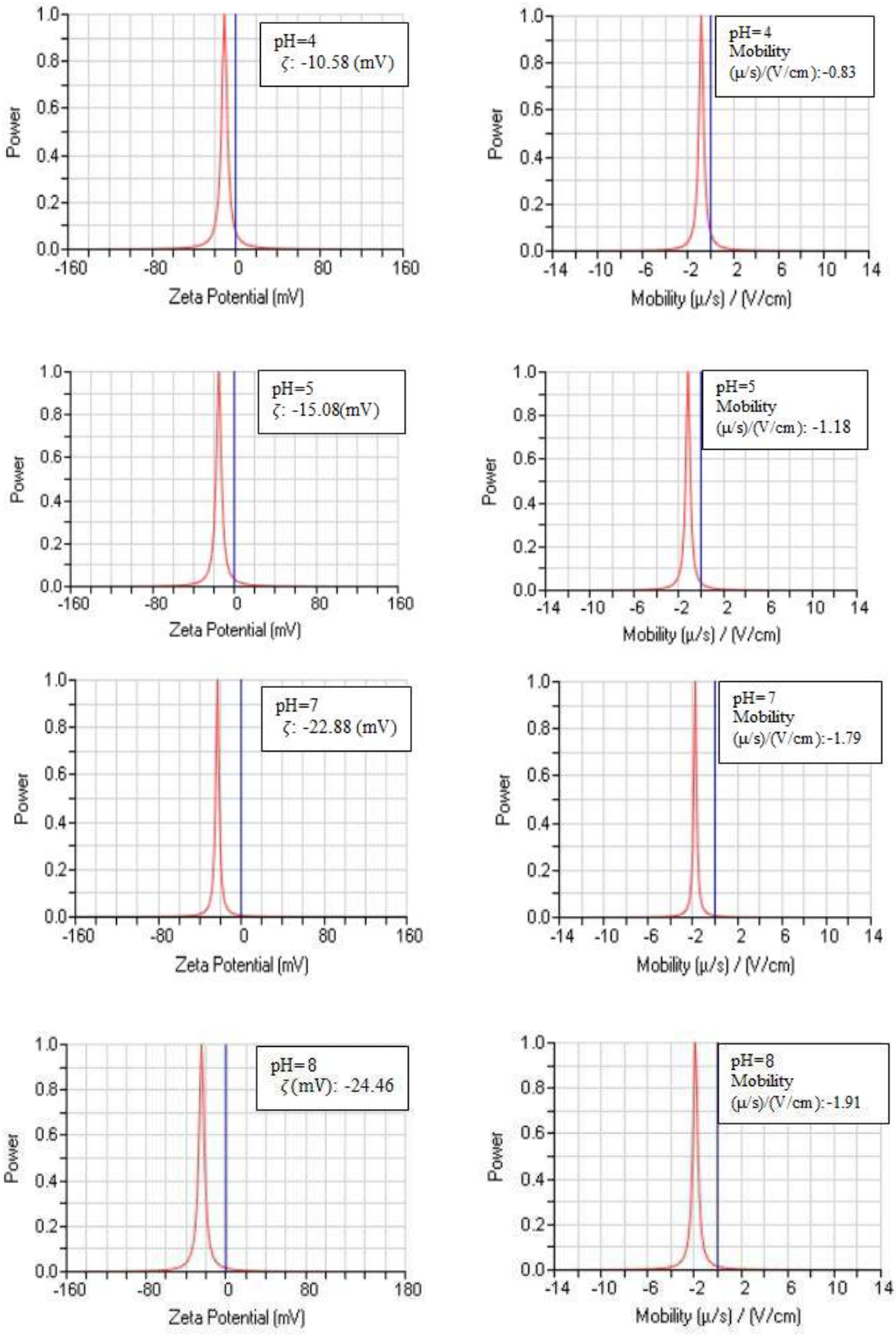

Fig. C.1.3 Zeta potential and mobility (microelectrophoresis method) at 0.1 M NaCl concentration for pH 4, 5, 7 and 8

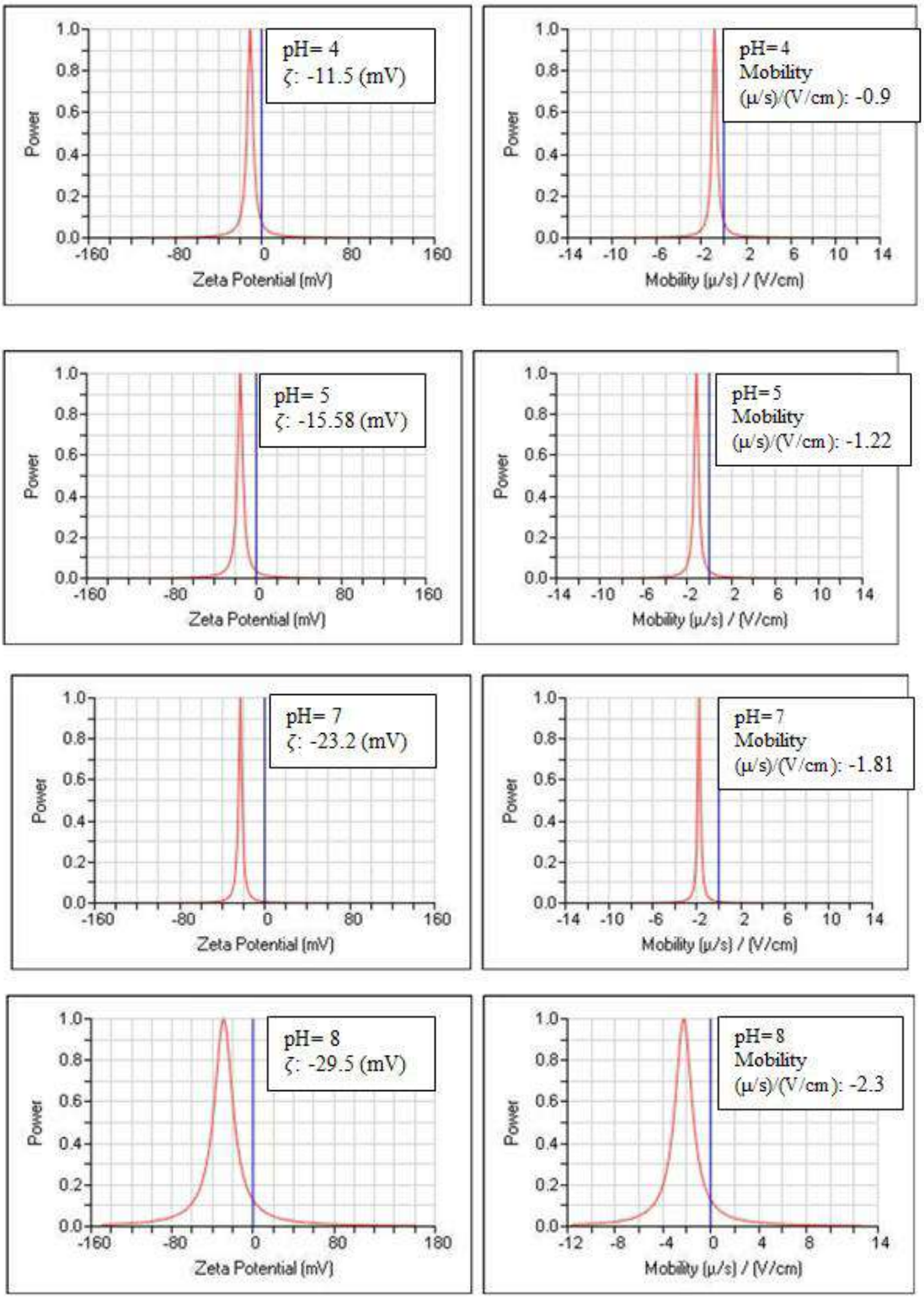

Fig. C.1.4 Zeta potential and mobility (microelectrophoresis method) at 5 ppm $CaCO_3$ concentration for pH 4, 5, 6, 7 and 8

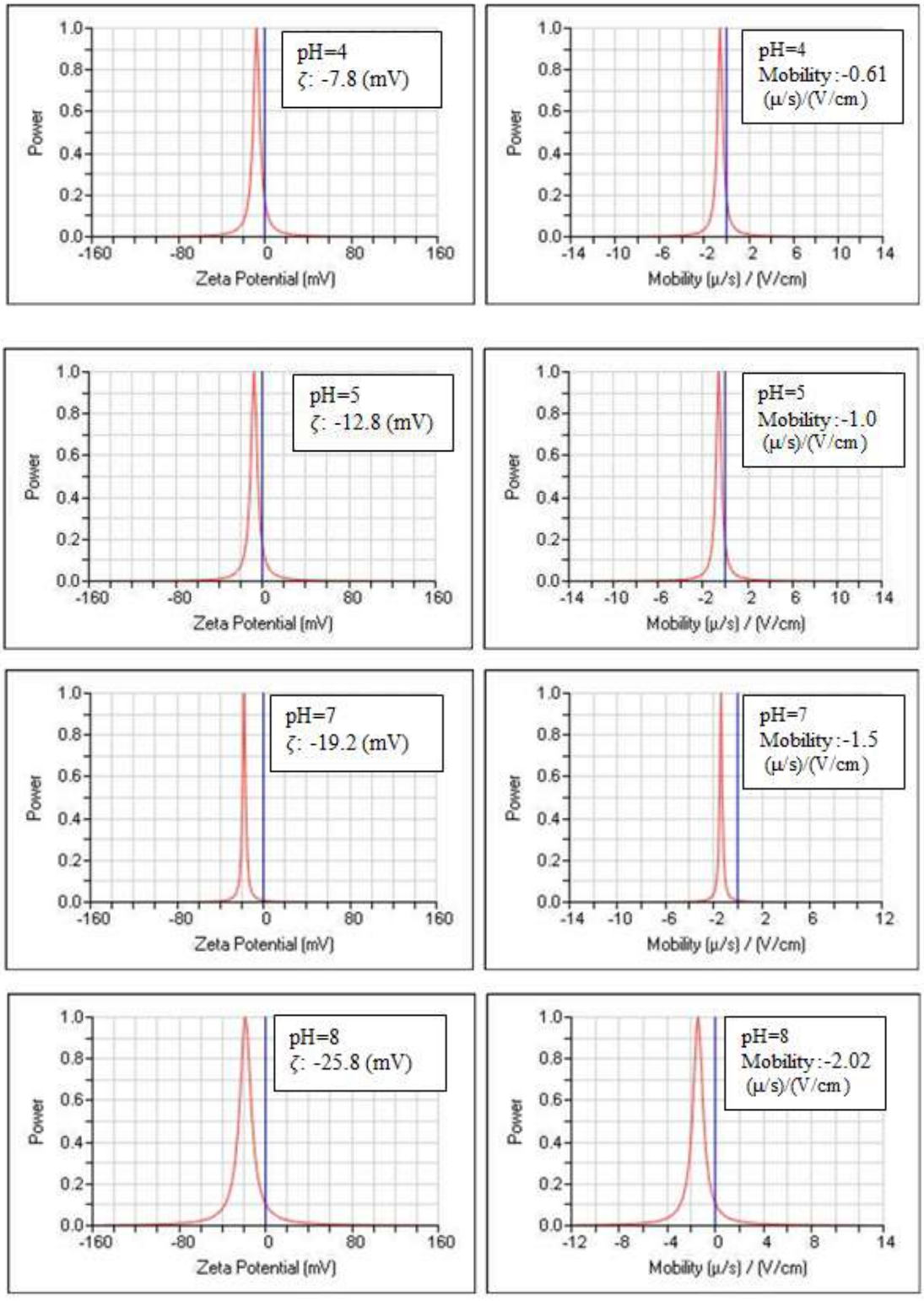

Fig. C.1.5 Zeta potential and mobility (microelectrophoresis method) at 10 ppm $CaCO_3$ concentration for pH 4, 5, 6, 7 and 8

Table C.1.1 Estimated Streaming Potential of 0.9 nm Titanium Dioxide NF Membrane over a Range of pH Values for Background Electrolyte Fixed at 0.01 and 0.1 M NaCl.

pH	Streaming potential (mv/bar) 0.01 M	Streaming potential (mv/bar) 0.1 M
3	8.7	4.4
4	-5.26	-2.9
5	-12.2	-9.6
6	-16.8	-13.3
7	-21.9	-15.7
8	-23	-17.6
9	-25	-18.2

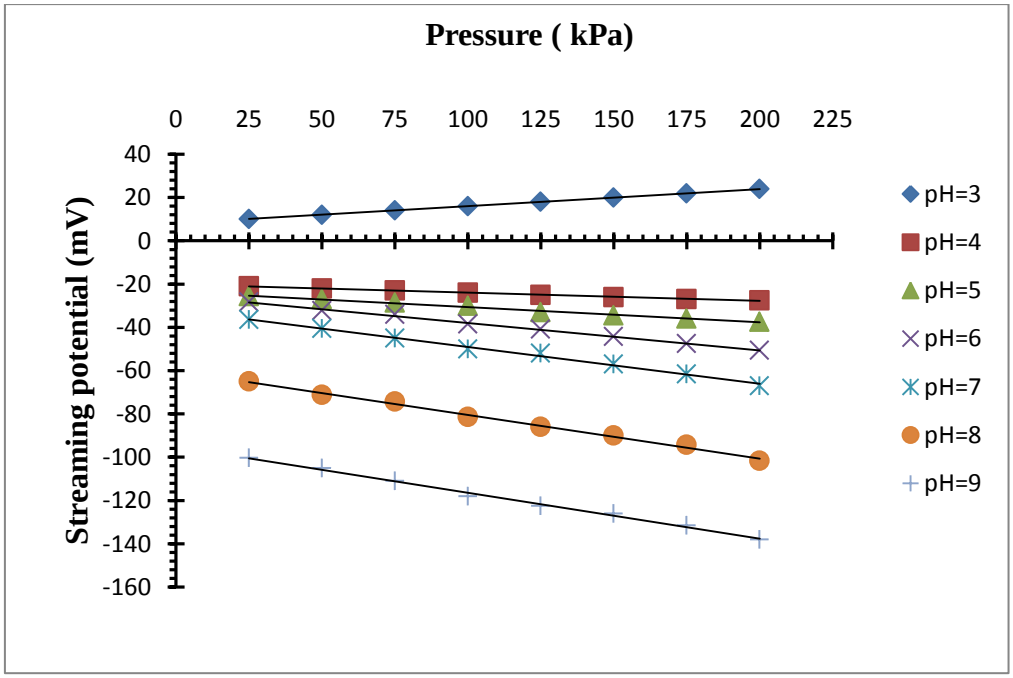

Fig.C.1.7 The streaming potential measurements of 0.9 nm titanium dioxide NF membrane versus applied pressure increment over a range of pH values for backgrounded electrolyte fixed at 0.01 M KCl.

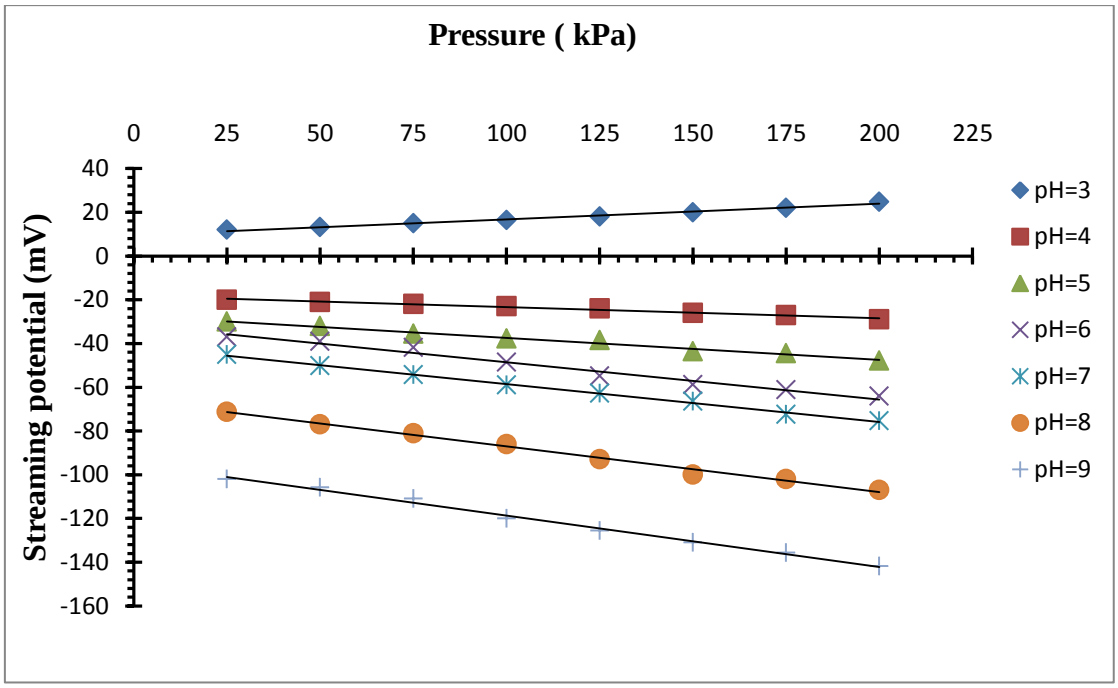

Fig. C.1.8 The streaming potential measurements of 0.9 nm titanium dioxide NF membrane versus applied pressure increment over a range of pH values for backgrounded electrolyte fixed at 0.01 M $NaHCO_3$.

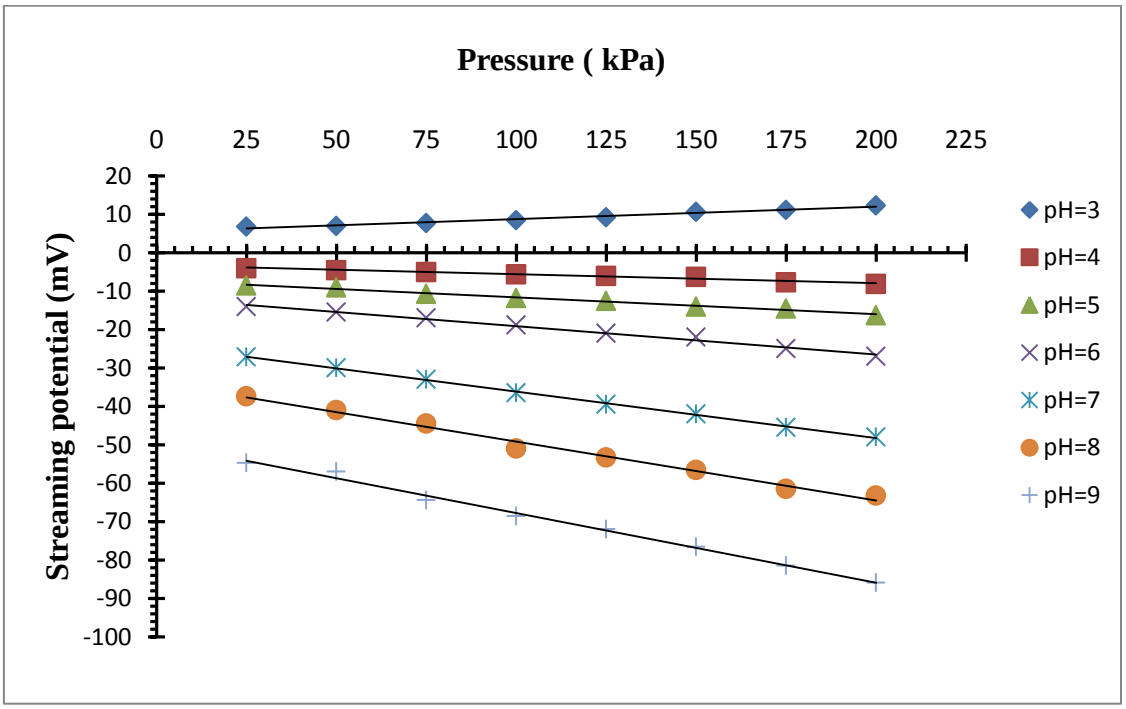

Fig. C.1.9 The streaming potential measurements of 0.9 nm titanium dioxide NF membrane versus applied pressure increment over a range of pH values for backgrounded electrolyte fixed at 0.01 M $CaCl_2$.

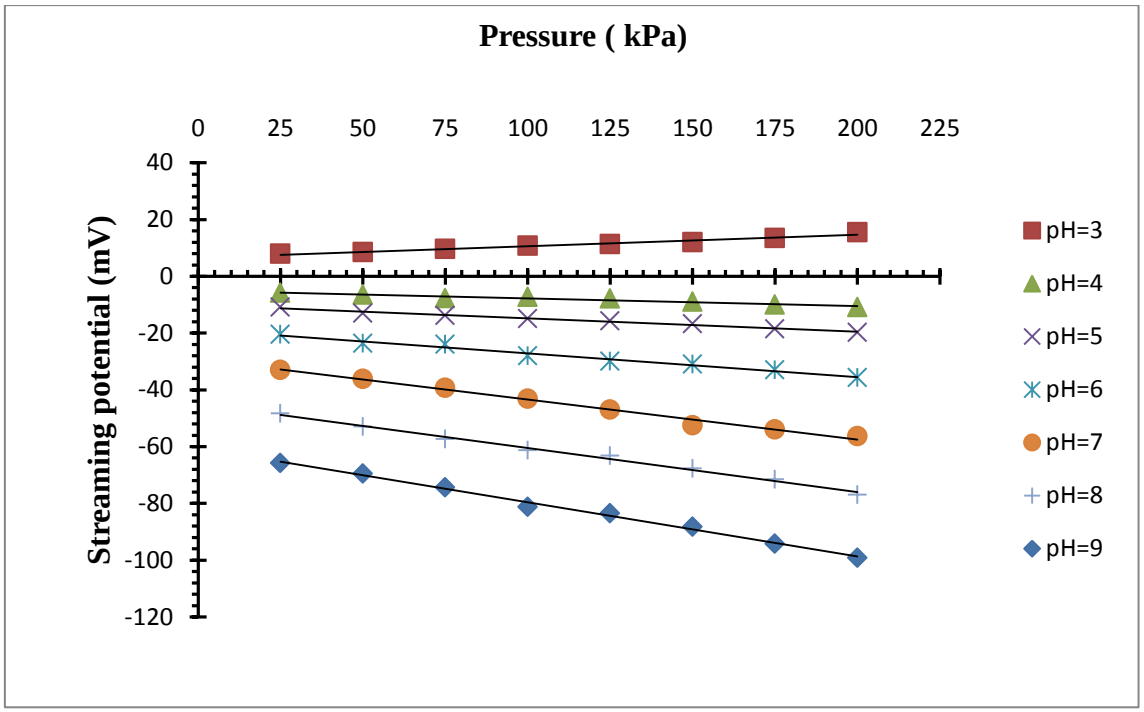

Fig. C.1.10 The streaming potential measurements of 0.9 nm titanium dioxide NF membrane versus applied pressure increment over a range of pH values for backgrounded electrolyte fixed at 0.01 M $MgCl_2$.

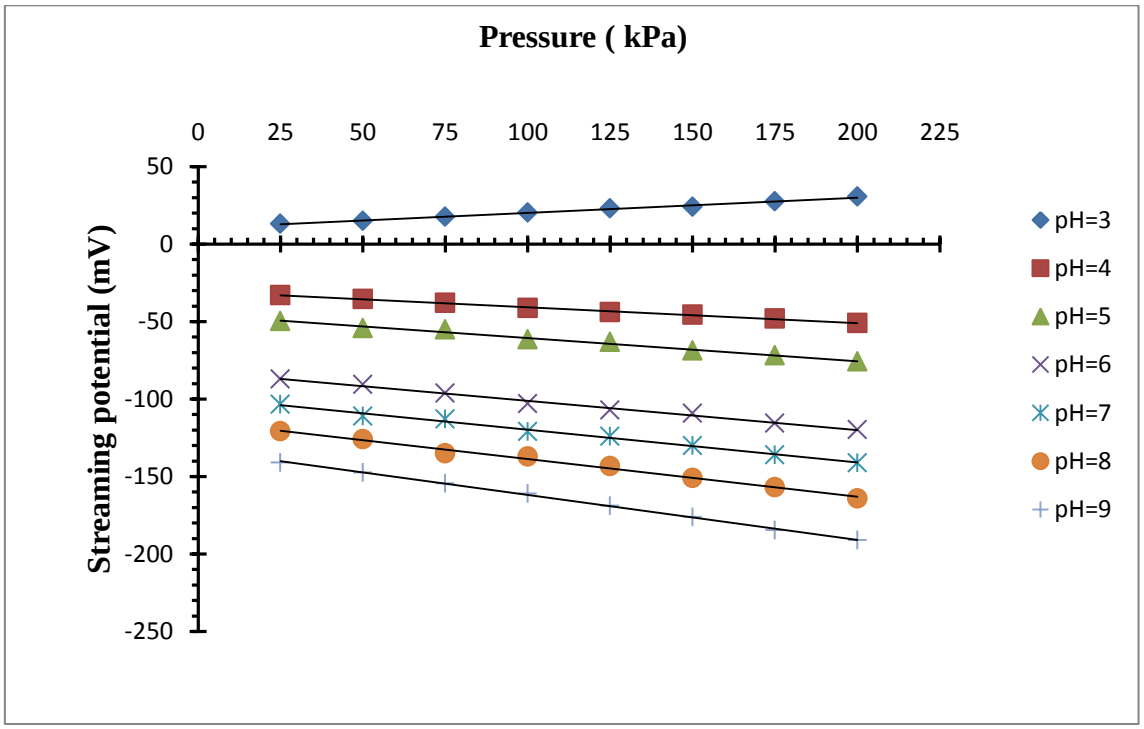

Fig. C.1.11 The streaming potential measurements of 0.9 nm titanium dioxide NF membrane versus applied pressure increment over a range of pH values for backgrounded electrolyte fixed at 0.01 M Na_2CO_3.

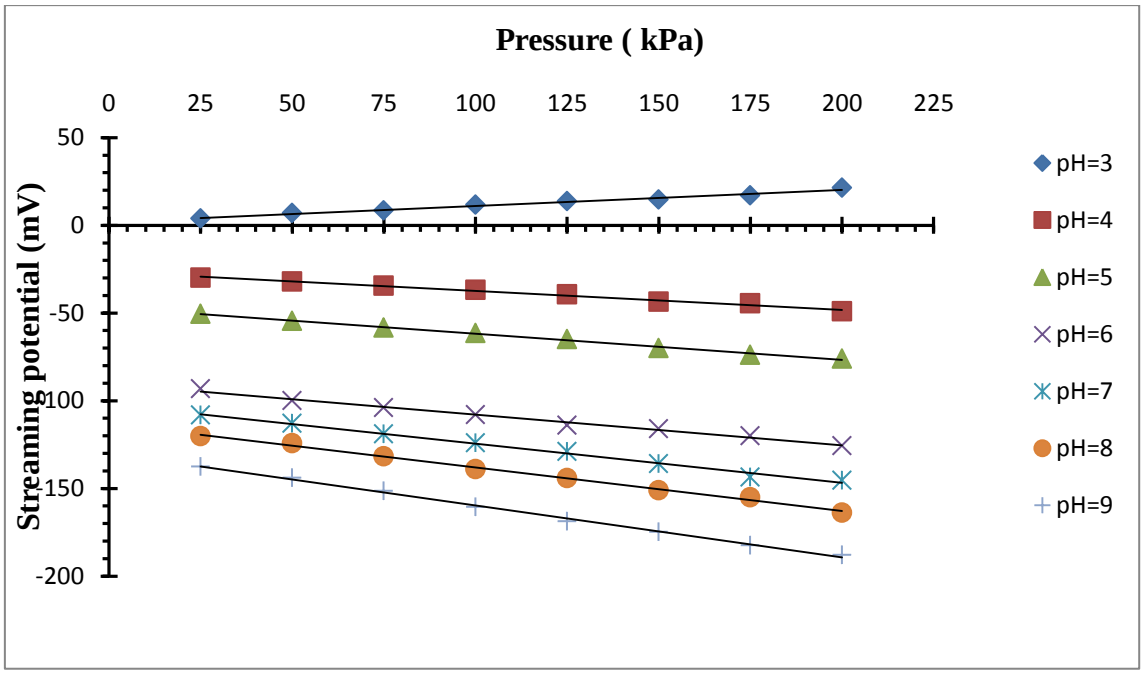

Fig. C.1.12 The streaming potential measurements of 0.9 nm titanium dioxide NF membrane versus applied pressure increment over a range of pH values for backgrounded electrolyte fixed at 0.01 M $MgSO_4$.

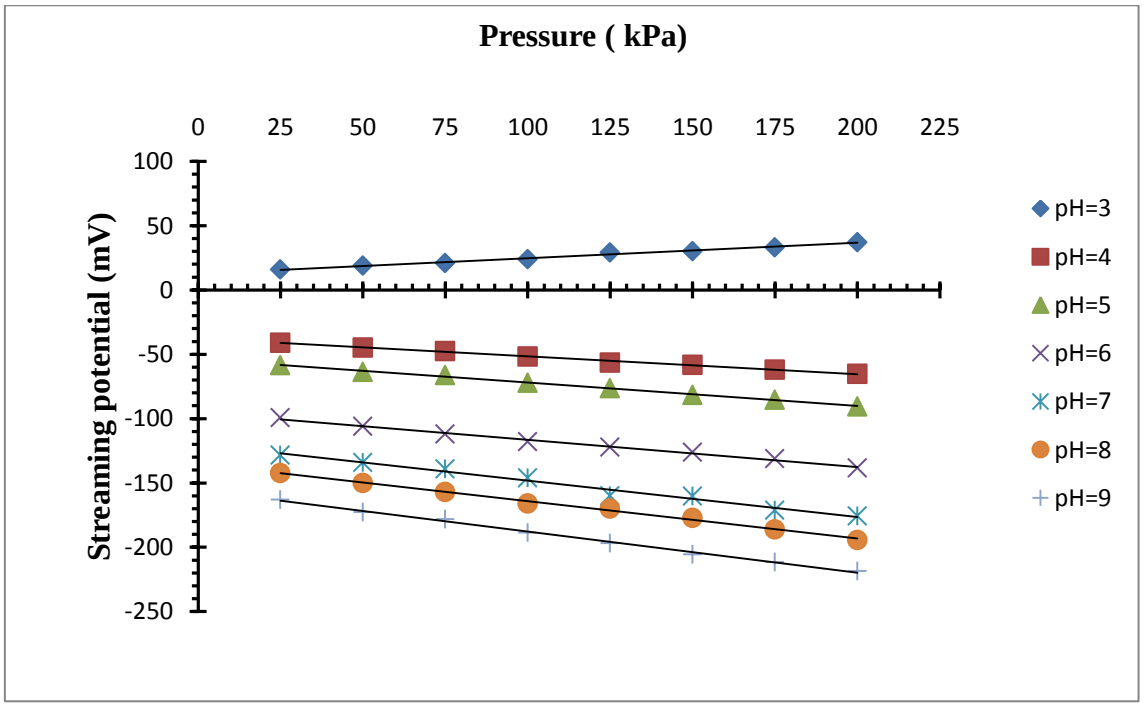

Fig. C.1.13 The streaming potential measurements of 0.9 nm titanium dioxide NF membrane versus applied pressure increment over a range of pH values for backgrounded electrolyte fixed at 0.01 M Na_2SO_4.

Table C.1.2 The Zeta Potential of 0.9 nm Ceramic Titanium Dioxide Nanofiltration Membrane Determined From Streaming Potential Plotted against pH for Background Electrolyte Fixed at 0.01 M (NaCl, $NaHCO_3$, Na_2CO_3, and Na_2SO_4)

pH	NaCl	$NaHCO_3$	Na_2SO_4	Na_2CO_3
3	12.39	9.3	15.53	12.9
3.6	0	0		0
3.8			0	
4	-10.08	-6.59	-17.7	-13.2
5	-15.1	-13	-23.36	-19
6	-22.62	-19.8	-28.5	-23.8
7	-26	-22.2	-34.6	-27.6
8	-28.99	-26.2	-38	-31.6
9	-31.9	-29.1	-40.62	-36.7

Table C.1.3 The Zeta Potential of 0.9 nm Ceramic Titanium Dioxide Nanofiltration Membrane Determined from Streaming Potential Plotted against pH for Background electrolyte Fixed at 0.01 M (NaCl, KCl, $MgCl_2$ and $CaCl_2$)

pH	NaCl	KCl	$CaCl_2$	$MgCl_2$
3	12.39	10.2	4	5.6
3.4			0	0
3.5		0		
3.6	0			
4	-10.08	-4.88	-3	-3.7
5	-15.1	-9.05	-5.75	-6.5
6	-22.62	-16.2	-9.5	-10.8
7	-26	-21.7	-15.3	-17
8	-28.99	-25.82	-18.9	-21
9	-31.9	-27.18	-22.84	-24.3

Table C.1.4 The Zeta Potential of 0.9 nm TiO_2 NF Membrane Determined from Streaming Potential Plotted against pH for Background Electrolyte Fixed at 0.01 M ($MgSO_4$ and Na_2SO_4)

pH	$MgSO_4$	Na_2SO_4
3	12.77	15.53
3.7	0	
3.8		0
4	-13.99	-17.7
5	-18.65	-23.36
6	-23.73	-28.5
7	-27.2	-34.6
8	-31.82	-38
9	-36.82	-40.62

C.2 Rejection Measurements of Membrane

Table C.2.1 Sodium Chloride Rejection at (0.001, 0.01 and 0.1 M) versus TMP

Applied TMP (bar)	NaCl 0.001 M	NaCl 0.01 M	NaCl 0.1 M
1	5.9	2.1	1.5
2	8.25	4.15	2.9
3	9.45	6.25	4.5
4	11	7.55	5.6
5	12.4	9	6.7
6	13.5	9.85	7.4
7	15.7	12.8	9.6
8	17.15	15.45	11.5
9	19.75	17.8	13.3
10	22.1	20.55	15.4
11	24.25	21.9	16.4
12	26.45	23.7	17.6
13	28.85	25.75	19
14	31.45	27.7	20
15	34.65	30.1	22.5

Table C.2.2 Magnesium Sulphate Rejection at (0.001, 0.005 and 0.01 M) versus TMP (1.0-15.0 bar)

Applied TMP (bar)	Magnesuim sulphate 0.01 M	Magnesuim sulphate 0.001 M	Magnesuim sulphate 0.005 M
1	22.5	28.9	27.1
2			
3	30.23	41.85	37.3
4			
5	36.34	45.65	42.3
6			
7	46.1	56.65	52.15
8			
9	53.8	60.85	56.45
10	57.86	65.25	62.35
11	59.8	68.85	64.65
12	61.05	74.75	67.91
13	61.75	76.95	69.7
14	62.2	80.8	70.43
15	62.75	85.25	70.99

Table C.2.3 Calcium Chloride Rejection at (0.001, 0.005, 0.01, 0.015 M) Versus TMP (1.0-15.0 bar)

Applied TMP (bar)	$CaCl_2$ 0.001 M	$CaCl_2$ 0.005 M	$CaCl_2$ 0.01 M	$CaCl_2$ 0.015 M
1	23.75	20	13.8	6.55
2				
3	30.65	26.6	21.3	10.45
4				
5	38.75	34.55	28.1	15.95
6				
7	44.8	39.6	35.25	21.1
8				
9	51.65	45.75	40.9	25.8
10	55.45	50.8	44.4	27.85
11	59.05	54.35	48.95	30.8
12	62.8	59.4	50.7	31.45
13	65.8	65	51.75	32.7
14	68.6	69	52.5	33.1
15	73.95	71.65	53.1	33.4

Table C.2.4 Sodium Sulphate, Magnesium Chloride and Sodium Bicarbonate Rejection at Constant Concentration (0.01 M) versus TMP (1.0-15.0 bar)

Applied TMP (bar)	$MgCl_2$ R%	$NaSO_4$ R%	$NaHCO_3$ R%
1	16	24.45	13
2			
3	26	33.5	20.4
4			
5	31	40.3	27.4
6			
7	40.1	49.25	34.1
8			
9	45	57	38.7
10	47.8		43.5
11	52	66.45	48.2
12	55		50.1
13	58.3	72.75	51
14	59		54
15	60	82	57

Table C.2.5 Calcium Carbonate Rejection as a Function of Applied (TMP) for the NF TiO_2 Membrane (1-15 bar) at three Concentration (5.0×10^{-5}, 10.0×10^{-5} and 13.0×10^{-5} M $CaCO_3$) and Constant pH (6.0).

Applied TMP (bar)	R% $CaCO_3$ 5×10^{-5} M	R% $CaCO_3$ 10×10^{-5} M	R% $CaCO_3$ 13×10^{-5} M
1	42	38	33
2	58	54	50
3	58.8	55.6	49
4	59.5	56.8	48.3
5	60.2	53	44.67
6	61	48.46	40
7	53.5	43	37.13
8	43.5	33.5	28
9	36.5	32.3	26.5
10	32	29.4	24.8
11	29	26	22.2
12	26.6	24	21.5
13	25	22.6	20.2
14	24	22	19.8
15	23.7	21.6	19.5

Table C.2.6 Calcium carbonate rejection as a function of applied (TMP) for the NF TiO_2 membrane (1-10 bar) at supersaturation concentration (50×10^{-5} M $CaCO_3$)

Applied TMP (bar)	R% $CaCO_3$ 50×10^{-5} M
1	34
2	23.21
3	16.63
4	2.785
5	-5.9
6	-17.2
7	-24.7
8	-28.87
9	-33.755
10	-37

Table C.2.7 Percentage of Salt (Sodium Chloride) Rejection versus pH in two Concentrations (0.01 M NaCl; 0.001 M NaCl), (Pressure 12 bar)

pH	0.001NaCl	0.01NaCl
3	29	25
3.8	21	17
5	28.6	24
6	33.29	29.3
6.5	35	31
7	36.4	32.3
8	37.3	33.4
9	38	34.2

Table C.2.8 $MgSO_4$ Rejection at pH (3.5, 6.0 and 9.0) and Constant Concentration (0.01 M) versus TMP (1.0-15.0 bar)

Applied TMP (bar)	Magnesuim sulphate pH 3.5	Magnesuim sulphate pH 6	Magnesuim sulphate pH 9
1	9.8	22.5	25.55
2			
3	22.7	30.23	33.85
4			
5	26.7	36.34	42.1
6			
7	31.5	46.1	50.1
8			
9	36	53.8	59.15
10	37.25	57.86	62.95
11	38.5	59.8	65.32
12	39.5	61.05	66.87
13	40.3	61.75	68.15
14	40.75	62.2	68.77
15	41.3	62.75	69.35

Table C.2.9 Calcium Carbonate Rejection as a Function of Applied (TMP) for the NF TiO_2 Membrane (1-15 bar) at three Different pH (3,6 and 9) and Fixed Concentration (5×10^{-5} M).

Applied TMP (bar)	pH 3	pH 6	pH 9
1	39	42	51
2	55.5	58	65
3	56.3	58.8	66.8
4	57	59.5	67
5	57.5	60.2	67.9
6	58	61	70
7	50.5	53.5	61.7
8	40.9	43.5	52.9
9	33.7	36.5	44.5
10	29.2	32	40.5
11	26.3	29	37
12	23.7	26.6	33.9
13	22	25	33.2
14	20.5	24	31.4
15	20.4	23.7	30.2

Table C.2.10 Calcium Chloride Rejection at (0.01 M) versus TMP (1.0-15.0 bar) at Cross Flow Velocity (1 and 2 m/s)

Applied TMP (bar)	$CaCl_2$ 1 m/s	$CaCl_2$ 2 m/s
1	13.8	16.4
2		
3	21.3	26.8
4		
5	28.1	33.65
6		
7	35.25	39.6
8		
9	40.9	44.6
10	44.4	48.1
11	48.95	51.45
12	50.7	54.15
13	51.75	57.4
14	52.5	60.4
15	53.1	64.5

Table C.2.11 Calcium Carbonate Rejection as a Function of Applied (TMP) for the NF TiO_2 Membrane (1-15 bar) at Cross Flow Velocity (1 and 2 m/s) and Fixed Concentration (10×10^{-5} M).

Applied TMP (bar)	$CaCO_3$ 10 ppm - Velocity 1 m/s	$CaCO_3$ 10 ppm - Velocity 2 m/s
1	38	43
2	54	58
3	55.6	58.8
4	56.8	60.7
5	53	59
6	48.46	52.7
7	43	46
8	33.5	37.6
9	32.3	35.2
10	29.4	32.5
11	26	30.4
12	24	28
13	22.6	26.7
14	22	25
15	21.6	23.8

Table C.2.12 NaCl, $NaHCO_3$ and Na_2SO_4 Rejection at Constant Concentration (0.01 M) Versus TMP (1.0-15.0 bar)

Applied TMP (bar)	NaCl R%	$NaHCO_3$ R%	Na_2SO_4 R%
1	2.1	13	24.45
2			
3	6.25	20.4	33.5
4			
5	9	27.4	40.3
6			
7	12.8	34.1	49.25
8			
9	17.8	38.7	57
10		43.5	
11	21.9	48.2	66.45
12		50.1	
13	25.75	51	72.75
14		54	
15	30.1	57	82

Table C.2.13 NaCl, $MgCl_2$ and $CaCl_2$ Rejection at Constant Concentration (0.01 M) versus TMP (1.0-15.0 bar)

Applied TMP (bar)	NaCl R%	$MgCl_2$ R%	$CaCl_2$ R%
1	2.1	16	13.8
2			
3	6.25	26	21.3
4			
5	9	31	28.1
6			
7	12.8	40.1	35.25
8			
9	17.8	45	40.9
10	20.55	47.8	44.4
11	21.9	52	48.95
12	23.7	55	50.7
13	25.75	58.3	51.75
14	27.7	59	52.5
15	30.1	60	53.1

Table C.2.14 $NaSO_4$ and $MgSO_4$ Rejection at Constant Concentration (0.01 M) versus TMP (1.0-15.0 bar)

Applied TMP (bar)	Na_2SO_4 R%	$MgSO_4$ R%
1	24.45	22.5
2		
3	33.5	30.23
4		
5	40.3	36.34
6		
7	49.25	46.1
8		
9	57	53.8
10		
11	66.45	59.8
12		
13	72.75	61.75
14		
15	82	62.75

Table C.2.15 Na_2SO_4, $MgCl_2$, $NaHCO_3$ $CaCl_2$, $MgSO_4$ and NaCl Rejection at Constant Concentration (0.01 M) versus TMP (1.0-15.0 bar)

Applied TMP (bar)	Na2SO4 R%	MgCl2 R%	NaHCO3 R%	CaCl2 R%	MgSO4 R%	NaCl R%
1	24.45	16	13	13.8	22.5	2.1
2						
3	33.5	26	20.4	21.3	30.23	6.25
4						
5	40.3	31	27.4	28.1	36.34	9
6						
7	49.25	40.1	34.1	35.25	46.1	12.8
8						
9	57	45	38.7	40.9	53.8	17.8
10	61.25	47.8	43.5	44.4	57.86	20.55
11	66.45	52	48.2	48.95	59.8	21.9
12	70.1	55	50.1	50.7	61.05	23.7
13	72.75	58.3	51	51.75	61.75	25.75
14	77.4	59	54	52.5	62.2	27.7
15	82	60	57	53.1	62.75	30.1

Table C.2.16 Ca^{+2}, Mg^{+2} and Na^{+1} Rejection Versus TMP 1-12 bar.

Applied TMP (bar)	Ca^{+2} R%	Mg^{+2} R%	Na^{+1} R%
1	14.2	14.6	12.4
2	20	21	15.2
3	28	29	19.5
4	33.2	34.6	23.6
5			
6	40.1	42	25.2
7			
8	41.5	43.6	27.5
9			
10	41.8	43.9	28.2
11			
12	42	44.1	28.5

Table C.2.17 TDS of Oilfield Produced Water Versus TMP 1-12 bar

Applied TMP (bar)	TDS of Oilfield Produced Water
1	55.78
2	54.25
3	51.12
4	48.5
5	
6	45.69
7	
8	45.37
9	
10	44.98
11	
12	44.73

C.3 Permeate Conductivity Measurements

Figs. (C.3.1, C.3.2 and C.3.3) show the conductivity of (NaCl) permeate at 0.001, 0.01 and 0.1 M respectively as a function of applied (TMP). From these figures it can be deduced that the conductivity of (NaCl) permeate for any concentration was reduced with raised applied (TMP).

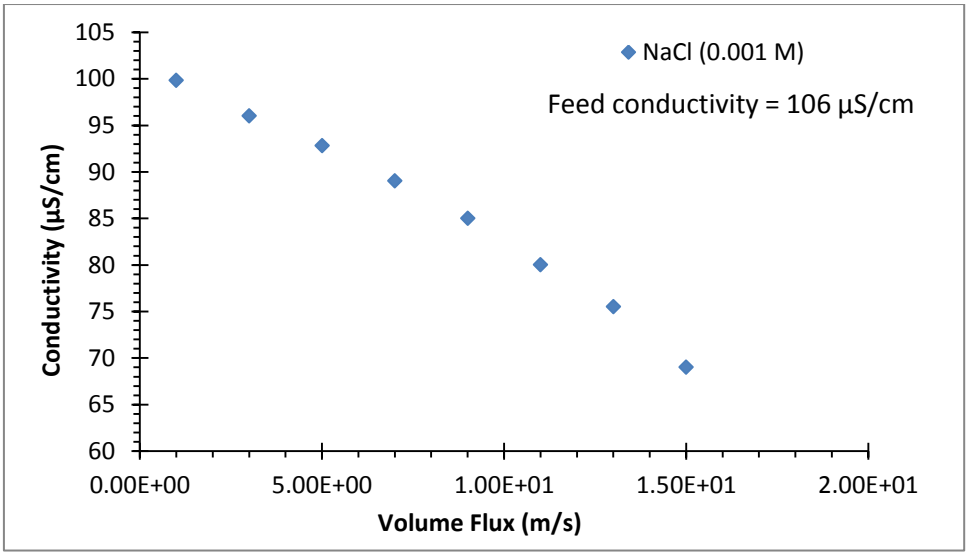

Figure C.3.1 Sodium Chloride Conductivity at 0.001 M versus (Jv) Volume Flux ($m^3/m^2.s$)

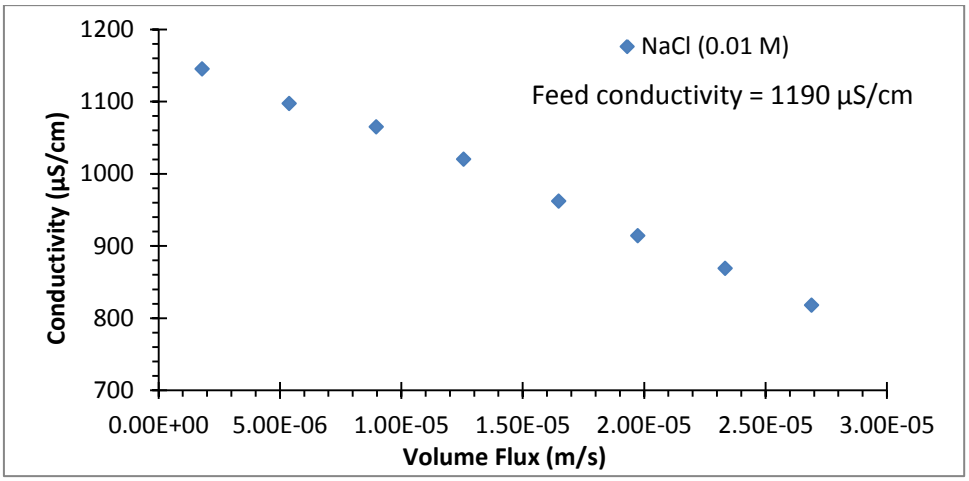

Figure C.3.2 Sodium Chloride Conductivity at 0.01 M versus (Jv) Volume Flux ($m^3/m^2.s$)

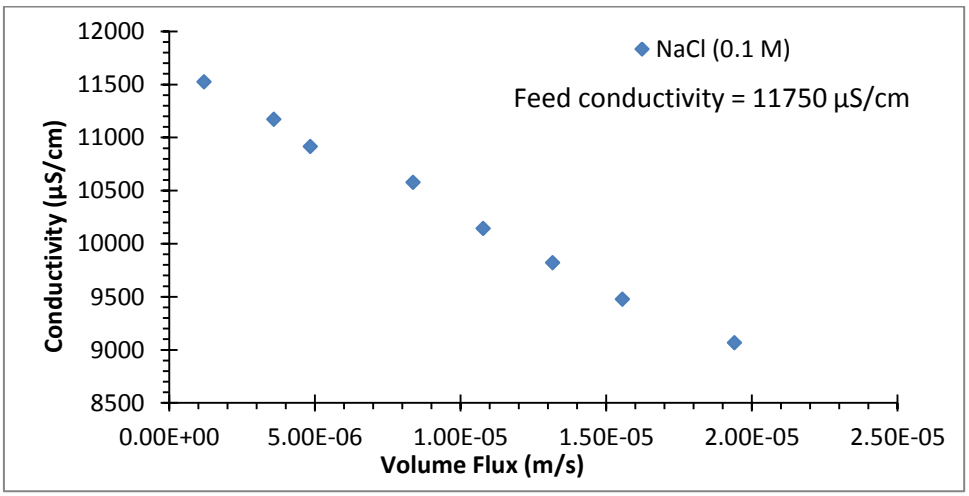

Figure C.3.3 Sodium Chloride Conductivity at 0.1 M versus (Jv) Volume Flux ($m^3/m^2.s$)

Figs. (C.3.4, C.3.5 and C.3.6) show the conductivity of magnesium sulphate permeates at (0.001, 0.005 and 0.01 M) respectively as a function of applied (TMP).

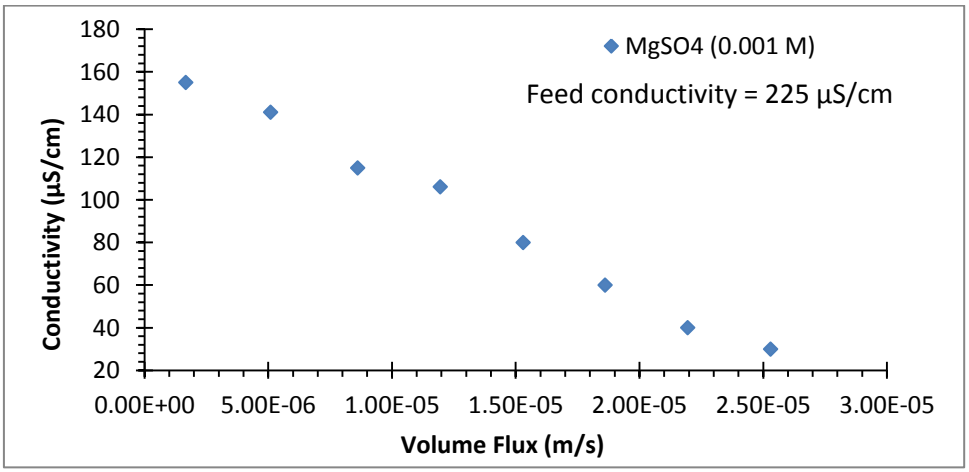

Figure C.3.4 Magnesium Sulphate Conductivity at 0.001 M versus (Jv) Volume Flux ($m^3/m^2.s$)

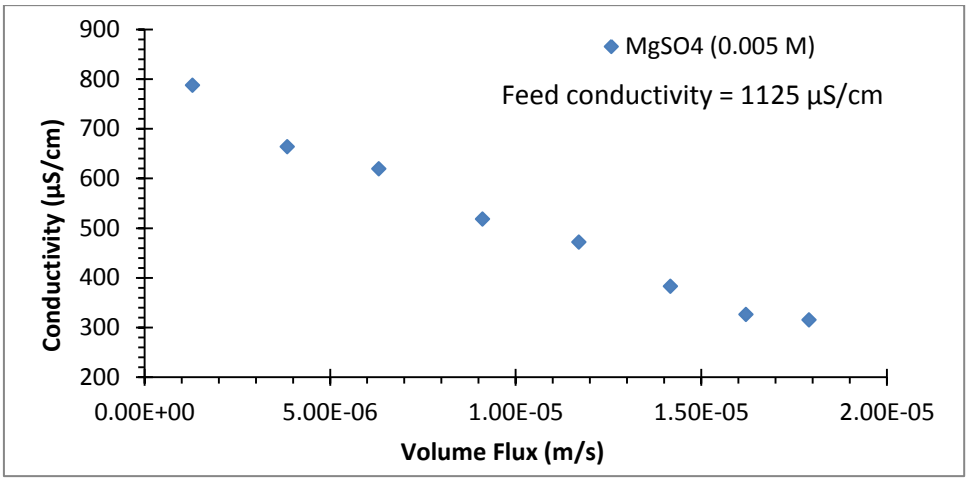

Figure C.3.5 Magnesium Sulphate Conductivity at 0.005 M versus (Jv) Volume Flux ($m^3/m^2.s$)

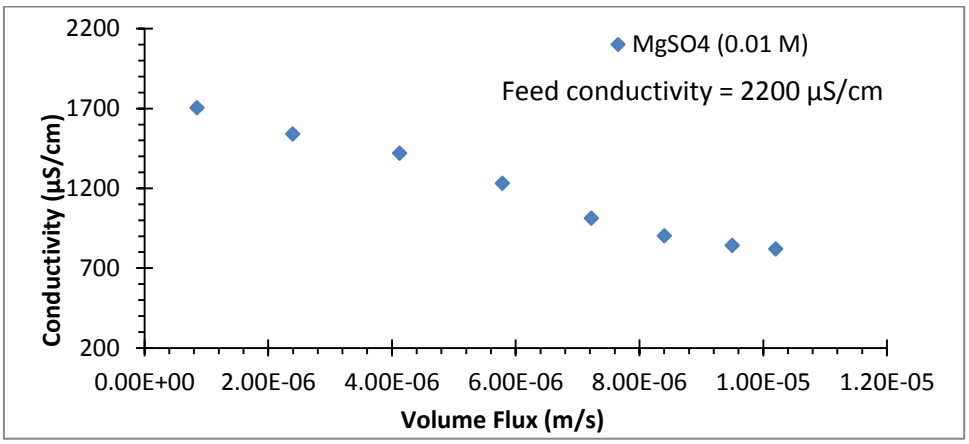

Figure C.3.6 Magnesium Sulphate Conductivity at 0.01 M versus (Jv) Volume Flux ($m^3/m^2.s$)

Figs. (C.3.7, C.3.8, C.3.9 and C.3.10) show the conductivity of $CaCl_2$ permeates at 0.001 M, 0.005 M, 0.01 M and 0.015 M respectively versus applied (TMP). Can be seen from these figures that the conductivity of calcium chloride permeate for any concentration were reduced with the increased applied (TMP).

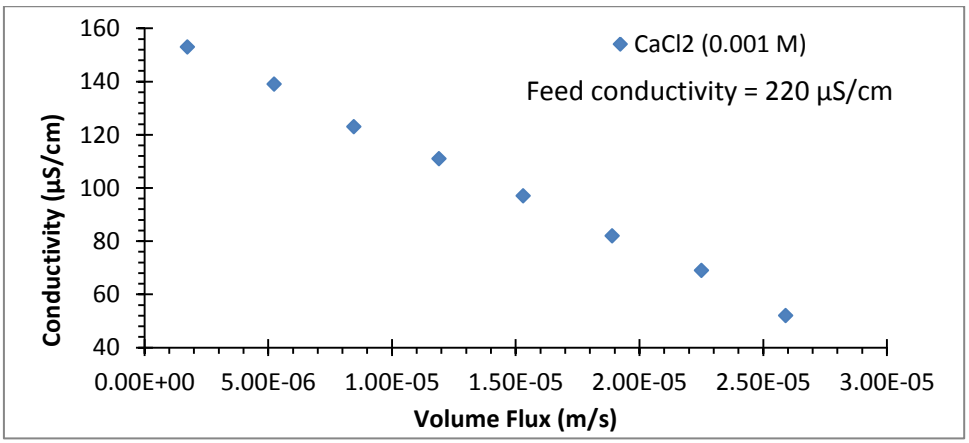

Figure C.3.7 Calcium Chloride Conductivity at 0.001 M versus (Jv) Volume Flux ($m^3/m^2.s$)

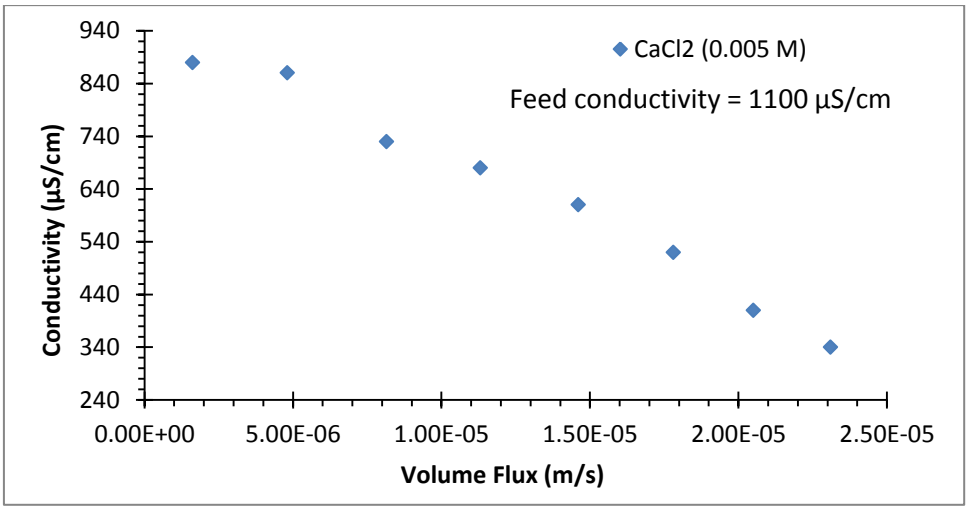

Figure C.3.8 Calcium Chloride Conductivity at 0.005 M versus (Jv) Volume Flux ($m^3/m^2.s$)

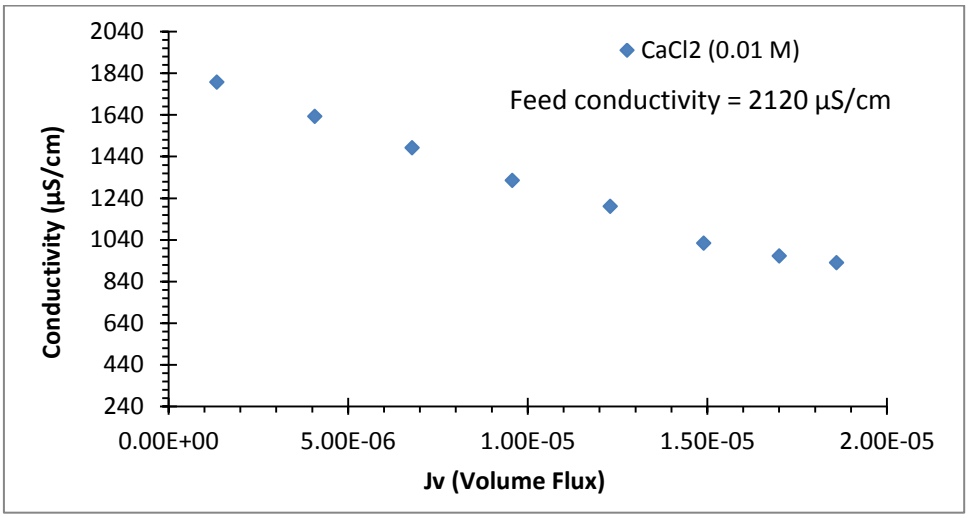

Figure C.3.9 Calcium Chloride Conductivity at 0.01 Mversus (Jv) Volume Flux ($m^3/m^2.s$)

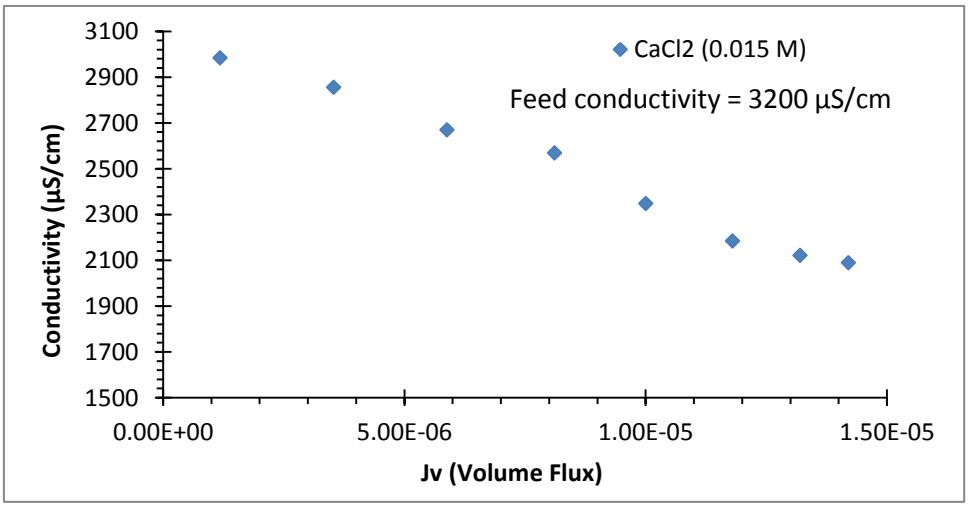

Figure C.3.10 Calcium Chloride Conductivity at 0.015 M versus (Jv) Volume Flux ($m^3/m^2.s$)

C.4 Critical Flux Determents

Table C.4.1 Critical Flux of (0.001, 0.005, 0.01M) $MgSO_4$

Applied TMP (bar)	pure water ($l/m^2.h$)	0.01 M $MgSO_4$	0.001 M $MgSO_4$	0.005 M $MgSO_4$
1	6.58E+00	2.967	6.1	4.64
2	1.32E+01	5.98	12	9.33
3	1.97E+01	8.613	18.6	13.83
4	2.63E+01	11.6	24.8	18.42
5	3.29E+01	14.833	31	22.73
6	3.95E+01	18.2	37	27.94
7	4.61E+01	20.814	43	32.78
8	5.26E+01	23.684	49	37.08
9	5.92E+01	26	55.08	42.2
10	6.58E+01	28.44	61	47.12
11	7.24E+01	30.24	67	51.2
12	7.90E+01	32.4	73	54.863
13	8.55E+01	34.2	79	58.474
14	9.21E+01	35.64	85	62.089
15	9.87E+01	36.72	91	64.396

Table C.4.2 Critical Flux of (0.001, 0.005, 0.01, 0.015 M) $CaCl_2$

Applied TMP (bar)	pure water ($l/m^2.h$)	0.001 M $CaCl_2$	0.005 M $CaCl_2$	0.01 M $CaCl_2$	0.015 M $CaCl_2$
1	6.58E+00	6.22	5.82	4.907	4.232
2	1.32E+01	12.321	11.74	9.77	8.47
3	1.97E+01	18.83	17.3	14.94	12.704
4	2.63E+01	25.12	23.28	19.8	16.914
5	3.29E+01	31.1	29.35	24.9	21.173
6	3.95E+01	37.8	34.92	30.2	25.43
7	4.61E+01	42.83	40.74	35.15	29.187
8	5.26E+01	50.24	46.36	39.56	33.02
9	5.92E+01	55.2	52.38	44.1	36
10	6.58E+01	61.4	58.1	48.8	39.4
11	7.24E+01	68.182	64.02	53.6	42.5
12	7.90E+01	74.64	69.3	57.5	46
13	8.55E+01	80.86	73.7	61.2	47.6
14	9.21E+01	87.08	78.6	64.5	49.5
15	9.87E+01	93.3	83	67	51

Table C.4.3 Critical Flux of (0.001, 0.01 and 0.1 M) NaCl

Applied TMP (bar)	pure water ($l/m^2.h$)	0.001 M NaCl	0.01 M NaCl	0.1 M NaCl
1	6.58E+00	6.46	5.7	4.31
2	1.32E+01	12.92	12.153	8.6124
3	1.97E+01	19.378	18.23	12.92
4	2.63E+01	25.837	24.31	17.225
5	3.29E+01	32.297	30.383	21.53
6	3.95E+01	38.756	36.46	25.84
7	4.61E+01	45.215	42.54	30.144
8	5.26E+01	51.675	48.6	34.45
9	5.92E+01	58.134	54.69	38.76
10	6.58E+01	64.59	60.77	43.1
11	7.24E+01	71.053	66.84	47.37
12	7.90E+01	77.512	72.92	51.675
13	8.55E+01	83.9713	78.99	55.981
14	9.21E+01	90.43	85.07	60.29
15	9.87E+01	96.89	91.15	64.59

Table C.4.4 Critical Flux 0.01M Na_2SO_4 and $NaHCO_3$

Applied TMP (bar)	pure water ($l/m^2.h$)	0.01 M Na_2SO_4	0.01 M $NaHCO_3$
1	6.58E+00	4.067	5.503
2	1.32E+01	8.134	11
3	1.97E+01	12.249	16.48
4	2.63E+01	16.244	22
5	3.29E+01	20.395	27.47
6	3.95E+01	24.43	33
7	4.61E+01	28.436	38.52
8	5.26E+01	32.5742	44
9	5.92E+01	36.603	49.49
10	6.58E+01	40.694	55
11	7.24E+01	44.737	60.6
12	7.90E+01	48.75	66
13	8.55E+01	52.2871	71.5
14	9.21E+01	56.978	77
15	9.87E+01	61	82.5

Table C.4.5 Critical Flux of 0.01 M $MgSO_4$ at pH 6.0 and 9.0

Applied TMP (bar)	pure water ($l/m^2.h$)	0.01 M $MgSO_4$ pH 6	0.01 M $MgSO_4$ pH 9
1	6.58E+00	2.967	4
2	1.32E+01	5.98	8
3	1.97E+01	8.613	11
4	2.63E+01	11.6	13.5
5	3.29E+01	14.833	17.4
6	3.95E+01	18.2	21
7	4.61E+01	20.814	24
8	5.26E+01	23.684	27
9	5.92E+01	26	30
10	6.58E+01	28.44	33
11	7.24E+01	30.24	35.3
12	7.90E+01	32.4	37.4
13	8.55E+01	34.2	39.5
14	9.21E+01	35.64	40.4
15	9.87E+01	36.72	42.6

Table C.4.6 Critical Flux of 0.01 M $CaCl_2$, $MgSO_4$ and NaCl

Applied TMP (bar)	pure water ($l/m^2.h$)	0.01 M $CaCl_2$	0.01 M $MgSO_4$	0.01 M NaCl
1	6.58E+00	4.907	2.967	6.08
2	1.32E+01	9.77	5.98	12.153
3	1.97E+01	14.94	8.613	18.23
4	2.63E+01	19.8	11.6	24.31
5	3.29E+01	24.9	14.833	30.383
6	3.95E+01	30.2	18.2	36.46
7	4.61E+01	35.15	20.814	42.54
8	5.26E+01	39.56	23.684	48.6
9	5.92E+01	44.1	26	54.69
10	6.58E+01	48.8	28.44	60.77
11	7.24E+01	53.6	30.24	66.84
12	7.90E+01	57.5	32.4	72.92
13	8.55E+01	61.2	34.2	78.99
14	9.21E+01	64.5	35.64	85.07
15	9.87E+01	67	36.72	91.15

Table C.4.7 Permeate Flux of Glucose as a Function Membrane of Applied Pressure for NF

Flux (m/s)	Applied pressure/8μ (s^{-1})
1.40E-06	1.25E+07
3.00E-06	2.50E+07
5.00E-06	3.75E+07
6.00E-06	5.00E+07
8.20E-06	6.25E+07
9.70E-06	7.50E+07
1.16E-05	8.75E+07
1.33E-05	1.00E+08
1.50E-05	1.13E+08
1.60E-05	1.23E+08
1.80E-05	1.38E+08
2.10E-05	1.50E+08
2.15E-05	1.63E+08
2.40E-05	1.75E+08
2.65E-05	1.88E+08

Table C.4.8 Rejection of Glucose as a Function of Permeate Flux for 0.9 nm (TiO_2) NF Membrane

Flux (m/s)	glucose rejection %
1.40E-06	2.90E+00
5.00E-06	7.40E+00
8.20E-06	1.14E+01
1.16E-05	1.52E+01
1.50E-05	1.83E+01
1.80E-05	2.18E+01
2.15E-05	2.50E+01
2.65E-05	2.90E+01

Table C.4.9 Critical Flux of Oilfield Produced Water

Applied TMP (bar)	Pure Water ($l/m^2.hr$)	Oilfield Produced Water ($l/m^2.hr$)
1	6.58E+00	2.6
2	1.32E+01	5.3
3	1.97E+01	7.5
4	2.63E+01	9.7
5	3.29E+01	12.2
6	3.95E+01	13.3
7	4.61E+01	15
8	5.26E+01	16.5
9	5.92E+01	17.08
10	6.58E+01	17.27
11	7.24E+01	17.95
12	7.90E+01	18.62

C.5 Donnan Potential

Tables (C.5.1), **(C.5.2)** and **(C.5.3)**: Membrane surface charge density, effective membrane charge and Donnan potential at pH (3-9) estimated from microelectrophoresis zeta potential measurements for background electrolyte constant at 0.001,0.01 and 0.1 M NaCl.

Table C.5.1 Surface Charge Density of Membrane, Effective Membrane Charge and Donnan Potential at pH from 3 to 9 Measured from Zeta Potential Measurements (Micro-Electrophoreses Method) for Background Electrolyte (Concentration) Constant at 0.001M NaCl and Temperature 25 ^{o}C.

pH	Membrane surface charge density (mC/m^2)	Effective membrane charge (mol/m^3)	Donnan potential (mV)
3.0	+0.62	+22.95	+2.95
3.7	0	0	0
4.0	-0.98	-36.3	-4.57
4.5	-1.25	-46.3	-5.89
5.0	-1.49	-54.98	-7
6.0	-1.98	-73.3	-9.34
7.0	-2.21	-81.8	-10.43
8.0	-2.32	-85.9	-10.97
9.0	-2.53	-93.67	-12.3

Table C.5.2 Surface Charge Density of Membrane, Effective Membrane Charge and Donnan Potential at pH from 3 to 9 Measured from Zeta Potential Measurements (Micro-Electrophoreses Method) for Background Electrolyte (Concentration) Constant at 0.01M NaCl and Temperature 25 ^{o}C.

pH	Membrane surface charge density (mC/m^2)	Effective membrane charge (mol/m^3)	Donnan potential (mV)
3.0	+0.87	+32.2	+0.58
3.5	0	0	0
4.0	-2.52	-93	-1.19
5.0	-4.1	-151.8	-2.0
6.0	-5.6	-208	-2.76
7.0	-6.49	-240.3	-3.19
8.0	-7.0	-258.97	-3.44
9.0	-7.46	-276.18	-3.66

Table C.5.3 Surface Charge Density of Membrane, Effective Membrane Charge and Donnan Potential at pH from 3 to 9 Measured from Zeta Potential Measurements (Micro-Electrophoreses Method) for Background Electrolyte (Concentration) Constant at 0.1 M NaCl and Temperature 25 ^{o}C.

pH	Membrane surface charge density (mC/m^2)	Effective membrane charge (mol/m^3)	Donnan potential (mV)
3.0	+0.55	+20.36	+0.03
3.3	0	0	0
4.0	-3.2	-118.45	-0.174
4.5	-7.65	-282.9	-0.377
5.0	-10.9	-410.2	-0.51
6.0	-15.41	-569.77	-0.758
7.0	-16.53	-611.95	-0.814
8.0	-17.67	-674.3	-0.87
9.0	-18.21	-719.56	-0.897

Table (C.5.4) Membrane surface charge density, effective membrane charge and Donnan potential at pH (3-9) estimated from streaming zeta potential measurements for background electrolyte constant at 0.01M NaCl.

Table C.5.4 Surface Charge Density of Membrane, Effective Membrane Charge and Donnan Potential at pH from 3 to 9 measured from Zeta Potential Measurements (Streaming Potential Method) for Background Electrolyte (Concentration) Constant at 0.01M NaCl and Temperature 25 ^{o}C.

pH	Membrane surface charge density (mC/m^2)	Effective membrane charge (mol/m^3)	Donnan potential (mV)
3.0	2.374	+43.94	+1.124
3.6	0	0	0
4.0	-1.45	-53.67	-0.7
5.0	-3.58	-132.5	-1.76
6.0	-4.9	-182	-2.46
7.0	-6.27	-232	-3.12
8.0	-6.69	-247.6	-3.28
9.0	-7.2	-266.4	-3.54

C.6 Results of Mathematical Model

Table C.6.1 Na^{+1} and Cl^{-1} Ions Concentration Inside the Membrane Active Layer Against the Step Size

Step Size (m)	Na^{+1} mol/m^3	Cl^{-1} mol/M^3
0	4.99E+00	5.54E+00
4.90E-07	4.58E+00	5.12E+00
9.80E-07	4.19E+00	4.73E+00
1.49E-06	3.84E+00	4.37E+00
1.99E-06	3.51E+00	4.05E+00

Table C.6.2 Sodium Chloride Rejection (Experimental and Theoretical) verses Applied Transmembrane Pressure (TMP) bar.

Pressure	NaCl Experimental R%	Numerical solution of (DSPM) sodium chloride
1	2.1	2.484
2	4.15	4.912
3	6.25	7.285
4	7.55	9.6
5	9	11.87
6	9.85	14.07
7	12.8	16.25
8	15.45	18.36
9	17.8	20.425
10	20.55	22.442
11	21.9	24.343
12	23.7	26.337
13	25.75	28.22
14	27.7	30.06
15	30.1	32

Appendix-D

D.1 Fortran Programme and Theoretical Results

D.1.1 Fortran Programme

```
      PROGRAM nanofiltration membrane fourth fifth order runge kutta
C     driver for routine membrane
      DOUBLE PRECISION cfed,cperm,flux
      DOUBLE PRECISION val,hind,hidc,abst,farcon,unigas,donnan,steric

!     .....................(Definitions & Units).................................
!     cfed: Ion feed concentration(mol/m^3), cperm: Ion permeate concentration(mol/m^3),
!     flux: permeate volume flux(m^3/m^2.s), val: Ion valance, abst : Absolute temp (K),
!     hind: Ion hindered diffusivity(m^2/s), hinc: Ion hindered concentration(dim.less),
!     farcon: Faraaday constant(C/mol),unigas: universal gas constant(J. mol^-1.K^-1),
!     donnan: Donnan potential(V), ster:Ion Steric partitioning coefficient(dim.less).

      COMMON/aleph/cfed(10,2),val(10,2),hind(10,2),hidc(10,2)
      COMMON/ale/steric(10,2),cperm(2000,2),donnan(10,2)
      COMMON/beth/farcon,unigas,flux,nep,abst,node
      INTEGER NSTEP,NVAR
      PARAMETER(NVAR=2,NSTEP=200)
      INTEGER i,j
      REAL xx(2000),x1,x2,y(2,2000),vstart(NVAR)

!     y: membrane concentration(mol/m^3), x1: membrane thickness at x=0(micron),
!     x2: membrane active skin layer thickness at x = Delta x(micron)
      COMMON /path/ xx,y
      EXTERNAL derivs

      OPEN(unit=5,file='memb.dat',status='unknown')
      OPEN(unit=6,file='memb.res',status='unknown')
      OPEN(unit=7,file='memb15.res',status='unknown')
      farcon=96487
      unigas=8.3145

!       convrg=1.0D-5
!       PRINT*,' auto 1 other 0'
!       read*,iauto

      iauto = 1
      IF(iauto.EQ.1)THEN
         READ(5,*)nep
         print*, nep
         write(6,*) nep
         READ(5,*)abst
         READ(*,*)flux
         print*,abst,flux
         write(6,*)abst,flux
         DO i = 1,nep
            DO j = 1,2
              READ(5,*)val(i,j),hind(i,j),hidc(i,j)
              READ(5,*)cfed(i,j),donnan(i,j),steric(i,j)
              PRINT*,i,j,val(i,j),hind(i,j),hidc(i,j)
              PRINT*,cfed(i,j),donnan(i,j),steric(i,j)
              WRITE(6,*)i,j,val(i,j),hind(i,j),hidc(i,j)
              WRITE(6,*)i,j,cfed(i,j),donnan(i,j),steric(i,j)
            END DO
            val(i,1)=ABS(val(i,1))
            val(i,2)=-ABS(val(i,2))
         END DO
```

```
      ELSE
         Print*,' Where is the data??'
         stop
      END IF

!     set the number of stepes (nstep or node)
      node=200

!     The initial permeate conc. was assumed to be equal to the feed conc. then:

      cperm(1,1)=cfed(1,1)/1.0
      cperm(1,2)=cfed(1,2)/1.0

!     set the intial value of y

!     Partitioning distribution at the feed interface(Feed - membrane interface):

      fixed1=EXP(-val(1,1)*farcon*donnan(1,1)/(unigas*abst))
      y(1,1)=cfed(1,1)*steric(1,1)*fixed1
      fixed2=EXP(-val(1,2)*farcon*donnan(1,2)/(unigas*abst))
      y(2,1)=cfed(1,2)*steric(1,2)*fixed2

      x1=0.0D-6
      vstart(1)=y(1,1)
      vstart(2)=y(2,1)
      x2=20.0D-6

      call membrane(vstart,NVAR,x1,x2,NSTEP,derivs)
      call output
      do 11 i=1,200
        print*,i,xx(i),y(1,i),y(2,i)
11    continue
      print*,1.0-cperm(1,1)/cfed,1.0-cperm(1,2)/cfed
      WRITE(7,*)1.0-cperm(1,1)/cfed,1.0-cperm(1,2)/cfed


      END

      SUBROUTINE derivs(x,y,dydx)
      REAL x,y(*),dydx(*)
      DOUBLE PRECISION cfed,cperm,flux
      DOUBLE PRECISION val,hind,hidc,abst,farcon,unigas,donnan,steric
      COMMON/aleph/cfed(10,2),val(10,2),hind(10,2),hidc(10,2)
      COMMON/ale/steric(10,2),cperm(2000,2),donnan(10,2)
      COMMON/beth/farcon,unigas,flux,nep,abst,node

!     The electrical potential gradient inside the membrane pores:

        fixed3= (val(1,1)*flux/hind(1,1))*(hidc(1,1)*y(1)-cperm(1,1))
        fixed4= (val(1,2)*flux/hind(1,2))*(hidc(1,2)*y(2)-cperm(1,2))
        fixed5= val(1,1)**2*y(1)
        fixed6= val(1,2)**2*y(2)
        fixed=-(fixed3+fixed4)/((farcon/(unigas*abst))*(fixed5+fixed6))

!     The ionic concentration gradient withen the membrane pores:

        fixed7 = (flux/hind(1,1))*(hidc(1,1)*y(1)-cperm(1,1))
        fixed8 = (val(1,1)*y(1)*farcon/(unigas*abst))*fixed
        fixed9 = (flux/hind(1,2))*(hidc(1,2)*y(2)-cperm(1,2))
        fixed10 = (val(1,2)*y(2)*farcon/(unigas*abst))*fixed
        dydx(1) = (fixed7-fixed8)
        dydx(2) = (fixed9-fixed10)

!     Partitioning distribution at the permeate interface(membrane interface - permeate):

        fixed11= EXP(-val(1,1)*farcon*donnan(1,1)/(unigas*abst))
        cperm(2,1)=y(1)/(steric(1,1)*fixed11)
        fixed12= EXP(-val(1,2)*farcon*donnan(1,2)/(unigas*abst))
        cperm(2,2)=y(2)/(steric(1,2)*fixed12)

!     permeate concentration change ratio
        ratio = ((cperm(1,1) - cperm(2,1))/cperm(1,1))
        ratio = ((cperm(1,2) - cperm(2,2))/cperm(1,2))

        relax=0.9

        cperm(1,1)=relax*cperm(1,1)+(1-relax)*cperm(2,1)
        cperm(1,2)=relax*cperm(1,2)+(1-relax)*cperm(2,2)
```

```
      print*,ratio,y(1),y(2),fixed,cperm(1,1)
      return
      END

      SUBROUTINE membrane(vstart,nvar,x1,x2,nstep,derivs)
      DOUBLE PRECISION cfed,cperm,flux
      DOUBLE PRECISION val,hind,hidc,abst,farcon,unigas,donnan,steric
      COMMON/aleph/cfed(10,2),val(10,2),hind(10,2),hidc(10,2)
      COMMON/ale/steric(10,2),cperm(2000,2),donnan(10,2)
      COMMON/both/farcon,unigas,flux,nep,abst,node
      INTEGER nstep,nvar,NMAX,NSTPMX
C     set the maximum number of functions(NMAX),and
C     maximum number of values to be stored(NSTPMX)
      PARAMETER (NMAX=2,NSTPMX=2000)
      REAL x1,x2,vstart(nvar),xx(NSTPMX),y(NMAX,NSTPMX)
      EXTERNAL derivs
      COMMON /path/ xx,y
CU    USES rk4
      INTEGER i,k
      REAL h,x,dv(NMAX),v(NMAX)
      do 11 i=1,nvar
         v(i)=vstart(i)
         y(i,1)=v(i)
11    continue
      xx(1)=x1
      x=x1
      h=(x2-x1)/nstep
C     h: the step size value
      do 13 k=1,nstep
        call derivs(x,v,dv)
        call rk4(v,dv,nvar,x,h,v,derivs)
       if(x+h.EQ.x)pause 'stepsize not significant in membrane'
        x=x+h
        xx(k+1)=x
        do 12 i=1,nvar
          y(i,k+1)=v(i)
12      continue
      print*,xx(k+1),y(1,k+1),y(2,k+1)
13    continue
      return
      END

      SUBROUTINE rk4(y,dydx,n,x,h,yout,derivs)
      DOUBLE PRECISION cfed,cperm,flux
      DOUBLE PRECISION val,hind,hidc,abst,farcon,unigas,donnan,steric
      COMMON/aleph/cfed(10,2),val(10,2),diff(10,2),hidc(10,2)
      COMMON/ale/steric(10,2),cperm(2000,2),donnan(10,2)
      COMMON/both/farcon,unigas,flux,nep,abst,node
      INTEGER n,NMAX
      REAL h,x,dydx(n),y(n),yout(n)
      EXTERNAL derivs

      PARAMETER (NMAX=2)
      INTEGER i
      REAL h6,hh,xh,dym(NMAX),dyt(NMAX),yt(NMAX)
      hh=h*0.5
      h6=h/6.
      xh=x+hh
      do 11 i=1,n
        yt(i)=y(i)+hh*dydx(i)
11    continue
      call derivs(xh,yt,dyt)
      do 12 i=1,n
        yt(i)=y(i)+hh*dyt(i)
12    continue
      call derivs(xh,yt,dym)
      do 13 i=1,n
        yt(i)=y(i)+h*dym(i)
        dym(i)=dyt(i)+dym(i)
13    continue
      call derivs(x+h,yt,dyt)
      do 14 i=1,n
        yout(i)=y(i)+h6*(dydx(i)+dyt(i)+2.*dym(i))
14    continue
      return
      END
```

```
      SUBROUTINE output
      DOUBLE PRECISION cfed,cperm,flux
      DOUBLE PRECISION val,hind,hidc,abst,farcon,unigas,donnan,steric
      COMMON/aleph/cfed(10,2),val(10,2),diff(10,2),hidc(10,2)
      COMMON/ale/steric(10,2),cperm(2000,2),donnan(10,2)
      COMMON/beth/farcon,unigas,flux,nep,abst,node
      INTEGER NSTEP,NVAR
      PARAMETER(NVAR=2,NSTEP=200)
      INTEGER i,j
      REAL xx(2000),x1,x2,y(2,2000),vstart(NVAR)
      COMMON /path/ xx,y
      i = 1
      write(6,10) i,xx(i),y(1,i),y(2,i)
      write(7,10) i,xx(i),y(1,i),y(2,i)


      DO i = 2,node
         iz = i/50
         ii = 50*iz
         IF(i.EQ.ii)THEN
           print*, i,xx(i),y(1,i),y(2,i)
           write(6,10)i,xx(i),y(1,i),y(2,i)
           write(7,10)i,xx(i),y(1,i),y(2,i)

         END IF
      END DO
10    FORMAT(i6,5(8x,e13.7))
      RETURN
      END
```

Table D.1.2 Theoretical Results

1	.0000000E+00	.4998912E+01	.5536204E+01
50	.4900000E-06	.4966248E+01	.5503540E+01
100	.9899993E-06	.4933124E+01	.5470416E+01
150	.1489999E-05	.4900210E+01	.5437502E+01
200	.1990002E-05	.4867507E+01	.5404799E+01

2.610835039329873 E-002
2.357452323402409 E-002

.....

1	.0000000E+00	.4998912E+01	.5536204E+01
50	.4900000E-06	.4933712E+01	.5471004E+01
100	.9899993E-06	.4868010E+01	.5405302E+01
150	.1489999E-05	.4803142E+01	.5340434E+01
200	.1990002E-05	.4739098E+01	.5276390E+01

5.162562593688325 E-002
4.661533153145148 E-002

.....

1	.0000000E+00	.4998912E+01	.5536204E+01
50	.4900000E-06	.4901309E+01	.5438601E+01
100	.9899993E-06	.4803568E+01	.5340860E+01
150	.1489999E-05	.4707686E+01	.5244978E+01
200	.1990002E-05	.4613627E+01	.5150919E+01

7.656322557631101E-002
6.913272182684782E-002

.....

1	.0000000E+00	.4998912E+01	.5536204E+01
50	.4900000E-06	.4869033E+01	.5406325E+01
100	.9899993E-06	.4739792E+01	.5277084E+01
150	.1489999E-05	.4613820E+01	.5151112E+01
200	.1990002E-05	.4491035E+01	.5028327E+01

1.009330176915796E-001
9.113741066664960E-002

.....

1	.0000000E+00	.4998912E+01	.5536204E+01
50	.4900000E-06	.4836889E+01	.5374181E+01
100	.9899993E-06	.4676675E+01	.5213967E+01
150	.1489999E-05	.4521519E+01	.5058811E+01
200	.1990002E-05	.4371257E+01	.4908549E+01

1.247472668428044 E-001
1.126404723278901 E-001

.....

1	.0000000E+00	.4998912E+01	.5536204E+01
50	.4900000E-06	.4804875E+01	.5342167E+01
100	.9899993E-06	.4614217E+01	.5151509E+01
150	.1489999E-05	.4430761E+01	.4968053E+01
200	.1990002E-05	.4254242E+01	.4791534E+01

1.480163735040975E-001
E-0011.336512979122873

.....

1	.0000000E+00	.4998912E+01	.5536204E+01
50	.4900000E-06	.4772989E+01	.5310281E+01
100	.9899993E-06	.4552406E+01	.5089698E+01
150	.1489999E-05	.4341530E+01	.4878822E+01
200	.1990002E-05	.4139935E+01	.4677227E+01

1.707509143895077 E-001
1.541794376573028 E-001

.....

1	.0000000E+00	.4998912E+01	.5536204E+01
50	.4900000E-06	.4741233E+01	.5278525E+01
100	.9899993E-06	.4491240E+01	.5028532E+01
150	.1489999E-05	.4253795E+01	.4791087E+01
200	.1990002E-05	.4028273E+01	.4565565E+01

1.929634653316855E-001
1.742362469033132E-001

.....

1	.0000000E+00	.4998912E+01	.5536204E+01
50	.4900000E-06	.4709606E+01	.5246898E+01
100	.9899993E-06	.4430713E+01	.4968005E+01
150	.1489999E-05	.4167539E+01	.4704831E+01
200	.1990002E-05	.3919202E+01	.4456494E+01

2.146641891238038E-001
1.938307555043795E-001

.....

1	.0000000E+00	.4998912E+01	.5536204E+01
50	.4900000E-06	.4678107E+01	.5215399E+01
100	.9899993E-06	.4370820E+01	.4908112E+01
150	.1489999E-05	.4082737E+01	.4620030E+01
200	.1990002E-05	.3812666E+01	.4349958E+01

2.358642752521720 E-001
2.129734651039673 E-001

1	.0000000E+00	.4998912E+01	.5536204E+01
50	.4900000E-06	.4646738E+01	.5184030E+01
100	.9899993E-06	.4311559E+01	.4848851E+01
150	.1489999E-05	.3999375E+01	.4536667E+01
200	.1990002E-05	.3708621E+01	.4245913E+01

2.565721970719859E-001
2.316718303692085E-001

1	.0000000E+00	.4998912E+01	.5536204E+01
50	.4900000E-06	.4615498E+01	.5152790E+01
100	.9899993E-06	.4252921E+01	.4790213E+01
150	.1489999E-05	.3917427E+01	.4454719E+01
200	.1990002E-05	.3607009E+01	.4144300E+01

2.767997130420978E-001
2.499361716908169E-001

.....

1	.0000000E+00	.4998912E+01	.5536204E+01
50	.4900000E-06	.4584383E+01	.5121675E+01
100	.9899993E-06	.4194899E+01	.4732191E+01
150	.1489999E-05	.3836871E+01	.4374164E+01
200	.1990002E-05	.3507777E+01	.4045071E+01

2.965566920485310E-001
2.677754277737691E-001

.....

1	.0000000E+00	.4998912E+01	.5536204E+01
50	.4900000E-06	.4553399E+01	.5090691E+01
100	.9899993E-06	.4137496E+01	.4674788E+01
150	.1489999E-05	.3757695E+01	.4294987E+01
200	.1990002E-05	.3410886E+01	.3948177E+01

3.158512241573159E-001
2.851977607662821E-001

.....

1	.0000000E+00	.4998912E+01	.5536204E+01
50	.4900000E-06	.4521245E+01	.5058537E+01
100	.9899993E-06	.4078321E+01	.4615613E+01
150	.1489999E-05	.3676621E+01	.4213914E+01
200	.1990002E-05	.3312338E+01	.3849631E+01

3.354791094339515 E-001
3.029205311163287 E-001

السيطرة على تكوّن التكلسات في غشاء ثاني اوكسيد التيتانيوم الخزفي النانوفلتر

اعداد

مظفر يعقوب حسين

اشراف

أ. د. احمد فائق حسن العلوي

د. عامر ناجي احمد النعيمي

الخلاصة

يهدف البحث إلى دراسة منع تكون الترسبات وحساب نسبة رفض كاربونات الكالسيوم ($CaCO_3$) والأملاح الأخرى (NaCl، KCl، $NaHCO_3$، $MgCl_2$، $CaCl_2$، Na_2CO_3، Na_2SO_4 و$MgSO_4$) لغشاء ترشيح دقيق (النانوفلتر: NF) سيراميكي أنبوبي ثاني أوكسيد التيتانيوم ذو حجم مسامي ٠,٩ نانومتر.

العوامل الأساسية المؤثرة على الترسبات والرفض لأغشية الترشيح (NF)، شحنة سطح الغشاء والتي تم قياسها باستخدام طريقة الترحيل الكهربائي (microelectrophoresis) وطريقة جهد الجريان (Streaming potential) لتحديد نقطة التعادل الكهربائي (IEP) للغشاء. لذلك تم تصنيع قطبين من مادة متراكبة مكونة من الفضة النقية و٤% ذهب لقياس جهد زيتا على سطح الغشاء مباشرةً للأملاح بطريقة جهد الجريان. كذلك تم تطبيق اسلوب خطوة بعد خطوة (step by step) لتحديد قيم التدفق الحرج كدالة لتجنب الترسبات على سطح الغشاء. قياسات جهد زيتا لملح كلوريد الصوديوم القياسي أجريت في دالة حامضية (٣-٩) بتراكيز مختلفة (٠,٠٠١، ٠,٠١ و٠,١ مولاري) وفي مجال ضغط (٠,٢٥-٢ بار). تشير النتائج إلى أن نقطة التعادل الكهربائي IEP متقاربة للطريقتين وكانت بحدود (٣,٣-٣,٥)، نقطة التعادل الكهربائي لبقية الأملاح كانت بحدود (٣,٤-٣,٨)، جهد زيتا يزداد مع زيادة الدالة الحامضية.

تمت دراسة العوامل التالية في تجارب نسبة الرفض والتدفق الحرج: التركيز (٥×١٠ $^{-٥}$ - ٥٠×١٠$^{-٥}$ مولاري) إلى $CaCO_3$، بينما الأملاح الأخرى (٠,٠١-٠,٠٠١ مولاري)، الدالة الحامضية (٣-٩)، سرعة الجريان (١-٢ متر/ثانية) وضغط مرور (١-١٥ بار).

تمت دراسة سلوك رفض $CaCO_3$ في دالة حامضية (٦) وسرعة ١م/ثا، الرفض يزداد مع زيادة الضغط ويصل إلى أعلى نسبة (٦١%) في ضغط ٦ بار وبتركيز ٥×١٠$^{-٥}$ مولاري، ومن ثم يبدأ بالنزول مع الضغط. نسبة الرفض تزداد مع زيادة الدالة الحامضية وسرعة الجريان، زيادة سرعة الجريان من (١م/ثا إلى ٢م/ثا) تؤدي إلى زيادة نسبة الرفض بحدود ٦% في دالة حامضية (٦) وتركيز ١٠×١٠$^{-٥}$ مولاري. أعلى نسبة رفض كانت تساوي (٧٠%) في ضغط ٦ بار وتركيز ٥×١٠$^{-٥}$ مولاري، دالة حامضية (٩) وسرعة جريان ٢م/ثا، وفي حالة فوق التشبع ٥٠×١٠$^{-٥}$ مولاري نسبة الرفض تقل مع زيادة الضغط منذ البداية.

نتائج رفض الأملاح الأخرى كانت حسب التسلسل التالي ($MgCl_2 < MgSO_4 < Na_2SO_4 < CaCl_2 < NaHCO_3 < NaCl$). أعلى نسبة رفض كانت إلى Na_2SO_4 تقريباً ٨٢.٢%. نسبة الرفض تزداد مع زيادة (جهد زيتا، سرعة الجريان، الضغط) وتقل مع زيادة التركيز.

نتائج التدفق الحرج تشير الى حصول التدفق الحرج فقط لمحاليل الملحين ($MgSO_4$ في التركيزين ٠,٠٠٥ و ٠.٠١ مولاري) مع تدفق للنافذ (٧٩ و ٥٤ لتر/م^{٢}.ساعة) على التوالي و ($CaCl_2$ حدث في التراكيز ٠,٠٠٥، ٠,٠١ و ٠,٠١٥ مولاري) مع تدفق للنافذ (٧٨.٦، ٥٧.٥ و ٤٣.٣ لتر/م^{٢}.ساعة) على التوالي. التدفق الحرج لم يحدث للاملاح الاخرى (NaCl، $NaHCO_3$ و Na_2SO_4). عموماً، عند زيادة التركيز يحدث التدفق الحرج في ضغوط واطئة. بينما زيادة كل من الدالة الحامضية pH والسرعة يؤدي الى حدوث التدفق الحرج في ضغوط عالية.

تم دراسة معالجة المياه المصاحبة لانتاج النفط والغاز (Oilfield produced water) (الناتجة من خزانات فصل الماء عن النفط) من حقل نفط بازركان في ميسان جنوب العراق. عملية المعالجة تتكون من معالجة اولية باستخدام غشاء ترشيح دقيق MF (٠,٣ مايكرومتر) وغشاء فائق الدقة UF (٠,٠٠٤ مايكرومتر) على التوالي وبعد ذلك معالجة لاحقة باستخدام غشاء نانوفلتر NF (٠,٩ نانومتر) وغشاء تنافذ عكسي RO (٠,٣ نانومتر). الازالة الكلية للمحتوى الكاربوني TOC ٩٥,٨% و ١٠٠%، ازالة الزيت (oil) ٩٩,٤% ، ١٠٠% وازالة الاملاح الصلبة الكلية الذائبة TDS ٣٠% و ٩٩,٤١% بعد غشاء النانوفلتر NF والتنافذ العكسي RO على التوالي.

تم استخدام موديل دونان الرياضي (DSPM) لحساب نسبة رفض ملح NaCl نظرياً. النتائج النظرية قريبة من النتائج العملية وأعلى نسبة رفض تساوي (٣٠,٣% و ٣٣,٦%) عملياً ونظرياً على التوالي في ضغط (TMP) ١٥ بار.

جمهورية العراق
وزارة التعليـم العالي و البحث العلمـي
جامعـــة بغـــداد
كليـــة الهندســـة
قسم الهندسة الكيمياويـة

السيطرة على تكوّن التكلسات في غشاء ثاني اوكسيد التيتانيوم الخزفي النانوفلتر

اطروحة مقدمة الى

كليـــة الهندسـة- جامعـة بغـــداد

كجزء من متطلبات نيل شهادة الدكتوراه في الهندســـة الكيماويـة

من قبل

مظفر يعقوب حسين
بكالوريوس هندسة كيمياوية - ١٩٨٨
ماجستيـر هندسـة كيـميـاوية - ٢٠٠٢

اب - ٢٠١٨